

# **Development of an Intelligent Robotic Manipulator**

by

**Trevor Holden**

A Thesis submitted to the University of Central Lancashire in partial fulfilment  
of the requirements for the degree of

**MSc (by Research)**

The work presented in this thesis was carried out at the School of Computing,  
Engineering and Physical Sciences

January 2012

## **Declaration**

I declare that while registered with the University of Central Lancashire for the degree of Master of Science I have not been a registered candidate or enrolled student for another award of the University of Central Lancashire or any other academic or professional institution during the research programme. No portion of the work referred to in this thesis has been submitted in support of any application for another degree or qualification of any other university or institution of learning.

Signed.....

Print.....

## Abstract

The presence of hazards to human health in chemical process plant and nuclear waste stores leads to the use of robots and more specifically manipulators in unmanned spaces. Rapid and accurate performance of robotic arm movement and positioning, coupled with a reliable manipulator gripping mechanism for variable orientation and a range of deformable and/or geometric and coloured products, will lead to smarter/intelligent operation of high precision equipment. The aim of the research is to design a more effective robot arm manipulator for use in a glovebox environment utilising control kinematics together with image processing / object recognition algorithms and in particular the work is aimed at improving the movement of the robot arm in the case of unresolved kinematics, seeking improved speed and performance of object recognition along with improved sensitivity of the manipulator gripper mechanism

A virtual robot arm and associated workspace was designed within the LabView 2009 environment and prototype gripper arms were designed and analysed within the Solidworks 2009 environment. Visual information was acquired by barrel cameras. Field research determines the location of identically shaped objects, and the object recognition algorithms establish the difference between them. A touch/feel device installed within the gripper arm housing ensures that the applied force is adequate to securely grasp the object without damage, but also to adapt to any slippage whilst the manipulator moves within the robot workspace.

The research demonstrates that complex operations can be achieved without the expense of specialised parts/components; and that implementation of control algorithms can compensate for any ambiguous signals or fault conditions that occur through the operation of the manipulator. The results show that system performance is determined by the trade-off between speed and accuracy. The designed system can be further utilised for control of multi-functional robots connected within a production line. The Graphic User Interface illustrated within the thesis can be customised by the supervisor to suit operational needs.

# Contents

<b>Declaration</b> .....	<b>ii</b>
<b>Abstract</b> .....	<b>iii</b>
<b>List of Figures / Tables / Plates</b> .....	<b>vi</b>
<b>Acknowledgements</b> .....	<b>xi</b>
<b>Abbreviations</b> .....	<b>xii</b>
<b>Chapter 1: Introduction</b> .....	<b>1</b>
1.1 Background.....	1
1.2 Robots within the Nuclear Industry.....	3
1.3 Literature review.....	5
1.4 Justification of the Research.....	9
1.5 Research Direction .....	10
1.6 Thesis Organisation .....	11
<b>Chapter 2: The Robot Arm Simulation</b> .....	<b>13</b>
2.1 The Design of the Virtual Robot .....	13
2.2 Robot Kinematics Solution.....	17
2.3 Inverse Kinematics solution for Virtual Robot.....	19
2.4 3D location kinematics solution used with virtual robot.....	22
2.5 Robot Arm Simulation Solution .....	27
2.6 Touch/Feel Application With FS Series Tactile Sensors .....	32
2.7 LabView Simulation of Visual Servoing mechanism .....	38
<b>Chapter 3: Design and Implementation of new gripper arms.</b> .....	<b>43</b>
3.1 Heuristic design of new gripper arms with inclusion of the force feedback sensor. ....	47
3.2 Prototype of Single Gripper Arm .....	51
3.3 Prototype of Dual Gripper Arm.....	54
3.4 Improvements to the prototype gripper arm designs .....	58
3.5 Design and implementation of replacement manipulator main body.....	61

<b>Chapter 4: Vision System Development</b> .....	<b>68</b>
4.1 Image Calibration from image acquisition .....	68
4.2 Colour Inspection. ....	70
4.3 Isolating a specific object from an image.....	73
4.4 8-bit greyscale image processing.....	74
4.5 Manipulation of greyscale images with logic operators.....	76
4.6 Greyscale Pattern and Object Matching .....	76
4.7 Additional vision control.....	78
<b>Chapter 5: Trials and Research Outcomes</b> .....	<b>80</b>
5.1 Virtual Robot and Kinematic Solution.....	80
5.2 Image Processing and Object Recognition.....	85
5.2.1 Initial image processing for object recognition algorithm - long scan position .....	90
5.2.2 Improvement in Long Distance image processing.....	96
5.2.3 Long Distance image processing Final Design.....	101
5.2.4 Object Recognition design for Close scan system .....	106
<b>Chapter 6: Conclusion and Recommendation for Further Work</b> .....	<b>116</b>
6.1 Further Work and improvements.....	123
<b>References</b> .....	<b>127</b>
<b>Appendix A</b> .....	<b>131</b>
Connection of Visual Servoing Mechanism to Manipulator .....	131
<b>Appendix B</b> .....	<b>132</b>
Visual Servoing Mechanism Commissioning Information .....	132
<b>Appendix C</b> .....	<b>135</b>
Virtual Manipulator Commissioning Information.....	135
<b>Appendix D</b> .....	<b>155</b>
Annealed Stainless Steel Gripper Arms Analysis .....	155
Simulation of prototype Stainless Steel gripper arms .....	155
<b>Appendix E</b> .....	<b>161</b>
FS-Series Force Sensor Manufacturers Datasheet.....	161

## List of Figures / Tables / Plates

### List of Figures

Figure 1	Aspects of an Intelligent machine.....	3
Figure 2	Parent - Child Relationship for design of the Virtual Robots.....	13
Figure 3	Building Blocks for the development of the Virtual Robot.....	14
Figure 4	LabView Front Page for Generation of Robot Tree .....	15
Figure 5	Robot Tree Joint Array Parameters .....	16
Figure 6	The Finished Virtual Robot Design .....	16
Figure 7	Number of Degrees of freedom of the Katana 6M180 with axis and rotation parameters .....	17
Figure 8	Rotation of a vector about an arbitrary axis.....	19
Figure 9	Rotation of a frame by angle.....	20
Figure 10	Frame Relationship between one link and a connected link.....	21
Figure 11	Robot Vision and Manipulator Sequence Structure .....	29
Figure 12	Ariel view of robot worksapce illustrating 'drop-off' locations of objects .....	31
Figure 13	Generation of Joint Array .....	31
Figure 14	Updating Joint Array using Kinematic Solution.....	32
Figure 15	Force Sensor Equivalent Circuit and Construction.....	33
Figure 16	DC Amplitude from Force Sensors with No Applied Load (x30).....	34
Figure 17	Control Algorithm for Force Feedback Control Response .....	36
Figure 18	Pulse Width Modulation (PWM) versus Angular Adjustment for Servo Motors ...	39
Figure 19	PWM Generation for Control of Both Servo Motors .....	40
Figure 20	Visual Servoing Algorithm Design.....	41
Figure 21	Existing SS Gripper Arm Design.....	44
Figure 22	Existing Katana 6M180 Gripper Mechanism .....	45
Figure 23	Existing Gripper Grasping Various Diameter Objects .....	45
Figure 24	Schematic Determining modest tolerance for position of Manipulator.....	46
Figure 25	Locations of Load and Restraint on existing Gripper Arm .....	46
Figure 26	Existing Gripper Displacement Chart for Maximum Load .....	47
Figure 27	Secure Mouning For Force Sensor PCB Board .....	47
Figure 28	Gripper Arm Front Plate including Slots for Additional Components.....	48

Figure 29 Gripper Design No.1 .....	49
Figure 30 Three finger Gripper Arm Design .....	50
Figure 31 Gripper Design to Permit Assisting an Object into the Gripper Mechanism .....	51
Figure 32 3D Single Gripper Arm Design .....	52
Figure 33 Locations of Restraint stress on Prototype Single Gripper Arm .....	53
Figure 34 Locations of Load on Prototype Single Gripper Arm .....	53
Figure 35 Stress and Displacement Model for Prototype Single Gripper Arm .....	54
Figure 36 Dual Gripper 3D Design .....	55
Figure 37 Locations of Restraint on Dual Gripper Arm .....	56
Figure 38 Locations of Load on Prototype Dual Gripper Arm .....	56
Figure 39 Stress and Displacement Model for Prototype Dual Gripper Arm .....	57
Figure 40 Final 3D Design of Single Gripper Arm .....	58
Figure 41 Final 3D Design of Dual Gripper Arm .....	59
Figure 42 Stress and Displacement Model for Final Design of Dual Gripper Arm .....	60
Figure 43 Schematic of Main Base Prototype .....	63
Figure 44 Intermediate Shell of Manipulator .....	64
Figure 45 Gripper Housing Mount to Manipulator Main Body .....	64
Figure 46 Design Schematic of Gripper Housing .....	65
Figure 47 Bevel Gear Arrangement for Operation of Gripper Mechanism .....	66
Figure 48 Gripper Mounting Onto Bevel Gears For Transient Operation .....	66
Figure 49 Example of calibration coordinate system .....	70
Figure 50 Hue colour Space to colour spectrum array relationship .....	71
Figure 51 Comparing colour spectrums of two images .....	72
Figure 52 Example of how to utilise all shades of grey to highlight greater details in captured images .....	75
Figure 53 Greyscale Pattern Matching x-correlation Methodology .....	78
Figure 54 Calculation of new reach coordinate for manipulator .....	79
Figure 55 Object Matching Operation .....	79
Figure 56 The Virtual Robot and Associated Workspace .....	81
Figure 57 Real World Manipulator Position to Virtual Manipulator Position .....	81
Figure 58 Position of Manipulator for the Short Image Acquisition Scan .....	82
Figure 59 Manipulator Movement after Grasping Object - First Trial .....	84

Figure 60 Long Distance Image Acquisition Algorithm Connection Diagram .....	90
Figure 61 3D View of Image Intensity Operation with Logic Operator .....	91
Figure 62 Closer Inspection of 3D View of Image Intensity Operation with Logic Operator	93
Figure 63 Measurement of Object Location Initial Trial .....	94
Figure 64 Location of Cable Causing Positional Issues.....	95
Figure 65 Design Time Frame Analysis for Initial Trial .....	95
Figure 66 Increased Spatial Calibration Grid and Resultant Corrected Image .....	96
Figure 67 Long Distance Image Acquisition with Improved Calibration and Pattern Matching Connection Diagram.....	97
Figure 68 Measurement of Object Location with Improved Calibration and Pattern Matching.....	100
Figure 69 Time Frame Analysis with Improved Calibration and Pattern Matching Algorithm .....	101
Figure 70 Long Distance Image Acquisition Final Algorithm Connection Diagram .....	102
Figure 71 Effect of Processed Image with Logic Operator - Final Design.....	103
Figure 72 3D representation and Histogram from Logic Operator - Final Design .....	104
Figure 73 Measurement of Object Location - Final Design.....	105
Figure 74 Long Distance Final Design Time Frame Analysis.....	106
Figure 75 Close Scan Image Acquisition Final Algorithm Design.....	108
Figure 76 Ensuring a Colour and Pattern Match for the Three Objects.....	110
Figure 77 Time Distribution Chart for Short Scan Algorithms .....	114
Figure 78 Operator GUI for Manipulator Control System .....	123
Figure 79 Parabolic interpolation for sub-pixel location .....	125
Figure 80 Edge Detection Once Object is Grasped.....	125

### **List of Tables**

Table 1 Excel Database for Control of Virtual Manipulator.....	30
Table 2 Control Algorithm Response for Force Feedback Control .....	37
Table 3 PC-10 Comparison of Single Gripper Arm Properties .....	59
Table 4 PC-10 Comparison of Dual Gripper Arm Properties.....	60
Table 5 Manipulator Maneuvres from Short Scan to Object Under Inspection.....	83

Table 6	Image Histograms for all Objects in the Image - Template Position .....	87
Table 7	Image Intensity for Objects - Template Position .....	88
Table 8	Intensity for PBOG Object in Different Location on the Workspace .....	89
Table 9	Histogram Charts Before and After Logic Operator .....	92
Table 10	3D View of Image Intensity Operation with Logic Operator with Improved Calibration and Pattern Matching .....	98
Table 11	Histogram Charts Before and After Logic Operator with Improve Calibration and Pattern Matching Algorithm .....	98
Table 12	Processed Image Operation with Brightness Control - Final Design .....	103
Table 13	Histograms Illustrating Colour Content of the Objects .....	108
Table 14	Close Scan ROI Colour Differences .....	109
Table 15	3D View and Histogram Charts after Pane Extraction - Short Scan Algorithm .....	110
Table 16	Results from Short Scan Algorithm .....	112
Table 17	Results from the GBOPO Determining a Pattern Match Error .....	113

### **List of Plates**

Plate 1	Nuclear waste Glovebox [Courtesy: Science photo library] .....	5
Plate 2	Three objects under inspection and manipulation .....	27
Plate 3	Location of visual servoing system on Katana Robot arm .....	42
Plate 4	Modification to Pressure Plate on Gripper Arms .....	61
Plate 5	Manufactured Prototype of PC-10 Manipulator with Stereo Vision Attached .....	67
Plate 6	Position of robot pose causing perspective errors within image .....	69
Plate 7	Initial Position of First Image Capture .....	85
Plate 8	Lighting Levels Upon Robots Workspace During Image Capture .....	86

**List of Figure, Tables and Plates in Appendices****Appendix A**

FigureA 1 Vision Servo Mechanism Mounting Bracket.....	131
--	-----

**Appendix B**

FigureB 1 Servo Adjustment From First Scan Position.....	132
FigureB 2 Servo Adjustment From First Scan Coordinates to Short Scan Coordinates.....	132
FigureB 3 LabView Frames Describing Servo Adjustment From Short Scan Coordinates to Grasp Position.....	134

**Appendix C**

FigureC 1 Calibration Encoder Settings Algorithm.....	136
FigureC 2 Virtual Manipulator Calibration Position.....	137
FigureC 3 POBG 'drop-off' Destination Position of Manipulator.....	148
TableC 1 Calibration Encoder Settings.....	135
TableC 2 Labview Frames from Calibration to First Image Scan Position.....	138
TableC 3 Labview Frames from Long Scan Position to Short Scan Coordinates.....	139
TableC 4 End Effector Position to Enable Object Grasp.....	140
TableC 5 Manipulator Movement to Lift Grasped Object Clear of Workspace.....	141
TableC 6 LabView Frames Illustrating Movement to Drop GBOPO Object.....	143
TableC 7 LabView Frames Describing Movement From GBOPO 'drop-off' Position to First Scan Coordinates.....	145
TableC 8 LabView Frames Illustrating Movement to Drop POBG Object.....	147
TableC 9 LabView Frames Depicting Movement from POBG 'drop-off' position to First Scan Position.....	149
TableC 10 LabView Frames Illustrating Movement to Drop PBOG Object.....	151
TableC 11 LabView Frames Illustrating Movement From PBOG 'drop-off' Location to Following Image Acquisition Scan.....	153

**Appendix D**

FigureD 1 FOS for Prototype SS Single Gripper Design.....	155
FigureD 2 Stress and Displacement Model for SS Single Gripper Arm.....	156
FigureD 3 FOS Limit for SS Single Prototype Gripper Arm Design.....	156
FigureD 4 Failure Analysis for SS Single Gripper Arm.....	157
FigureD 5 FOS for Prototype Design SS Dual Gripper Arm.....	158
FigureD 6 Stress and Displacement Model for SS Dual Gripper Arm.....	158
FigureD 7 FOS for Prototype Design SS Dual Gripper Arm.....	159
FigureD 8 Failure Stress Analysis for SS Dual Gripper Arm.....	159
FigureD 9 FOS Limit for Prototype SS Dual Gripper Arm Design.....	160
TableD 1 Annealed SS Single Gripper Arm Properties.....	155
TableD 2 Annealed SS Prototype Dual Gripper Arm Properties.....	157

## Acknowledgements

I would like to express the most sincere gratitude to Dr Javad Yazdani, my Director of Studies, for all the invaluable discussions and consistent support throughout the year. Special accolade goes to Dr Jonathan Francis who encouraged me and offered additional support in tough times throughout the year.

I would also like to thank Professor Waqar Ahmed for his support and advice throughout the year. Also special acclaim to all the technicians who have assisted me throughout the year, helping to resolve the software and hardware issues encountered that involved substantial inconvenience for the technicians themselves (e.g. the use of the prototype machine, Windows 7 issues, compatibility issues etc.; thank-you to all of them).

I could not have even started this course without the support of my friends and family, who have placed faith in me to obtain the Masters degree and encouraged me into bettering myself in this tough economic period. It has seen one of the hardest years I have encountered, with various issues both professional and personal – so your invaluable support and the odd tease has helped me keep going.

I have met some new friends and learned the processes involved in academia which will add to my knowledge gained in industry. A tough year but a fruitful year – can't wait to do it all again!

## Abbreviations

AI -	Artificial Intelligence	Min	Minimum
Ap	First Acquired Image	mm	Millimetres
Bp	Second Acquired Image	ms	Milliseconds
B&W	Black and White	mV	Millivolts
CAD	Computer Aided Design	N	Newton force
CCD	Charged Coupled Device	NE	North East
CFR	Code of Federal Regulation	Op	Logic Operator
Cos	Cosine	PBOG	Pink Blue Orange Green
CPU	Central Processing Unit	PC	Personal Computer
DAQ	Data Acquisition	PC	Polycarbonate (gripper design section only)
DC	Direct Current	PCB	Printed Circuit Board
DOF	Degrees of Freedom	POBG	Pink Orange Blue Green
DSP	Digital Signal Processing	POMDP	Partially Observed Markov Decision Process
FIFO	First In – First Out	PWM	Pulse Width Modulation
FOS	Factor of Safety	Ref	Reference
FS	Force Series (manufacturer's ref.)	RGB	Red Green Blue colour space
GBOPO	Green Blue Orange Pink Orange	ROI	Region of Interest
GUI	Graphic User Interface	SIL	Safety Integrity Levels
HD	High Definition	Sin	Sine
HSL	Hue Saturation Luminance	SS	Stainless Steel
H&S	Health and Safety	STL	Stereo lithography
Hz	Hertz (measurement of frequency)	TV	Television
I/O	Input / Output	USB	Universal Serial Bus
IR	Infra-red	VI	Virtual Instrument
LV	LabView (Software Application)	XOR	Exclusive OR
Lux	Light levels	2D	Two Dimension
Max	Maximum	3D	Three Dimension

# Chapter 1

## Introduction

### 1.1 Background

Most effective robotic systems need some form of human control (i.e. need to be supervised), generally with the use of a joystick or with a bio-mechanical mechanism connected to the human arm [1]. The presence of hazards to human health in chemical process plant and nuclear waste stores leads to the use of robots and manipulators in unmanned spaces, with custom manipulators designed for certain application (e.g.. decommissioning nuclear power stations, or for use within glovebox technologies) [2,3]. Speedy and accurate performance of robotic arm movement and positioning, coupled with reliable manipulator grip for use with variable and possibly unpredictable orientation or range of deformable and/or geometrical and coloured products, will lead to smarter operation of high precision equipment [4]. In order to achieve this flexibility and improve performance over non intelligent systems, a robotic manipulator is required to increase its own autonomous decision making and operation ability, to solve more complex tasks in increasingly challenging domains. This requires the manipulator to receive information about its own on-board systems and surrounding environment. In interacting with the real world, autonomous systems will be forced to rely on sensor data in order to infer the state of their environment [5]. Unfortunately, sensor data has limited accuracy and is subject to noise. The ability of an autonomous system to counteract these limitations at an affordable cost requires a system to combine data from multiple sensors, control algorithms and on-board databases.

Many robots are able to compute complicated mathematical transforms in order to control their spatial movement. They have inbuilt 'smart' functions. However, it is recognised that a significant deficiency in robots without intelligence, is their lack of flexibility, e.g. [6], "No robot can be called intelligent, if it is without significant sensing capabilities or has a rigid control sequence". As with any operation, there is a degree of uncertainty as to whether the operation was as successful as intended. In the computer world calculations occur with the fortune of no outside interference or external events but by contrast, in the robot world a

number of factors/solutions must be designed into the computer controlled system to resolve issues such as :-

- a) Components do not always stay in the same place and deteriorate with use.
- b) The same movements can sometimes produce different results especially where robotic structures are required to interact with other systems (e.g. fluid flow from pressurised systems that can become clogged).
- c) There are always some unknowns about aspects of the task, either in the form of risk or uncertainty.
- d) External interference is possible, from minor effects of the local environment to major catastrophes.

Thus the design of the robot system has significant intrinsic difficulties to deal with, in addition to those associated with implementing computer-based systems. Figure 1 illustrates the characteristics required for an autonomous machine to be intelligent and thereby, instigate or counteract the aforementioned issues. The robot is programmed with a specific task; the robot then has to utilise intelligence in order to complete the task. Information from sensors and recognition ability (from databases or previously actioned tasks loaded from the memory) will assist the robot in learning from the environment. Depending on the information from the sensor system, the robot will need to adapt: a good example is a manipulator which senses an obstruction from a previously clear path; hence a different path is required to achieve the same objective. Communication is required to programme the robot with a specific task in addition to communicate the monitoring/fault information to a supervisor.

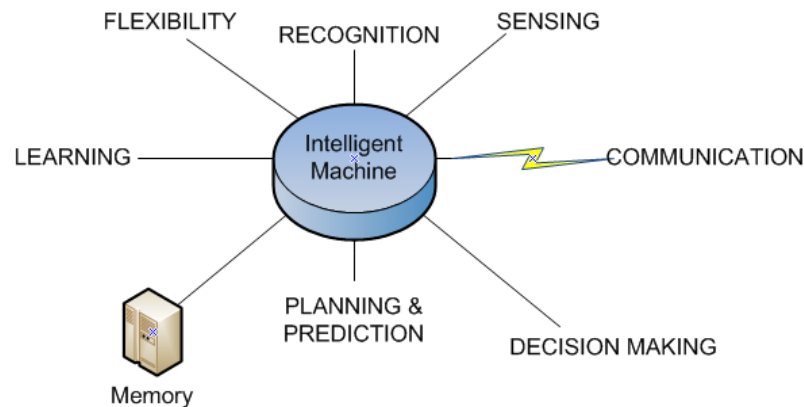


Figure 1 Aspects of an Intelligent machine

## 1.2 Robots within the Nuclear Industry

The use of robots for handling toxic substances, monitoring and data acquisition are of equal importance. Concerns with radiation causing functional problems and efficiency difficulties are major issues regarding the use of robots within this field (e.g. [1],[3],[5]). The main application where robots are valuable in the nuclear industry is to perform automated and repetitive work, or to execute hazardous tasks that are dangerous to human health. Performing these functions reliably, over time carries considerable benefit, which has been recognized by Marian and Rowan [7]. Reduction of manpower excursions into hazardous environments is a significant health and safety task that is augmented by a reliable robotic system. The use of robot manipulators, within the nuclear industry, is to replace the human arm where the radiation level compromises the safety of the personnel. The ability to adapt to unplanned occurrences is a major advantage for unmanned spaces. Thus an ability to alter the orientation of the end effector to manipulate fallen or misplaced object is the key to their success.

Their flexibility originates from the number of Degrees-of-Freedom (DOF) that the manipulator possesses: as the DOF increases so does the flexibility. It is this flexibility that enables the manipulator to copy the movements of a human arm, but traditionally it has remained human intelligence that provides control. It is this distinction which allows the use of manipulators for the transportation of hazardous material that is executed by a master/slave system: the operator manipulates a master arm that is mechanically connected to a slave robot in a hot cell; as such the robot reproduces every movement of the operator. The advantages of

this system are its simplicity and affordability. The shortcomings are a low payload and a limited distance between the operator and the robot. Since the manipulator is used in place of a human arm, it is not sufficient to simply visualize an operation to be able to operate correctly. A good example is the handling of an egg. An operator can see how well a gripper holds an egg on a monitor but this is not enough. The operator needs a force feedback system to avoid squeezing the egg too hard and avoid breaking or dropping it. This feedback is made with force and torque sensors and requires a significant amount of electronics and control algorithms [8].

Where this flexibility becomes useful is within very small contained areas such as Gloveboxes that are designed to allow manipulation of objects in a separately pressurized environment, a typical example of a Glovebox used within a nuclear environment is illustrated in Plate 1. Nuclear workers sort equipment for disposal after us in the nuclear industry, as such the glovebox permits workers to manipulate hazardous materials, through gloves, without exposure to themselves or subsequent unfiltered release of the material to the environment. In the Nuclear Industry, gloveboxes provide confinement and protection of radioactive material handling of a diverse range of chemical, oxygen-sensitive, hazardous and nuclear materials, however strict controls are required on seals and internal environmental pressure to provide full protection. Another drawback to the use of gloveboxes is that the interior workspace is reserved for primary operating purposes on the box floor between the glove ports and within reach of the gloved hand; and remote handling capabilities other than tool extensions for the gloved hand, are usually not provided. Installing a robot arm manipulator in these low-level radioactive environments would provide additional flexibility and improve the amount of human interaction with radioactive materials.



Plate 1 Nuclear waste Glovebox [Courtesy: Science photo library]

Two key points of this research are therefore, the demonstration of manipulator capability that integrates force sensors and camera inputs in recognizing and manipulating objects; and using intelligence or control algorithms to use with a displaced environment.

### 1.3 Literature review

In 1975, Rollies [9] discussed the purpose of verification vision in verifying and updating the location of an object based on a selected number of image features by searching in small “area-of-interest” within in the acquired image. To speed up the process of interpreting vision inputs, actual image features instead of the object’s position are used as the feedback signal for the controlling of the manipulator: these features can be directly related to the control parameters of the robotic system, as explained by Weiss and Sanderson in [10].

In 1990, Howe and Cutkosky [11], discussed the flexibility and robustness of a manipulator with an attached tactile sensor. A two fingered gripper mechanism was used to determine the grasp quality and applied force. The smoothness and control of both the gripper mechanism and manipulator during operation were investigated. It was found that clumsy grasping resulted in issues with accurate and efficient control of the manipulator; the design of the gripper mechanism and the placement of the tactile sensor affected the operation, in addition sharp movements of the manipulator accounted for some sensing error within the testing stages. By comparing how humans grasped and moved objects with the manipulator design, they were able to account for variations in load throughout the operation. A similar control

structure is used for this research under tighter tolerance levels, with the ability to integrate the vision system into the grasping control.

In 1996, Bell, Wilson and Huk [12], explained that vision systems can adequately measure, and therefore control, a maximum of 3 feature characteristics independently, e.g. perceived feature position (in  $x$  and  $y$ ) and orientation (about  $z$ ). In position based control systems, features are extracted from the image to estimate (with the geometrical model of the target) the pose of the target in the configuration space with respect to the position of the camera. The error between the actual and the desired position of the end-effector is evaluated. They explain that this method has the limitation of being sensitive to calibration errors, since the feedback signal is calculated using estimated values that are functions of the system calibration parameters. The matter is further clarified by the work of Koditshek and Rizzi [13]. Moreover, in image based control systems, the error signal is calculated by comparing the location of the features in the current image with the desired location as discussed by Malcom [14]. The feedback is given by the location of the features in the image plane of the current image. The dynamics of the system are described by a Jacobian matrix: relating the changes in the image to the ones in the arm position. The motion of the object in the image is computed by inverting the matrix. Thus, the position accuracy of the end-effector is less sensitive to camera calibration errors. The limitation of the image based method is that the Jacobian matrix is a function of the distance between the camera and the target, which is difficult to calculate.

An important aspect of the current research is the use of visual data in the approach of a robot manipulator to an object as discussed by Kelly in 1996 [15], addressing the visual servoing of a planar robot manipulator, in bringing the end effector to a desired target using a fixed camera. A Jacobian matrix with the standard kinematics function is combined with a known, followed by an unknown camera orientation in order to resolve positional coordinates using a 2-link rigid robot manipulator. Joint velocities are the main feedback into the control system to enable the vision system to be added in correctly calculating the end effector position. The work is further advanced by Cojocaru and Tanasie [16] who discussed the importance of camera calibration (for positioning and orientation) in the accuracy of image feature extraction for the positioning of a manipulator arm.

In 1997, Eggenberger [17], argued that there are distinct advantages in training a neural network to improve the operation of a robot arm. The research used a fixed stationary camera focussed onto the workspace and involved the manipulator learning to bring an object into the centre of field of view. This method permitted for a greater degree of accuracy and less calibration issues when the robot arm was moving as all pre-set parameters remained the same throughout the operation. However, the time taken for the weights to be calculated in order to allow the manipulator to function within a real time environment outweighed the benefits gained as close inspection of a specific Region-Of-Interest (ROI) and correction of manipulator position was difficult to accomplish with a fixed camera system.

In 2001, Horaud and Skordas [18] discussed a strategy for recognizing objects using binary images, from which silhouettes were extracted and global features measured. The object is said to be recognized whenever a set of measured features matches a set of pre-stored features that best describe the part. They summarize their work by describing a vision system for use within a robotics environment that should be capable of recognizing objects when they touch or partially overlap each other – having the ability to detect more than one object and making a decision which one to manipulate first, could be very useful for achieving flexible automation. Horaud and Skordas also stress the importance of the manipulator being designed with the object characteristics in mind.

Agarwalla and Hutto [19], discussed the benefits of combining information from multiple sources in order to improve efficiency of various systems, including robotics. They consider that it is not only important to combine both internal and external sensor data, but also data from other computer locations, such as databases, to ensure optimisation. They explain that sensor integration is necessary for the automation of a large number of critical systems, in order to make the correct decisions in the presence of faulty data. (This is ultimately the task required for mission critical robotic applications especially in the nuclear industry.) Decision algorithms within the software management system take a number of binary inputs and determine what the final answer should be. Several independent sensors were combined into a network (Image and/or tactile) in order to provide capabilities that one simple sensor alone

is unable to provide. The work in 2004 [19] demonstrated the possibility of meeting a key challenge for some years e.g. [20] and [21].

In 2004, Gomez and Eggenberger [22], used a learning algorithm to determine the colour difference between objects under detection. The camera in this case was mounted in a fixed position external to the workspace, on a tripod mount, looking onto the manipulator and its workspace. With the vision system, the robot could recognize the difference in colour between objects using a Hebbian learning algorithm. Matrices are created for red, black and white and a weight score is calculated to distinguish the difference between each. Once the colour is recognized the distance and length away from the end of the manipulator is calculated then the movement of the arm is augmented by the relationship of the red inputs to those of other colours. This method achieved success with a 3 DOF manipulator. The 6 DOF Katana that was later used, failed to successfully follow the colour due to the increased complexity of the kinematics required to control the joints.

Also in 2004, Harri [23], utilized a similar concept to the one discussed in [9] but with the addition of a software management system to produce a hierarchical architecture was introduced involving a top-down approach to simplify input signals into a robot control system. The discussion in [23] is concentrated on the information needed from an imaging system to perform a certain task and removing other redundant operations. This is further advanced in [24], which is concerned with the extraction of useful information specifically from motor and sensor control, by designing sensory management schemes to improve the speed of real time operation. Using a combination of information about what and when to learn/engage was found to be more useful than either alone. The success was found to be dependent on the functional and management hierarchy. These techniques were used in this current research with some success.

An advancement to the work by Eggenberger in [21], Ashutosh [25] used a stationary camera mounted over the workspace and another on the manipulator 'neck'. The manipulator gained positional information from the overhead camera and then uses the other to determine gasp position. Unfortunately the two separate coordinate systems contradicted each other and errors in position were obtained.

The problem of integrating grasp and vision was considered recently. In 2009, Saxena and Driemeyer [26], discussed the problem of grasping an object through the use of a vision system. In this case, the camera is mounted onto the manipulator neck and through the vision algorithms; the manipulator calculates the best location, using a probabilistic model to grasp the object to ensure security when lifted from the workspace. The ability to scan the captured image, then using the 2D representation to detect the location of the object for the end effector to position itself, has considerable merit in saving process time from generating a 3D view of the robot's workspace in order to calculate the joint space of the manipulator. This concept was also used in this research.

#### **1.4 Justification of the Research**

It is vitally important that the robot manipulator is designed to match its working environment. Currently there is widespread use of manipulators that are either pre-programmed with a map plan, or connected to a human supervisor (via a master/slave system). However neither has the ability to efficiently counteract abnormalities within the robot's workspace: the master/slave system is slow to react and must rely on the human operator, using various sensor data, to alter the movement to the connecting joint; whereas a combination of map planning and sensor data assists in overcoming the drawbacks. For a robot manipulator, addressing the reaching and grasping problem without knowing the precise location of the target is of utmost importance regarding the control of the manipulator in joint space, thus current research described in this thesis is concentrated in this area of control and not on the aspects of the harsh environment.

The manipulator control system utilized/developed here uses visual information to locate the target/objects; and to control the reach and orientation of the manipulator. The use of touch/feel sensing within the manipulator end effector determines the presence of an object. Generally with these elements being fused together, a mechanism of visual servoing is generated. The thesis describes how many image features are necessary to control the direction on the end effector to the object. In doing this, use is made of the approach

contained in [26], where the 3D workspace is converted into a 2D representation, as all the objects will be located on the robot's workspace.

There is no criterion for originality within an MSc thesis, but a degree of originality exists here in that unique software management architectures are used for both image processing and the arm kinematics. Forward, direct and inverse kinematics are highly complementary, thus combined to ensure full control of all the joints on the manipulator, along with software constraints to ensure hazardous conditions, such as collision with robot workspace, is avoided. The vision system is fused with a software database and force feedback sensors in the grippers, to ensure an object is present.

### **1.5 Research Direction**

During the early stages the research project was directed on communication to a Katana 6M180 robot arm (refer to Chapter 2.2 for details on 6M180 Katana robot arm) with the LabView 2009 environment; connection was achieved however the Katana 6M180 robot arm was not required until the second half of the year. At the testing stage, the Katana 6M180 robot arm became unavailable, due to University responsibilities at other campuses. This was unforeseen at the beginning of the MSc, this circumstance caused a change of direction of the research. Additional development time was needed for the generation of the virtual robot arm and workspace. Moreover, the required change of research direction included: concentration on improving efficiency of recognition; and kinematic operation using hard coded algorithms. The author was able to obtain use of the robot arm for a small period of time, to allow images to be captured for use with the virtual robot image processing algorithms; and it is these captured images which show the objects in various areas of the robot's workspace that are used for this MSc thesis. In addition, operational cycles of the robot arm could not be recorded to prove the physical attributes of the vision and kinematic control but given the change in research direction, this may be suitable for PhD. Hence attention has been given improving detection accuracy and minimising the decision time for the manipulator to grasp the recognised object and transport it to the correct 'drop-off' location.

All the elements to provide an autonomous control of a robot manipulator positioned within a glovebox, are discussed. The Katana 6M180 robot arm and associated workspace is reproduced virtually to test the improvements of the kinematic control of all joints. Images of the objects are stored in a database with all instructions as to where the object is required to be transported to. The vision system, attached to the manipulator 'neck', will direct the end effector to the desired object location by the use of image processing and recognition algorithms. To assist in securing the transportation of the object, improvements in the gripper arm are discussed and developed to ensure that damage to the object is avoided. The physical size of the gripper arms are used in conjunction within the kinematic calculations to prevent any collision with the workspace or the robot arm's interconnected joints. Several elements that are required to ensure efficient operation are discussed throughout the thesis and how each element is related to the correct operation of the autonomous robot arm manipulator.

## **1.6 Thesis Organisation**

Chapter 2 describes the design of the virtual manipulator and workspace within the LabView 2009 environment, and how the virtual manipulator joints relate to the kinematic control algorithms. In addition, ancillary devices such as vision servo motor control and tactile feedback system are discussed in detail, with Chapter 3 providing details of the development of the new gripper mechanism and how the design relates to the correct operation of the tactile feedback system discussed in Chapter 2.

Chapter 4 gives a detailed description of the various vision algorithms used to direct the end effector to the object location and how the success of these algorithms rely on the correct operation of the ancillary connected devices discussed in Chapter 3 and the correct resolution of the kinematic algorithms described in Chapter 2.

Chapter 5 presents the investigative methodology and contains the main results of the trials, along with insights gained.

Chapter 6 briefly describes an overall summary of the research project and discusses the implications and advantages to the design. Brief discussions about sensor fusion techniques

used have a benefit to the efficiency of the control system, and also allows for the electronic devices to be used within a hazardous environment. Comparison with findings from other researchers within the field of robotics and discussions on the human supervisory role and how to improve supervision not only of one unit manipulator but numerous robots being monitored on one Graphic User Interface (GUI): in-case of failsafe interrupts are required; in addition to describing possible improvements to the research.

## Chapter 2:

### The Robot Arm Simulation

This chapter discusses the design of the virtual robot arm simulation and how it relates to the robot arm control kinematics. The LabView 2009 environment is used for the creation of the virtual robot arm with the design measurements of the linkages and joints taken from the Katana 6M180 robot arm. The designed robot arm and workspace is saved in a dat file, which is then imported into the simulation to operate with the kinematic algorithms as detailed in Chapter 2.5.

#### 2.1 The Design of the Virtual Robot

All the elements that are required for the operation of the physical robot arm is reproduced within the virtual environment i.e. Workspace, bin locations (drop-off positions of the objects) and the robot arm. For ease of design a parent-child relationship is utilised to build the virtual arm and workspace. A global space was created using the Property Node ActiveX function that creates a blank scene to which element were added to reproduce the Katana robot and workspace virtually, as seen in Figure 2. A Top-Down approach was used beginning with the workspace, and then the robot arm was built in stages using basic geometric shapes, as such that the connected element (child) is positioned with respect to its parent (WRTP).

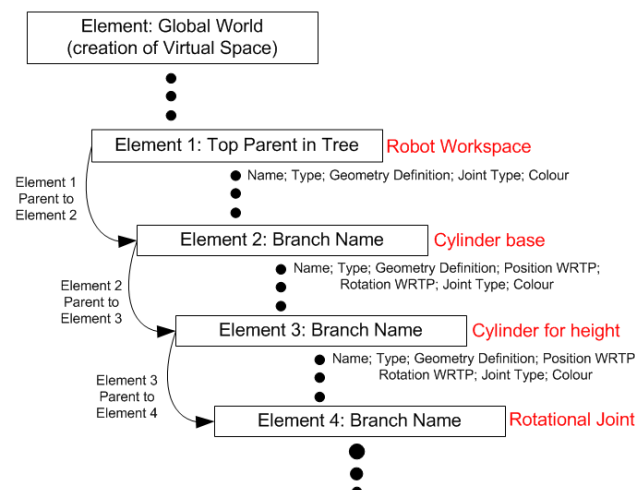


Figure 2 Parent - Child Relationship for design of the Virtual Robots

The child elements incur two positioning parameters: position WRTP, Rotation WRTP; which enables the child element to be situation anywhere and at any angle of rotation with respect to its parent element. The operation of the robot arm has to be included within the design of the virtual robot; the Katana has two main actions, rotation about an axis, and translation within an axis (used for the gripper mechanism). These two actions were incorporated within the design as a new joint of a child element as such does not incur any dimensional characteristics. An array of elements describing a scene was produced incorporating the building blocks of the robot design as seen in Figure 3 and further clarified in Figure 5. The name of each corresponding element is important as it enables quick referencing if alteration of an attribute is required.

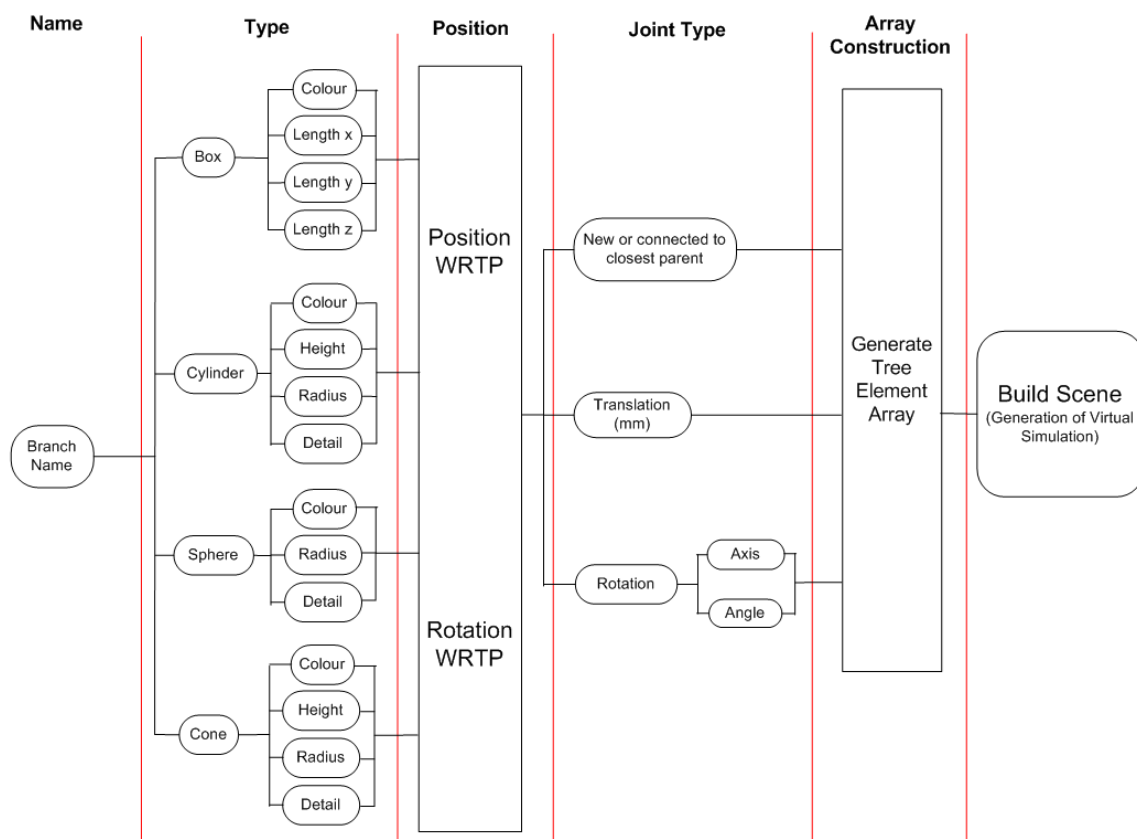


Figure 3 Building Blocks for the development of the Virtual Robot

The Generation of the Joint array is simplified by operator prompts on the front page of the design Virtual Instrument (vi), illustrated in Figure 4. Each element in the design tree was given a name (generated automatically using numerical system), the type section determines the geometric shape of each element i.e. Box, cylinder, sphere or cone. The WRT Parent determined the position and rotation of the child element to its parent element – the position

of such element is seen instantly within the scene. A property node was used to import the windows palette for the selection of the element colour. Virtual buttons are used to build/add or remove elements from the tree structure. An additional function ‘delete children’ was added to delete all children, if a parent element was to be removed with the connected children elements.

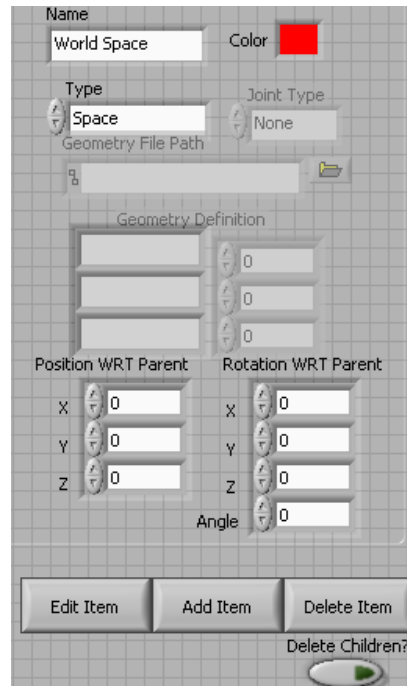


Figure 4 LabView Front Page for Generation of Robot Tree

In Figure 5, the robot configuration column illustrates the name of the robot element and associated parent child relationship; the robot workspace highlighted in blue to signify the main functional parent in the tree. The type column determines what shape of object is used to build the respective element. In the joint type column, Boolean logic is used to determine locations of joints and the associated axis of rotation, as a result ‘None’ determines that the child is positioned WRTP and fixed in this position. If a joint is allocated as a child element, the children elements following the joint, incurs the actions of the joint. The physical sizes of the objects are shown in the Geometry definition column (the geometry path column has been added in-case of importing an stl file, not used during the research). The WRT parent columns determine the location of the child element WRTP in addition to the rotation of the element WRTP. The colour column is stated as a 32bit integer number representing the associated colour selected from the windows colour palette where ‘0’ indicates black.

Robot Configuration	Type	Joint Type	Geometry Definition	Geometry Path	Pos WRT Parent (X,Y,Z)	Rot WRT Parent (X,Y,Z,Angle)	Color
World Space	Space	None	0,0,0		0,0,0	0,0,0,0	16711680
Base	Box	None	1600,10,1600		0,0,5,0	1,0,0,90	16448250
World Space_3	Cylinder	None	12,20,1		350,0,350	1,0,0,90	65302
World Space_3_2	Cylinder	None	12,35,1		500,0,75	1,0,0,90	16711680
World Space_3_2_2	Box	None	40,12,40		-565,0,0	0,0,0,0	0
World Space_3_2_2_2	Cylinder	None	12,50,1		350,0,-350	1,0,0,90	15719424
World Space_3_2_2_2_2	Box	None	60,12,60		0,0,-450	0,0,0,0	499456
Base_3_2_2_2_2	Box	None	130,50,260		0,0,450	0,0,0,0	0
Base_3_2_2_2_1	Box	None	5,20,83		-30,0,0	0,0,0,0	9868950
Base_2	Cylinder	None	14,55,1		0,32,0	1,0,0,90	9521152
Base_2_2	Cylinder	None	30,48,1		0,0,-14	0,0,0,0	9521152
Base_2_3	Cylinder	None	13,44,1		0,0,-22	0,0,0,0	9521152
Base_2_3_2	Cylinder	None	62,40,1		0,0,-20	0,0,0,0	9521152
Base_2_3_2_1	Cylinder	None	10,44,1		0,0,-36	0,0,0,0	9521152
Base_2_3_2_2	Cylinder	None	12,44,1		0,0,-11	0,0,0,0	14248960
Base_2_3_2_3	Joint	Rot_Z	0,0,0		0,0,-11	0,0,0,0	1970943
Base_2_3_2_4	Box	None	93,95,62.5		0,0,-23.5	0,0,0,0	9521152
Base_2_3_2_5	Joint	Rot_Y	0,0,0		0,0,-31.25	0,0,0,0	16711880
Base_2_3_2_6	Cylinder	None	95,46,1		0,0,0	1,0,0,90	4539717
Base_2_3_2_7	Cylinder	None	10,27.5,1		0,0,47.5	0,0,1,90	14248960
Base_2_3_2_8	Cylinder	None	10,27.5,1		0,0,-95	0,0,1,90	14248960
Base_2_3_2_9	Cylinder	None	13,32.5,1		0,0,-10	0,0,1,90	0
Base_2_3_2_10	Cylinder	None	13,32.5,1		0,0,115	0,0,1,90	0
Base_2_3_2_11	Cylinder	None	190,17.5,1		-95,0,-57.5	0,1,0,90	9521152
Base_2_3_2_12	Joint	Rot_X	0,0,0		0,0,-95	0,0,0,0	16711680

Figure 5 Robot Tree Joint Array Parameters

The completed design of the virtual robot and workspace is seen in Figure 6 with the robot arm mounted onto the grey workspace. The robot arm is reproduced mainly using two geometric shapes: boxes and cylinders as seen in the robot tree of Figure 5, the location of the joints does not produce a new element on the scene, however the elements following the joint location will incur the ability to be manipulated by associated rotation or translation parameter (rot\_x, rot\_y, rot\_z, tran\_x, tran\_y, tran\_z) of the joint in one of the three axes. Between each joint, are connected links that determine the reach of the robot arm; this will be discussed further throughout this chapter. With using the robot tree, new elements can be added and moved up the configuration tree to be positioned next to its correct associated parent element. In this case the addition of the visual servo system mounted onto the manipulator ‘neck’ and the colour coded bins (positioned on the workspace) were added and relocated further up the robot tree next to its corresponding parent, as seen in Figure 5 and Figure 6.

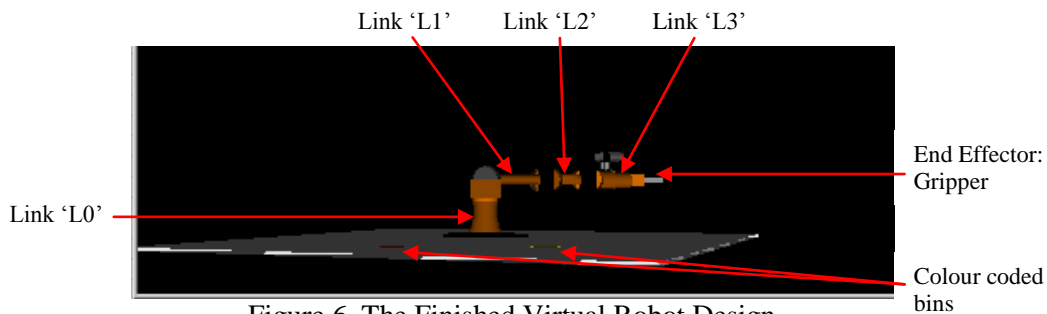
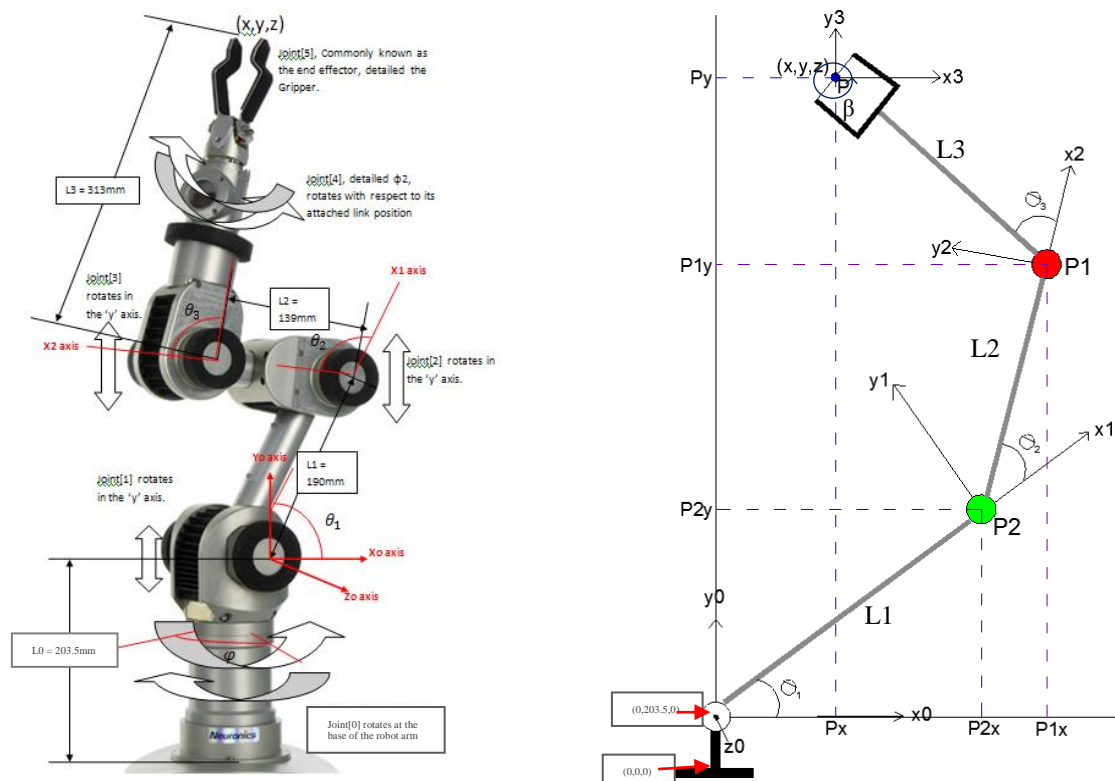


Figure 6 The Finished Virtual Robot Design

## 2.2 Robot Kinematics Solution

Each joint location on the virtual robot arm determines a variable condition which is altered by angular movement. This angular movement is controlled by the kinematic solution. Kinematics is simply described as the study of how a robot moves in its workspace. It is directly linked to the intended movement, position and orientation of the end effector (in this case a gripper mechanism) [27]. A manipulator consists of a series of links, connected together by joints. Each link can be considered to have a coordinate frame. Homogeneous transformations describe the position and orientation between coordinate frames (links). The length and angular position of the links will determine the reach of the manipulator, therefore it is important to know the maximum reach given the pose (or orientation) of the end effector (attached to the last link of the arm). Since the virtual manipulator is based on the Katana 6M180, the number of (and the length of) the links is required to reproduce the robot arm, and to enable the kinematic equations to be created and thus solved. A schematic of the Katana 6M180 depicting the length of the links and number of DOF moveable joints in any axis) is shown in Figure 7a and b.



a) Katana 6M180 Number DOF and length of Joints

b) 3Dimensional axis and rotation Angles for virtual Katana.

Figure 7 Number of Degrees of freedom of the Katana 6M180 with axis and rotation parameters

The robot arm has a total of 5 DOF with an attached gripper arm, thus possesses 6 joints. Each link attached to each DOF all vary in length; hence the robot has a maximum reach of:

$$\begin{aligned} \text{Max horizontal reach (MHR)} &= L1 + L2 + L3 \\ \text{MHR} &= 190 + 139 + (125 + 115 + 73) = 642\text{mm} \\ \text{Maximum Vertical Reach (MVR)} &= L0 + L1 + L2 + L3 \\ \text{MVR} &= 203.5 + 190 + 139 + 313 = 845.5\text{mm} \end{aligned}$$

The operation of the robot manipulator can be described by the relationship between one link and the next. Therefore, the position of the end effector utilising a 3Dimensional (3D) space coordinate system can be described by angular relationship with each connected joint (see Figure 2b), hence,

$$\begin{aligned} x &= (L1 \cos \theta_1 + L2 \cos(\theta_1 + \theta_2) + L3 \cos(\theta_1 + \theta_2 + \theta_3)) * \cos \varphi \\ y &= L0 + (L1 \sin \theta_1 + L2 \sin(\theta_1 + \theta_2) + L3 \sin(\theta_1 + \theta_2 + \theta_3)) \\ z &= -(L1 \cos \theta_1 + L2 \cos(\theta_1 + \theta_2) + L3 \cos(\theta_1 + \theta_2 + \theta_3)) * \sin \varphi \text{ or } -X \sin \varphi \end{aligned}$$

With  $\varphi$  - angle of rotation of joint 0 in the y axis.

$\theta_1$  - angle of rotation of joint 1 in the x axis.

$\theta_2$  - angle of rotation of Joint 2 from the normal of joint 1 in the  $x_1$  axis.

$\theta_3$  - angle of rotation of joint 3 from the normal of joint 1 in the  $x_2$  axis.

The positional origin of the robot arm (i.e. x,y,z = 0,0,0) is the centre of the cylindrical base, as seen in Figure 7.

The above equations are commonly used for forward kinematics solutions (joint space method); they assume that the manipulator already has information as to the correct angular position of the joints.

### 2.3 Inverse Kinematics solution for Virtual Robot

The inverse kinematics problem consists of the determination of the joint variables corresponding to a given end-effector position and orientation [28,29]. The solution to this problem is of fundamental importance in order to transform the motion specifications, assigned to the end effector in the operational space, into the corresponding joint space motions that allow execution of the desired motion. The inverse kinematics problem is far more complex than forward kinematics for a number of reasons:-

- 1) Multiple solutions may exist
- 2) The equations are far more complex
- 3) There may be no admissible solution, in view of the manipulator structure[30,31].

The homogeneous transformation describing the relationship between one link and the next is generally called an A matrix. This A matrix describes the relative translation and rotation between link coordinate systems (i.e.  $A_1^0$  - describes the first link,  $A_2^1$  - describes the second link in relation to the first,  $A_3^2$  - describes the third link in relation to the second, and so on...). Hence the position and orientation of the last link of a three link manipulator in base coordinates is given by the matrix product, generally called a T matrix, thus:-

$$T_3^0 = A_1^0 A_2^1 A_3^2$$

A rotation matrix describing a body orientation with respect to a reference frame also constitutes a matrix operator that rotates a vector by a given angle about an arbitrary axis in space, as shown in Figure 8.

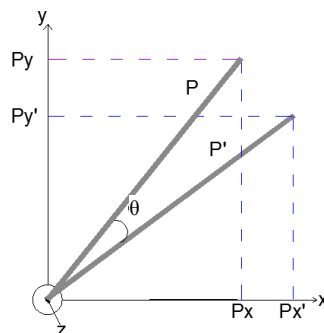


Figure 8 Rotation of a vector about an arbitrary axis

$P'$  is a vector in reference frame 0- $x'y'z'$  with the same norm as  $P$ , but rotated, according to rotation matrix 'Rot', hence the relationship between  $P$  and  $P'$  is given by:

$$Px = Px' \cos\theta - Py' \sin\theta$$

$$Py = Px' \sin\theta + Py' \cos\theta$$

$$Pz = Pz'$$

Thus representing the coordinate transformation between the coordinates of a point expressed in two different frames with common origin, and are characterised by nine elements which are not independent but related by six constraints due to the orthogonality conditions given in  $Rot^T Rot = I$  (identity matrix). Three parameters are sufficient to describe orientation of a rigid body in space, by rotations about the  $x, y$  and  $z$  axes by an angle  $\theta$  ( $Rot = [x' y' z']$ ), as seen in Figure 9.

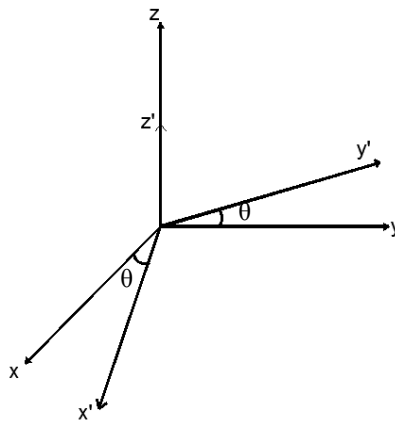


Figure 9 Rotation of a frame by angle

From which the rotation by angle  $\theta$  about the axis  $z$  becomes:

$$x' = \begin{bmatrix} \cos\theta \\ \sin\theta \\ 0 \end{bmatrix} \quad y' = \begin{bmatrix} -\sin\theta \\ \cos\theta \\ 0 \end{bmatrix} \quad z' = \begin{bmatrix} 0 \\ 0 \\ 1 \end{bmatrix}$$

Thus the rotation matrix of frame 0- $x'y'z'$  with respect to 0- $xyz$

$$Rot(z, \theta) = \begin{bmatrix} \cos\theta & -\sin\theta & 0 \\ \sin\theta & \cos\theta & 0 \\ 0 & 0 & 1 \end{bmatrix}$$

A transformation of the space H is a 4x4 matrix and represents translation by a vector  $ai+bj+ck$ , where  $i, j$  and  $k$  are unit vectors along the  $x, y$ , and  $z$  coordinate axes and  $w$  is a constant, hence:-

$$\text{Point vector } v = \begin{bmatrix} x \\ y \\ z \\ w \end{bmatrix} \text{ where } \begin{matrix} a = x/w \\ b = y/w \\ c = z/w \end{matrix} \text{ thus, } H = \text{Trans}(a,b,c) = \begin{bmatrix} 1 & 0 & 0 & a \\ 0 & 1 & 0 & b \\ 0 & 0 & 1 & c \\ 0 & 0 & 0 & 1 \end{bmatrix}$$

Thus, the transformation corresponding to rotations about the  $x, y$  or  $z$  axis by angle  $\theta$  are determined by:-

rotation by angle $\theta$ about the axis $x$ $\text{Rot}(x,\theta) = \begin{bmatrix} 1 & 0 & 0 & 0 \\ 0 & \cos\theta & -\sin\theta & 0 \\ 0 & \sin\theta & \cos\theta & 0 \\ 0 & 0 & 0 & 1 \end{bmatrix}$	rotation by angle $\theta$ about the axis $y$ $\text{Rot}(y,\theta) = \begin{bmatrix} \cos\theta & 0 & \sin\theta & 0 \\ 0 & 1 & 0 & 0 \\ -\sin\theta & 0 & \cos\theta & 0 \\ 0 & 0 & 0 & 1 \end{bmatrix}$	rotation by angle $\theta$ about the axis $z$ $\text{Rot}(z,\theta) = \begin{bmatrix} \cos\theta & -\sin\theta & 0 & 0 \\ \sin\theta & \cos\theta & 0 & 0 \\ 0 & 0 & 1 & 0 \\ 0 & 0 & 0 & 1 \end{bmatrix}$
---	---	---

As seen in Figure 10, a link is characterized by the Denavit-Hartenberg convention, by two dimensions,  $a_i$  normal distance (length) and the angle  $\alpha_i$  between the axis in a plane perpendicular to  $a_i$ , known as the twist of the link. When a connecting link is  $L_{i-1}$  is not directly in line with the normals of  $L_i$ , two parameters are measured between the normals along joint  $i$  axis:  $d_i$  – relative position of two connected links and  $\theta_i$  - angle between the normals measured in a plane normal to the axis.

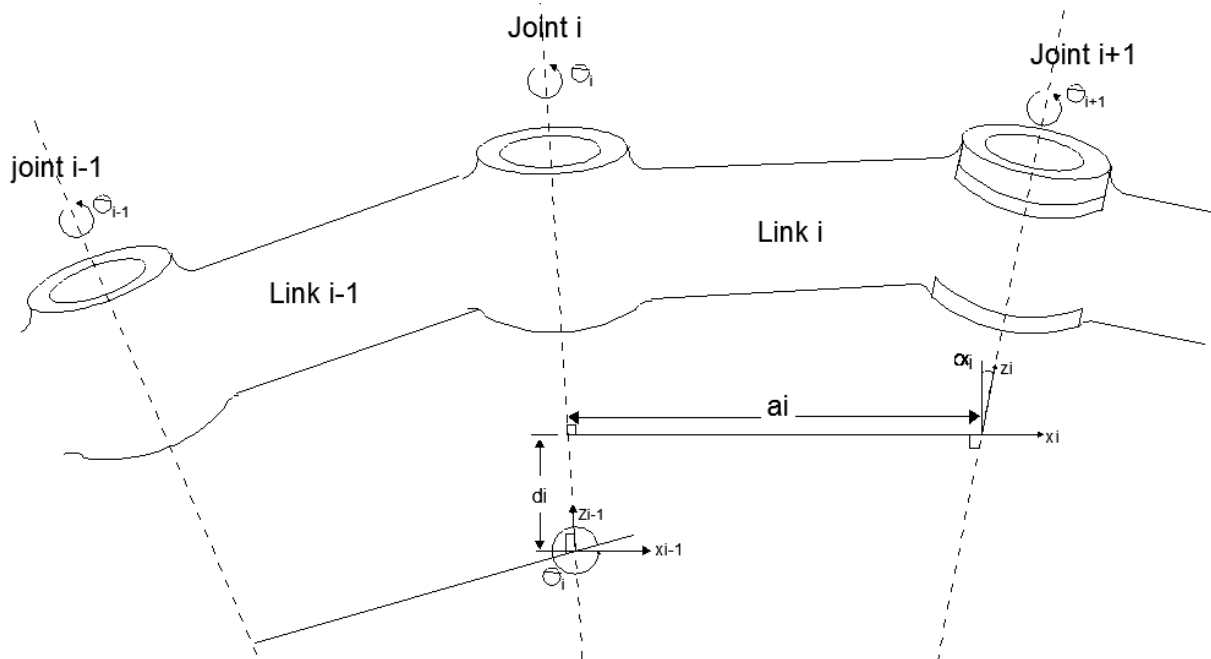


Figure 10 Frame Relationship between one link and a connected link

The relationship between successive frames of reference (Coordinate frame at joint  $i-1$  and coordinate frame at joint  $i$  (see Figure 8 and Figure 9))  $i-1,i$  is described by:

- 1) Rotation about  $L_{i-1}$ , at angle  $\theta_i$ .
- 2) Translate along  $L_{i-1}$ , a distance  $d_i$ .
- 3) Translate along rotated  $x_{i-1}$ , a length  $a_i$ .
- 4) Rotation about  $x_i$ , twist angle  $\alpha_i$ .

Hence the homogeneous transformation depicting the relationship between the two links is expressed as an A matrix:

$$A_i = \text{Rot}(z,\theta)\text{Trans}(0,0,d_i)\text{Trans}(a_i,0,0)\text{Rot}(x,\alpha_i)$$

$$A_i = \begin{bmatrix} \cos\theta_i & -\sin\theta_i & 0 & 0 \\ \sin\theta_i & \cos\theta_i & 0 & 0 \\ 0 & 0 & 1 & 0 \\ 0 & 0 & 0 & 1 \end{bmatrix} \begin{bmatrix} 1 & 0 & 0 & a_i \\ 0 & 1 & 0 & 0 \\ 0 & 0 & 1 & d_i \\ 0 & 0 & 0 & 1 \end{bmatrix} \begin{bmatrix} 1 & 0 & 0 & 0 \\ 0 & \cos\alpha_i & -\sin\alpha_i & 0 \\ 0 & \sin\alpha_i & \cos\alpha_i & 0 \\ 0 & 0 & 0 & 1 \end{bmatrix}$$

$$A_i = \begin{bmatrix} \cos\theta_i & -\sin\theta_i\cos\alpha_i & \sin\theta_i\sin\alpha_i & a_i\cos\theta_i \\ \sin\theta_i & \cos\theta_i\cos\alpha_i & -\cos\theta_i\sin\alpha_i & a_i\sin\theta_i \\ 0 & \sin\alpha_i & \cos\alpha_i & d_i \\ 0 & 0 & 0 & 1 \end{bmatrix}$$

For simplicity  $\cos\theta_i$  and  $\sin\theta_i$  is shortened to  $C_i$  and  $S_i$  respectively. With both connecting joint, shown in Figure 10, directly in-line with each other to create an extension of the first joint, hence  $\alpha_i$  and  $d_i$  become constants equal to zero, the homogeneous transformation becomes:-

$$A_i = \begin{bmatrix} C_i & -S_i & 0 & a_iC_i \\ S_i & C_i & 0 & a_iS_i \\ 0 & 1 & 1 & 0 \\ 0 & 0 & 0 & 1 \end{bmatrix}$$

## 2.4 3D location kinematics solution used with virtual robot

The Katana 6M180 is a three link manipulator, as a result the direct kinematic function is described by the T matrix:

$$T_3^0 = A_1^0 A_2^1 A_3^2$$

Substituting  $A_i$  into  $T_3^0$  to find associated angles  $\theta_1, \theta_2, \theta_3$  gives,

$$T_3^0 = A_1^0 A_2^1 A_3^2 = \begin{bmatrix} C_{123} & -S_{123} & 0 & L_1 C_1 + L_2 C_{12} + L_3 C_{123} \\ S_{123} & C_{123} & 0 & L_1 S_1 + L_2 S_{12} + L_3 S_{123} \\ 0 & 0 & 1 & 0 \\ 0 & 0 & 0 & 1 \end{bmatrix}$$

Where  $L_2 C_{12}, L_2 S_{12}$  describes the relationship of joint 2 with respect to joint 1

$L_3 C_{123}, L_3 S_{123}$  describes the relationship of joint 3 with respect to joint 1 and joint 2.

$C_{12}$  represents  $\text{Cos}(\theta_1 + \theta_2)$ ,  $S_{12}$  represents  $\text{Sin}(\theta_1 + \theta_2)$ ,  $C_{123}$  represents

$\text{Cos}(\theta_1 + \theta_2 + \theta_3)$ ,  $S_{123}$  represents  $\text{Sin}(\theta_1 + \theta_2 + \theta_3)$ .

To simplify the calculation, specifying the position and orientation in terms of a minimum number of parameters, such as two coordinates (Px and Py) and angle  $\Phi$  with axis  $x_0$ .

$$x = \begin{bmatrix} Px \\ Py \\ \Phi \end{bmatrix} = k(J) = \begin{bmatrix} L_1 C_1 + L_2 C_{12} + L_3 C_{123} \\ L_1 S_1 + L_2 S_{12} + L_3 S_{123} \\ \theta_1 + \theta_2 + \theta_3 \end{bmatrix}$$

With which, the orientation of the robot and the relationship with the joint angles can be determined as:-

$$\Phi = \theta_1 + \theta_2 + \theta_3$$

By using a coordinate frame  $x_3$  (which is horizontal to  $x_0$ ), declaring the orientation  $\beta$  from  $x_3$  and the length of the final section  $L_3$ , the coordinates of the end of joint 2, given by P1 can be found. As such the x,y coordinates for P1 can be described as:-

$$P1x = P_x - L_3 C_\phi = L_1 C_1 + L_2 C_{12}$$

$$P1y = P_y - L_3 S_\phi = L_1 S_1 + L_2 S_{12}$$

These solutions consider the first two angles  $\theta_1$  and  $\theta_2$ , thus using the law of cosines to calculate  $\theta_2$  (being an external angle), by Summing and squaring the above equations, yields:-

$$P1x^2 + P1y^2 = L_1^2 + L_2^2 + 2L_1 L_2 C_2$$

Thus,

$$C_2 = \frac{P1x^2 + P1y^2 - L_1^2 - L_2^2}{2L_1L_2}$$

$\theta_2$  could be obtained from the arc cosine, however obtaining  $S_2$  and using tangent rule will resolve issues with inaccuracies. At this point the extreme of the arm reach requires to be taken into consideration; therefore the value of  $C_2$  can only be between  $-1 \leq C_2 \leq 1$ . Thus:

$$S_2 = \pm \sqrt{(1 - C_2^2)}$$

This equation certifies whether the posture of the arm (at this position) is either up or down posture (- and + respectively). The angle  $\theta_2$  can be computed:-

$$\theta_2 = \text{atan}(S_2, C_2) \approx \text{acos } C_2$$

Also, the angle  $\theta_1$  is calculated taking into account position P as:

$$\theta_1 = \tan^{-1}(P2_x/P2_y)$$

However, there are instances where the position is unresolved due to large variation of positional and rotational movement, therefore a further calculation to check the correct angle calculation for  $\theta_1$  is required. Hence by substituting  $\theta_2$  in  $P1x$  and  $P1y$ , yields:-

$$S_1 = \frac{(L_1 + L_2C_2)P1_y - L_2S_2P1_x}{P1_x^2 + P1_y^2}$$

And,

$$C_1 = \frac{(L_1 + L_2C_2)P1_x - L_2S_2P1_y}{P1_x^2 + P1_y^2}$$

Thus

$$\theta_1 = \text{atan}(S_1, C_1)$$

Alternatively,

$$\theta_1 = \sin^{-1}((P1_y * (L_1 + L_2) - P1_x * L_2 * S_2) / (P1_x^2 + P1_y^2))$$

As a result, the joint positions in 3D space can be calculated by specifying the end effector position and the orientation of the manipulator. However, the main obstacle with kinematics is that there is a high chance that the end effector, during the calculations and respective movement will collide with the ground or itself, unless numerous positional samples (i.e. additional coordinates stored in the database), are placed in the map plan that controls the movement of the manipulator. However, with the end effector position calculated using a combination of vision sensors and 3D coordinates positions from a database these additional sample positions will decrease efficiency and needlessly increase the size of the database.

In an attempt to resolve this issue, a combination of numerous calculations for joint angles as above is actioned to ensure that each calculation returns the identical result (considering rounding errors) in addition to the following algorithm.

```

IF 'y' position new ≤ 57mm
  THEN
    Action speed change on joint (1,2, or 3) to
    ensure that gripper does not crash into ground
IF 'y' position now ≤ 30mm
  THEN
    Re-check 'θ, θ2, θ3' to ensure position y ≥ 0
      IF y ≤ 0;
        THEN
          Report error in system;
      IF y > 0;
        THEN
          Stop decrease in y; AND
          Alter joint angles to ensure end effector orientation can be reached
          Check calculations THEN
          Return to main routine, resume kinematic solution.

```

The algorithm ensures when the end effector position is close to the surface, the inverse kinematic function is interrupted and a decision is made based on the current and future coordinate positional information. Once the end effector is 57mm above the surface, depending of the current joint angles and the end angle positions of each respective joint a decision is made about which joint of the manipulator to speed up to ensure no collision occurs. When the end effector is calculated at 30mm above the surface, an additional decision

transpires to ensure the end position can be reached, but also to halt angular movement in the joint or joints to stop collision occurring. This function will inherently not override the kinematics but offer additional control when a possible hazardous condition arises.

An optimisation approach allows incorporating in a natural way important parameters for a specific task by specifying details for each parameter. The set of functions can be task dependent, as well as being dependent on one another, in addition, these functions can be parameterised by sensory input. For instance, when manipulating a radioactive liquid within a beaker as described as how the manipulator is programmed in the research, the orientation of the manipulator and force/pressure of the gripper is more important than the quickest route to reach its destination. The pose of the manipulator in this case is required to be a constant of  $0^\circ$  to the workspace, hence by using the position of the other two joints,  $\theta_3$  can be found by the following algorithm.

$$\theta_3 = (90 + \theta_1) + (\theta_2 - 90)$$

The equation above depict that the current rotational positions of joint 1 and 2 are used to ensure that  $\beta$ , the pose of link three with respect to link one and two of the manipulator remains at  $0^\circ$  to  $x_0$ . This algorithm will work in conjunction with the forward and inverse kinematic equations to ensure the manipulator is fully aware of the position and pose at any one time.

To ensure the manipulator has reached it final position, multiple AND gates are used with the current and post angular positions of each joint. The joint angles are used to determine the correct end position of the present movement, with the current angle positions of the arm placed in the 'now' world coordinates and the new position of the angles calculated from the inverse kinematics equations placed in the 'new' world coordinates, to enable stored values to be updated and utilised on multiple sub.vi's on each iteration. Total control can be accomplished by continually monitoring the arm position with the end coordinates, then permitting a decision to be made about the direction of each joint attached to the manipulator. The values of  $px, py, p1x, p1y$  are continually monitored also to ensure correct placement in 3D space of the end effector. The algorithm will function in conjunction with round up/down.vi

with a tolerance of  $0.5^\circ$  of angular rotation (gathered from the specifications of the Katana servo feedback mechanism. When the new position has been reached a Boolean control is activated, along with a Boolean control for both end effector position ( $P_x, P_y$ ) and P1 position ( $P_{1x}, P_{1y}$ ), utilising a 3 input AND gate to ensure accurate positioning and resolution of the kinematic equations.

## 2.5 Robot Arm Simulation Solution

The prime objective of the research is to detect the presence of a recognised object on the workspace from a database of images, and allow the robot manipulator to operate with the visual information obtained from the cameras mounted on the manipulator 'neck'. The three objects used are all the same size, shape, and weight, the only difference between the three objects is the colour pattern as seen in plate 2.



Plate 2 Three objects under inspection and manipulation

Object 1: Pink, orange, blue, green (POBG).

Object 2: Green, blue, orange, pink, orange (GBOPO).

Object 3: Pink, blue, orange, green (PBOG).

*Note: Each colour is applied to the whole of a specific size (diameters) of the objects; each tapered portion of the object is multi-coloured.*

To save on resources and to assist in prolonging lifespan of electronic devices working in hazardous environments (gloveboxes), the ancillary devices are only used when required, thus quick image acquisition snap shots of the workspace were taken, to direct the robot

manipulator to accurately move towards the recognised object. A block diagram describing the operation is shown in Figure 11. A combination of information from the vision system and positional information from the database shown in Table 1 are used to ensure the manipulator accomplishes its task. To enable synchronisation with a physical Katana 6M180 robot arm, the virtual robot arm is required to manoeuvre to an exact position that matches the physical robot arm. Therefore the Katana 6M180 initial task is to perform a calibration routine to reset the on-board encoders to a pre-set value (see Appendix C); The virtual robot arm initial position will be with all joints at zero degrees as seen in Figure 6, thus by uploading the joint positions of the Katana calibration routine, from the database, synchronisation with the Katana 6M180 can be accomplished.

The first image acquisition (long distance scan) produces an estimate about the location of the recognised object, the coordinate information gathered from this scan is used to direct the manipulator so as to be 200mm horizontal distance ( $x_0$ , refer to Figure 7) away from the recognised object. At this position, a second image acquisition task (short distance scan) is performed, this time gathering information about the colour properties and rechecking the coordinates of the object situated on the workspace. Once the object has been recognised, a sequence structure that ensures the respective coordinate information for the object, is actioned. The manipulator also corrects any positional error returned from the first image acquisition scan in order to grasp the object. The gripper mechanism will grasp the object, and the manipulator control will activate the gripper feedback system to measure the applied force on the object so as to avoid slippage or damage through transportation. A further image scan can be accomplished at this position, utilising edge detection in combination with the force feedback system to further ensure security of the object whilst being manipulated to its destination.

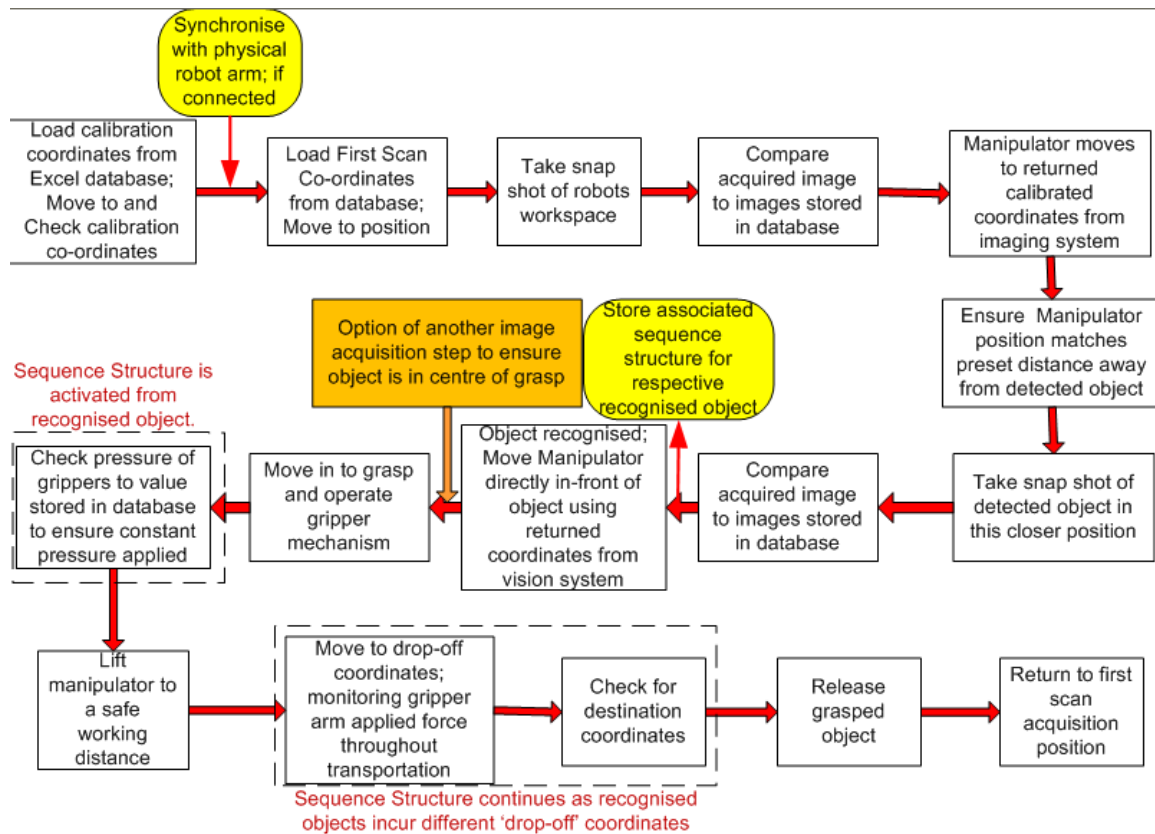


Figure 11 Robot Vision and Manipulator Sequence Structure

The sequence illustrates the basic operation of the programmed Manipulator system, with the addition of a further inspection once the object has been successfully grasped to ensure no slippage occurs.

The coordinate database that the manipulator control system interrogates to ensure correct operation of the virtual manipulator is produced in Microsoft Excel as seen in Table 1. The initial movement to calibration position is stored in the database as angle coordinates for each respective joint. Following this manoeuvre, however the correct functioning of the system is reliant of visual data gathered from the camera system, as such the database utilises 3D coordinate positions with 2D coordinates calculated from the vision system: to direct the end effector of the manipulator. The ability to utilise this procedure is permitted because the robot arm is secured to the surface of the workspace and the objects are also placed on the same workspace. The values stored in the database are for ideal location of the object ( $Id_{loc}$ ) and the ideal position and pose of the manipulator. The vision system clarifies the position of the object with respect to the end effector, if found that the object is not situated in the ( $Id_{loc}$ ), the returned calibrated coordinates from the vision system is used with the values in the database to alter the position and orientation of the manipulator. Once an object stored in the image

database (the image database is stored as a link within the address column of Table 1) has been recognised, the manipulator control system reads the values within the respective column on the database to ensure the object is successfully transported to its ‘drop-off’ location on the workspace, in addition to receiving information about the amount of applied force required by the gripper mechanism to ensure security of the object throughout the process. Further control of the gripper mechanism is also shown by placing an angle limitation of  $20^\circ$  for the joint that controls the gripper mechanism so no collision occurs once connected to a physical manipulator (refer to Chapter 3).

Table 1 Excel Database for Control of Virtual Manipulator  
The coordinate positions are stated in ‘mm’ and the orientation, gripper and phi are entered as angle positions to correspond to the virtual robot design.

Function	address	PHI	THETA 1	THETA 2	THETA 3	PHI 2	Gripper	
Calibration		-75	-55	-125	-115	103	0	
Function	address	x = y	height	orientation	gripper	phi	Force in Newtons	Object
long scan	n/a	255	217	40	0	var	n/a	
close scan	n/a	365	77	46	0	var	n/a	
grasp	n/a	605	40	5	20	var	0.002354	
pick up	n/a	605	164.9	5	20	var	0.002354	
red	..\..\..\All	544.455	55.5	0	20	-170.5	0.002354	POBG
green	..\..\..\All	533.243	55.5	0	20	-135	0.002354	GBOPO
yellow	..\..\..\All	544.455	55.5	0	20	132	0.002354	PBOG
green/sq	..\..\..\All	482.528	66	0	20	90	0.002354	Not assigned
before grasp	n/a	543	51.715	13	0	var	n/a	

The ‘drop-off’ locations for the objects are situated in differing locations on the workspace and are identified by different coloured geometric shapes as seen in Table 1 and clarified in Figure 12.

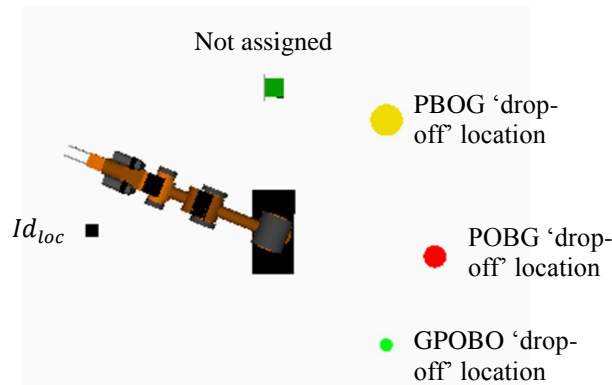


Figure 12 Ariel view of robot workspace illustrating 'drop-off' locations of objects

The design of the virtual robot was discussed in Chapter 2.1 that generates a scene of the virtual robot arm and associated workspace along with the joint locations and corresponding actions will function with the kinematic algorithms discussed in Chapter 2.3 and 2.4. To permit the virtual robot design to operate with the kinematic algorithms, concentration is only required for control of the joints themselves. As such the joints are to be separated from the robot tree as seen in Figure 13. All the functions required to produce the virtual robot are not required, as such the only action is to import the scene and associated tree elements, thus permitting access to the parent/child relationship within the design. The parent/child for the joints are then separated in order of appearance in the main tree beginning with joint 0 to the last joint 5. The actions of the joints are then attached to the new joint array; as such the characteristics of the children of the joints within the scene can be updated without generating a new tree that will describe any updates to the scene on the Graphic User Interface (GUI).

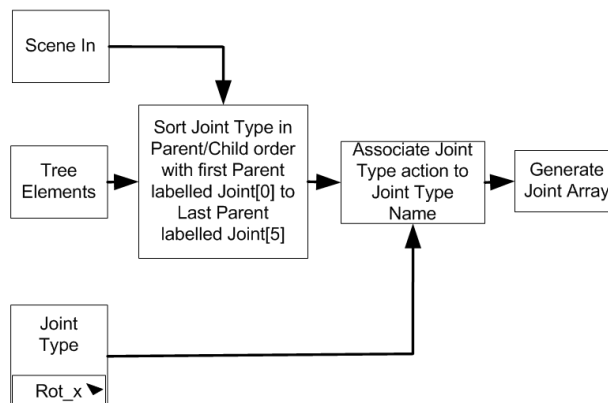


Figure 13 Generation of Joint Array

The kinematic algorithms, which calculate the joint angles given the 3D coordinates of the end effector, are used to amend the values of the joints within the joint array. The joint array is then used to update the position of the virtual robot arm links that are attached to the joints with the parent/child relationship within the main scene on the GUI as seen in Figure 14. The new angle positions of the joints are stored within a global variable within the main program to be used with numerous sub.vi's: to keep full control of the movement of the virtual manipulator with utilising a combination of forward, direct and inverse kinematics.

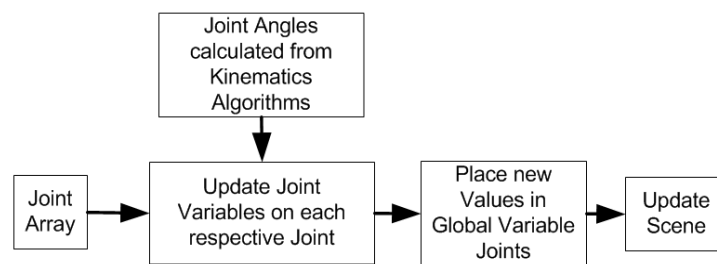


Figure 14 Updating Joint Array using Kinematic Solution

## 2.6 Touch/Feel Application with FS Series Tactile Sensors

In most applications the current drawn from the motor, which drives the gripper mechanism is used as the sole feedback control to inform the manipulator control system that the gripper arms have firmly grasped an object. However, the main flaw in this design is that the gripper mechanism, due to positional error of the manipulator, has grasped nothing and the additional current draw is from both gripper arms acting against each other.

In this research, the vision system is utilised to ensure positional accuracy of the end effector whilst the force sensor is used to determine a physical presence of an object. A combination of these two elements working together, a secure grasp of the object was possible [41]. A motor/gearbox combination is used to drive the gripper mechanism (the gearbox has a ratio of 1014:1). When stopped, the worm drive within the gearbox ensures that the applied load working onto the gearbox, will incur no reverse movement within the drive mechanism, thus preventing a decrease in applied force on the object, thus the motor does not need to be supplied with power continuously in order to maintain the required force.

The force sensor utilises a piezo-resistive micro-machined silicon sensing element, the stability is achieved via an unamplified Wheatstone bridge circuit. The force sensor operates on the principle that resistance will increase as the piezoresistor flexes under applied force.

The force is applied to a stainless steel (SS) plunger, directly to the sensing element. The amount of resistance change is directly in proportion to the amount of force applied and results in a mill volts (mV) output, the equivalent circuit can be seen in Figure 15a. The sensor is protected by an elastomeric technology moulded within plastic and can withstand load of up to 43.15Newtons (over-force); the construction of which can be seen in Figure 15b (*refer to datasheet in Appendix E for specifications of sensor*).

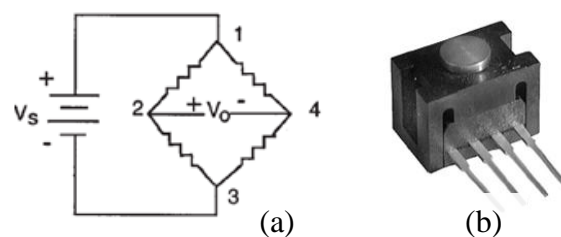


Figure 15 Force Sensor Equivalent Circuit and Construction

The main advantage with this type of sensor is the sensor output characteristics do not change with respect to mounting orientation. The force sensors are mounted onto a Printed Circuit Board (PCB); the PCB is installed internal to the gripper arms. The stainless steel plunger surface area is increased by the addition of a spring plate that will lay over the plunger, when an object comes into contact with the plate, the differential voltage produced by the sensor will simultaneously increase. The sensor outputs are directly connected to a Data Acquisition (DAQ) board, which then communicates directly to the PC.

For the feedback system to work accurately, design imperfections have to be taken into account. With the stainless steel (SS) plunger mounted on a silicone base (to prevent oxidation) variations between devices are expected. The feedback values from the force sensors with no force are seen in Figure 16; the volts/newton feedback value has been amplified in circuit by a scale of 30 to obtain further tolerance to the design imperfections.

The variation is the differing Direct Current (DC) voltage generated from the Wheatstone bridge by the SS plunger on the silicone base. There is a difference in the maximum DC voltage generated by the electronics between the force sensor in the single gripper (0.44mV) and the dual gripper (0.74mV). This variation is not due to the design of the gripper arms, but of the force sensor; which is counteracted in the design of the control algorithms to ensure no false detection is recorded. Using the feedback from each gripper arm as separate measurements, tolerances for each individual force sensor can be inbuilt into the design. For research purposes the object that is required to be grasped can easily be damaged if too much force is applied. Therefore strict tolerance in applied force is needed: set to  $(5.884 \times 10^{-4} \text{N})$ .

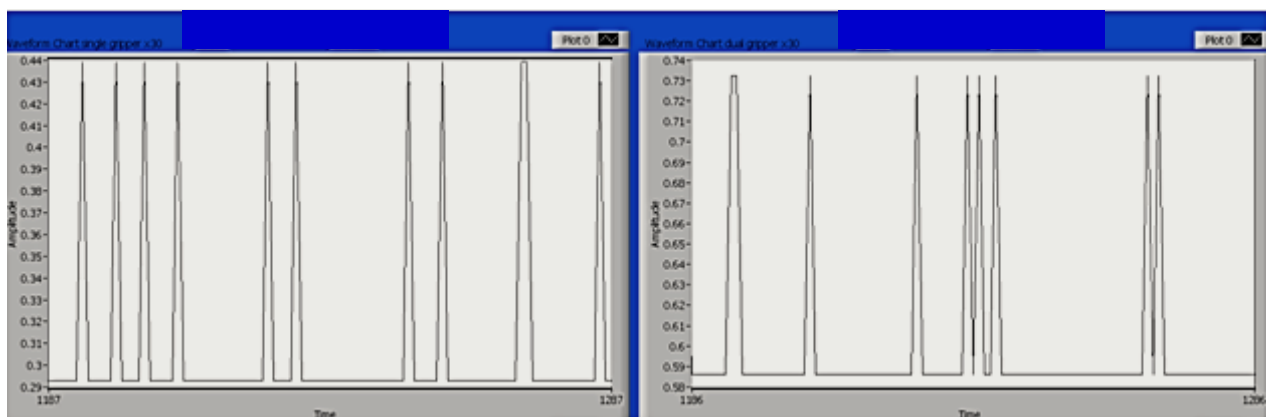


Figure 16 DC Amplitude from Force Sensors with No Applied Load (x30)

The left hand image shows the measured applied force from the single gripper with no load; the right hand image shows the applied force from the dual gripper with no load. The x axis is measured in seconds and the y axis is measured in volts/newton

The gripper mechanism requires three operating functions: grip, reverse and hold. The results from each gripper arm are correlated together to determine what operation is required to ensure security of the grasped object. If the control determines that more applied force is required, the motor will operate in grip mode until the hold position is obtained. Likewise, if too much applied force is sensed on any gripper, the motor will reverse until hold position is obtained. The motors are connected to the PMD Data Acquisition (DAQ) device; dual software interlocks are used to ensure that the motor cannot be driven in both directions at once and create an overload condition. The feedback values from previous iterations are used to ensure motor direction (forward and reverse operation) are separated by Boolean expressions. The design of the algorithm is an advancement from the work accomplished by Howe in [41], who discussed the necessity for combining robotic manipulation with tactile

sensing for the development of smooth manipulator operation, in addition to finding contact locations, contact forces and determining contact conditions. The modified algorithm used for the research, uses a combination of sensing and control schemes to compensate for undesirable characteristics of both object being grasped and the operation of the manipulator, in addition to providing the necessary control to incorporate tactile information into real-time operation. Thus creating a manipulator system that can respond to information gathered from the sensors and provide machine dexterity, in applications where small forces and displacements must be controlled. Figure 17 illustrates the activation of the PMD device inputs to receive information from the force sensors, shown in Section1 Figure 17. The applied force specifically for the recognised object is uploaded from the database, and tolerance levels are set for both individual gripper arms. The input voltages from each Wheatstone bridge are compared to the database value, and a decision is made to the operation of the gripper mechanism, shown in Section2 Figure 17. The Boolean outputs to the motors are monitored to ensure dual signals (forward and reverse) are not activated at the same time. As the gripper mechanism begins to grasp the object, a timer will begin that will monitor how long the 'grip' function has been operated before any feedback voltage values from the force sensors is received, as shown in Section3 Figure 17. If no DC value is obtained from the gripper mechanism within a certain time period, the manipulator control will decide that the object is not present and take alternative actions, which could include additional vision acquisition scan in order to gain confidence of a presence of an object. The designed control continuously monitors the force feedback throughout the transportation to the objects destination point. Once this position has been reached, the power to the force sensors is released to save on resources: only when the manipulator is required to grasp, is power enabled and only when fully released is power disabled to the force sensors.

The tight tolerance values are essential since the manipulator may be required to work within environments containing water and oil and therefore the gripper mechanism has to adapt to these circumstances to ensure security of the grasped object. The operation of the control designed in Figure 17, can be seen visually by the LabView frames shown in Table 2, with the applied load set to  $(2.354 \times 10^{-3} \text{N})$ , which is adequate to grasp the objects.

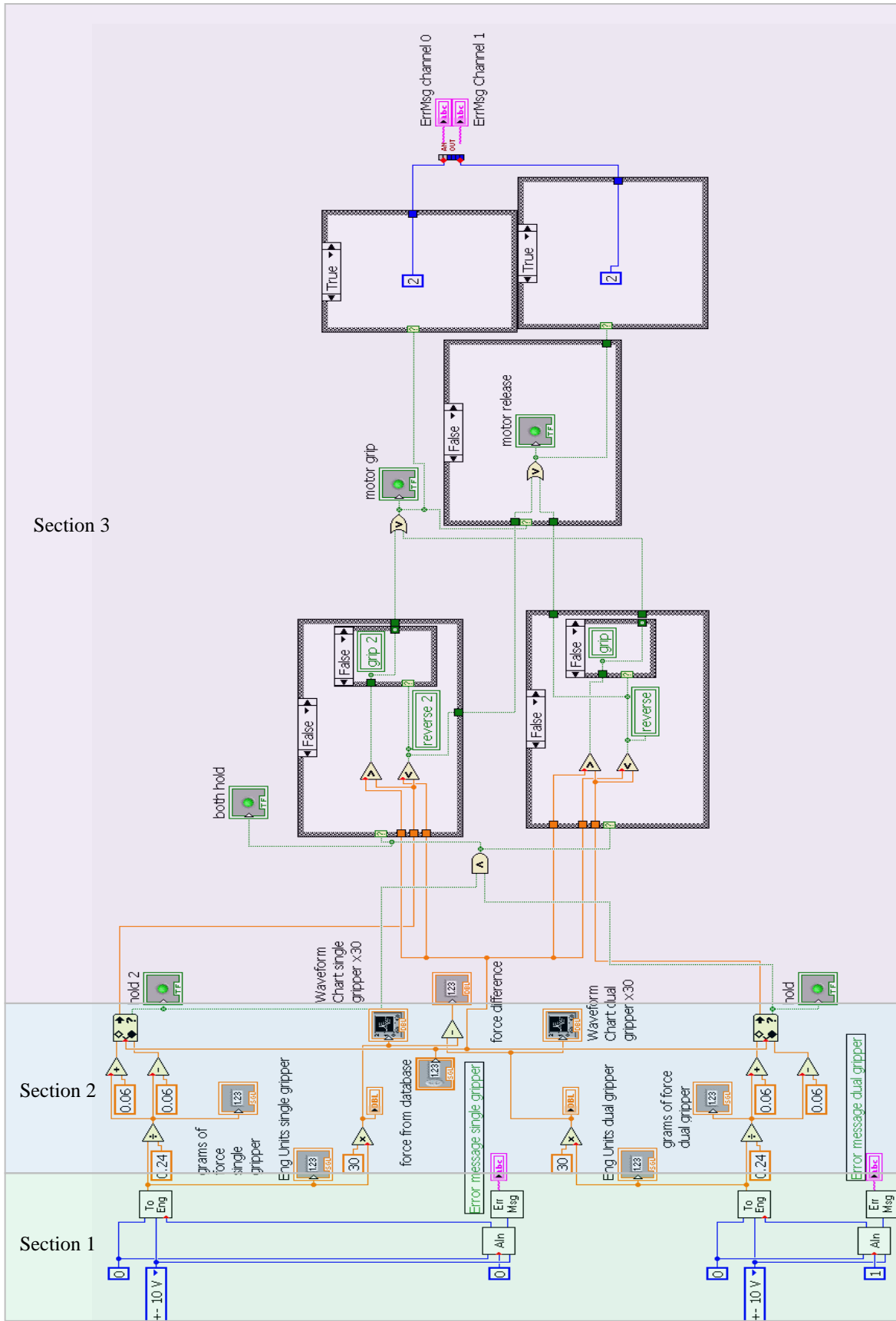


Figure 17 Control Algorithm for Force Feedback Control Response

Table 2 Control Algorithm Response for Force Feedback Control

Single Gripper	Dual Gripper	Operation of Gripper mech.
<p>When the manipulator is in position, power is engaged onto the gripper mechanism, with the gripper being in the open position, both left and right gripper arm are programmed to grip as seen on the right figure above. (Feedback value shown corresponds to the design specifications of the Force Sensor, see Appendix E)</p>		
<p>grams of force single gripper: 0.2237 Eng Units single gripper: 0.054</p>	<p>grams of force dual gripper: 0.2441 Eng Units dual gripper: 0.059</p>	
<p>The gripper mechanism begins to close, once the pressure plate comes into contact with the object, the applied load increases. One the applied load comes to within the stringent tolerance setting, the motor that controls the gripper mechanism stops and the hold function activates; the gear ratio will ensure that no slippage occurs within the mechanics of the arms.</p>		
<p>grams of force single gripper: 0.3662 Eng Units single gripper: 0.088</p>	<p>grams of force dual gripper: 0.284E Eng Units dual gripper: 0.068</p>	
<p>If one of the gripper arms records an over-applied load, the mechanism will operate in reverse. Above the single gripper arm has recorded this, and as seen on the right hand side, reverse function is operated. Although this fault condition will occur rarely, a swift voltage spike in the motor could cause both grippers to create an over applied force, whilst the shape of an object could also cause the above fault condition.</p>		
<p>grams of force single gripper: 0.1831 Eng Units single gripper: 0.044</p>	<p>grams of force dual gripper: 0.1627 Eng Units dual gripper: 0.039</p>	
<p>The most common occurrence is under force conditions, moreover caused by slippage of the object under grasp. Both applied forces from both gripper arms has reduced, however only the dual gripper has recorded the applied force below the tolerance level (the single gripper is just within the tolerance limit). To compensate for this the gripper mechanism activates to close (grip). Once both applied forces are again within tolerance, the control will revert back to hold condition. This control is actioned throughout once the manipulator has grasped the object: to prevent slippage.</p>		

## 2.7 LabView Simulation of Visual Servoing mechanism

To enable efficient image processing and accurate control of the manipulator, the object under detection requires to be located near the centre of the acquired image. To enable this, the camera system is mounted onto a visual servoing mechanism to permit ‘homing’ of the manipulator to the recognised object. Two cameras are attached to the manipulator ‘neck’ (see appendix A), via a quick release bracket: to facilitate possible advancement to 3Dimensional images to be acquired or to provide a failsafe system in-case of fault condition with one of the cameras. There are numerous methods to control this type of visual servoing system, the main three are:

- 1) Permanently attach each camera to ensure the focal point is at 90° straight at the robots workspace and use the difference in measurements, once both images are combined into a single image, between the same object in each camera: to determine the distance and angle from the end effector.
- 2) Allow the individual servo motors to be controlled separately to ensure that the object is in the centre of the field of view in both cameras. Then take measurements from each captured image and angular difference between each servo to determine the correct location of the object in the robots workspace.
- 3) Permit the servo motors to be synchronised together and operate on the horizontal distance away from the object detected. Measurements can be taken from the image captured from either camera or both to determine the location coordinates of the object on the robots workspace.

The simplest method of control however, is to have both servo motors operate with one algorithm. This saves on resources and reduces complexity of the algorithm design; hence Method 3 is utilised to permit the servo motor rotational position to depend upon the horizontal distance away from the detected object and the orientation of the manipulator. The servo motors are controlled by a Pulse Width Modulated (PWM) waveform, with 180° of movement, as seen in Figure 18.

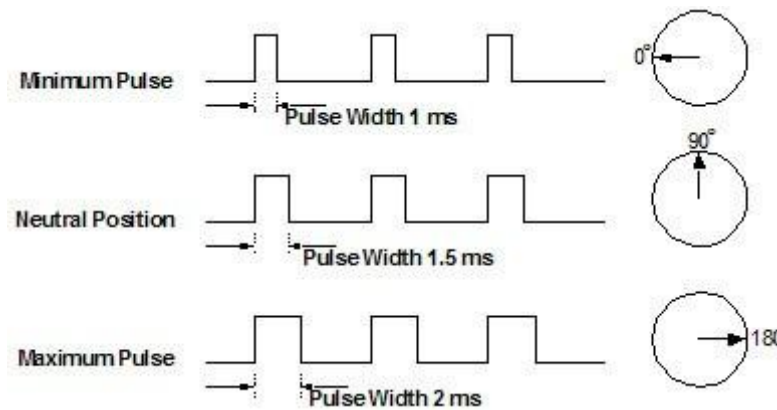


Figure 18 Pulse Width Modulation (PWM) versus Angular Adjustment for Servo Motors

Figure 18 illustrates the correlation between pulse width and angle of movement. The pulse width is directly controlled by the calculated distance from the object given by the vision algorithms (see Chapter 4), and is also interconnected to the simulated encoder feedback system of the joints. To reduce the number of calculations required, both servo-motors are controlled from one variable. The inclusion of the following control algorithm will ensure that both servo-motors will operate as a mirror image of one another.

$$x = \text{maxd} - (n - \text{mind})$$

Where  $x$  = duty cycle of PWM servo 2  
 $\text{maxd}$  = Max\_duty\_cycle\_var  
 $\text{mind}$  = Min\_duty\_cycle\_var (default -50)  
 $n$  = duty cycle of PWM servo 1

Figure 19 illustrates the PWM generation for the control of both servo motors, demonstrating that each servo motor will function as a mirror image of the other. The top 2 graphs show the left camera pointing all the way to the left and the right camera pointing all the way to the right. The middle graphs shows the duty cycle equal for both servomotors positioned at 90° (1.5ms), directed forward onto the workspace and the bottom graphs shows the duty cycle of the left at 180° (2ms) and the right at 0° (1ms); thus both servo motors are synchronised together.

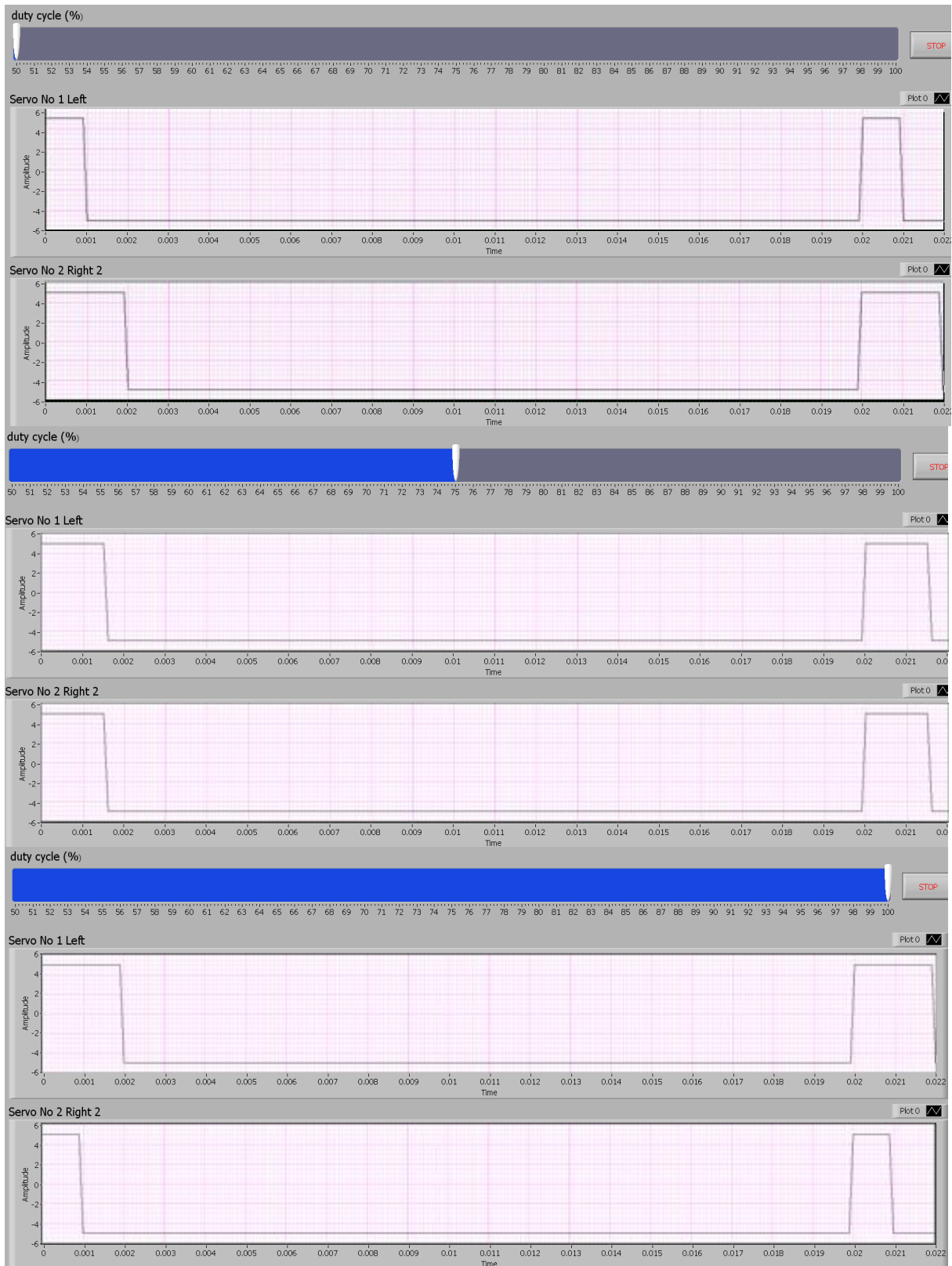


Figure 19 PWM Generation for Control of Both Servo Motors

The Virtual Instrument designed enables the servo motors to be powered off until requested by the manipulator control system to permit another image acquisition task, as shown in Figure 20. Both servo motors are controlled from the same variable and are generated independently. The time power is enabled to the servo motors is restricted to 1sec (adequate to permit a 90° rotation on each motor), seen on the right hand side of the sequence structure. Additional functions are added to the main control including amplitude and frequency adjustment in order to tune in the servo motors to avoid jitter. The mounting arrangement of the visual servoing system can be seen in Plate 3 with additional information in Appendix A.

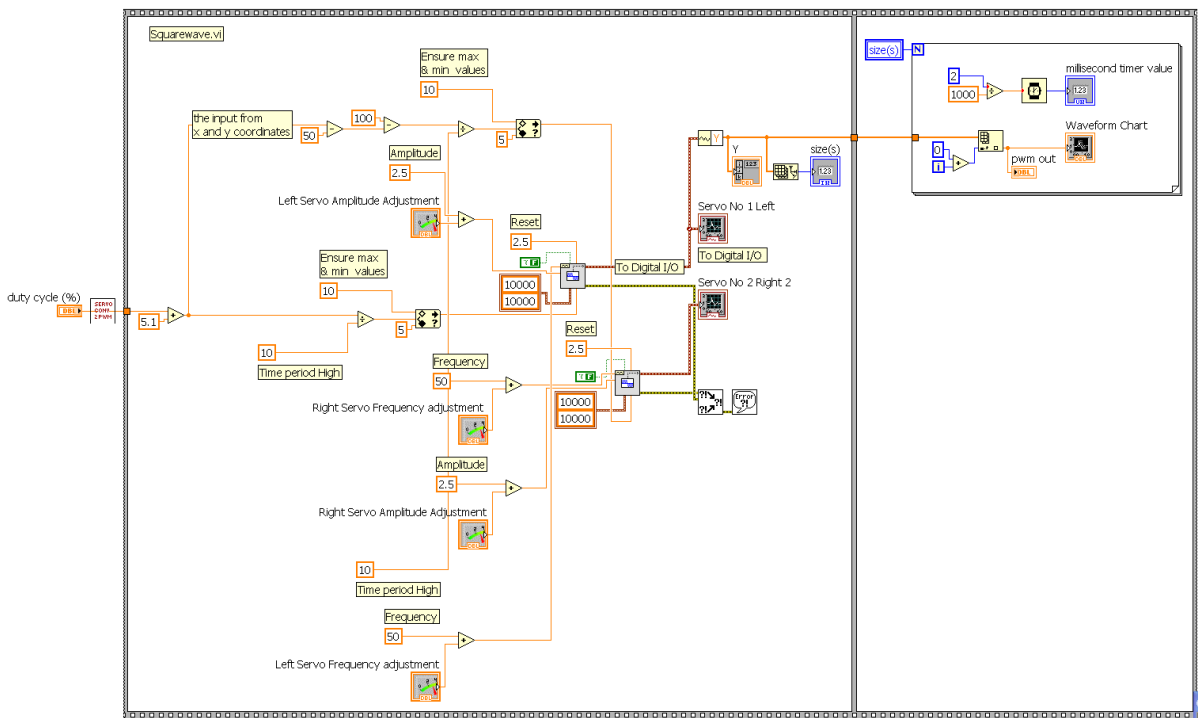


Figure 20 Visual Servoing Algorithm Design

This algorithm is called from the main program within the LabView environment. The sequence structure ensures that the calculation for angle adjustment occurs once and the servo motors are engaged for a one second period to reach the corresponding calculated angle.

Plate 3 illustrates a physical the manipulator (Katana 6M180) positioned in the grasp position with the rotation of each servo motors at an angle to ensure that the Region of Interest (ROI) remains toward the centre of the field of view within the captured image.



Plate 3 Location of visual servoing system on Katana Robot arm  
The Manipulator is in grasp position with both cameras directed towards the object, operated by PWM signal from above algorithm

*Note: With designing the visual servoing system with the facility for a second camera, one camera will remain in standby until an error or fault condition is reported or a check on recognition and positional information is required, thus providing a failsafe system.*

The visual servoing system will be initialised at the first image acquisition position (long distance scan). The angular position is loaded from the database to ensure the  $Id_{loc}$  coordinates is within the centre of a camera(s) field of view. As the manipulator manoeuvres closer to the recognised object, the visual servoing mechanism ensures that the object appears towards the centre of an acquisitioned image to improve the efficiency of object recognition and thus the estimated object location coordinates. For commissioning information refer to Appendix B.

## Chapter 3:

### **Design and Implementation of new gripper arms.**

To assist a physical robot arm to successfully transport a deformed object, gripper arms are used. The standard gripper arms supplied with the Katana 6M180 robot arm are shown in Figure 21. The left and right gripper arms are identical in shape and as discussed in this chapter have distinct weaknesses, as such incur limitations to the functionality of the gripper mechanism. With the research concentrating on improving the operation of a manipulator the gripper mechanism is one of the most important considerations, therefore in order to improve the weakness of the existing gripper arm, additional design and development was required to incorporate the force feedback system and to create a multifunctional gripper mechanism. The attached arms require the ability, not only to encompass the FS series force sensor, but to allow the facility of a range of different sensors to be installed within the gripper arms and permit manipulation of deformed objects.

The main criteria for the design of new gripper arms are therefore:

- 1) To remove the weakness of manufacturer standard grippers
- 2) Inclusion of force sensor feedback system.
- 3) To permit small objects to be grasped securely
- 4) Permit the gripper arms to assist the object into the gripper mechanism – in case of manipulator position error.
- 5) Add additional strength to the gripper arms to permit additional tasks.

The first criterion is to examine the properties of the existing gripper arms to determine the location of stress and the degree of displacement that occurs when the gripper mechanism is under load. The existing grippers are manufactured from 201 annealed stainless steel, the design of which is seen in Figure 21.

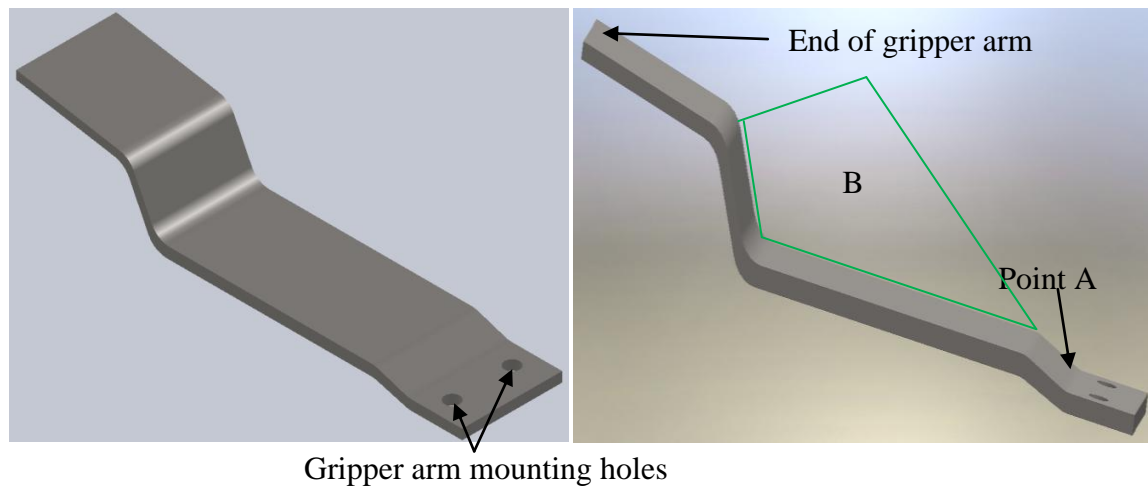


Figure 21 Existing SS Gripper Arm Design

The depth of each gripper arm is 20mm is width and designed to grasp objects either at the end of the gripper arm or centrally within location labelled B.

Figure 21 illustrates the design of the gripper arm used for both sides of the gripper mechanism of the katana 6M180. There are three main issues with this design of gripper arm:-

- 1) There is only the current drawn from the gripper drive motor to inform the control system that an object has been successfully grasped or present, but no feedback mechanism within the gripper arms.
- 2) There is a significant gap when both gripper arms come together (this area is identified within the green line boundaries depicted by B in Figure 21 and further illustrated in Figure 22), which would only allow small objects to be grasped by the small surface area at the end of the gripper arms.
- 3) When under load the arm has the tendency to flex at the fold, located at point 'A' Figure 21, this combined with a small surface area limits the characteristics of the object being manipulated with the gripper mechanism.

The limitation to the object sizes to be grasped by the gripper arms are seen in Figure 22. The permitted width of the object(s) are  $<48.04\text{mm}$  at the end of the gripper arm and  $>35.29\text{mm}$  for a secure grasp central within the gripper mechanism.

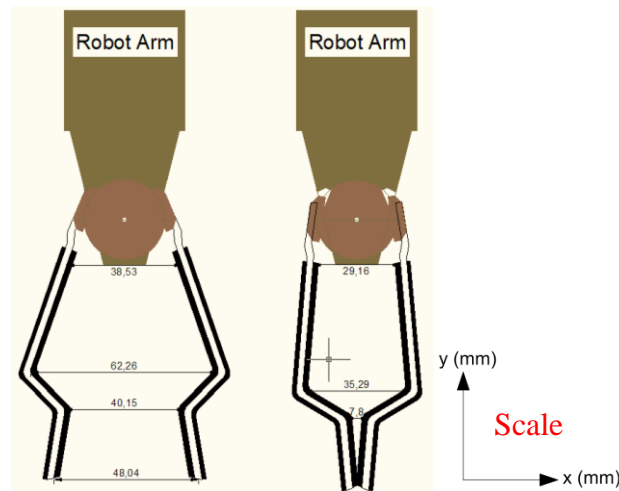


Figure 22 Existing Katana 6M180 Gripper Mechanism  
All dimensions are depicted in mm and drawn to scale

In Figure 23 the gripper mechanism is shown grasping various cylindrical objects of differing diameters from 5mm to 30mm. Although all the object(s) have been successfully grasped the gripper can fully close without a good grip on the smallest object.

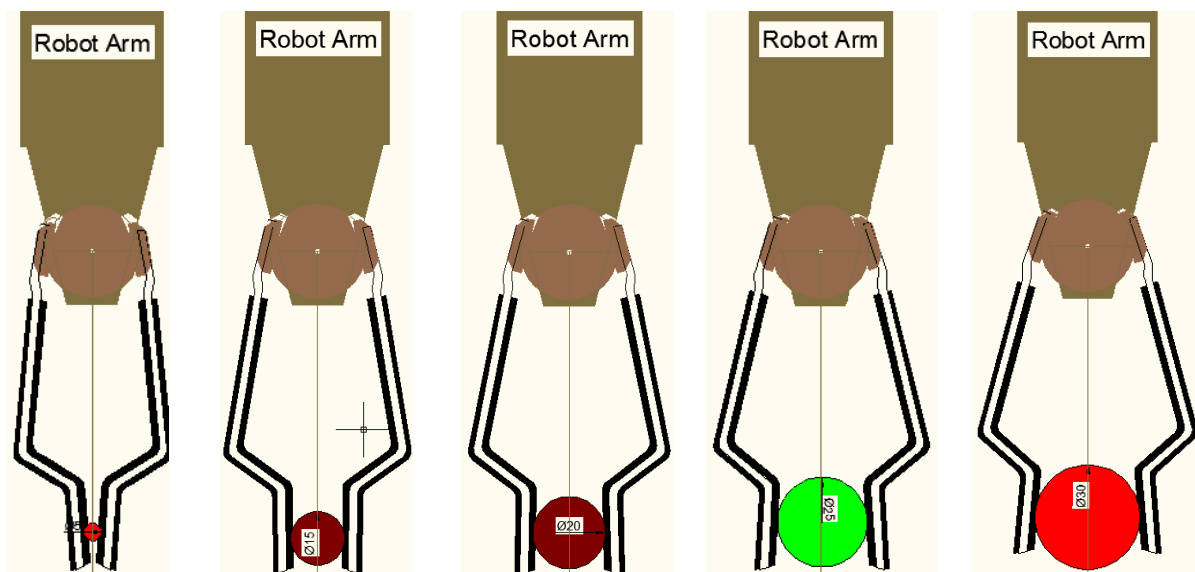


Figure 23 Existing Gripper Grasping Various Diameter Objects  
The gripper mechanism has successfully grasped all sizes from 5mm (far left) to  $\Phi$ 30mm (far right). However positioning of the end effector requires to be accurate: to ensure security of the object being manipulated.

As seen in Figure 23, if the robot manipulator is not in the exact position, the shape of the gripper arms do not lend themselves to ease the object into the gripper mechanism, thus causing the manipulator to move the object rather than grasp it. There is also only modest

tolerance for forward motion of the manipulator, towards the object, before the gripper mechanism fully closes and grasps nothing. Figure 24 illustrates only the largest of the objects have the possibility of being successfully grasped; if the manipulator moves too far. The other objects due to the small surface area have low probability of being grasped successfully; therefore the manipulator control has to be extremely accurate.

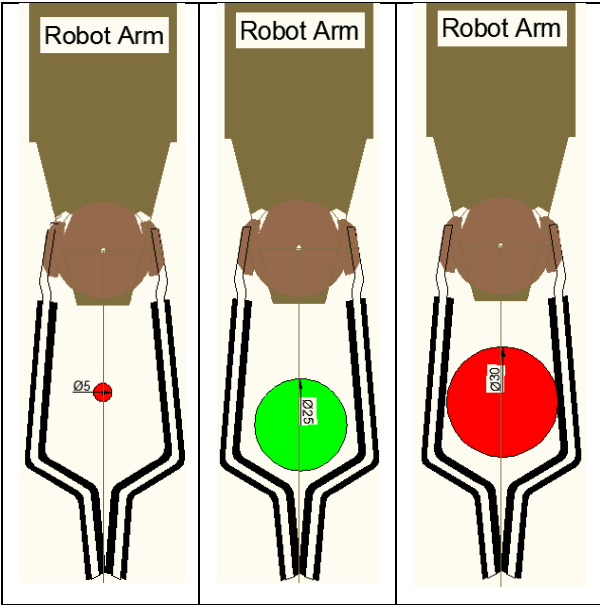


Figure 24 Schematic Determining modest tolerance for position of Manipulator

In order to improve on the existing design, stress simulations are conducted with approximately 0.787N (with 3% added as a safety margin) maximum permitted load that the force cell can measure effectively without damage. As seen in Figure 25, the locations of load (including direction of load to the part, shown in blue) and restraint (fastening point of the gripper arm, which will be under strain during load conditions, shown in red) are determined.

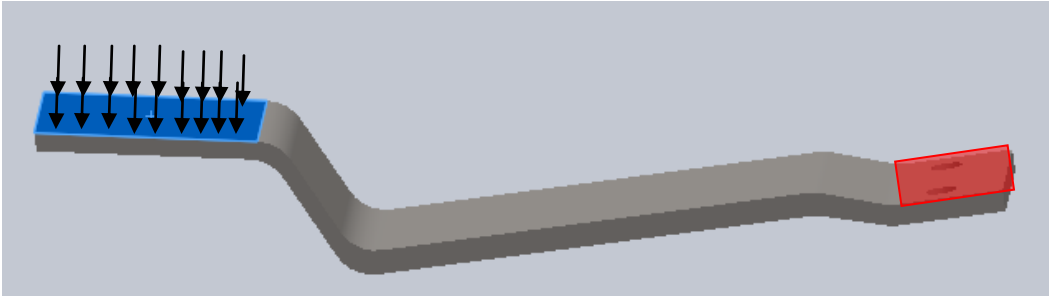


Figure 25 Locations of Load and Restraint on existing Gripper Arm

A Factor of Safety (FOS) is calculated to determine whether any failure points occur with the design and also the location of these failure points. Figure 26 illustrates the location of stress (shown in red) situated just past the gripper arm mounting bracket at the fold labelled point A in Figure 21. However, the lowest FOS is calculated at 2.96, which is above the minimum value of 1 that concludes the critical areas of the design given the stress applied to the part. The data gathered from the simulation is used as the minimum performance criteria for the new design of gripper arm.

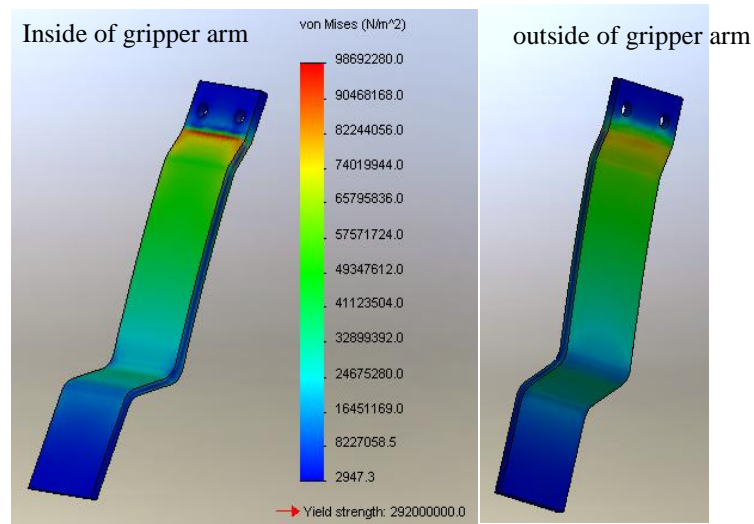


Figure 26 Existing Gripper Displacement Chart for Maximum Load

### 3.1 Heuristic design of new gripper arms with inclusion of the force feedback sensor.

Numerous designs for the improved gripper arms are illustrated within this section, with the maximum opening distance to match the existing gripper mechanism. The base of the gripper arm will incorporate a mounting plate to secure the PCB board that the force sensor is mounted onto, in addition to a back-plate to support the sensor when in contact with an object; this will form the base of the gripper arm, as seen in Figure 27.

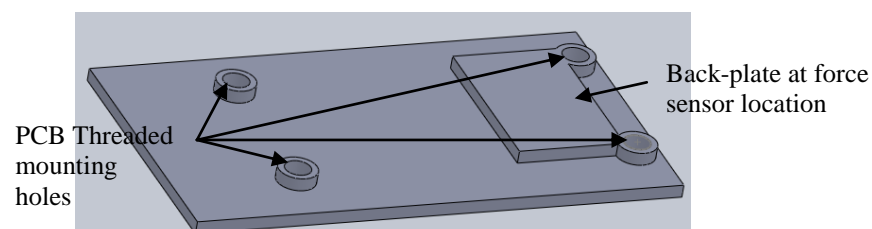


Figure 27 Secure Mouning For Force Sensor PCB Board  
The plastic casing of the FS series Force sensor will be supported by the back plate and the PCB board is secured using the four mounting holes.

The location of the force sensor plunger is of utmost importance in the design of the gripper arm: if the object does not come into contact with the plunger, force cannot be measured and therefore the manipulator will continue to grasp as the feedback signal will inform the control that no object has been detected. (The AutoCAD 2009 package was used to test various designs, which are described below.)

To increase the surface area of the plunger, a spring steel flat bar was used. The bar is inserted into the front plate resting on the plunger of the force sensor, a 3D view of the front plate is shown in Figure 28. The central square hole, labelled A, depicts the location of the force sensor, the plate locates securely around the force sensor casing adding additional security to the sensor. The spring steel flat bar inserts through the slots, labelled B, therefore any contact with the flat bar will register as a voltage change through the Wheatstone bridge circuit; thus determining that an object is present. The operation of the design can be seen in Figure 29.

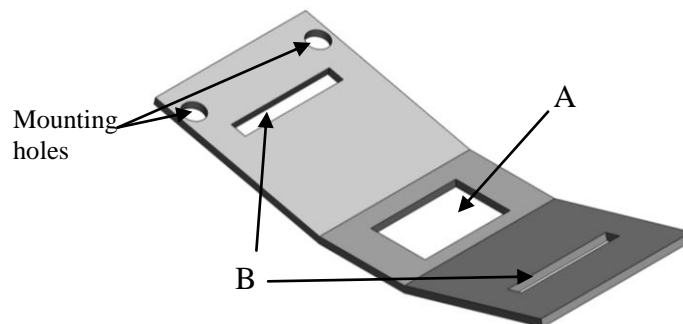


Figure 28 Gripper Arm Front Plate including Slots for Additional Components  
The FS series force sensor will be positioned at position A. The front plate will be secured to the main gripper arm with the mounting holes (upper left).

As seen in Figure 29, increasing the surface area of the plunger, the gripper mechanism will be able to pick-up the smallest object (5mm dia.) to the largest (30mm dia.). With the internal walls of the gripper mechanism, labelled A, on an angle reduces the problem of objects slipping further into the manipulator, in addition by rounding in the end of the gripper arm, labelled B, the effect of the object slipping out is reduced, but not resolved. The robot manipulator can be expected to work within environments that contain: water, oil etc. and within other hazardous areas that could reduce the effectiveness of the gripper mechanism.

Consider the right schematic in Figure 29, if the object incurs an oily/slippery surface and the gripper attempts to grasp the object with the manipulator in this position, there is a possibility that the object would slip through the arms. By using a human hand to test the theory, it became apparent that no matter how much force is applied to an oily object the object has a strong possibility of slipping through the grasp using a two finger approach. By using two fingers and a thumb, rather than a thumb and a finger, the security of the object was significantly improved. The same philosophy was used to alter the design to allow for additional overlap between left and right gripper arms to compensate for this issue.

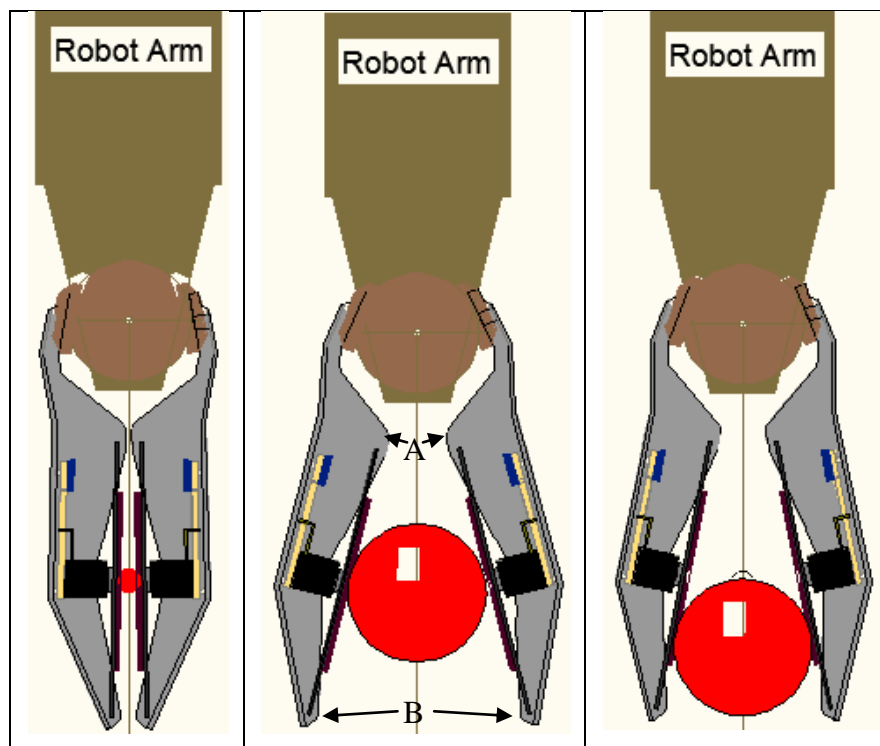


Figure 29 Gripper Design No.1

The force sensors are mounted in one arm for both the left and right grippers. The third finger is used for additional support and does not contain any electronics and is predominantly used for additional security for the object being transported. Figure 30 illustrates an improvement to the initial gripper design, with the right gripper comprising of two fingers (third finger not shown in 2D design, as positioned behind as viewed from the top) to permit the left gripper to slide in-between and thus create the overlap. All sizes of objects are accommodated; the facility of three finger mechanism ensures the object can be held securely within the grasp

without the possibility of slipping out. The ends of the gripper arms are angled inwards to prevent the largest object sliding through once the gripper mechanism begins to close. In addition the inner section of the fingers are stretched inwards, labelled A, to prevent the smallest object being positioned between the gripper mechanism and the manipulator body, labelled B; It also assists in the objects being positioned on the pressure plates to improve the operation of the force feedback control system. However, the design illustrates issues with the ends of the gripper arms: with a small clearance between the gripper mechanism being fully opened and the largest size of object, there is a possibility of the manipulator pushing the object over or out of the way whilst manoeuvring to grasp. If the object being manipulated is a beaker full of liquid, any movement not in the desired way has to be avoided. In addition, a reduction in the surface area at point A, would simplify the design, lighten the gripper arms and still perform the identical task, with reduced complexity and cost of manufacture.

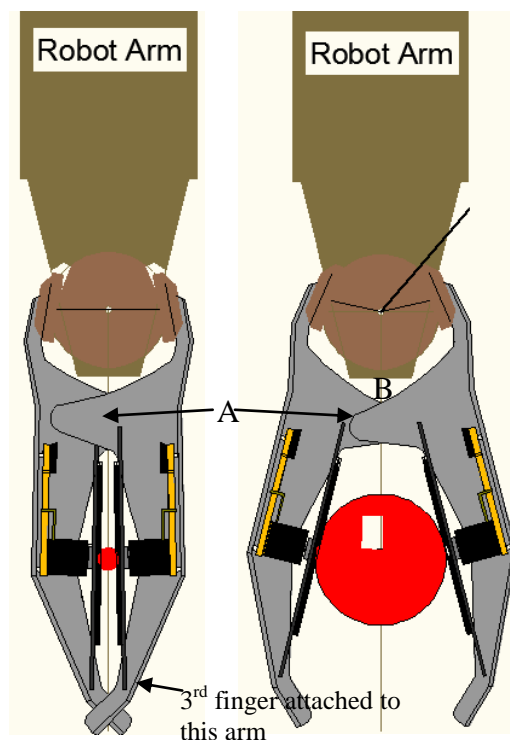


Figure 30 Three finger Gripper Arm Design

The aforementioned improvements are illustrated in Figure 31. The ends of the gripper arms are rounded to assist in feeding the objects into the mechanism, in addition to the internal 'arc' at position A in Figure 30 being reduced. This 2D model was then used to heuristically test the various diameter objects within the simulation at different locations within the gripper

mechanism: the design was transferred into 3D using the Solidworks 2009 application for further analysis and prototyping.

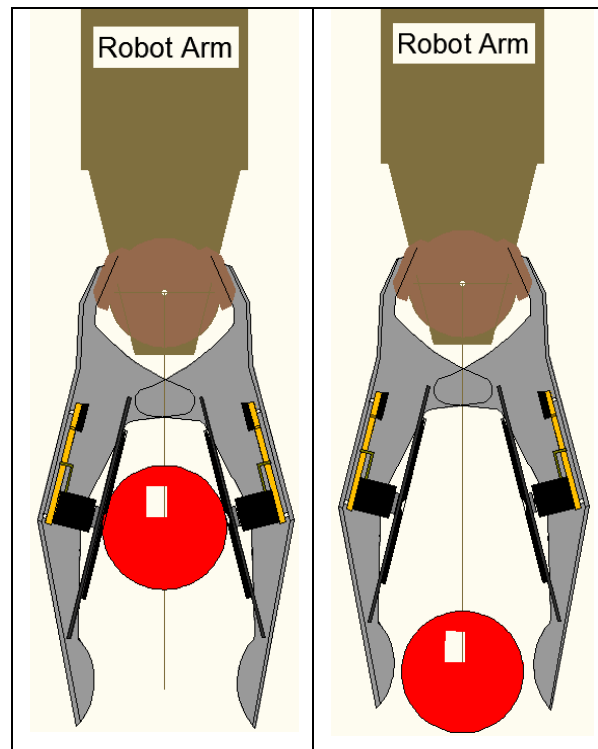


Figure 31 Gripper Design to Permit Assisting an Object into the Gripper Mechanism

### 3.2 Prototype of Single Gripper Arm

To ensure the design of gripper arms along with the force feedback control system functioned efficiently together, the arm were required to be physically manufactured. Solidworks 2009 enables the designed 3D image to be saved in binary format 'stl file', which can be uploaded to the rapid prototyping machine to be manufactured from high viscosity polycarbonate PC-10 material. The manufactured part(s) are then assembled together to produce a new manipulator with attached gripper mechanism that is used to test the operation of the ancillary devices of the intelligent manipulator described throughout this thesis. To generate the specification of the final annealed stainless steel (SS) gripper arms, further analysis is conducted to calculate mean time before failure (MTBF). The results for these SS gripper arms are described in Appendix D, as only the PC-10 gripper arms are utilised within this research, as such are designed to function with the weight characteristics of the objects used,

whilst the SS equivalent will permit additional functions and the ability to transport heavier objects without causing critical failures to the gripper arms themselves.

Using the measurements obtained from the 2D design schematics, the prototype of the single gripper arm was produced, as shown in Figure 32. To permit the force sensor PCB board to be fitted internal to the gripper arm, the depth of the main body is increased from 20mm to 25mm. To allow for fitting on the Katana robot, the depth of the front of the arm remained at 20mm to ensure a secure fit, shown on the right hand side of Figure 32. The front mounting plate slides under the locating rim and secured to the two threaded mounting holes.

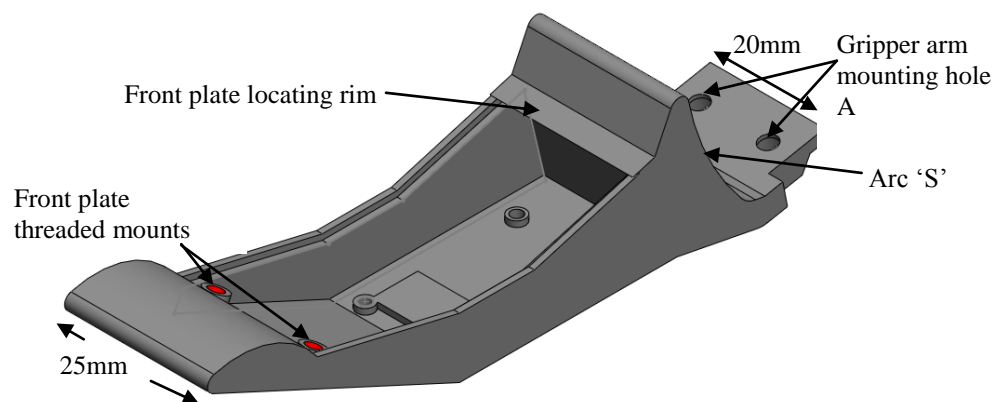


Figure 32 3D Single Gripper Arm Design

The depth of the gripper arm is increased to 25mm to incorporate the Force sensor and PCB mounting. On the right of the figure the width remains at 20mm to allow for mounting to the Katana robot arm.

With increased complexity of the design compared with the existing gripper arms the locations of stress are more detailed. The mounting holes on the far right of Figure 32, and on the underside there is also a recess for the 'cap-head' bolts that secures the gripper arm to the manipulator, will also take some strain. All the restraints are identified as shown in Figure 33.

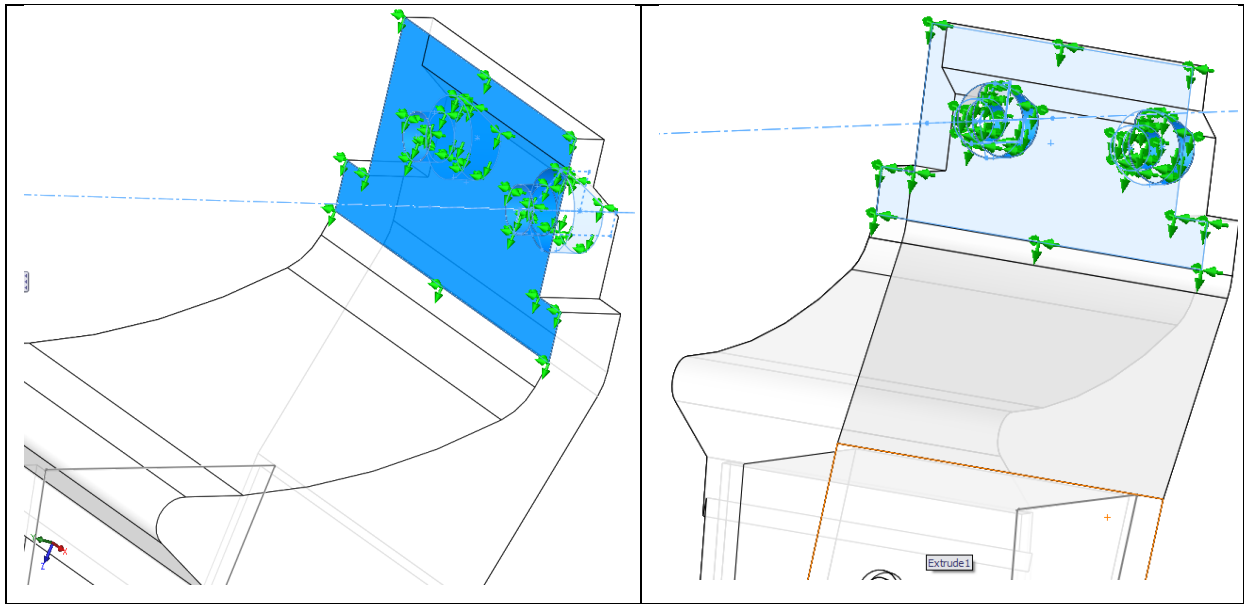


Figure 33 Locations of Restraint stress on Prototype Single Gripper Arm  
The locations of restraint includes the mounting area that attaches the gripper arm to the manipulator, but also the internal areas where the cap-head bolt will be located.

The positions of the load are situated in two different locations: on the mount that will support the force sensor, shown as position A in Figure 34, and the supports for the mounting plate that will house the pressure plate. The part has been designed so that the load is normal to the selected faces and evenly distributed.

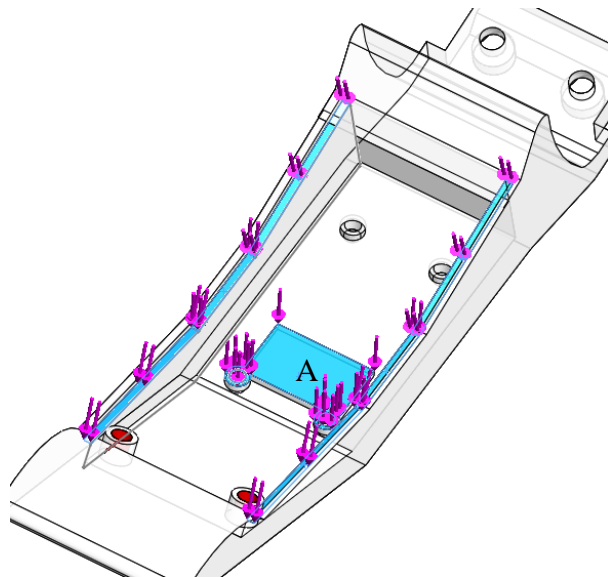


Figure 34 Locations of Load on Prototype Single Gripper Arm  
The front plate that is positioned onto the gripper arm incurs the smallest support surface area, therefore will be the weakest area of the part. Increased load however will be directed onto the force sensor mounting plate

The stress and displacement distribution charts are shown in Figure 35 using the identical parameters (force exerted on the gripper) used for the existing gripper, simulated in the previous section. Figure 35 illustrates the maximum stress location of the prototype single gripper arm; the location of stress is identical as with the existing gripper, however the deformation is decreased for the same applied load. There is significant displacement at the ends of the gripper arm that will increase the possibility of the object under transportation to slip once grasped. This could also result in the possibility of a break at the location shown in red of the left hand side of Figure 35, if the polycarbonate gripper is used under this load for a considerable amount of time.

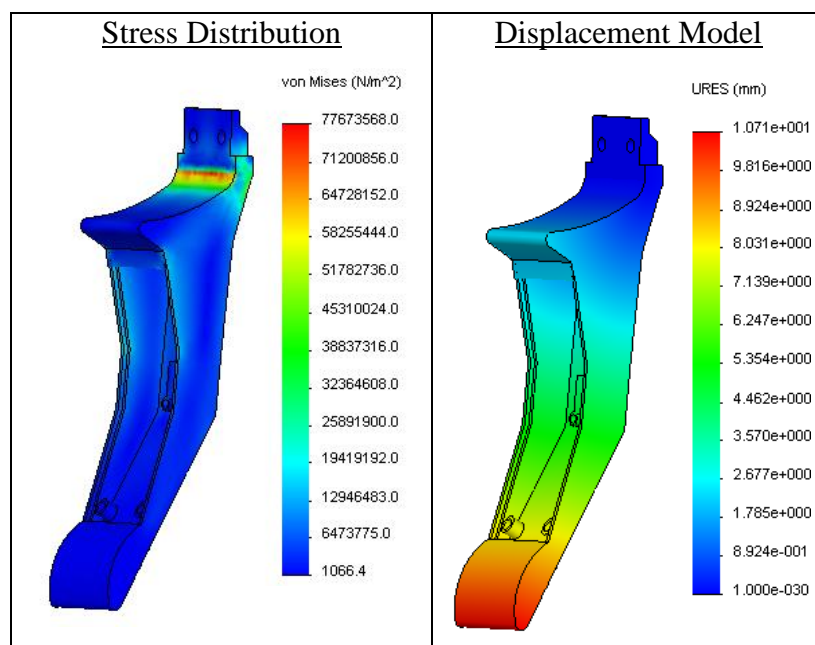


Figure 35 Stress and Displacement Model for Prototype Single Gripper Arm  
The prototype is made from High Viscosity Polycarbonate (PC-10) material manufactured by the rapid prototype machine. Unfortunately Solidworks 2009 cannot calculate yield strength of the part made from this material. The simulations of the above charts are used by the author to fully determine whether the manufactured part could withstand the applied force required to manipulate the selected objects.

### 3.3 Prototype of Dual Gripper Arm

The dual gripper arm is designed with two fingers: the force feedback electronics installed in one and the other is used for additional support. The prototype 3D design is shown in Figure 36. The two finger gripper arm is designed to permit the single gripper arm to slot into the gap between the fingers when closed. The finger that houses the force sensor electronics is an

identical copy of the single gripper arm. The other finger, is attached by an extending mounting plate, support plate and support beam to prevent any major distortion in shape of the part when under load. The support finger is designed to be narrower than the main finger and a spring steel flat bar is inserted along the slots of this finger to correspond with the other finger. As with the single gripper arm the restraint revolves around the mounting holes, the left gripper however has an increase in surface area on the underside as shown in Figure 37.

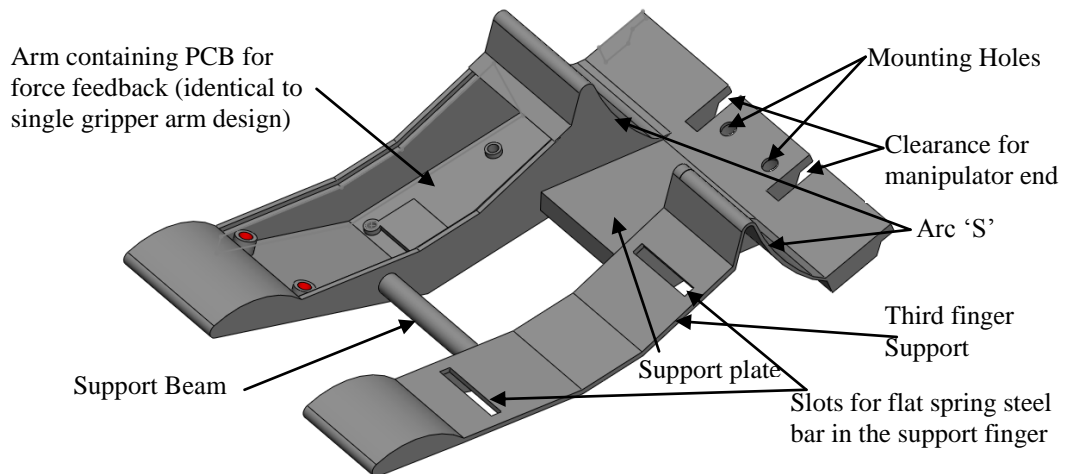


Figure 36 Dual Gripper 3D Design

The section of the dual gripper arm shown on the North-West area of the figure is a duplicate of the single gripper arm in the previous section. The support bar depth is 20mm and attached by an extended mounting plate and a support beam to allow some additional displacement for grasping deformed objects.

As seen in Figure 37, the restraint area is extended from that of the single gripper arm, the main area of restraint, however is identical, but the surface area and strength, due to the dual finger design, is increased.

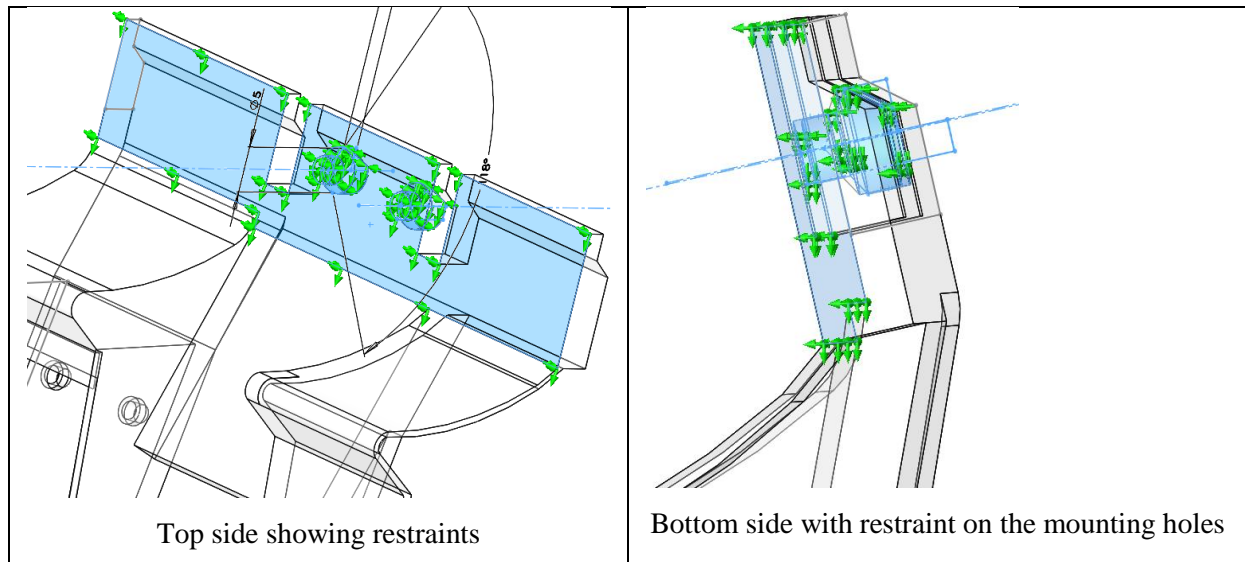


Figure 37 Locations of Restraint on Dual Gripper Arm

The section that mounts onto the Katana robot determines the area of restraint. With the extendable mounting plate to allow the third finger, the restraint is spread more evenly across the entire surface.

The load being applied on this part is located in several locations: three of these are identical to the single gripper arm; however the load conditions are distributed between both fingers. Thus part will have load evenly distributed across two planes, the main location of load is on the mount that will support the force sensor. The locations of load are illustrated in Figure 38.

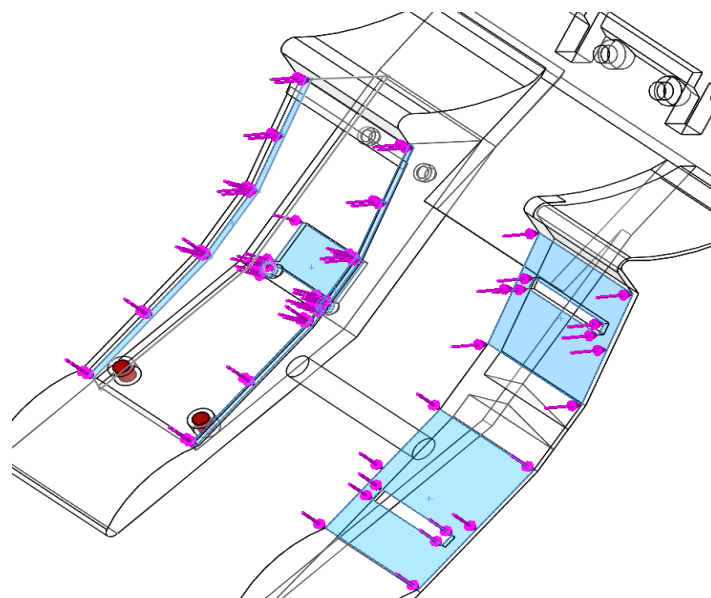


Figure 38 Locations of Load on Prototype Dual Gripper Arm

The areas of load are identical as the single gripper arm, however the addition of the third finger allows the load to become displaced from the main gripper arm, thus improving load resistivity of the part when compared with the single gripper arm.

The stress and displacement distribution are shown in Figure 39 using the identical parameters used for the single gripper in previous section. By comparison with the single gripper arm, the maximum stress location is displaced from where the gripper arm attaches to the manipulator. The inclusion of a much greater surface area of the part causes a decrease in deformation on the part for the same applied load. The support plate and beam alleviate the stress to the main finger and as a result the displacement of the main finger is considerably reduced. Most of the displacement occurs in the support finger due to the hollow design. There is no significant risk of the part failing under the maximum operational load: no areas depicted in red near the restraint on the simulation.

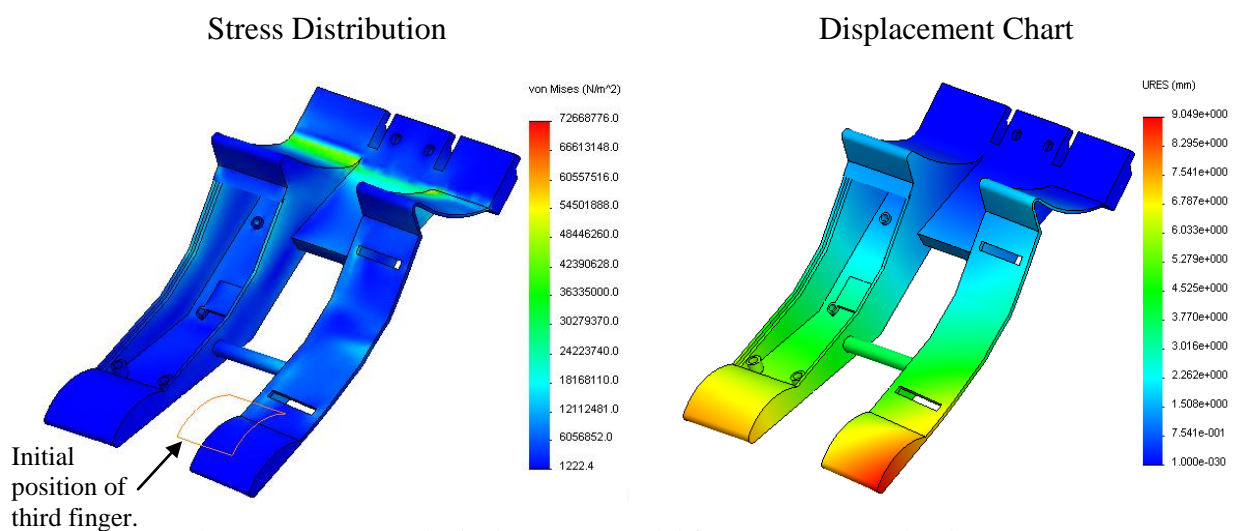


Figure 39 Stress and Displacement Model for Prototype Dual Gripper Arm As with the single gripper arm. The prototype is made from High Viscosity Polycarbonate (PC-10) material, manufactured by the rapid prototype machine. The Stress distribution chart above illustrates the effect of the load onto the part by indicating the amount of displacement, with the right chart determining the location of maximum displacement.

Both Gripper arms were manufactured using the prototype machine, and used as a trial fitting with the katana robot and to determine other issues with the shape of the gripper arm and how well the combination of both grippers worked together. When installed, the rear of the area labelled 'arc S' in Figure 32 and Figure 36 failed to include an adequate radius to avoid contact with the manipulator and therefore when closing the gripper mechanism, this area of the gripper arm collided with the end bracket. This caused the part to displace at the location of maximum stress, hence causing additional functional issues with the gripper mechanism:

the main one being occasional collision with the opposite gripper arm upon grasping the smaller objects.

With designing prototypes issues like these are common place; as such prototypes are generally used to determine any design weaknesses before finalising the design to produce a workable model. In addition a cost analysis is generally conducted to identify whether improvements to the prototype can be accomplished whilst saving material usage and cost.

### 3.4 Improvements to the prototype gripper arm designs

A strengthening rib across the main area of stress has been included to strengthen the single gripper arm against the possibility of shattering during the testing period and to reduce the displacement on the part when under load. In addition the arc radius 'arc S' has been increased to permit adequate clearance between the gripper arm and the end of the manipulator when closing; all other dimensions have remained identical. The improvements to the single gripper arm can be seen in Figure 40 and the dual gripper arm in Figure 41.

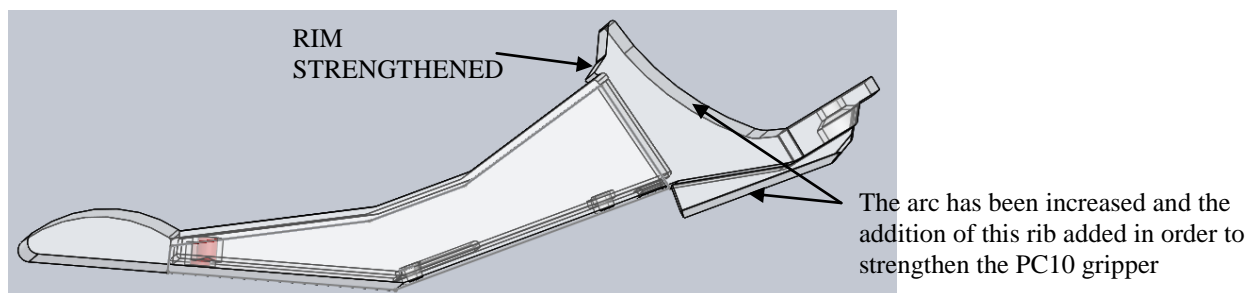


Figure 40 Final 3D Design of Single Gripper Arm

As seen in Figure 41, similar modifications were made to the dual gripper arm; however two strengthening ribs have been added at the two locations where the stress levels were recorded at maximum: A rib placed at the mounting point to the manipulator and a rib on the section that houses the force sensor. In addition the flexible support shown at the top of the schematic in Figure 41 is strengthened to remove the amount of flexibility in this area that assisted in decreasing the 'potential' slip of the object being transported.

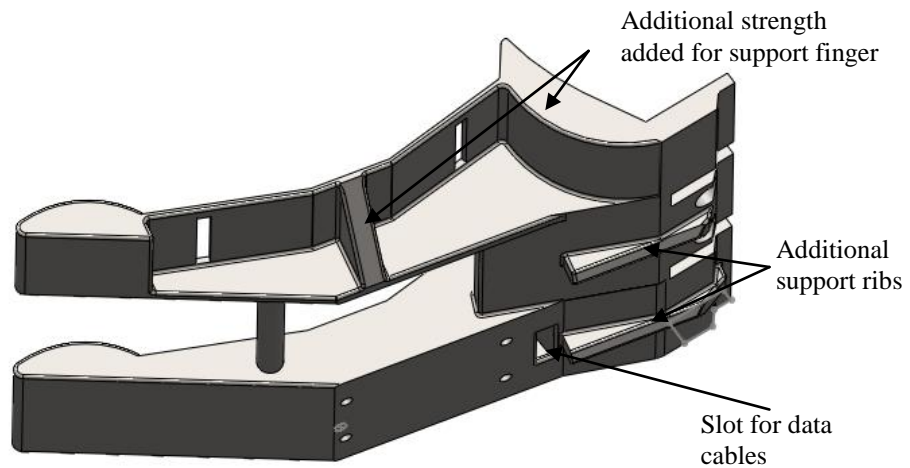


Figure 41 Final 3D Design of Dual Gripper Arm

Table 3 shows a comparison between the original prototype and the new modified version of the single gripper arm. By strengthening the front plate locating rim, increasing the radius of the arc and installing a support rib underneath the location of maximum stress, the mass of the part, volume and surface area has decreased; thus the quantity of material to manufacture the part as a result had also decreased. The stress on the part is reduced with the strengthening rib added, also the total displacement under the same applied load is reduced, hence under maximum load (0.787N), the gripper arm attained superior performance than the original prototype and incurred the ability to maintain its original shape better under load conditions.

Table 3 PC-10 Comparison of Single Gripper Arm Properties

Mass properties of prototype		Mass properties of modified prototype	
Mass	0.01436 kg	Mass	0.01351 kg
Volume	0.000013422 $m^3$	Volume	0.000012625 $m^3$
Surface area	0.010467 $m^2$	Surface area	0.010305 $m^2$
Original Prototype properties		Modified prototype properties	

As seen in Table 4, by strengthening the dual gripper arm, the mass increased by 12%, however the additional supports that are added to prevent considerable distortion of the support finger has the advantage of reducing the amount of displacement the part incurred whilst under load.

Table 4 PC-10 Comparison of Dual Gripper Arm Properties

Mass properties of existing gripper Output coordinate System: -- default --		Mass properties of existing gripper Output coordinate System: -- default --	
Mass	0.02603 kg	Mass	0.0296 kg
Volume	0.000024331 m <sup>3</sup>	Volume	0.000027663 m <sup>3</sup>
Surface area	0.020595 m <sup>2</sup>	Surface area	0.020408 m <sup>2</sup>
Original Prototype properties		Modified prototype properties	

Figure 42, further clarifies the improvements on the prototype design; the stress is more evenly distributed on the part (50% superior with the applied load). The maximum displacement has changed to the main finger, but again the modified part has considerable tolerance against distortion under load.

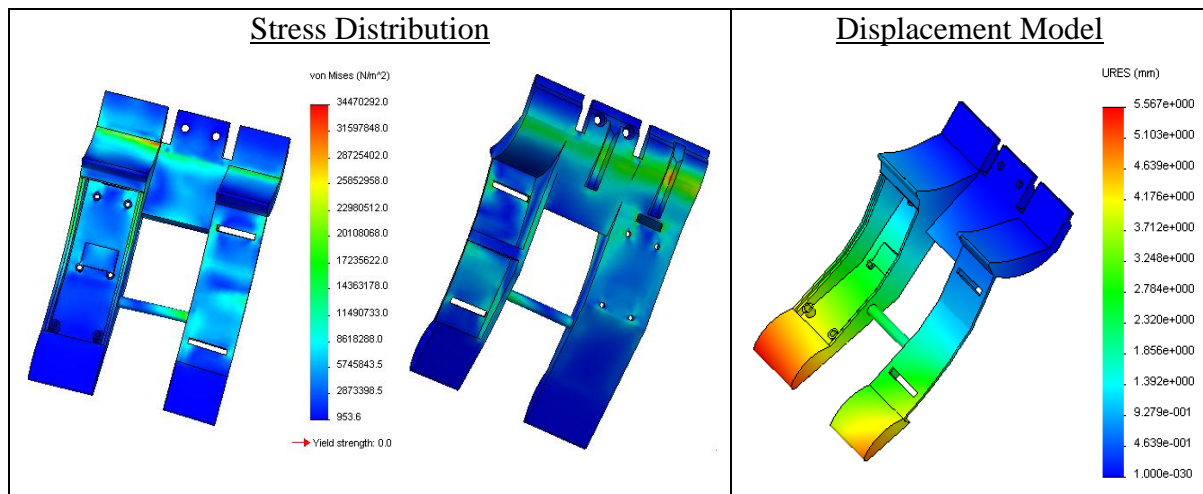


Figure 42 Stress and Displacement Model for Final Design of Dual Gripper Arm When compared with the original charts (Figure 39), a significant improvement in the way the part behaves under load conditions is achieved with only a slight increase in mass. With the improvements the main area of displacement is situated on the main finger and not on the support finger.

The gripper arms were designed to ensure mechanical protection for the on-board electronics, and to permit a pressure plate to act upon the object causing a voltage feedback value to the main control system. The design of the pressure plate due to unavailability of appropriate resources (i.e. access to workshop), required to be modified for physical testing. Thus for physical testing, the front plate is absent from both arms and replaced by 1.5mm spring steel plate as shown in Plate 4, secured at the front of the gripper arm by two tapped mounting holes. The operation of the gripper mechanism itself has not been altered, only the placement

of the object requires to be precise, so as not to be trapped between the end of the spring steel plate (point A) and point B.

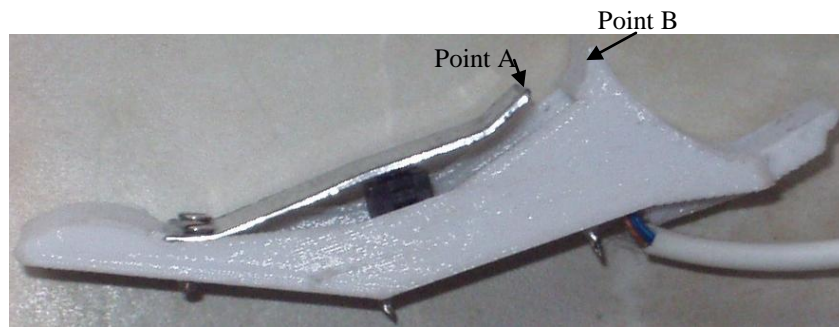


Plate 4 Modification to Pressure Plate on Gripper Arms

Thus with the pressure plate not being secured at each end, the measured changes in applied force became more abrupt, hence the control system became more sensitive to external influences, (hence the  $2.356 \times 10^{-3} \text{N}$  of force entered into the software database as illustrated in Figure 17). This incurred a better touch/feel mechanism if delicate and fragile objects required to be manipulated. The three finger gripper mechanism design will permit various shaped and sizes of object(s) to be manipulated, the dual grip would allow flexibility in order to grip around deformed objects. The maximum allowable size of the object is constrained by the maximum opening distance of the gripper mechanism. The design of the gripper arms ensures maximum strength with minimum material usage. The manufacturer standard gripper arms have proven to have considerable weakness in their design, and therefore less adaptability than the purpose designed gripper arms described in this chapter.

### **3.5 Design and implementation of replacement manipulator main body**

The following section discusses the design for a replacement Manipulator for ease of maintenance to improve uptime of a robotic system. The replacement manipulator was manufactured from PC-10, and used with the PC-10 gripper arms to test the security of the objects used in this research. The manipulator is designed to permit quick disassembly and replacement of all parts using off-the-shelve tools and components. The final designed and manufactured manipulator is then illustrated at the concluding part of the chapter to visually identify that the R&D conducted in this research, with respect to improving the mechanics of

the manipulator, can be installed directly into an industrial manufacturing cell / line to offer additional advantages that current manufacturer supplied manipulators do not.

One of the main criterion for robots being used for mission critical tasks is the reliability and the cost, both in time and money, of maintaining the mechanics and electronics in-case of fault conditions. Generally maintenance aspects of such autonomous machines are overlooked and most of the consideration is given to the economical option of manufacturing and assembling the machine / robot. The current Katana 6M180 is no exception, specialist tools and considerable time is required in order to replace any faulty component (with the exception of the gripper arms) and would be difficult to resolve fault conditions if an electronic component caused adverse effects on the correct operation of the manipulator. The following discusses the improvements to the existing manipulator to enable quick disassembly and thus efficient change of parts. Measurements are taken from the Katana 6M180 to enable the new manipulator to be attached to the rest of the physical robot arm.

The vision sensor clamp is 60mm in diameter (see Appendix A) to enable a secure fitting, but also to enable quick removal (designed specifically in-case the Katana is required by other researchers during the completion of this project). Therefore base is 60mm in diameter and ribs have been added to the base for positioning of the vision sensor clamp, as can be seen in Figure 43.

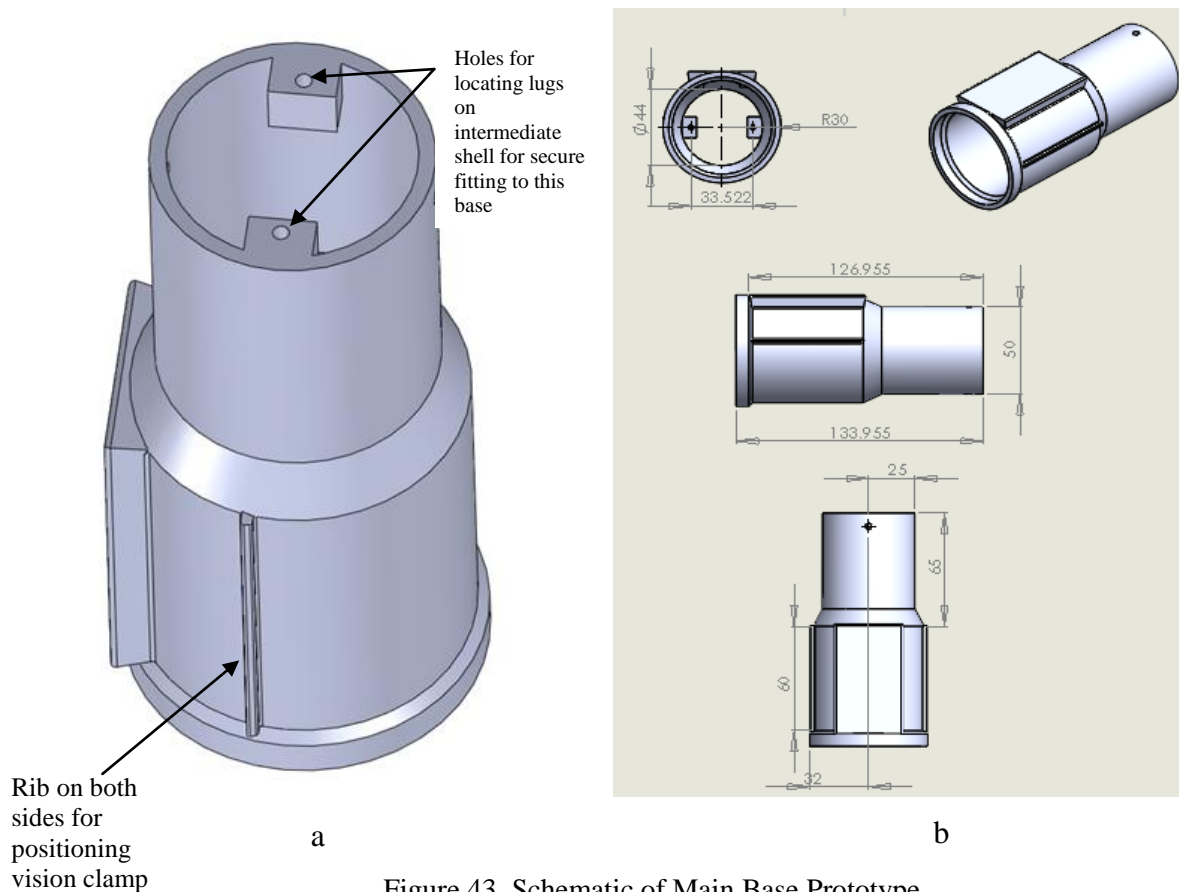


Figure 43 Schematic of Main Base Prototype

The flat foot is added to the main base to improve stability when placed on a surface to enable testing of the transient movement of the gripper mechanism and the servo motor positioning.

For additional strength and to account for a small but defined section of the Katana manipulator, the shell illustrated in Figure 44, is designed. The two cones internal to the structure are for location into on main body, with the addition of being fastened into place by the external mounting holes. The front of this shell has additional mounting holes for securing the gripper housing.

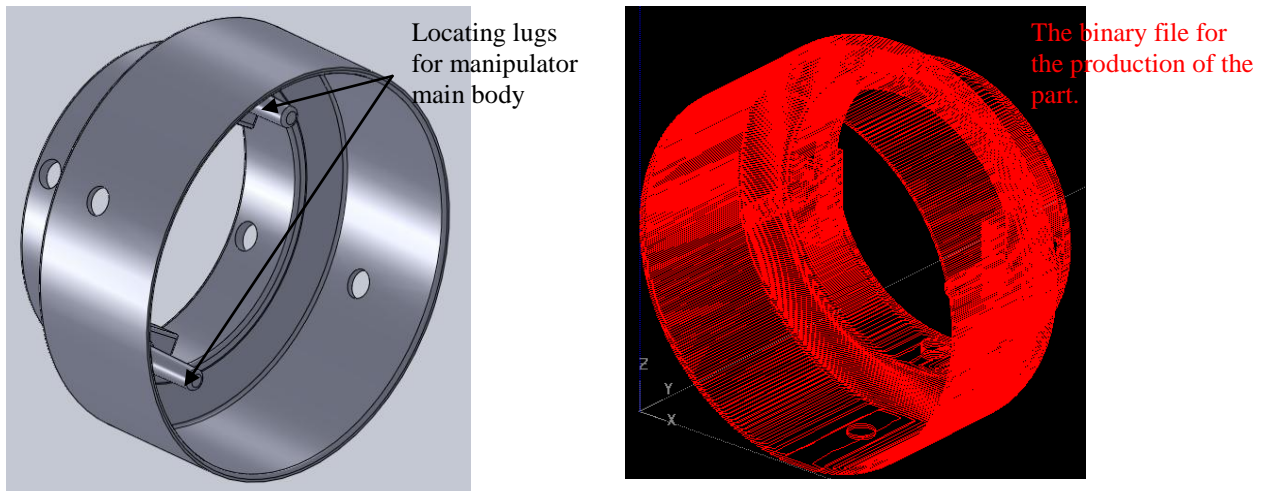


Figure 44 Intermediate Shell of Manipulator

An efficient positioning design was chosen to enable assembly in hazardous areas or areas with poor lighting. The right figure illustrates the binary image used to produce the part on the rapid prototyping machine.

The design is based on a quick release system that requires very few tools to separate. Knowing that strength is required with the use of modest material, to keeping cost down, a gripper mount housing is designed to connect to the shell of Figure 44. The part illustrated in Figure 45 was designed to secure the gripper housing and the incorporated motor drive system. The part has been design with symmetrical spacing blocks, which will allow the gripper housing to be designed in two halves.

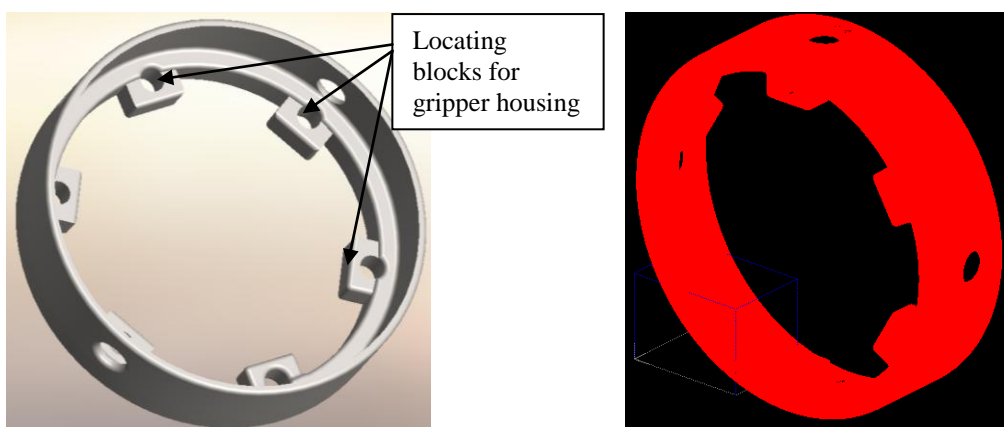
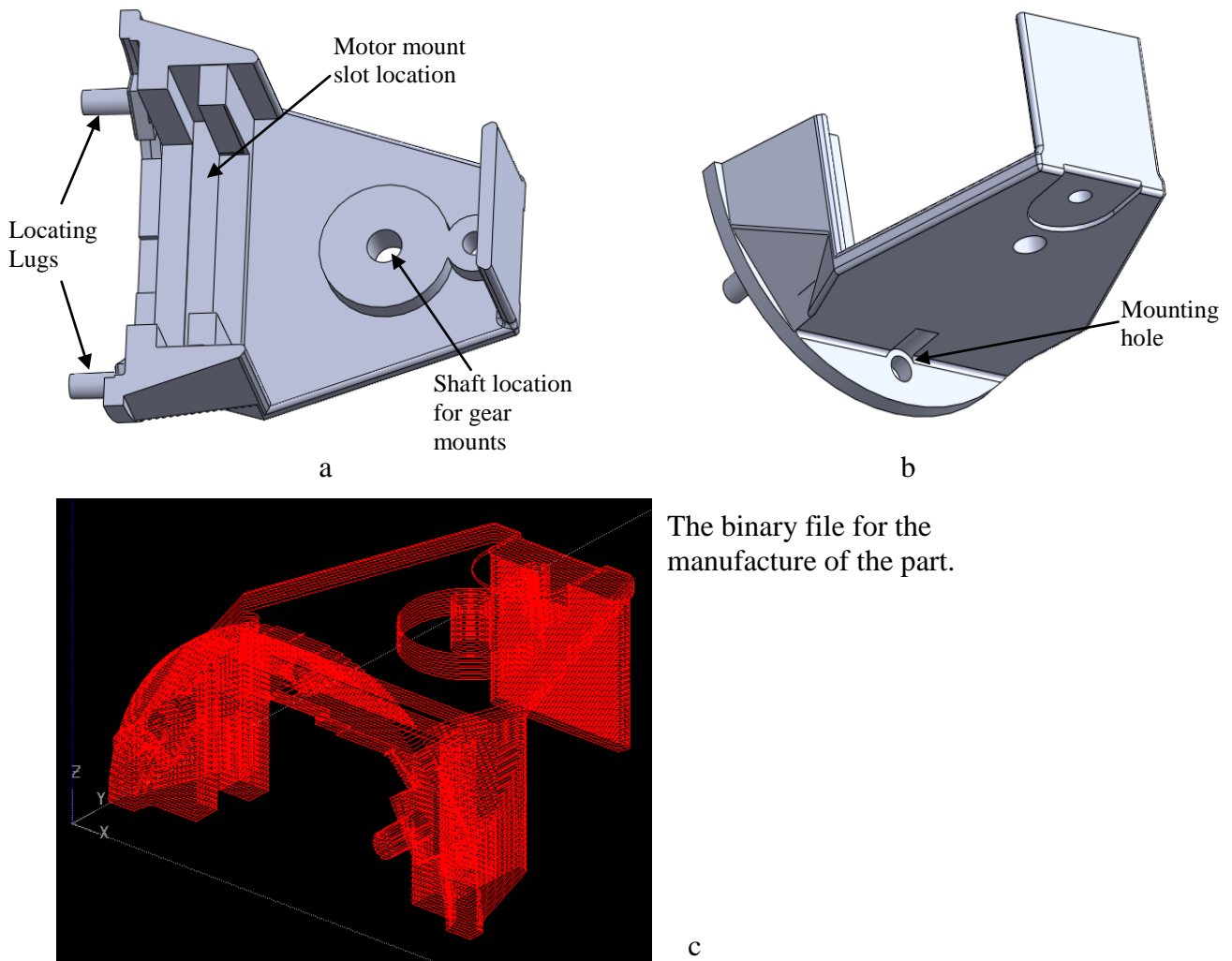


Figure 45 Gripper Housing Mount to Manipulator Main Body

The mount is designed to be secured with two mounting holes each  $180^\circ$  apart. The locating blocks are evenly distributed to allow accurate positioning of the gripper housing using locating lugs.

The gripper housing is where the gripper mechanism and the electromechanically parts that produce the transient movement are installed (the gears that will activate the gripper arms are also installed within the gripper housing). The motor mounting is located on a slot mechanism within in the gripper housing as illustrated in the schematic of Figure 46. The schematic labelled ‘a’ on Figure 46 clearly shows the slot for the motor mount. The slot is 3mm wide and 30mm in length. The hole to the right of this slot is the central location of the gears, which will rotate on the circular extruded base. In order to connect the motor to the gripper arms, a 2:1 gear ratio is used as seen in Figure 47.



The binary file for the manufacture of the part.

Figure 46 Design Schematic of Gripper Housing

A 20tooth bevel gear is attached to the motor whilst two 40tooth bevel gears are fastened to shafts that are secured to the gripper housing, the arrangement is seen in Figure 47. In order to produce a transient movement from the rotational movement of the motor, two mounting brackets have been produced as illustrated in Figure 48, in which the gripper arms attach to

the gripper mechanism to produce the grasping motion. These brackets will be positioned to rotate on the identical shaft of the 40tooth bevel gear; in addition the gear will also be attached to the bracket through three mounting holes. Once the Gripper housing is separated, all parts can be removed and quickly replaced providing efficient maintenance operation.

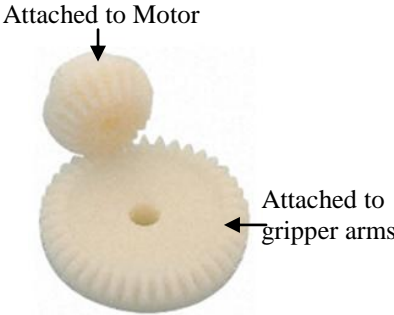
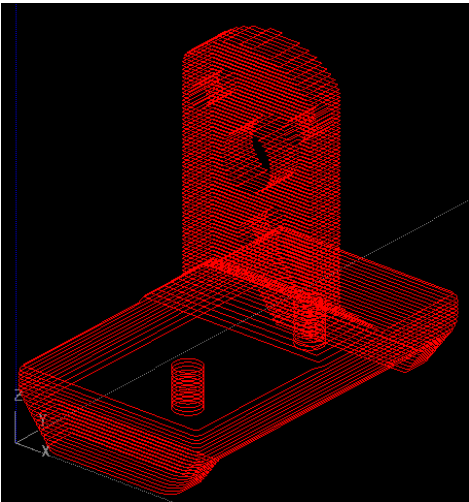
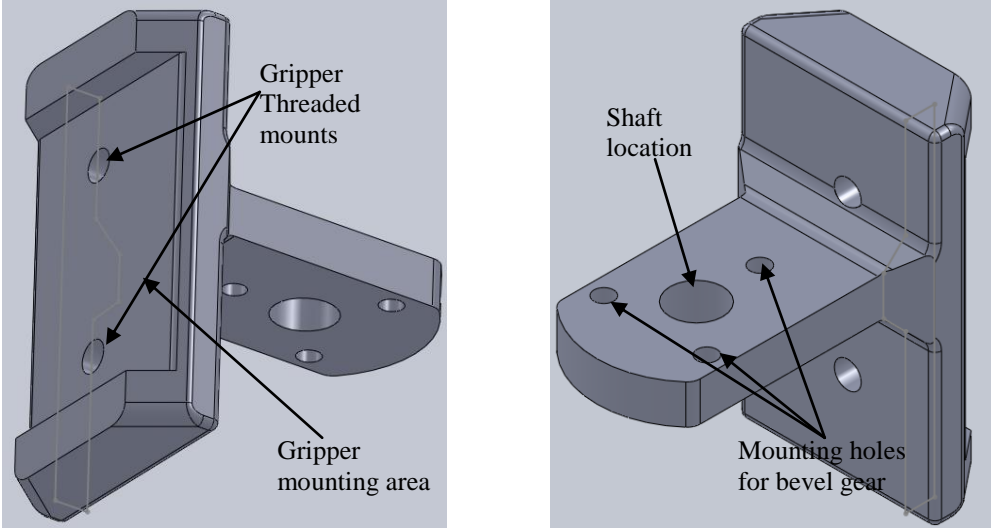


Figure 47 Bevel Gear Arrangement for Operation of Gripper Mechanism

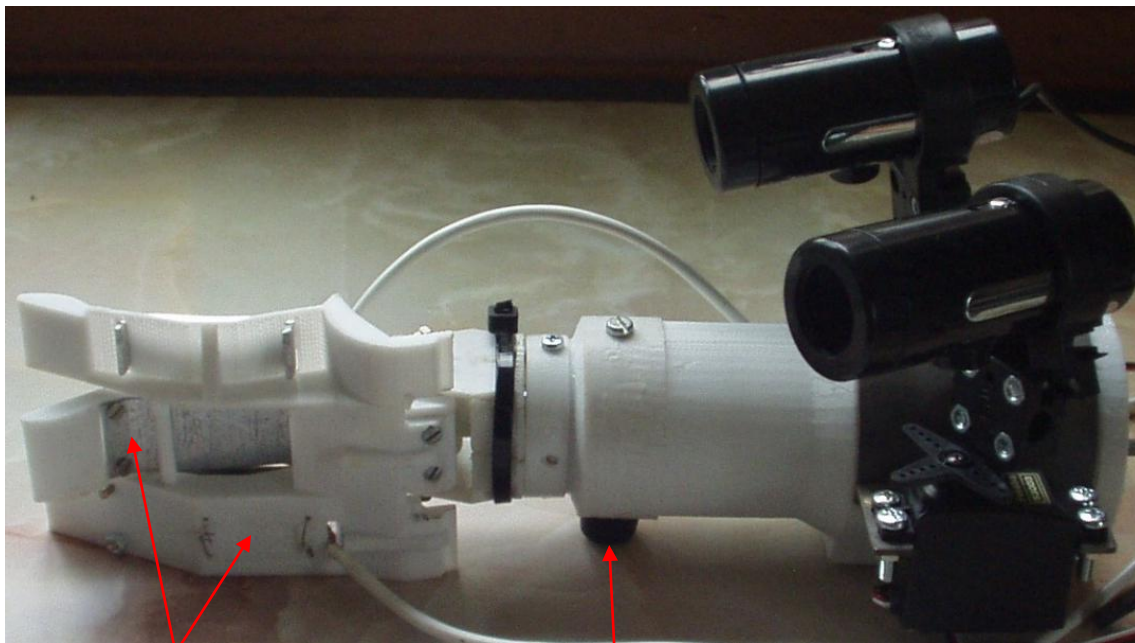


The binary file for the manufacture of the part.

Figure 48 Gripper Mounting onto Bevel Gears for Transient Operation

The replacement manipulator is floor standing with the final design of the gripper arms attached as shown in

Plate 5. The force sensors are installed in the middle and bottom fingers of the gripper mechanism and the visual servoing system is clipped to the main base. This manipulator was used to conduct functional tests on the efficiency of the grasp control algorithms, in addition to testing the PWM control of the servo motors. As can be seen by comparison to Plate 3, the identical visual servoing system and the gripper arms can be fitted to the Katana 6M180, thus providing machine dexterity in the use of the ancillary devices used to accomplish the development of the intelligent manipulator. The PC-10 manipulator proved a valuable tool in testing the main control that generates the autonomous actions; it will also provide a learning tool for students to gain knowledge in feedback systems and mechanical design.



The two finger that house the force sensor electronics

Additional rubber foot added to life main base, once gripper arms are attached, to enable operation.

Plate 5 Manufactured Prototype of PC-10 Manipulator with Stereo Vision Attached

## Chapter 4:

### Vision System Development

In order to use a camera to control the operation of an intelligent machine such as a robot in real time, the image is required to be encoded so the information it represents can be used to realise feature information for an object within the image [32,33]. For the speed of operation to be sufficient to allow quick decisions to be made, the image from the image acquisition device (camera), is encoded onto 8-bit Red, 8-Green, 8-Blue (RGB) image and/or Hue, Saturation, Luminance (HSL) image for colour matching algorithms to identify colour patterns of the object within the image. The resulting colour image is then converted to an 8-bit (1 byte) greyscale image to obtain information such as the shape of the object within the image.

#### 4.1 Image Calibration from image acquisition

With the camera(s) being attached to the robot manipulator the field of view, working distance and resolution values constantly vary depending on where the robot arm is in 3D space [34,35]. With the manipulator and attached camera directed towards the robot's workspace as in Plate 6, perspective errors occur in the captured image with the camera being positioned in a non-vertical position onto the workspace. To correct this perspective error a calibration step is included within the vision algorithms that will, in addition to correcting this error, transfer from pixel coordinates into real world coordinates stated in millimetres (mm). The visual servoing bracket is mounted on the manipulator directed towards the object. The cameras are mounted onto servo motors that control the field of vision, so that the position of the end effector can be corrected as the manipulator manoeuvres closer to the object. The point labelled  $Id_{loc}$  is the programmed coordinate of the ideally located object on workspace, stored in the software database.

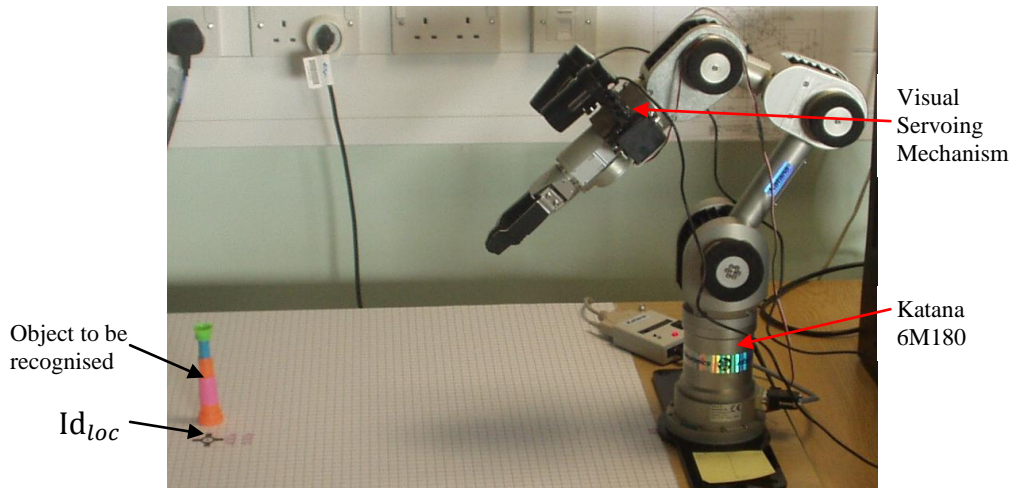


Plate 6 Position of robot pose causing perspective errors within image

A grid is produced on the image with known scale to assist counteracting the perspective errors. The grid is a finite set of points uniformly distributed over a rectangular size of 'w x h' with an increment step that first is represented by 2-Dimensional (2D) pixel coordinates  $(x,y)$ , which has an intensity value of  $v(x,y)$ , and then each pixel coordinate is manually calibrated to match real world 2-D coordinates  $Cal(x,y)$ . This distortion can be cancelled out by the use of a spatial calibration technique that maps grid positions of an image onto non grid positions [36]. (The coordinate system requires an origin, angle, and axis direction.) The algorithm is concerned with a mathematical matrix determining the corrected image, with the addition of converting the 3D image into 2D form due to the object being placed on the identical surface that the robot arm is mounted to.

Hence, the calibrated image  $Cal(x,y)$  equals the transform  $T^x$  and  $T^y$  of pixel coordinates  $(x,y)$  (selected coordinates on the captured image), throughout the 2-D image; in the new image the transformed grid points do not match the grid points of the original image, thus:-

$$Cal(x,y) = (T^x(x,y), T^y(x,y))$$

Using a grid of dots, as pixel location, within an image, the distance and moreover the real world units are entered as seen in Figure 49. The distance between A to B can be inputted, likewise B to C, C to D, and A to D. The calibration algorithm then uses the image of the grid, and the spacing between the dots in the grid to generate image  $Cal(x,y)$ : the list of pixels to real-world mappings. Although this is not a pre-prescribed method, the positive outcomes

demonstrated in Chapter 5 proved reliable. In order to improve the quality and accuracy of the calibration the number of grid position can be increased to further improve the calibrated feedback coordinates from the vision system.

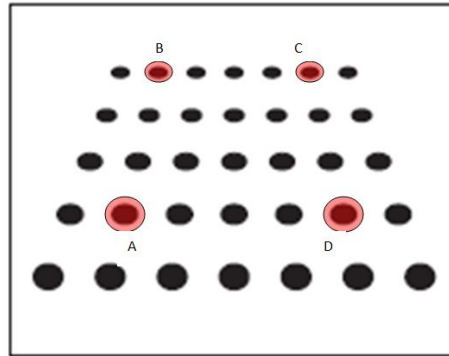


Figure 49 Example of calibration coordinate system  
Selected points on the image are selected that correspond to  
in line axis in order to counteract perspective distortion.

Due to an increase in lens distortion towards the image borders, pixels close to the centre of the image have lower error values than pixels at the image borders. Therefore, calibration of real world coordinates is focussed towards the centre of the image and away from the image borders. With the robot arm being situated in a fixed position, and the reach of the robot arm predetermined from the length of the links, the calibration coordinate system will be identical no matter where the robot arm is positioned. Therefore once the vision system is calibrated to the operation pose of the manipulator, the robot arm can be positioned anywhere as long as the same control system is used throughout the operation.

## 4.2 Colour Inspection.

The 3D colour information (RGB/HSL colour space) within an image is represented in a concise 1D form, used mainly to generate a combined histogram determining the intensity of each colour in the ROI: to allow for efficient colour matching, colour location, and more importantly colour pattern matching. A HSL conversion matrix is needed to represent the colour image in HSL space, hence:

$$X1 = \sqrt[3]{G - B}$$

$$X2 = 2R - G - B$$

$$\text{Luminance} = 0.299R + 0.587G + 0.114B = \text{greyscale value}$$

$$\text{Hue} = 256 \tan^{-1}\left(\frac{X1}{X2}\right)/(2\pi)$$

$$\text{Saturation} = 255\left(1 - \frac{3 \min(R, G, B)}{R + G + B}\right)$$

The Hue space is divided into sectors, each sector is subdivided into one part representing high saturation and the other representing low saturation values; each of these parts correspond to a colour bin and thus an element in the colour spectrum array. Each element of the colour spectrum array corresponds to a bin of colours in the HSL space; with the last two elements of the array representing black and white respectively. This can be visually seen below in Figure 50 which illustrates the separation of the colour image into a 1D representation.

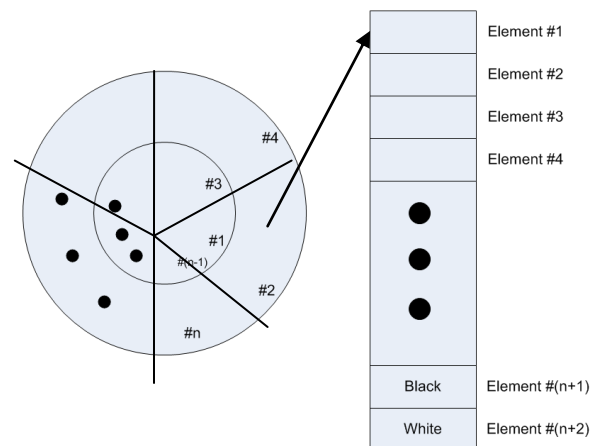


Figure 50 Hue colour Space to colour spectrum array relationship

The value of each element in the colour spectrum indicates the percentage of image pixels in each colour bin. The colour inspection algorithm counts the total number of pixels in the image in the appropriate element within the spectrum array.

The 1D array is used to produce a histogram chart to determine the colour content of the ROI. The generated histogram chart is also used to compare a template image to an acquired image.

Colour Matching is an intensity based similarity measure that quantifies which colours and how much of each colour exist in a region of an image and the difference between intensities of corresponding pixels. The algorithm compares the colour information in the entire image (or selected regions of the image) to the learned colour spectrum (template from the database), calculating a match score: higher the score - better the match, similar to the methods described in [17]. The match score is computed based on the similarity between two colour spectrums using the Manhattan distance between two vectors in a grid-like path, the algorithm is presented below:-

$$d(X, Y) = \sum_{i=1}^n |x_i - y_i|$$

Where  $n$  is the number of variables, and  $x_i$  and  $y_i$  are the values of the  $i$ th variable between the two images, at points  $X$  and  $Y$  respectively.

To express the vague knowledge about the importance of matching colour from the template image to the acquired image, a fuzzy membership weighting function is applied to each colour spectrum before computing the distance between them (the weighting function compensates for any errors that may occur during the creation of the 1-D arrays that represents the colour content of the image) [37,38]. From this a quantitative match score is acquired and a decision based on whether the colour score is high enough to engage further inspection of the workspace. A block diagram of the colour comparison between two images is shown in Figure 51.

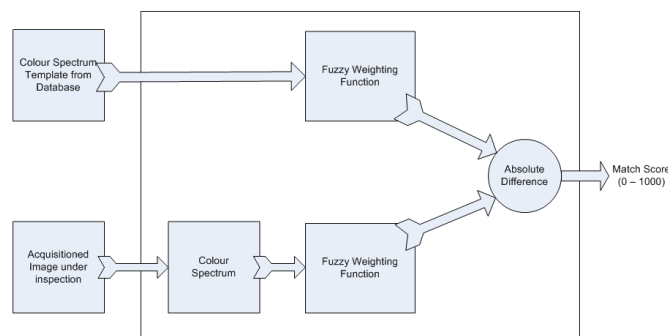


Figure 51 Comparing colour spectrums of two images  
 The fuzzy membership weighting function compensates for some errors that may occur during the binning process in the colour space.

Location of the colour match involves moving the region the size of the template (from the database) across the acquired image, from the top of the image to the bottom of the image. At each pixel location, the function computes the colour spectrum from the region of interest. The associated colour spectrum from the image acquisition is then compared to the template spectrum and the match score is generated.

$$f(u_i) = 1000 - \arg \min |Ix_i - Iy_i|$$

Where  $f(u_i)$  is the colour match score, and  $Ix_i - Iy_i$  are the intensity values of the template image and the acquired image respectively. (The value of 1000 is chosen to obtain a sizeable scale from 0 – 1000 in order to improve the location of the colour match without unnecessary delay due to increased calculations).

The procedure to attain the location of the match involves a coarse-to-fine search strategy (10% of the width and height of the template is used as the step size for the coarse search from the top left to bottom right of the image), which roughly identifies all the possible locations within the image that could be potential matches to the template information; followed by a hill climbing algorithm: performed around each match to produce accurate location coordinates of the match.

### **4.3 Isolating a specific object from an image.**

In order to detect a specific object within the image, isolation of the object features from the rest of the image is required [39]. To do this the specific object is to be masked. An image mask is an 8-bit binary (greyscale) image that is the same size of the inspection image. Pixels in the acquisitioned image are processed if corresponding pixels in an image mask have values other than zero. An image tolerance algorithm is required to make a decision of the value of the pixel within the image to ensure the image mask processing detects the Region-of-Interest (ROI) in a noisy or distorted image. Hence,

$$z = \frac{(x - y)}{v - y} \cdot 255$$

Where  $z$  is the 8-bit (unsigned) pixel value representing values between 0 and 255  
 $x$  is the 16-bit (signed) integer greyscale value representing values  
between -32,768 and +32,767  
 $y$  is the minimum Intensity value  
 $v$  is the maximum Intensity value.

The algorithm permits a tolerance on the dynamic range of pixels to be mapped to 0 or 255 respectively.

#### 4.4 8-bit greyscale image processing

To highlight details in the ROI that contain significant information 8-bit greyscale processing is used to further improve the contrast and brightness of an image by modifying the dynamic intensity of regions with poor contrast, to conduct analysis on images.

The transformation applied to transform  $S(x) - x$  represents the input grey-level intensity value – over a specified input range [rangeMin, rangeMax]:

$$S(x) = \begin{cases} \text{dynamicMin} & \text{if } x \leq \text{rangeMin} \\ f(x) & \text{if } \text{rangeMin} < x \leq \text{rangeMax} \\ \text{dynamicMax} & \text{if } x > \text{rangeMax} \end{cases}$$

where  $\text{dynamicMin} = 0$  (for 8-bit images) or the smallest initial pixel value (for 16-bit images).

$\text{dynamicMax} = 255$  (for 8-bit images) or the largest initial pixel value (for 16-bit images).

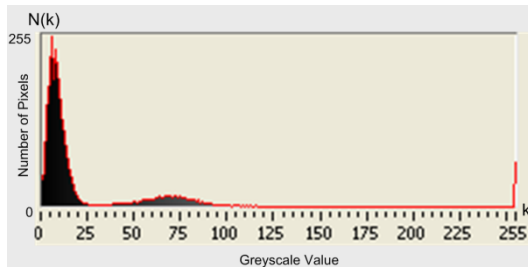
$\text{dynamicRange} = \text{dynamicMax} - \text{dynamicMin}$ .

$f(x)$  represents the new value.

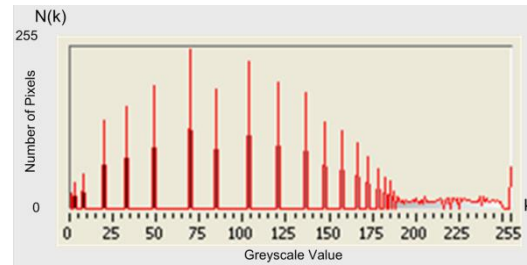
The function scales  $f(x)$  so that  $f(\text{rangeMin}) = \text{dynamicMin}$  and  $f(\text{rangeMax}) = \text{dynamicMax}$ .

For 8-bit resolution, the index element (256 elements) of the array represents an input grey level value. The value of each element indicates the output value; This value is shown on a

histogram chart as in Figure 52 that illustrates that the image is using only a small variation of the possible greyscale values that is available. With specifying a dynamic range, all greyscale levels can be utilised and enhance the features within the ROI for further processing as seen in Figure 52b.



a) Example of histogram created from pixel intensity of acquired image



b) Example of histogram created after equalization process

Figure 52 Example of how to utilise all shades of grey to highlight greater details in captured images

Filtering the greyscale image using a 2D kernel filter enhances the quality of the image by removing noise, and more importantly enhances the edge information in the image so that additional measurement can be performed. The filtered value of a pixel is a weighted combination of its original value and the values of its neighbouring pixels. The filtering operation, involves moving the kernel from leftmost and topmost pixel in the image to the rightmost and bottommost point in the image. Each central pixel becomes weighted average of its neighbours, therefore, the stronger the weight of a neighbouring pixel, the more influence it has on the new value of the central pixel, the low pass filtering of the image is described by the following algorithm:-

```

IF  $P_{(x,y)} - M > S$ 
    THEN  $P_{(x,y)} = P_{(x,y)}$ 
    ELSE  $P_{(x,y)} = M$ 
END

```

Where,  $P_{(x,y)}$  represents then intensity of pixel P with coordinates (x,y)  
M is the mean value of  $P_{(x,y)}$  and its neighbours  
and S is their standard deviation.

Given M and S, each pixel  $P_{(x,y)}$  is set to the mean value M if it falls outside the range [M-S, M+S].

#### 4.5 Manipulation of greyscale images with logic operators.

A simple method to mask, combine, and compare images is to use a logic operator function such as: AND, OR, XOR, or even using a constant to alter contrast or brightness of an image, the algorithm is described by.

$$I_p = A_p \cdot Op \cdot B_p$$

Where

- Ip is the new image value of pixel p
- Ap is the value of pixel p in image A
- Bp is the value of pixel p in image B (or a constant value)
- Op is the logic operator

Advantages of this type of image manipulation is elimination of light drifts and indeed in exceptional cases add a time delayed version of the image for comparison (ideal for motion tracking systems [39]). The logic operator produces an image in which its pixels are derived from the values of pixels with the same coordinates in other images.

For the absolute difference between two images or an image and a constant the following algorithm is used:-

$$I_p = |A_p - B_p|$$

If resulting value  $I_p$  is negative, the value is set to zero, if it is greater than 255, the value is set to 255.

#### 4.6 Greyscale Pattern and Object Matching

To strengthen the analysis from the colour pattern matching algorithm, a greyscale (8-bit) pattern matching algorithm predominantly locates the pattern of an object within an image. The pattern matching algorithm has three main tasks:-

- 1) Finding the pattern template in the image.
- 2) The orientation of the pattern in the image.
- 3) The position of the template in the image.

The algorithm uses a non-uniform sampling technique in order to describe the template. By utilising the template pixel values – or relative changes in values – the algorithm can detect the rotation of the pattern within an image. This technique reduces the redundant information and emphasises the respective feature to allow for an efficient, x-correlation implementation that can detect rotation of up-to 320°. As shown in Figure 53,  $w(x,y)$  is the template image of size  $K \times L$  within an image  $f(x,y)$  of size  $M \times N$ , where  $K \leq M$  and  $L \leq N$ . The correlation between  $w(x,y)$  and  $f(x,y)$  at a point  $(i,j)$  is given by:

$$C(i,j) = \sum_{x=0}^{L-1} \sum_{y=0}^{K-1} w(x,y)f(x+i,y+j)$$

Where  $C = x$ -correlation value  
 $i=0,1,\dots,M-1$ ,  
 $j=0,1,\dots,N-1$ , and the summation is taken over the region is the image where  $w$  and  $f$  overlap.

With the origin ‘ $f$ ’ of the processed acquisitioned image (green) being the top left corner of the image  $(0,0)$ , seen in Figure 53. The process involves moving the template (red) around the image area and computing the value  $C$  in that area. The correlation value is calculated by multiplication of each pixel of the image with the overlapping pixel in the template and then summing the results over all the pixels of the template. The maximum value of  $C$  indicates the positions where the template best matches within the acquired image.

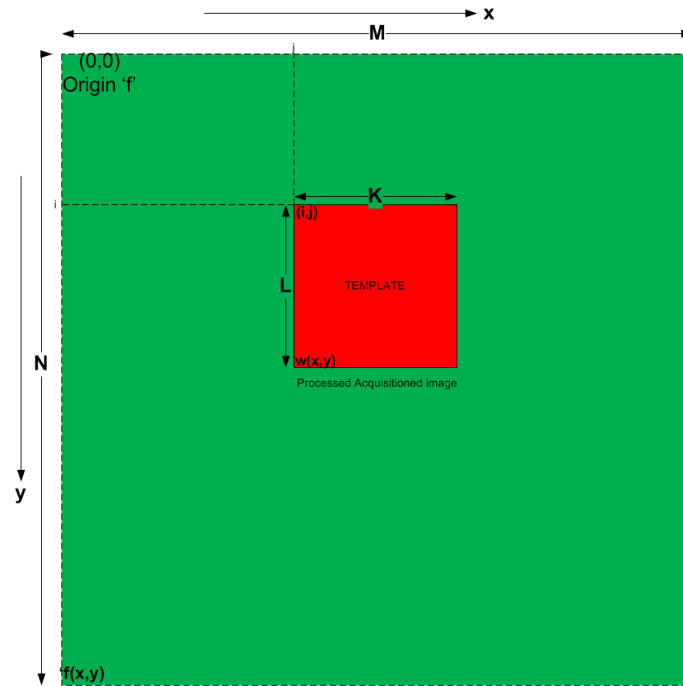


Figure 53 Greyscale Pattern Matching x-correlation Methodology

#### 4.7 Additional vision control

By combining multiple vision algorithms in order to achieve accurate detection and moreover location information, the intelligent manipulator control system can make decisions of where to move within its workspace. The accuracy and speed of these calculations is examined throughout this thesis, the main goal is to achieve accurate positional information with minimum errors to allow the manipulator to grasp and manipulate objects without the need for human intervention. Figure 54 shows the coordinate position for  $Id_{loc}$  is loaded from the database and subtracted from the new 'Cal y' distance, calculated from the image scans. The distance from the end effector to the object, measured from the image, is then used to calculate the associated adjustment in angular and distance measurements for the end effector to move to. The difference value is then used to calculate the new  $P1x$  and  $P1y$  position (refer to Figure 7). The process is repeated for the second image acquisition step until the gripper mechanism is in the position to grasp the object.

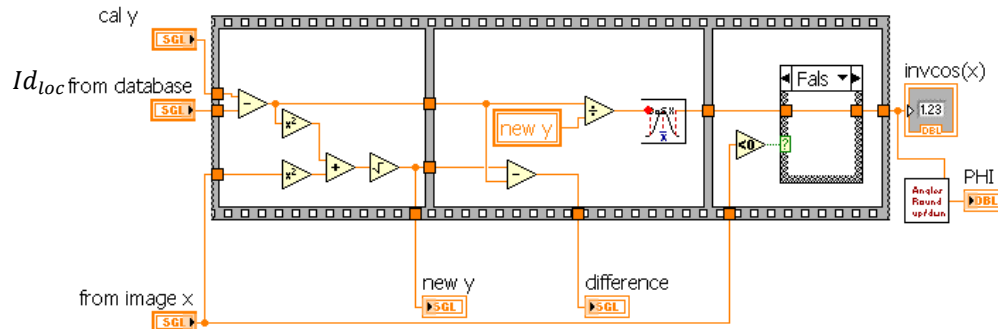


Figure 54 Calculation of new reach coordinate for manipulator The AngularRoundUp/Down.vi is used to ensure that any rounding error is resolved with an accuracy of 0.5° for each joint angle (specification taken from Katana 6M180). This sub.vi is utilised for all kinematic calculations for this reason.

The image processing stage that determines the colour content and object matching uses a three input AND gate to ensure an object has been recognised that matches a template image, the operation of the AND gate is seen in Figure 55.

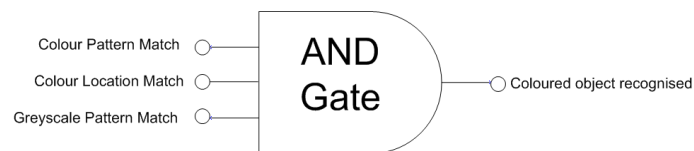


Figure 55 Object Matching Operation

The three input AND gate is used to determine the presence of a colour match in the second image acquisition scan (short scan), as a result all three algorithms have to recognise the object under inspection in the captured image, for the manipulator to move to the measure coordinates, generated from the greyscale pattern match, as discussed in Chapter 5.

## **Chapter 5**

### **Trials and Research Outcomes**

The first topic in this chapter discusses the successes of the kinematic algorithms with respect to the operation of the virtual robot, followed by the results of the robot vision system that encompasses various trials to demonstrate improvements in accuracy of the positional information gathered to control and interact with the manipulator kinematics solution.

The function of this manipulator control system is to allow accurate detection and location of an object within its own workspace, with the inclusion of an efficient design. To permit this efficiency, the virtual manipulator is design with the ability to synchronise with a real world robot arm in the calibration position, thus the calibration coordinates are read from the database and actioned. When the coordinates are reached, the database is again interrogated to receive the first image acquisition position. When the manipulator has confirmed this position has been reached, the image acquired is used to identify that an object, matching an object template within the image database, is located within the workspace and generates positional coordinates for the object. As a result of potential positional inaccuracies with this long distance scan, a second image acquisition position is required, which requires the end effector to be positioned approximately 200mm ( $x_0$ ) distance away from the detected object to enable the calibration of the acquisitioned image to be a constant: thus every cycle undertaken by the robot arm, the image calibration for the short scan will remain unchanged. Once the manipulator has confirmed the new position has been reached, the colour information on the object is considered and any positional error from the first scan is corrected. The manipulator then moves in to grasp the object, and transports the object to the ‘drop-off’ location ensuring, in this instance, the manipulator is positioned horizontal to the workspace (normal to  $x_0$ ). The manipulator movement/commissioning information is viewed by LabView frames shown in appendix C.

#### **5.1 Virtual Robot and Kinematic Solution.**

As described in Chapter 2, the robot manipulator and associated workspace is reproduced virtually. In Figure 56 the virtual workspace (large white rectangle) has numerous coloured

location points that the manipulator will transport the grasped object to (bins that the object will be dropped into). The decision of where the manipulator will move to is based on the information from the database in conjunction with the information received from the vision system. The  $Id_{loc}$  (the ideal object location) is shown by the black square, directly underneath the virtual end effector in Figure 56, the Figure also illustrates the initial starting position of the virtual robot.

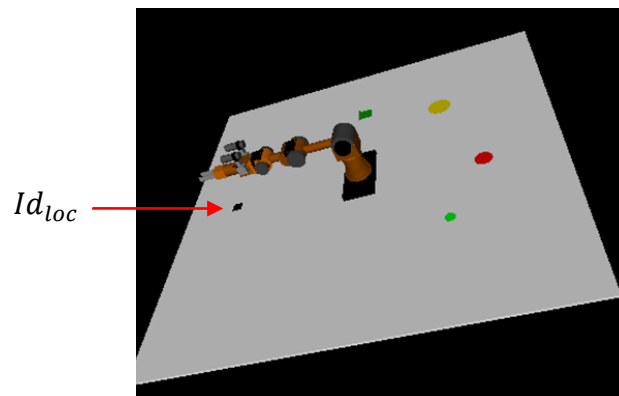


Figure 56 The Virtual Robot and Associated Workspace

After the calibration routine has completed, the manipulator manoeuvres to the first image acquisition position. The first scan coordinates are stored in the excel database as the end position and orientation of the end effector. Using Euler's distance formula, the kinematics calculates the quickest route in order to achieve the end position for each joint. The posture for the manipulator for this scan is seen in Figure 57, which compares the joint positions of the virtual robot arm to that of the Katana 6M180.



Figure 57 Real World Manipulator Position to Virtual Manipulator Position

With the manipulator in this pose, the vision system, once an object has been recognised, will supply the new coordinate location for the end effector; the manipulator will remain in this position until a positive object match has been determined. The excel database is interrogated to determine the ideal location and orientation of the end effector within 3D space, this information is used with the new values of 'x' (that effects joint 0) and 'y' (end effector reach) from the vision system. The manipulator will then make a decision on the 3D location for the second image acquisition position (short scan) as seen in Figure 58: to obtain more information about the object under inspection.

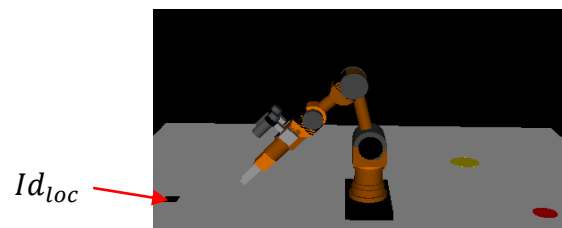
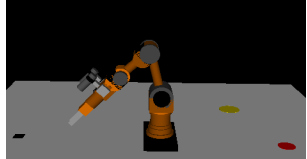
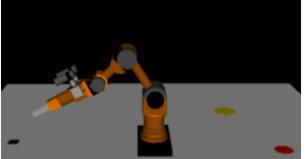
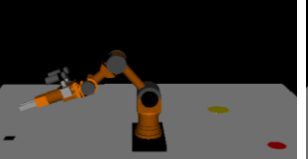
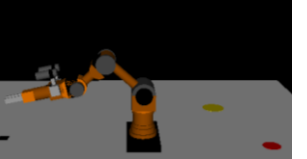
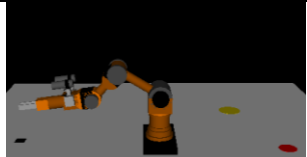
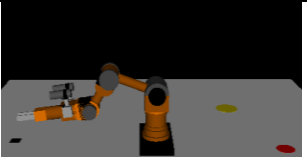
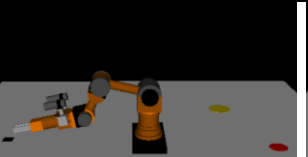


Figure 58 Position of Manipulator for the Short Image Acquisition Scan

In the position illustrated in Figure 58, the end effector is positioned 200mm ( $\pm 2$ mm) horizontal ( $x_0$ ) distance away from the object under inspection to permit an enhanced image to be to determine greater details of the object properties/characteristics, such as colour location. The new coordinates for the end effector is calculated with the same procedure used for the initial image scan and any positional error is corrected, so the finish position of the end effector, is situated just in-front and in-line with the object on the workspace. In this position the end effector is only 77mm above the workspace, hence, the kinematics algorithm is informed of the close proximity of the workspace and alters the solution to ensure no collision occurs. The movement from the short scan is shown in Table 5.

Table 5 Manipulator Maneuvres from Short Scan to Object Under Inspection

 <pre> nearest Encoder 0 18160 nearest Encoder 1 -2061 nearest Encoder 2 47247 nearest Encoder 3 6145 nearest Encoder 4 15269 nearest Encoder 5 30000 x position y position Z position 362.236 75.3011 6.322E </pre>	 <pre> nearest Encoder 0 18160 nearest Encoder 1 2450 nearest Encoder 2 41390 nearest Encoder 3 12332 nearest Encoder 4 15269 nearest Encoder 5 30000 x position y position Z position 480.727 134.195 8.3911 </pre>	 <pre> nearest Encoder 0 18160 nearest Encoder 1 4156 nearest Encoder 2 39174 nearest Encoder 3 14612 nearest Encoder 4 15269 nearest Encoder 5 30000 x position y position Z position 515.152 155.636 8.9920 </pre>	 <pre> nearest Encoder 0 18160 nearest Encoder 1 6350 nearest Encoder 2 36325 nearest Encoder 3 17542 nearest Encoder 4 15269 nearest Encoder 5 30000 x position y position Z position 550.312 182.326 9.6057 </pre>
 <pre> nearest Encoder 0 18160 nearest Encoder 1 8789 nearest Encoder 2 34900 nearest Encoder 3 20799 nearest Encoder 4 15269 nearest Encoder 5 30000 x position y position Z position 564.719 170.742 9.8572 </pre>	 <pre> nearest Encoder 0 18160 nearest Encoder 1 11592 nearest Encoder 2 34900 nearest Encoder 3 24543 nearest Encoder 4 15269 nearest Encoder 5 30000 x position y position Z position 559.097 120.128 9.7590 </pre>	 <pre> nearest Encoder 0 18160 nearest Encoder 1 13299 nearest Encoder 2 34900 nearest Encoder 3 25357 nearest Encoder 4 15269 nearest Encoder 5 30000 x position y position Z position 546.81 65.9811 9.5446 </pre>	 <pre> nearest Encoder 0 18160 nearest Encoder 1 14762 nearest Encoder 2 32051 nearest Encoder 3 23892 nearest Encoder 4 15269 nearest Encoder 5 30000 x position y position Z position 555.289 41.4944 9.6926 </pre>

As seen in Table 5, from the short scan position the manipulator makes a decision to position joint 3 of the manipulator before fully engaging the other joints. The manipulator realises that moving all joint simultaneously at the same speed could cause a hazardous condition with all likelihood that the end effector will come in contact with the workspace; therefore Euler's distance calculation is overridden by the top software loop of the algorithm on page 25, to ensure the manipulator avoids a hazardous condition.

With the object grasped, even with the addition of the full algorithm(on page 25), the first attempt for the manipulator to move to the desired location failed, the manipulator ignored the height of the end effector and began to move all joints to the desired end position and pose, as seen in Figure 59.

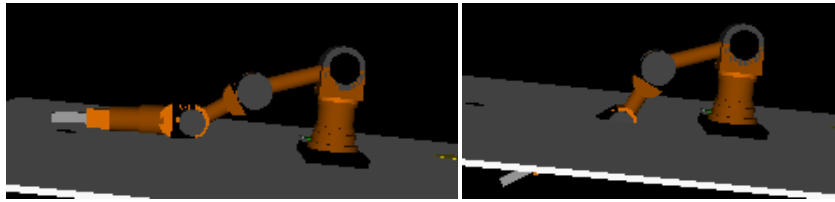


Figure 59 Manipulator Movement after Grasping Object - First Trial

This hazardous operation occurred due to one of the ‘drop-off’ locations: the joints of the robot became compact, as a result the dual calculations used for joint  $\theta_1$  and  $\theta_2$  did not match; thus the kinematics of the robot arm became unresolved and the manipulator became undecided causing the end effector to collide with the workspace (shown going through the workspace on the right hand of Figure 59). In addition, once the object has been grasped, joint3 of the manipulator, due to being programmed for manipulating liquids, should position itself in a horizontal position to the workspace irrespective of the location of other joints on the robot arm. The solution was to add an additional algorithm that interoperates with the two other joints (described on page 26) and to increase the height of the end effector before continuing calculations to the ‘drop-off’ location (seen as ‘pick-up’ in Table 1). This additional sample placed in the map plan was the only additional coordinate point added to the operation of the intelligent manipulator to efficiently complete its task. As a result the complication of several sample points in the map plan is removed, therefore the database interrogated by the main control remains simple to amend and understand. Only the minimum operation joint coordinates in addition to the ideal locations of the objects and ‘drop-off’ locations are entered, thus the intelligent manipulator performs mathematical calculations with calibrated coordinates returned from the vision system. The values from the database to ensure the end effector is directed towards the recognised object. Thus the database becomes easy to maintain and understand and specialist training to add additional tasks is kept to a minimum.

All the commissioning information includes the success of the manipulator in deciding which coloured object is present and where it is located on the robot's workspace, along with how the manipulator operates to drop the object in their respective bin locations, are seen in Appendix C.

## 5.2 Image Processing and Object Recognition.

Images to be used for the research are captured with the object manually moved around the workspace. The initial manipulator pose of the first image capture is directly related to the ideal position of the object, as shown in Plate 7. The testing area is far from idyllic, lighting levels and colour rendering in the area are constraint to those produced by fluorescent room lights as such allows for additional improvements in the design of the image algorithms for use in well-lit process areas and gloveboxes, but robots are commonly called upon to work in environments that are far from ideal. With the manipulator in this pose, considerable areas of the workspace are within focus of the electronic vision system, including the areas that would normally not be enclosed. The end effector is aimed directly towards the  $Id_{loc}$  (shown in green) and both cameras are positioned by the visual servoing system, so that  $Id_{loc}$  appears in the centre of the captured image. The lighting levels, taken with the Sekonic Flashmate L-3088s, within the workspace are seen in Plate 8.

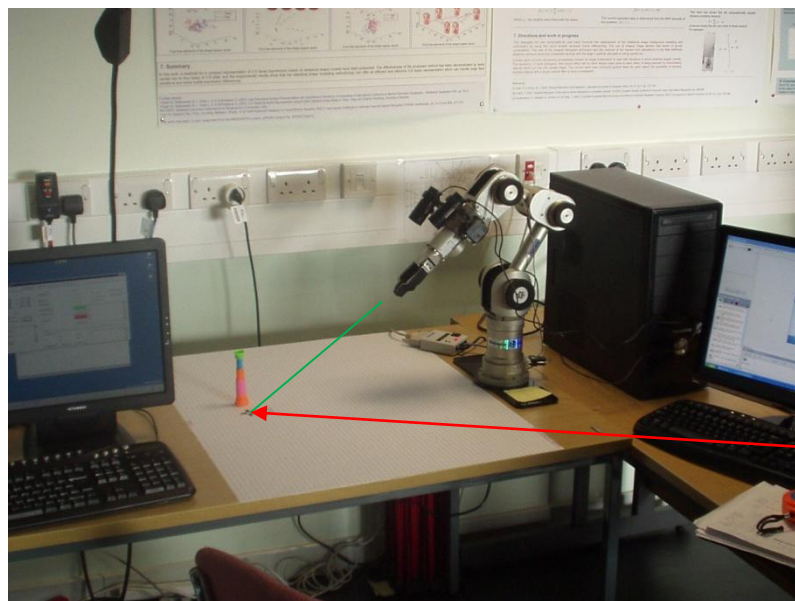


Plate 7 Initial Position of First Image Capture

The Katana robot arm is utilised to capture the images used throughout the research project. The robots arm is fastened to an office desk with the lighting being provided by the room fluorescent lighting.

The lighting levels are not at a level that is expected within a well-lit office (500Lux), as seen in Plate 8. Most of the recorded values are towards the 300Lux mark (minimum for reading) and therefore far from ideal for image capturing. This notwithstanding, clearly the object under inspection is easily identifiable with a human eye, however for object recognition, the

frequency and intensity of the colour is necessary to determine the content within the image. The image processing algorithms are used to determine the difference between three identically shaped objects. Each of these objects have identical colours, but the region of these colours within the object vary.

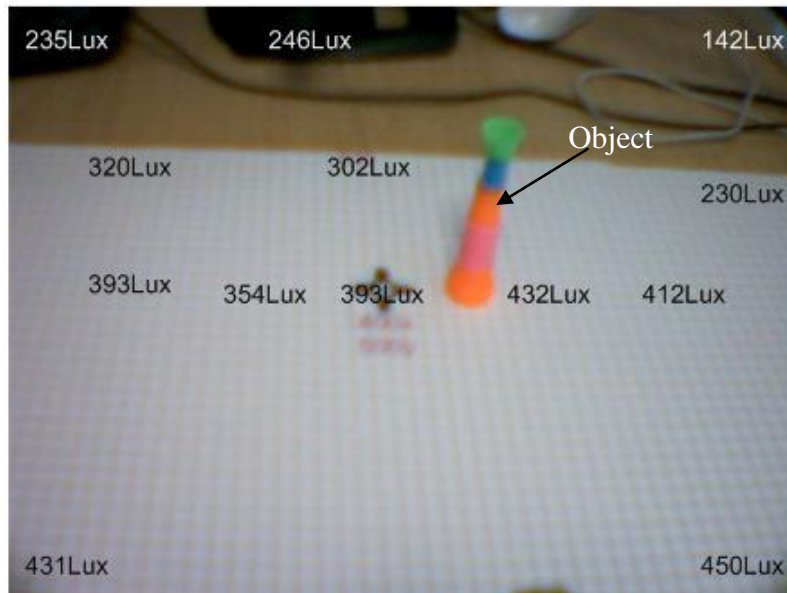
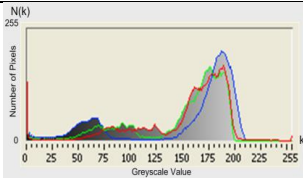
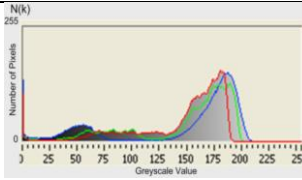
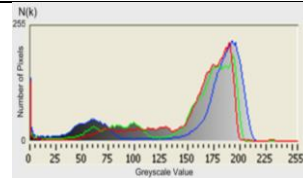
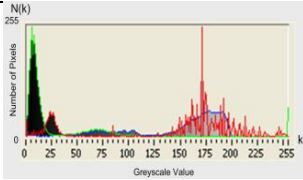
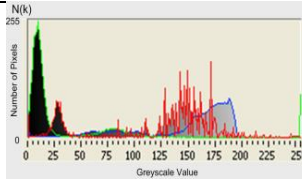
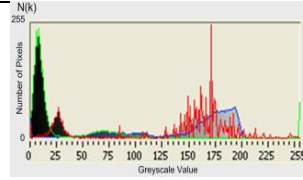


Plate 8 Lighting Levels Upon Robots Workspace During Image Capture  
The readings external to the robots workspace produce low lux readings due to the combination of light positions and shadows caused by the computer monitor. The object illustrated is situated in a location known throughout this chapter as the template location.

The initial inspection is conducted with the object in one location, known as the template location. This template location is used for fine tuning the vision algorithms, which are then hardened for the object appearing within different locations within the robots workspace. Table 6 describes the intensity values of the captured image with a histogram chart. The image is converted into an 8-bit representation for each colour, of values from 0 to 255 ( $2^8$ ). By comparing the histograms (a, b and c) in Table 6, with Plate 7 and Plate 8 there is considerable amount of grey and brown within the captured image, hence the number of pixels are towards the 130-215 intensity region. Although there is modest difference in the number of pixels for each object in this region, careful analysis does reveal that the number of identified pixels can be correlated to the different tapered sections of the objects within images. Hence the object with the greater orange content (PBOG) shown in 'c' has the

highest number of pixels identified in the red region. The GBOPO object shown in ‘a’, although the orange content is situated in two sector of the object, the amount of visible orange is less than in the PBOG, hence the number of identified pixels is reduced. The POBG object shown in ‘b’ has only a limited orange content, thus the number of identified pixels is considerably less than the other two objects. Likewise the HSL content also illustrates poor lightness/contrast of the captured image but also indicates the dominance of the blue and red wavelength content in both GBOPO ‘d’ and PBOG ‘f’ objects showing peaks at the 175 intensity region, whilst the POBG object shown in ‘e’ illustrates no colour sectors in dominance but shows an increase in the cyan content.

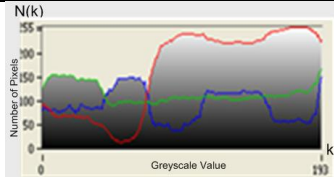
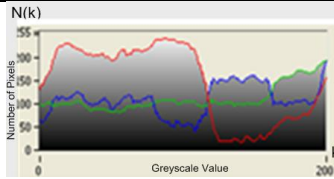
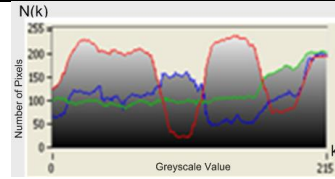
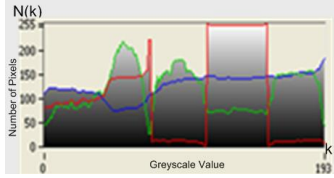
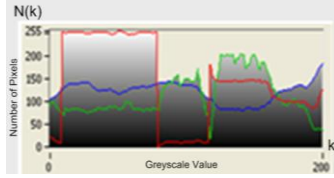
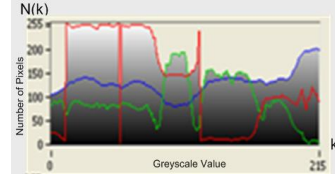
Table 6 Image Histograms for all Objects in the Image - Template Position illustrating both the RGB and HSL Histograms can be used describe the scene within an image.

	<u>Green Blue Orange Pink</u> <u>Orange</u>	<u>Pink Orange Blue Green</u>	<u>Pink Blue Orange Green</u>
<u>RGB content</u>	 <p>(a)</p>	 <p>(b)</p>	 <p>(c)</p>
<u>HSL content</u> Red – Hue Green – Saturation Blue - Luminance	 <p>(d)</p>	 <p>(e)</p>	 <p>(f)</p>

With all the objects comprising multi-coloured characteristics, discerning the specific differences between each object is required. The intensity values cannot be easily distinguished between each sample as pixel values (0-255) are approximate for each and are concentrated on the entire image. Hence, by confining the ROI specifically on the object, more details of the colour content of each image was realised as seen in Table 7. Consider the RGB content of all the objects, the GBOPO object distinctly illustrates a strong orange content (90-193) on the object, when compared with the physical object the two dominant colours sectors are orange and pink. The histogram also identifies the green (7-47) and blue (47-90) content, hence by comparing the object to the histogram, from top of the object (0) to bottom of the object (193) the colour content in the histogram fully describes the make-up of

the physical object. Closely examining the histogram in ‘c’ the blue sector of the object is described at (84-117), when the number of pixels describing the red content is reduced significantly, this change is also clarifies the blue plane being position the furthest away from the red plane in RGB inspection plane. In the HSL content, the pink sector of the object is described by the peak in hue values in the histograms, the green sector of the object is described by average hue content, orange described by low hue content.

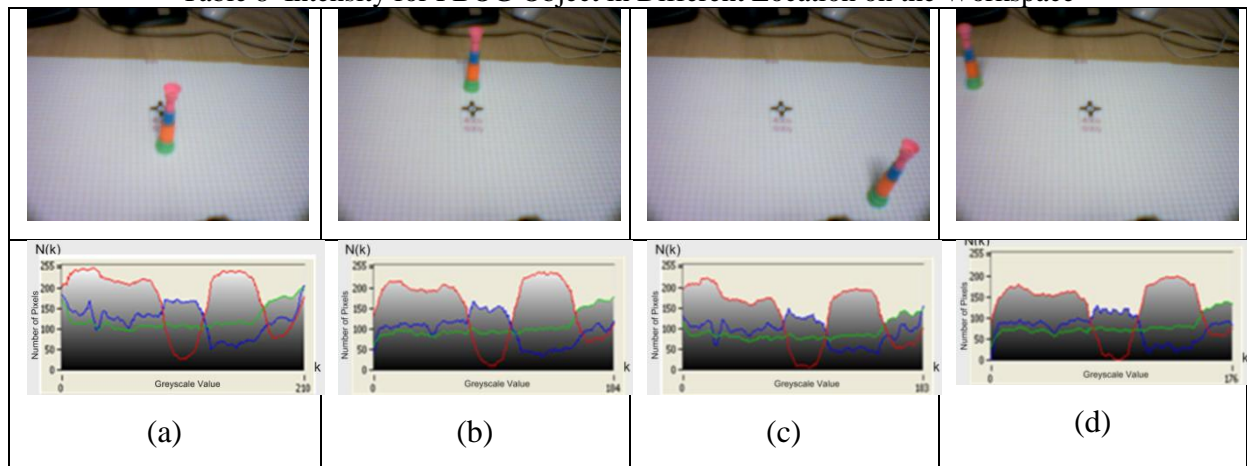
Table 7 Image Intensity for Objects - Template Position

	<u>Green Blue Orange Pink</u> <u>Orange</u>	<u>Pink Orange Blue Green</u>	<u>Pink Blue Orange Green</u>
<u>RGB</u> <u>content</u>	 <p>(a)</p>	 <p>(b)</p>	 <p>(c)</p>
<u>HSL content</u> Red – Hue Green – Saturation Blue – Luminance	 <p>(d)</p>	 <p>(e)</p>	 <p>(f)</p>

With the object in-line with the focal lens of the camera as in Table 8a and b, only scale-able differences in the number of pixels that describe the colour content of the object is seen, however the characteristics of the object can still be deciphered from the histogram charts. When the object appears offset from the focal point of the camera lens as in ‘c’ and ‘d’, this characteristic changes, the colour sectors of the object will appear to include less colour content in each sector due to the perspective distortion effects and the distance away from the camera lens, as seen by comparing histograms ‘a and b’ with ‘c and d’. The histograms illustrate considerable differences in describing the colour content of the object with the orange sector in dominance as in ‘b’ and ‘d’, compared with the two that are closer to the camera lens showing the pink sector in dominance, as it is the number of pixels that describes the object, this difference in describing the content will cause detection issues. As seen in ‘c’, an additional issue of the object creating a shadow within the image could affect the accuracy of the object location algorithm(s). When attempting to decipher between objects of

similar colour content this variation is unacceptable and will cause considerable error in recognition. This variation of light intensity and significant colour detection differences are an unacceptable quantity to be used for colour detection, as there is a possibility of a critical error in functionality of transporting the detected object to the wrong location. Hence, from this long distance image capture position, there are only two interests, one to identify that a recognised shape object is present within the workspace and second to calculate the coordinates of the object.

Table 8 Intensity for PBOG Object in Different Location on the Workspace



### 5.2.1 Initial image processing for object recognition algorithm - long scan position

As with the research conducted by Bell and Wilson in [12], to counteract the perspective distortion, a spatial calibration algorithm was utilised that will also convert pixel coordinates to real world coordinates used for the positioning of the end of the end-effector. A combination of extracting the blue pane from the RGB image then performing arithmetic and logical operations on the 8-bit greyscale image for correction of image backgrounds to eliminate light drifts is actioned. In addition, altering contrast and brightness in an attempt to counteract the differences in colour between the objects under inspection, and highlight the changes of pixel intensity within the workspace. The software management scheme can be seen in Figure 60.

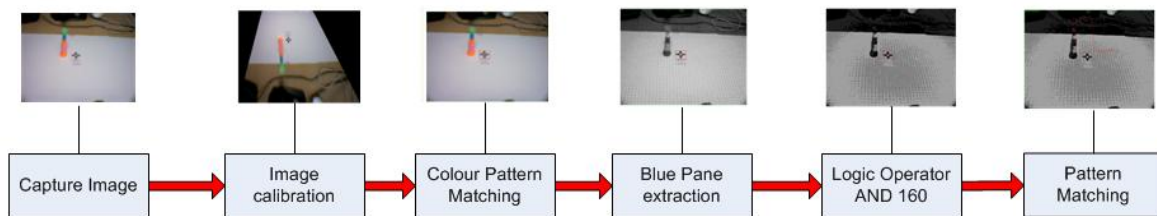


Figure 60 Long Distance Image Acquisition Algorithm Connection Diagram  
The image calibration algorithm produces the transpose matrix that is used to transfer pixel coordinates to real world coordinates and to correct the perspective error that occurs with the camera being offset to the workspace. The colour match is utilised to ensure that a recognised object is present and greyscale processing to find the location of the recognised object.

The Logic operator will ‘AND’ a constant to the blue pane image to darken the image in order to highlight the differences between the object and the robot workspace, followed by greyscale pattern matching algorithm to detect and locate the object and thus return positional coordinates of the object. From various trials it was found that a constant of 160 darkened the image to produce a distinct intensity difference between the object and the workspace, a higher constant, darkened the grid significantly on the workspace around the  $Id_{loc}$  location which would cause potential issues with the pattern matching algorithm. The resulting 3D view generated by the logic operator is shown in Figure 61. By comparison, the logic operator increases the pixel intensity of the lighter colours (white), and allows the darker colours within the image to be more distinctive, in addition to reducing the frequency content of the image. As such the robots workspace is seen as the white intensity block, with the object appearing as a cut out within the workspace area. Various intensity changes occur

through the robot workspace in-front of the object due to the lines of the grid darkening the surrounding the area. This can be visually seen by examining the histogram of both before and after the logic operator stage, seen in Table 9.

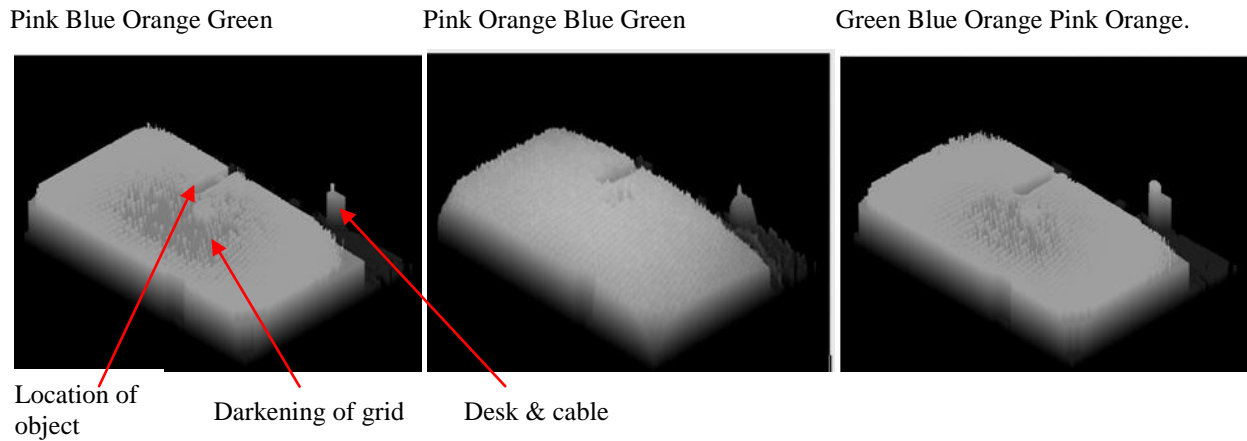
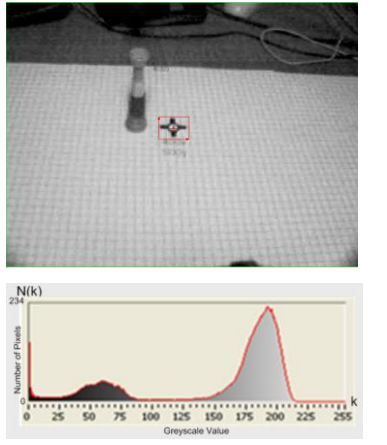
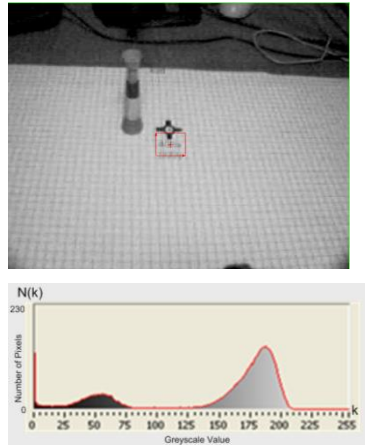
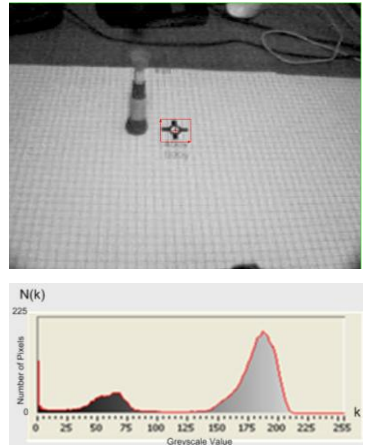
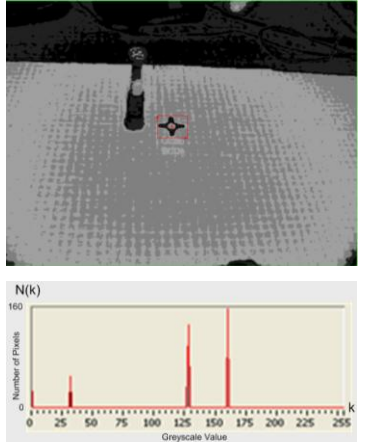
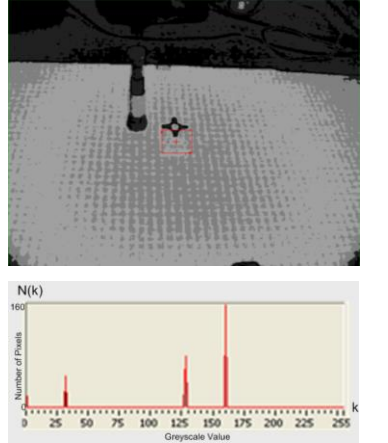
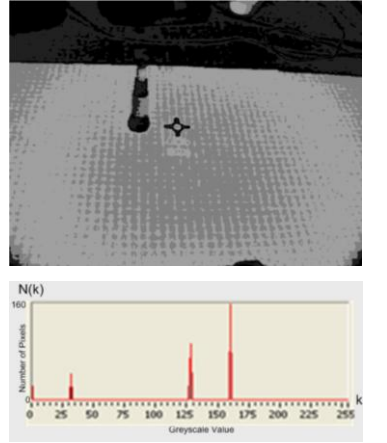


Figure 61 3D View of Image Intensity Operation with Logic Operator

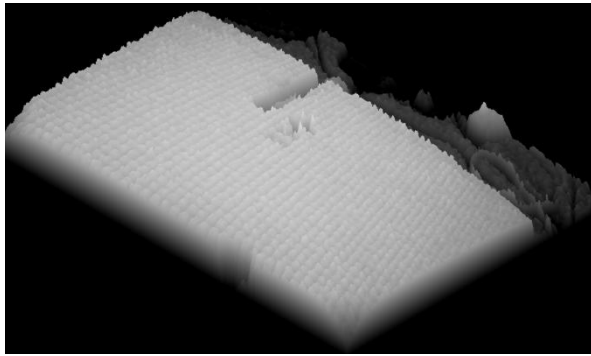
Concentrating on the top row of Table 9, each three objects attain the same grey-scale content, which varies in the number of pixels detected between the three objects. This has the advantage of allowing all the three different objects to be detected with one algorithm; however, there are still considerable variations in the greyscale content that will cause issues with pattern location. The logic operator in this case reduces the greyscale content, as seen in the histograms of the bottom row of Table 9. Three distinct peaks (at 32, 127 and 160 greyscale range) are revealed that describes the image content, as a result the greyscale range of the image is reduced considerably, hence providing increased accuracy for the pattern location algorithm: visually seen as darkening the object in relation to the workspace.

Table 9 Histogram Charts Before and After Logic Operator

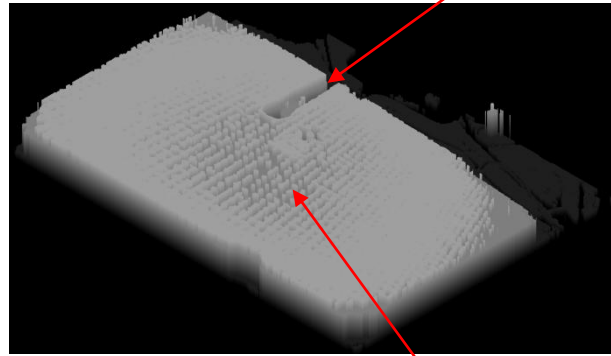
Pink Blue Orange Green	Pink Orange Blue Green	Green Blue Orange Pink Orange.
<p>After extraction of blue pane</p> 	<p>After extraction of blue pane</p> 	<p>After extraction of blue pane</p> 
<p>After logic operator</p> 	<p>After logic operator</p> 	<p>After logic operator</p> 

On the left hand side of Figure 62, the image pixel intensity changes describing the image are dramatic, causing pixels to incur values that are undesirable when locating a specific object within the image. Hence, the grey scale values describing the image is reduced (seen clearly on the North East corner of both images) highlighting the edges between the object and the workspace as can be seen on the right-hand side of Figure 62 and on the histograms of Table 9. For the object situated in different locations, only the intensity (No. of pixel) will vary with position. The pattern matching algorithm searches throughout all the robots workspace for the template image loaded from the image database, the results in Figure 63 describe the pixel location of the template within the image.

Before logic operator



After logic operator



Clear indentation of object

Grid lines causing fluctuations in intensity

Figure 62 Closer Inspection of 3D View of Image Intensity Operation with Logic Operator

The physical position of the object on the workspace is illustrated by the blue diamonds, whilst the returned coordinates (in mm) from the vision system for the objects are identified by different colours and shaped as seen in Figure 63. Only 4 samples from the PBOG object, labelled 'g', 'i', 'j', 'k', returned calibrated coordinates close to the physical location of the object: due to the associated object being used as the template to produce this algorithm, whilst one POBG object labelled 'd', returned a coordinate near to the physical position of the object. By using the Katana 6M180 robot arm, to acquire the short distance scan image acquisition in conjunction with the programmed distance away from the detected object, tolerance of the measurement system was produced. Using the coordinates of the recognised object as (0,0 (values of x, y in mm)), it was found that the returned coordinates for this long distance scan can be as much as (-60,-30) to (60,60) from the object location, for the left and right mounted cameras on the manipulator 'neck' (viewed from the rear of the robot arm), for the short distance scan position to correct any positional error to enable the end effector to successfully grasp the recognised object. With this considerable tolerance designed within the system, it is clear that the POBG object, labelled 'd' is (-18,+55.7) from actual position and therefore correctable with the short distance scan. However, there is significant number of returned samples at coordinates at  $y = 800$  to  $815$ ; It was found that the detected coordinates were external to the robots workspace, (i.e. the desk or more specifically a cable lead laid/positioned on the desk as seen in Figure 64.

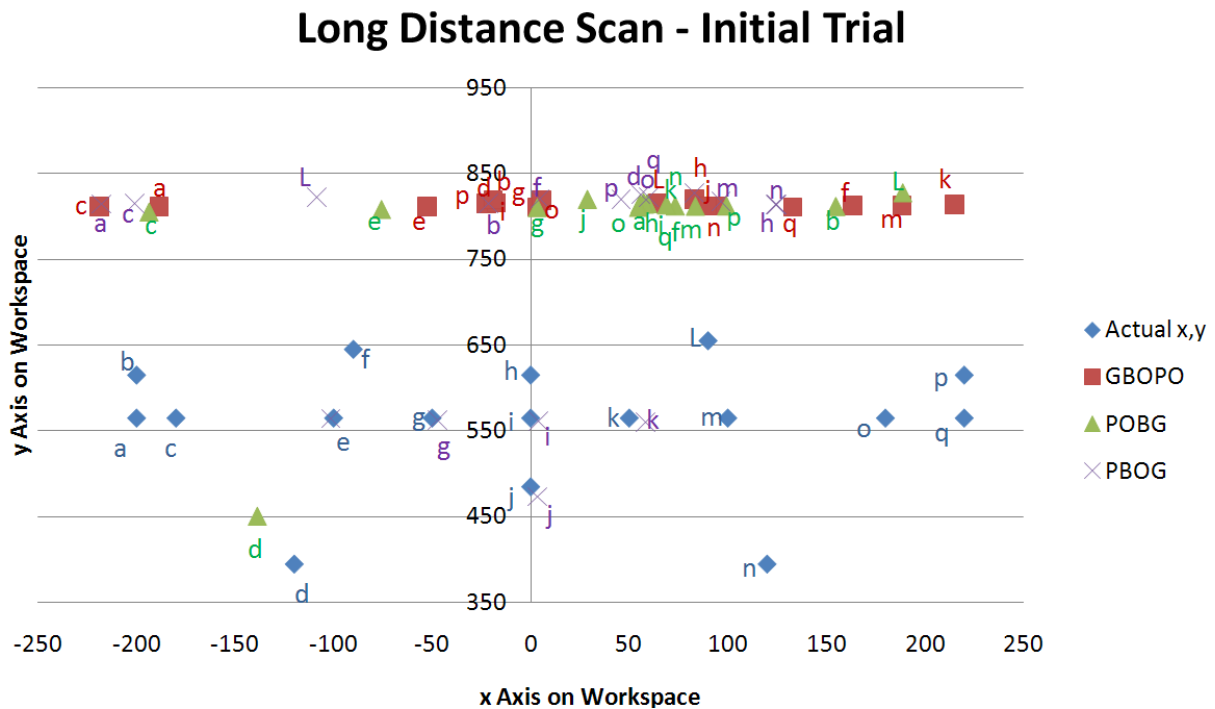


Figure 63 Measurement of Object Location Initial Trial  
 Actual x,y describes the actual object location on the workspace  
 The x axis represents distance in mm from current direction, the  
 y axis represents distance in mm from the centre of robot arm base.

The cable incurs a better match score (using greyscale pattern matching) than the actual object on the robot workspace, due to the light-dark-light area surrounding it and therefore returns the coordinates of the cable to the control system as seen in Figure 63. The ROI is confined to the maximum height of the object when situated in its furthest position on the workspace that the manipulator can reach; as a result the cable is just inside the ROI. Thus to improve the vision system, there are three issues to address:-

- 1) Increasing the accuracy of the spatial transformation on image calibration.
- 2) Further confining the ROI to concentrate on the workspace only, whilst ensuring the shape of the object is recognised.
- 3) Light intensity changes around the workspace affecting the efficacy of object detection.

Therefore, there is considerable merit on improving these algorithms in an attempt to counteract these issues.

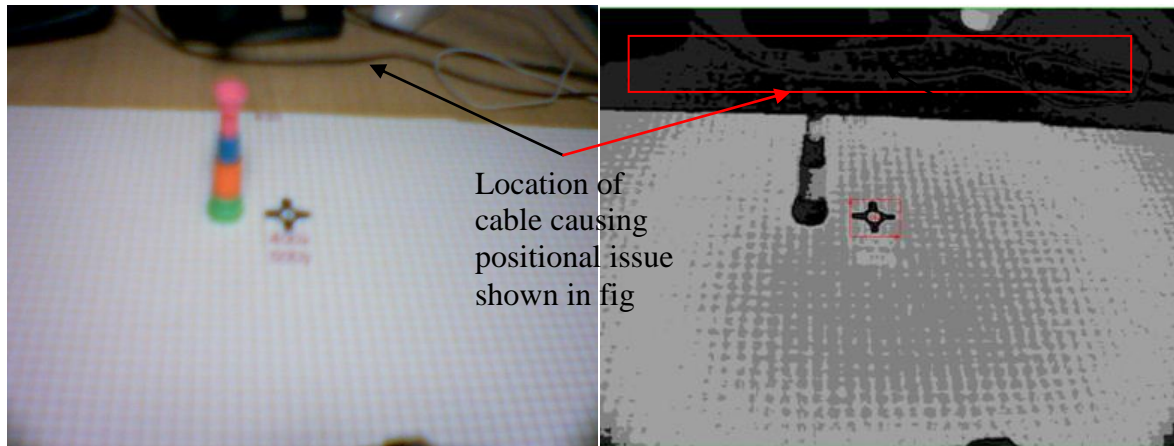


Figure 64 Location of Cable Causing Positional Issues

The time to complete the image processing is shown in Figure 65. The colour pattern matching algorithm uses 59.6% of the total time and greyscale pattern matching uses 37.6% for this particular object recognition algorithm, with the average time for inspection calculated as 46.44ms. Although the colour pattern matching algorithm is not directly used to determine the location of the object, it is useful in detecting the presence of the colour characteristics within the robots workspace, thus is extremely useful in preventing false activation of the manipulator if a foreign object arrives in the workspace. The total time taken although in processing time is considerable, to real time applications of this nature, 46.44ms will not cause considerable delay time in the manipulator deciding where to position itself in the workspace.

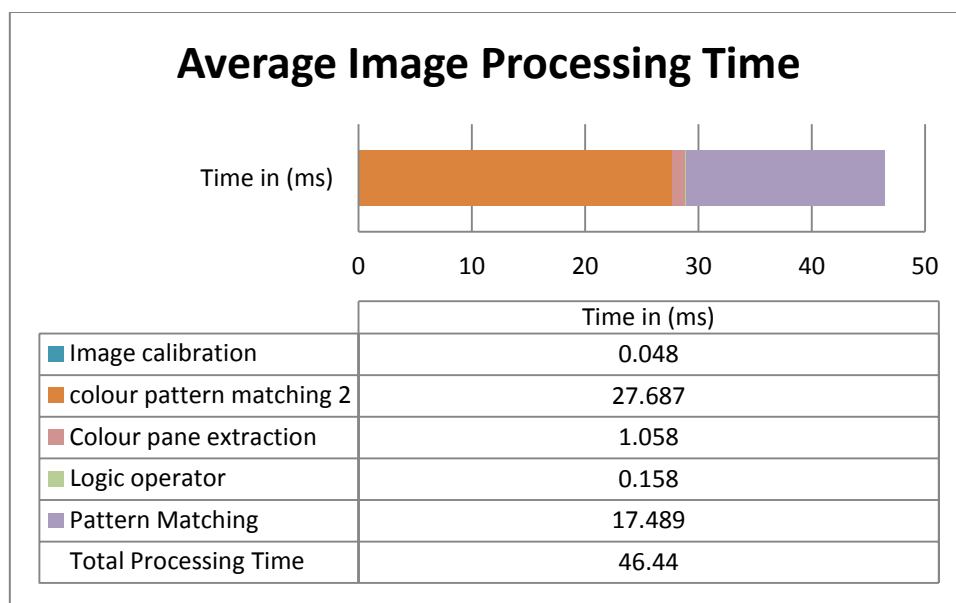


Figure 65 Design Time Frame Analysis for Initial Trial

### 5.2.2 Improvement in Long Distance image processing

Increasing the number of spatial calibration points will improve the coordinate location accuracy of the matching algorithms within the acquired images. Nine sample points are selected, instead of four used in the initial design, as shown in Figure 66. A number of spatial calibration points have been chosen towards the image borders including two directly centred onto the  $Id_{loc}$  and the object (shown in the image) to further improve the algorithms ability to correct for perspective distortion.

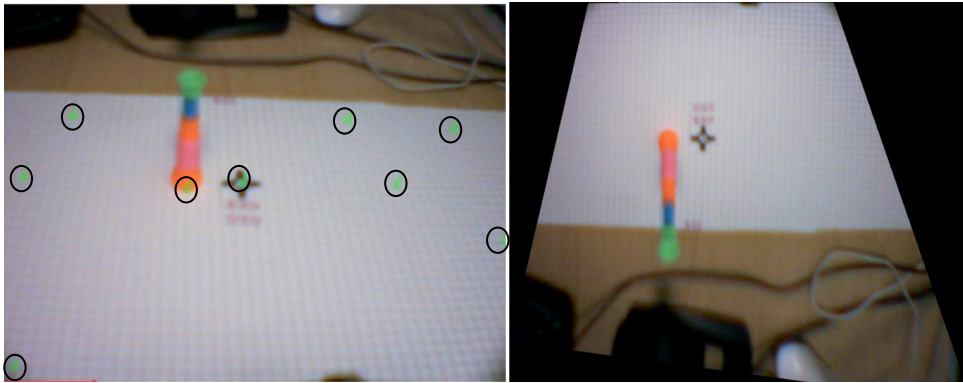


Figure 66 Increased Spatial Calibration Grid and Resultant Corrected Image

The correlation between the template and the image with greyscale pattern matching is sensitive to amplitude and light changes and therefore can give results that are not expected i.e. detection of a template within an image where the object is not positioned – or be it with a low match score (as seen in the previous trial). This will cause values of  $C$  to increment or decrement at a scale controlled by the intensity of image ‘ $f$ ’ (refer to page 77 for initial pattern matching algorithm). To help counteract this effect, a normalized correlation coefficient is calculated to average the intensity values of both the image and the template, as shown below:-

$$R(i, j) = \frac{\sum_{x=0}^{L-1} \sum_{y=0}^{K-1} (w(x, y) - \bar{w})(f(x+i, y+j) - \bar{f}(i, j))}{\left[ \sum_{x=0}^{L-1} \sum_{y=0}^{K-1} (w(x, y) - \bar{w})^2 \right]^{1/2} \left[ \sum_{x=0}^{L-1} \sum_{y=0}^{K-1} (f(x+i, y+j) - \bar{f}(i, j))^2 \right]^{1/2}}$$

Where  $\bar{w}$  is the average intensity of the template  $w$ .

$\bar{f}$  is the average value of ‘ $f$ ’ in the region coincident with the current location of  $w$  (see Figure 53.)

The value  $R$  lies in the range  $-1$  to  $1$  and is independent of scale changes in the intensity values of the image 'f' and template 'w'.

Counteracting the light intensity changes with this algorithm provides improved detection and thus the calibrated coordinates returned by this algorithm are used for final location of the end effector, the improved design can be seen in Figure 67. In the initial trial the workspace generated a higher intensity value than the object; hence the pattern matching was looking for a dark object on a light area. In this trial, the saturation plane is extracted from the RGB image to highlight the dark areas and darken the light areas, allowing the object to stand out on the workspace.

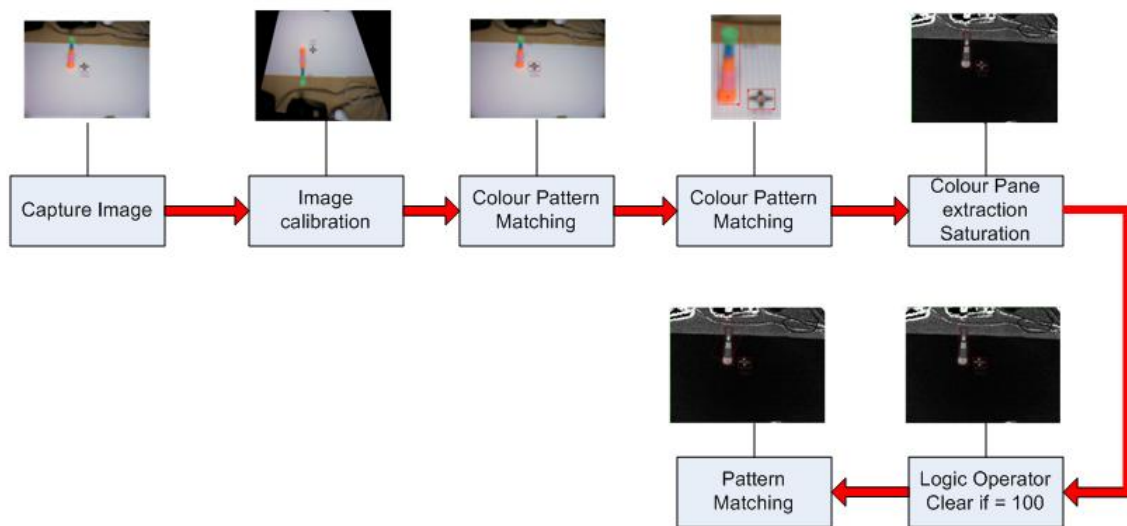
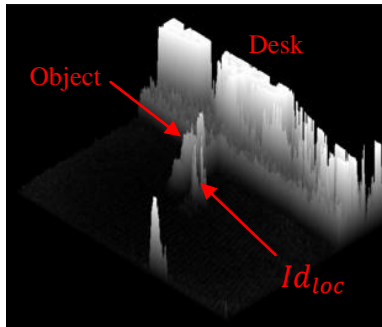
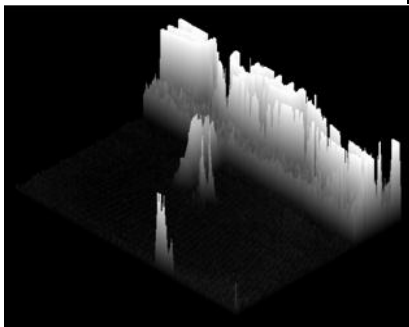
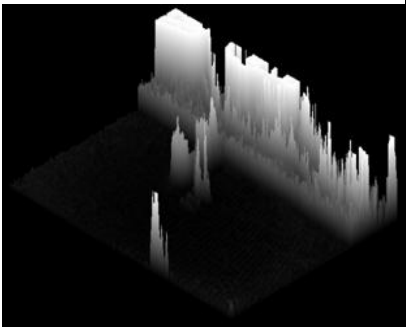


Figure 67 Long Distance Image Acquisition with Improved Calibration and Pattern Matching Connection Diagram

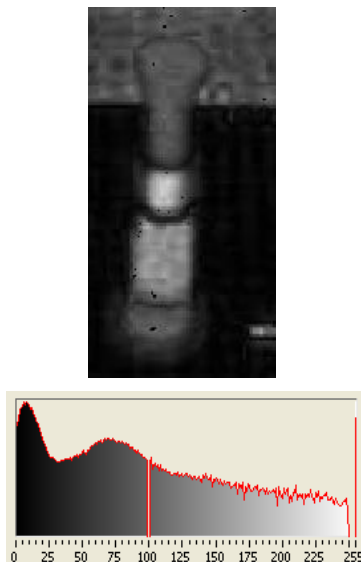
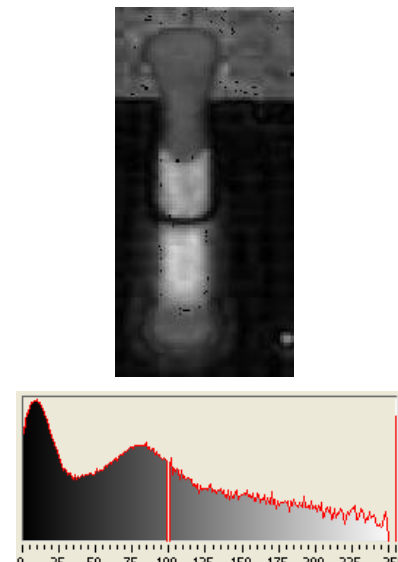
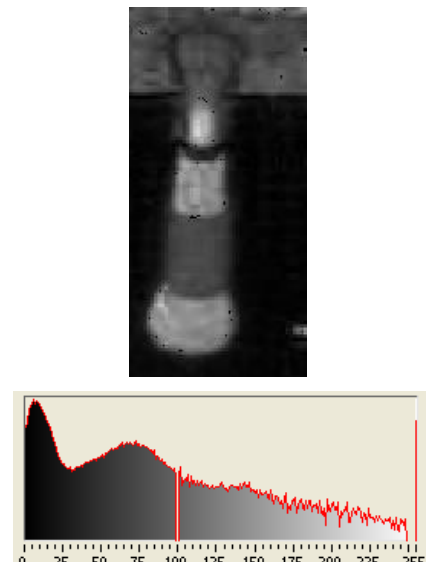
The results from this processing, shown in Table 10, four items are clearly seen. The first is the desk area external to the robots workspace (shown in the North-Eastern quadrant), second is the object clearly shown just North-West of the centre of the image; the third is  $Id_{loc}$  described by the two spikes in the centre of the image and the fourth appears at the South-Western quadrant that was found to be part of the Katana mounting bracket.

Table 10 3D View of Image Intensity Operation with Logic Operator with Improved Calibration and Pattern Matching

Pink Blue Orange Green	Pink Orange Blue Green	Green Blue Orange Pink Orange.
After Logic operator	After Logic operator	After Logic operator
		

The results shown in Table 10 and Table 11 illustrate, the ‘clear if = 100’ logic operator is used to darken and sharpen areas in the ROI by forcing pixel values to equal 0 if the pixel intensity is equal to the constant value of 100; otherwise the pixel remains the same intensity value. The content of the image remains the same, however the intensity of the pixels within the image are highlighted, as seen by the different patterns of black ‘dots’ illustrated on the objects. The histogram illustrates the operation of the logic operator.

Table 11 Histogram Charts Before and After Logic Operator with Improve Calibration and Pattern Matching Algorithm

Pink Blue Orange Green	Pink Orange Blue Green	Green Blue Orange Pink Orange.
After logic operator	After logic operator	After logic operator
		

As with the previous algorithm, the pattern matching algorithm searches throughout the ROI for the template image loaded from the image database, the results in Figure 68 illustrate the real world coordinates (mm) of the recognised template within the image. The results in this trial clearly show a significant improvement in locating the correct position of the object within the robots workspace. Some samples taken are directly on the actual coordinates of the object with only  $\pm 16\text{mm}$  positional error; this would permit the end effector of the manipulator to be directed close to the object for the second image acquisition scan with low positional error. The POBG and PBOG labelled 'c' will program the end effector to manoeuvre too far from the actual object location and thus cause a hazardous condition, with the likelihood of the end effector coming into contact with the object 'c' without expecting it; the exact opposite has occurred with the POBG 'g' coordinate that wouldn't cause the end effector to reach the actual position of the object and thus grasp nothing. In addition, three samples from 'a', one from GBOPO 'c' and one from POBG 'b' have returned coordinates of (-173,358), which would cause the manipulator to arrive in a location to grasp nothing, however, the returned coordinates are the default coordinates the vision algorithm returns when an object on the workspace has not been recognised. Thus the 'AND' gate within the control will ensure the manipulator will remain in the long distance position until a recognised object is present. The other samples have returned coordinates well within the tolerance specification but the different shades of grey that characterise the object after the logic operator for pattern matching, causes the error in return coordinates by producing a better match somewhere else on the object. However the fundamental issue with this trial is not all the objects have been recognised in the different positions on the workspace.

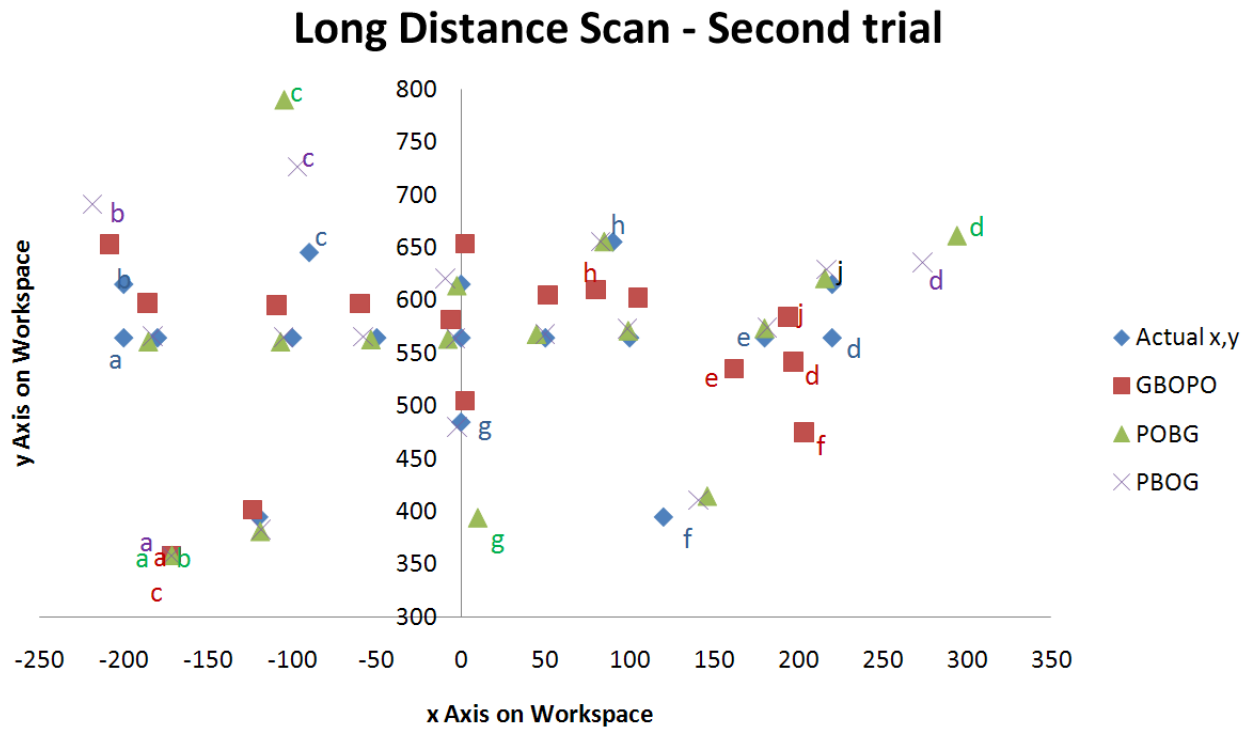


Figure 68 Measurement of Object Location with Improved Calibration and Pattern Matching

Actual x,y describes the actual object location on the workspace

The x axis represents distance in mm from current direction, the y axis represents distance in mm from the centre of robot arm base.

There is considerable time being used for the colour detection of the object: 87.8% of the total time of inspection that has increased from 46.44ms for previous trial to 139.7ms, shown in Figure 69, thus a 300.8% increase in processing time achieving a significant improvement in detection with all but eight samples permitting the manipulator to be moved into a position that would allow the second image acquisition to correct any positional error. Thus by using a sharper image and a combination of colour matching and greyscale pattern matching with confining ROI, the false detection from the area beyond the robots workspace has been significantly improved. However, further concentration is required to improve positional accuracy and to ensure the pattern matching algorithms recognises the object and returns more accurate calibrated coordinate results.

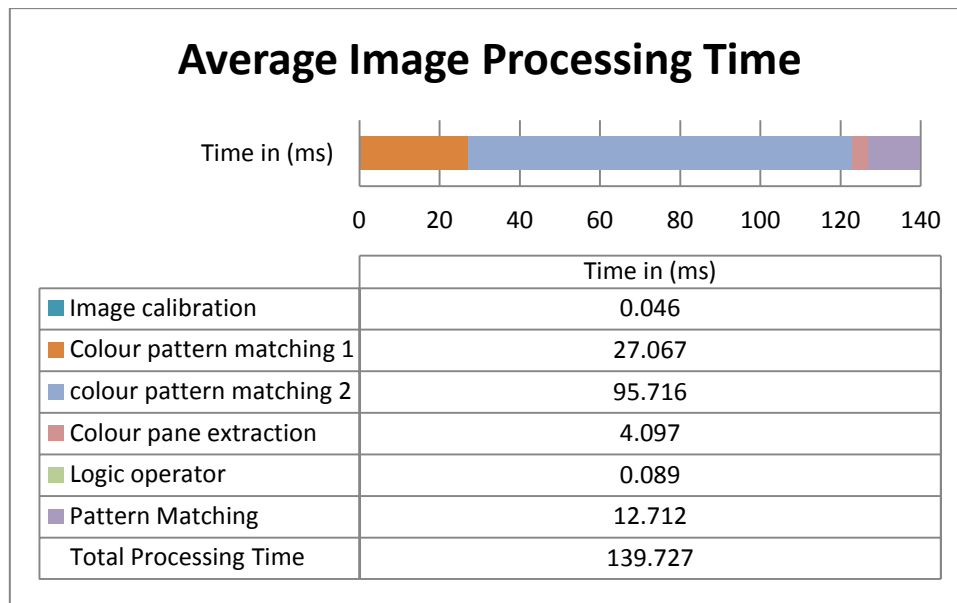


Figure 69 Time Frame Analysis with Improved Calibration and Pattern Matching Algorithm

### 5.2.3 Long Distance image processing Final Design

From the previous trials, extracting the saturation plane from the RGB image produces an image that can easily determine the location of both the  $Id_{loc}$  and the object as seen by the 3D representations of Table 10 in the previous section. From additional trials it has also become apparent that detecting a black object on a white background is considerably more successful than detecting an object with different shades of grey (varied pixel intensities). Therefore, by altering brightness of the 8-bit greyscale image to allow for greater distinction should assist in the determination of the correct shape and location of the object in the robots workspace. The final algorithm design can be seen in block form in Figure 70.

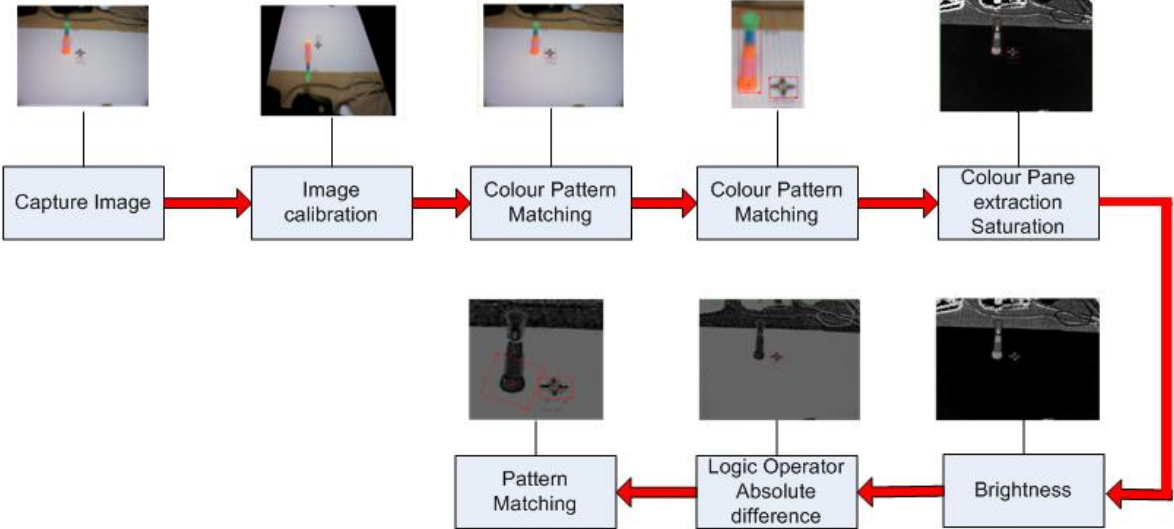
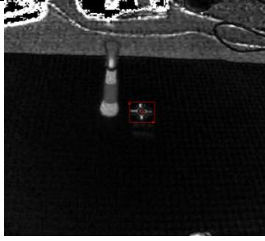
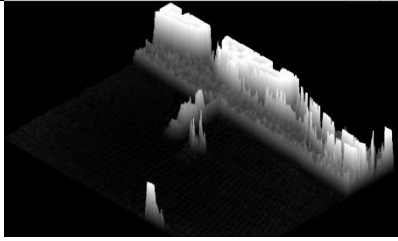
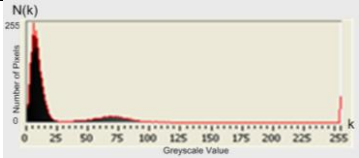
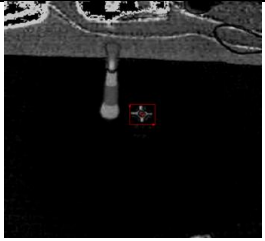
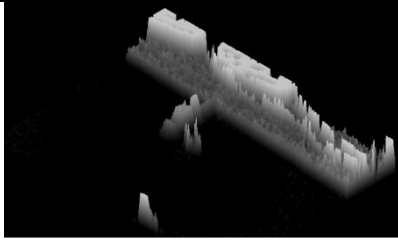
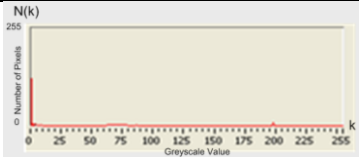


Figure 70 Long Distance Image Acquisition Final Algorithm Connection Diagram

As seen in Figure 70, the resulting image from the pane extraction is darkened to improve the distinction from the previous image processing task. The only potential issue is the dark areas on the desk are also highlighted, which could cause a repeat of the issues seen in trial one and two where pixel intensity is matched on the cable laid on the desk. The template used for object recognition is modified so part of the object is detected, which will allow further confinement of the ROI to remove the false detection from where the robots workspace meets the desk. As seen in the Table 12, the brightness control causes the image to appear darker and reduces the overall greyscale values of the entire image as seen by the histogram on the right hand side of row two in Table 12. This accentuates the ROI within the image to allow for easy inspection and removes the issue of the workspace grid darkening the area.

Table 12 Processed Image Operation with Brightness Control - Final Design

	Image	3D Representation	Histogram
After pane extraction			
After Bright-ness control			 Max value: 198 <div style="border: 1px solid black; padding: 5px; display: inline-block;">                         settings                          Brightness 72,                          Gamma 0.54,                          contrast 44.4                     </div>

The logic operator determines the absolute difference between each pixel within the image and a constant of 100, to ensure the workspace is plain grey (no grid lines) and the object incurs a similar shade of grey throughout each tapered section, as seen in Figure 71. Also illustrated in the image is the top of the object on the 2D image, appearing external to the workspace, the greyscale pattern matching is confined to the bottom  $\frac{3}{4}$  of the object to permit the ROI to concentrate on the workspace only. The colour pattern matching algorithm however, still concentrates on the whole object, thus by using the 'AND' function in the control, the colour and shape of the object is still required to achieve a positive match.



Figure 71 Effect of Processed Image with Logic Operator - Final Design

Unlike previous trials, there is a definite distinction between the workspace and the object with the advantage that there is no significant changes to the shades of grey that characterises the objects. Each coloured object produces an identical image to the one shown in Figure 71. Additional inspection results are illustrated in Figure 72. The robots workspace has greater concentration of pixel intensity compared to the object being detected. With the confinement of the ROI, the North-Eastern area of the image (the desk) does not interfere with the results and the object has a clear indentation. The workspace is described by one shade of grey (100) due to the logic operator, at a low intensity value due to the darkening effect of the brightness control, as seen on right of Figure 72.

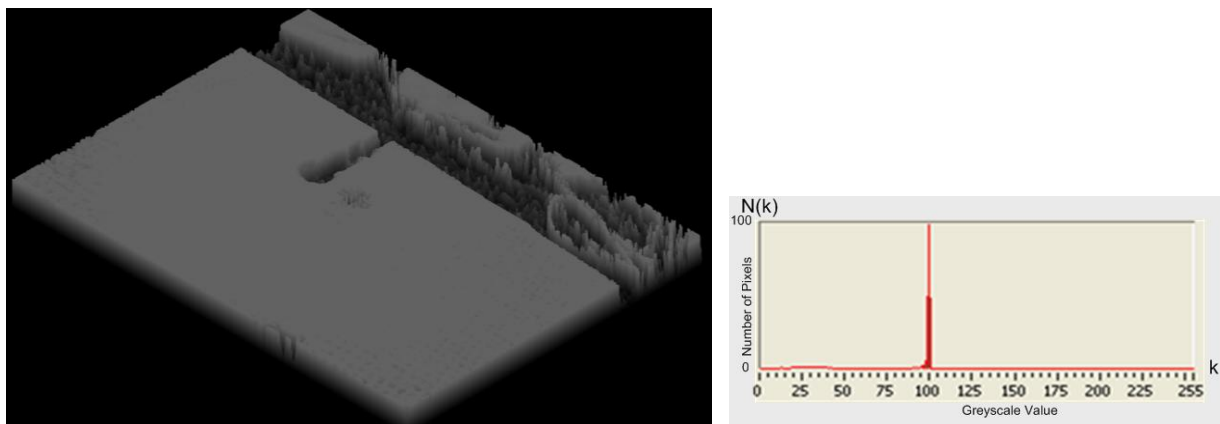


Figure 72 3D representation and Histogram from Logic Operator - Final Design  
The Histogram on the right describes the lighter colours in the associated image is made up from a greyscale value of 100 with an intensity of 100. The robots workspace is represented by the maximum value and the object represented by zero as seen by the 3D representation on the left.

As seen in Figure 73 only one sample from the GBOPO 'c', returning a coordinate at the very edge of the workspace, has failed to return a coordinate match that would enable the manipulator to correct its position, . Three samples labelled 'd' has returned a match on the right edge of the object, whilst samples labelled 'f' has returned a match on the left edge of the object. Thus showing a significant improvement in detection accuracy from previous trials with the vast majority of recorded results directly in line with the object and some result recorded with  $\pm 10\text{mm}$  positional error in each direction. From the authors perspective, due to the 480K pixel quality camera used, these result a far better than expected, with only 1 samples from GBOPO images being returned that would put the manipulator nowhere near the object under inspection and therefore un-correctable.

### Long Distance Scan - Final Trail

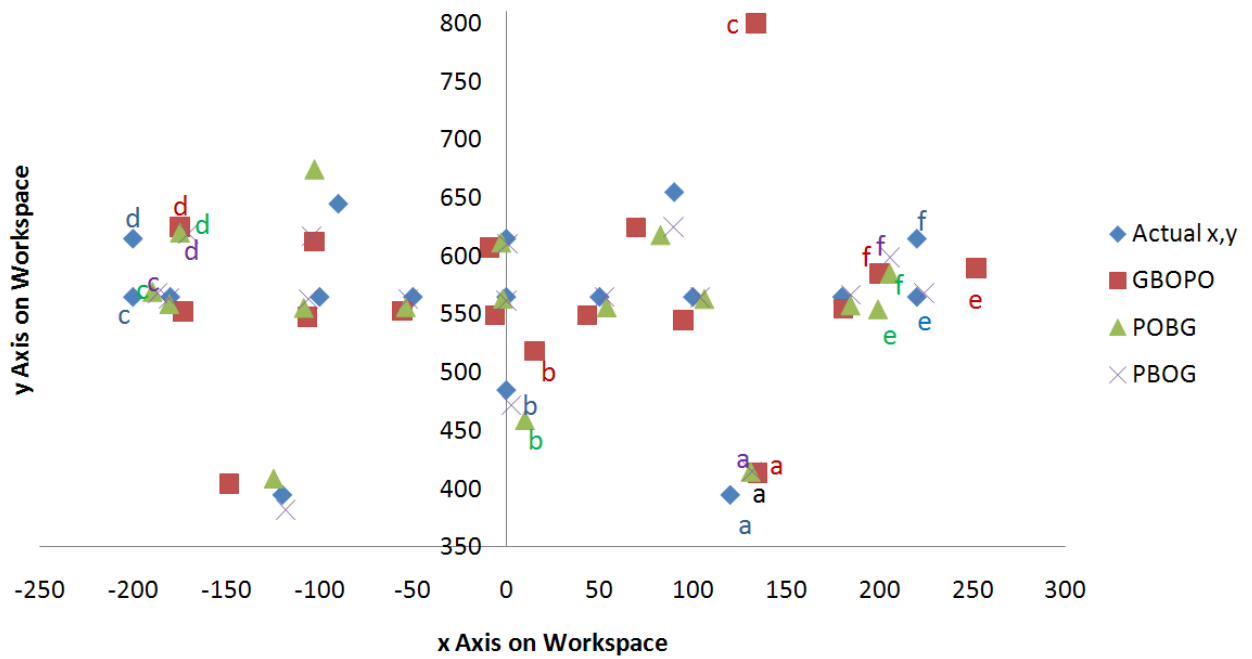


Figure 73 Measurement of Object Location - Final Design  
 Actual x,y describes the actual object location on the workspace  
 The x axis represents distance in mm from current direction, the  
 y axis represents distance in mm from the centre of robot arm base.

The inclusion of the improved pattern matching algorithm and the modification of the ones existing from previous trials have increased the total time taken for the completion of the object recognition algorithm, from 139.7ms to 142.7ms as seen in Figure 74, however the delay is still not deemed as a long delay time in real time applications in robotics. The trade-off between accuracy and time has incurred a significant improvement from the initial trial, as all but one sample produce the correct positioning of the manipulator for the close image acquisition scan.

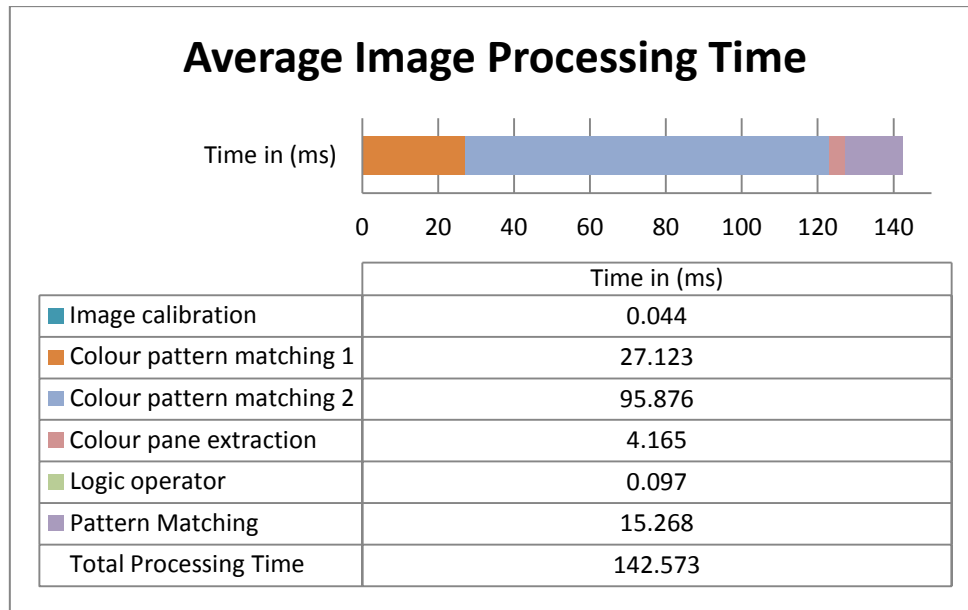


Figure 74 Long Distance Final Design Time Frame Analysis

A significant tolerance in detection coordinates permits the long distance scan algorithm to be extremely efficient in real-time applications. Prior knowledge of a further inspection scan, to correct positional error, assists in the effective operation of the robotic manipulator.

#### 5.2.4 Object Recognition design for Close scan system

The second image acquisition pose position is uploaded from the software database into the manipulator control system. These values are used in conjunction with the returned coordinates from the initial long distance scan, a calculation occurs to obtain the appropriate 3D position ( $x,y,z$ ) for the manipulator to manoeuvre so the robot arm will position itself with the line of sight of the camera is pointed directly at the object and the end effector is approximately 200mm ( $\pm 2$ mm) horizontal ( $x_0$ ) distance away from the object under detection (see Commissioning information in Appendix C). The visual servoing system will automatically adjust the camera angles based on the angular position and encoder feedback of the virtual robot arm so the object position determined from the long distance scan will be positioned central within the acquired image. Once the manipulator has acknowledged that the short scan position is reached, the image acquisition task is undertaken. There is a possibility that the object in this second scan could be a maximum of  $\pm 30$ mm in both axes, from the centre of the image, due to the estimated calibrated coordinates returned for the

object from the initial image acquisition task. Therefore there are three main reasons why the close scan is conducted:

- 1) Corrections in manipulator position due to possible inaccuracies of initial long distance scan.
- 2) To determine the colour difference between the objects.
- 3) To ensure an efficient algorithm design that searches through an image database to make a correct decision about what and where the object is required to be transported to.

The obvious advantage with this second image acquisition scan is that the colour quality does not vary considerably as the manipulator end effector is close to the object under detection. There are three algorithms that will be introduced in this section - one for each different coloured object. The algorithms will be connected together within a step sequence: if the first algorithm does not detect a match, the program will 'bridge over' to the next sequenced algorithm and so on. Once an object is recognised a sequence number is generated that will activate a sequence structure in the main program to upload the 'drop-off' coordinates and force required for the recognised object.

Image calibration is identical to the first image acquisition scan, as seen in Figure 75: the same workspace. The colour pattern matching algorithm identifies the colour within the ROI, the colour location algorithm is used to identify the colour differences of the object and return a positional coordinate. A colour database is created to identify each respective tapered coloured sectors of the object(s). The greyscale pattern matching algorithm will work in conjunction with the other algorithms to ensure that a correct and accurate location of object is determined; it will be the coordinates returned by this algorithm which will manoeuvre the end effector of the manipulator successfully to the object.

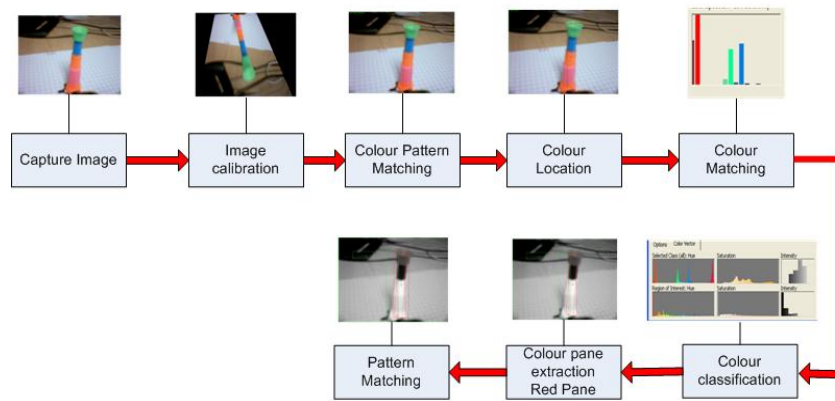


Figure 75 Close Scan Image Acquisition Final Algorithm Design

With the object being close to the camera lens a good inspection of the colour content of the object is now possible. The differences between the objects can be seen by the use of the colour space within a histogram chart. As seen in Table 13, the RGB histogram illustrates, there is no distinct difference between all three objects when looking for the object through the entire image. However, clearly the pixel intensity of each object is dissimilar with all three objects being positioned in an identical position as shown on the right of Table 14. This difference in pixel intensity will be used for the manipulator to distinguish the exact object under inspection. To assist this algorithm a separate database is produced that will classify the colour difference of the objects using the colour spectrum as a foundation.

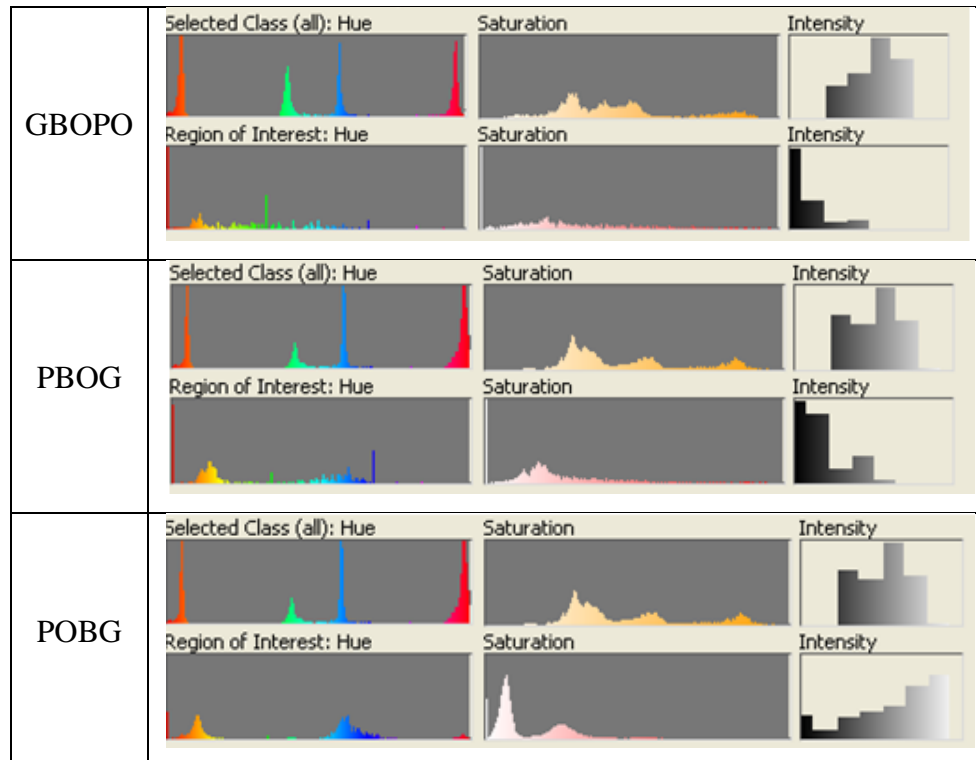
Table 13 Histograms Illustrating Colour Content of the Objects

GBOPO (RGB & HSL)	PBOG (RGB & HSL)	POBG (RGB & HSL)

As seen in the top column of each row in Table 14, there are variations of image quality and intensity between the acquired images for each different object, this noise has to be taken into account when performing the analysis. By confining the ROI onto the object itself, as in the

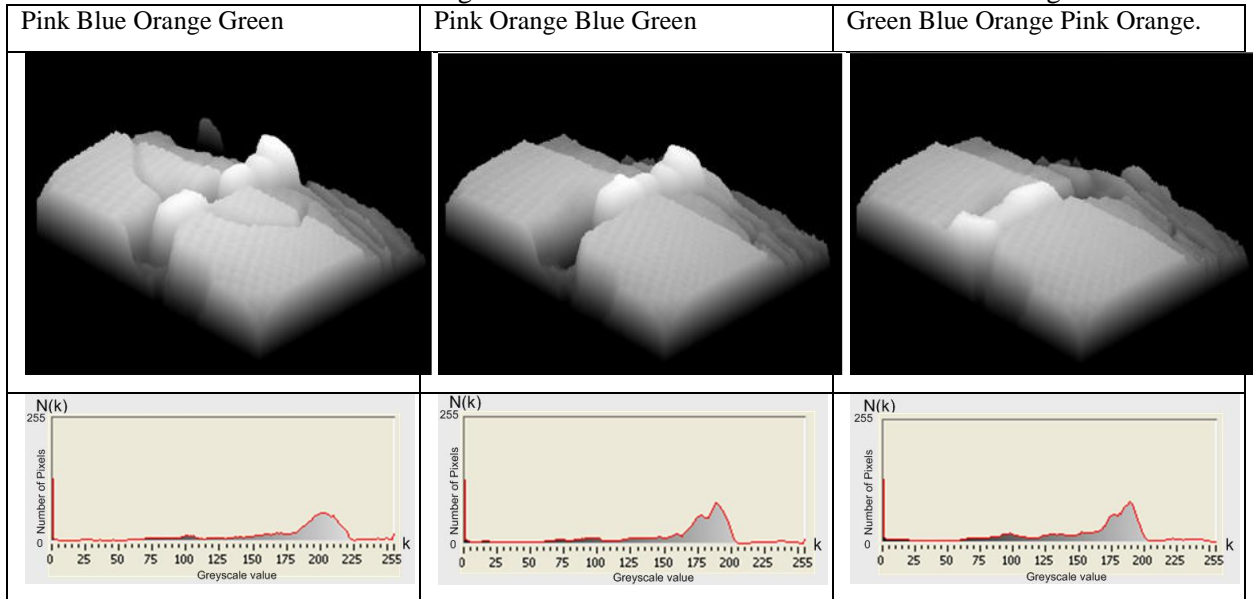
bottom column of each row, there is little difference between Hue and Saturation of GBOPO and PBOG, the greater difference between all three object is within the intensity pane, as a result a combination of these characteristic are used to determine the colour location within the image. The red pane is extracted from the colour image and then a greyscale pattern matching algorithm, similar to the one used previously, is actioned. The results are seen in Table 15.

Table 14 Close Scan ROI Colour Differences



From the histogram charts in Table 15, produced after the pane extraction, the three objects cannot be easily distinguished from each other, however further inspection of the 3D representational images (diagonally 'NE' through centre), the object outline can be clearly seen. The different colours within the object have different intensity values, thus, parts of the object have a high intensity value whilst other areas have a low intensity value (sectors of the object appear to be missing). This difference in intensity is used for the pattern matching algorithm to determine the location of the object and the difference between each. Looking closely at the 3D images clearly the orange and pink colours within the objects have significantly lower intensity values than the other colours in the object, thus discerning the difference as clearly seen in the top row of Table 15.

Table 15 3D View and Histogram Charts after Pane Extraction - Short Scan Algorithm



Functioning in conjunction with the colour location algorithm and colour matching algorithm (as software failsafe mechanism), the disparity between the objects can be established and the accurate real world coordinates can be calculated. Only when all three algorithms return a match will the manipulator have information on where the object is and where it requires to be transported to: using a three Input AND gate to ensure definite match has been detected. If any of the three algorithms do not return a match, no match is deemed to be found; therefore the manipulator will remain stationary and await further instructions, as seen in Figure 76.



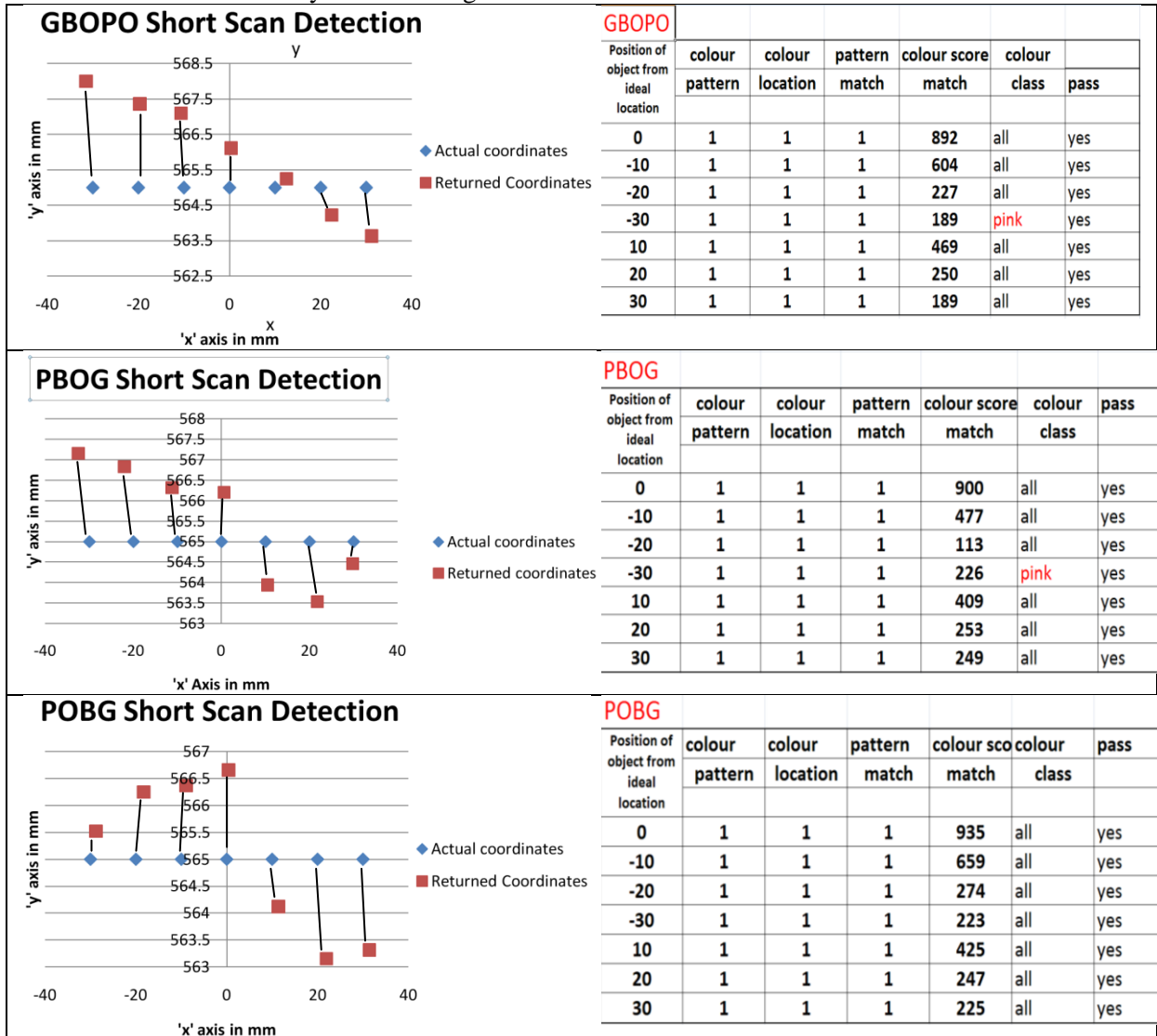
Figure 76 Ensuring a Colour and Pattern Match for the Three Objects

Table 16 illustrates that when the object under inspection matches the images stored within the database all parameters under evaluation (Colour Pattern, Colour Location and Pattern Match) return a value of '1', which concludes that a positive match has been found within the ROI. The colour match score is at highest with the object in direct line of site with the camera lens. If, due to positional error from the initial image acquisition scan, the object is not centred in the image, the colour match score reduces dramatically. The results from the colour classification determine whether all colours stored have been recognised. Only one sample from GBOPO and one sample from PBOG has produced a match with only 'pink' being recognised with the object being -30mm (x axis) from centre of the image. When the first algorithm, that detects the GBOPO object (top table), does not successfully return a positive match, the acquired image is transferred to the second algorithm within the ladder, which detects the PBOG object and so on.

The results obtained for the GBOPO algorithm returned accuracy for locating the object of  $\pm 2.5\text{mm}$  (max.) in all axes, the PBOG algorithm accuracy is recorded as  $\pm 2\text{mm}$  (max.) in all axes whilst the POBG algorithm returned accuracy of  $\pm 1.7\text{mm}$  (max.) in all axes. All algorithms are successful in only detecting the respective object it is looking for, thus returning a 'not detected' to the control when other objects are present in order to transfer the image through the control sequence of the control structure. The positional error recorded will not cause the gripper arms to come in contact with the object due to the physical size of the object compared to the maximum opening of the gripper mechanism. Therefore, as with the previous algorithm, the error pertained is within the acceptable tolerance of the gripper mechanism design.

Table 16 Results from Short Scan Algorithm

To ensure the round up/down sub.vi manoeuvres the manipulator as close to the detected object as possible, measurements to 100<sup>th</sup> mm are returned by the vision algorithms.



Depending on the lighting levels on the workspace, the quality of the acquired image, there is a possibility that an additional match is found by two out of the three algorithms used to detect a positive match, as seen in Table 17. The algorithm is designed to recognise the GBOPO object only, two algorithms, the colour location and the greyscale pattern matching algorithm has determined a match is present within the image, with the PBOG object in the workspace. It is only the third colour matching algorithm that has successfully rejected the object as a match. Thus, the three input AND gate has successfully filtered out this object from being fully recognised. Although a pattern match location has been generated, the

Boolean value has ensured the manipulator does not manipulate and transport the object to the incorrect location, thus preventing a critical operational error.

Table 17 Results from the GBOPO Determining a Pattern Match Error

PBOG	colour		colour location		pattern match		colour	colour	pattern	colour score	colour	
saved	match location		match location		match location		pattern	location	match	match	class	pass
file	x	y	x	y	x	y						
0	-	-	373	366	-	-	0	1	0	763	all	no
-10	-	-	337	349	377.46	56.31	0	1	1	496	all	no
-20	-	-	285	366	-	-	0	1	0	87	all	no
-30	-	-	231	366	-	-	0	1	0	197	all	no
10	-	-	456	345	-	-	0	1	0	379	all	no
20	-	-	507	342	-	-	0	1	0	216	all	no
30	-	-	559	325	-	-	0	1	0	230	all	no

Figure 77 illustrates that the average inspection time for the GBOPO is 110.8ms, whilst the average inspection time for POBG is 215.6ms and the average inspection time for PBOG is 166.7ms. Hence, the time-scale to run through all the object recognition algorithms is an average of 494.1ms for three objects. The interesting result from Figure 77, is the GBOPO object which possesses more different colour content than the other two, returned the minimum inspection time, due to the slight difference in colour frequency between the orange and pink colours, therefore it is easier for the algorithm to process through. Obviously the more complex and the more colour content of the object, this time delay would increase. The results shown here have proved that accurate and efficient results can be obtained with very minimum processes time delay in real time operations. This time delay can be reduced even further, with better quality of acquisitioned images and better lighting on and around the robot workspace, thus with these conditions met, there is a distinct possibility of an image processing stage being removed. Hence the maximum inspection time from the initial long distance scan to the full recognition of the object is 358.7ms, thus little inspection time is required in order for the manipulator to operate autonomously in deciding what and where an object is and needs to be transported to.

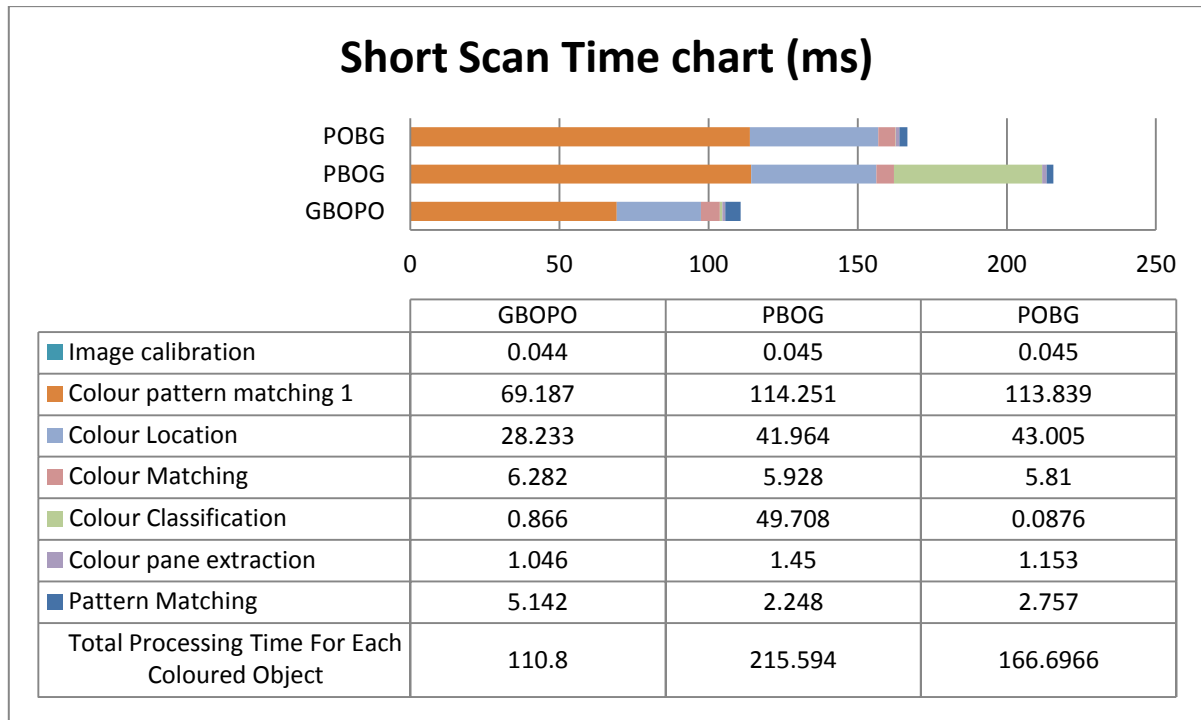


Figure 77 Time Distribution Chart for Short Scan Algorithms

Throughout the trials and improvement in accuracy of the vision system, in detecting the position of the object has improved, with only a slight increase in processing time used for the vision algorithms. The lessons learned from the first two trials of the long distance scan proved to be beneficial with the short distance scan. With allowing the different tapered colour sections of the object be transformed into one shade of grey that described the shape of the object improved the efficiency of the algorithms. The design procedure permitted that the long distance scan concentrated on the detection of the shape of the template rather than the colour, as such once the shape had been recognised the colour detection algorithm confirmed that the object is comprised of the colours described by the histogram charts. This will allow the manipulator to quickly decide that a recognised object is on the workspace and manoeuvre to the short distance scan where the differences in the objects that caused an issue with the first two trials of the long distance scan, became the solution in deciding the difference between the objects. Three algorithms are used in conjunction with each other to avoid false detection, as seen up to two of the three algorithms can incorrectly return a positive result for very similar shape and coloured object, only the third algorithm prevents a critical error in operation of the manipulator. In the short distance scan, the colour algorithms ensure that false detection is prevented by describing the colour tapered sectors of the object in position

they appear on the object and then decide to successfully produce a match, which is then used with the greyscale pattern matching algorithm through the 'AND' gate, which will then ensure the identical shape and similar coloured objects are recognised as being different and thus program the manipulator to 'drop-off' the object in the respective intended destinations as seen in the commissioning information in Appendix C.

As the manipulator manoeuvres to grasp the object from the information received from the two image acquisition scans, another image acquisition step can be introduced as seen in Figure 11. This will enable the manipulator to position itself so as to ensure the object is directly centred within the gripper mechanism in all axes. This additional step will introduce the availability of edge detection and object tracking, to detect whether the object has moved whilst grasped and being transported. The measurements taken from the object whilst grasped will be used in conjunction to comparing one acquired sample image to another in quick succession to detect any movement of the object. This can be used in interoperation with the tactile sensor in the gripper mechanism to ensure security of the object being manipulated.

## **Chapter 6**

### **Conclusion and Recommendation for Further Work**

The research programme focussed on the aspect of autonomous control and operation of a robot manipulator in recognising the difference between identically shaped objects; whilst ensuring accuracy in grasp position with security for the object being manipulated. Several disciplines have been discussed including Kinematics, feedback systems, visual servoing and in the case of improving the security of the object being transported; new gripper arms have been developed: removing the weaknesses of the existing manufacturer supplied gripper. The first chapter introduced the basic knowledge of autonomous control of robots with brief discussions about the work conducted by other researchers in the field of robotics, vision systems, intelligence and outstanding issues that require further research to resolve.

Chapter 2 described the design and implementation of the virtual robot arm and illustrated that the control of the scene revolved around the control of the joints placed within the robot tree; as such the joints became the master control whilst the other items in the tree became the slaves. The design methodology proved to be effective in real-time applications as updating the scene, which updates the position of all elements in the tree, became as simple as amending the values of the joints only, which in turn updated the positions of all the element in the tree within the scene. The identical methodology used in creating the scene can also be used as the basic building block for additional automated machinery to be quickly designed to enable a conclusion to be reached about the physical attributes of the created machine. The design of the robot tree allows the confinement of a robot arm with a glovebox structure, as such given the physical (internal) dimensions of a glovebox; a robot arm can be designed within the scene to function under these constraints. As a result purpose designed links and joints of manipulators can efficiently be created and the function can be tested within the virtual robot arm application. This chapter also introduced the kinematic control for the joints of the robot arm and how to utilise the algorithms to check positional information to ensure full control of all joints. A number of kinematic algorithms have been employed; Reverse kinematics is used for the main control, working with a basic map plan from an excel spreadsheet whose values are amended, in the main control with new positional coordinates values from the vision system to direct the end effector to the object location. Throughout the

movement, forward and direct kinematics are used as a ‘checksum’ to ensure calculations in joint space match the reach and pose of the manipulator from the reverse kinematics to counteract the issue of unresolved kinematics, which is a common problem in reverse kinematic operation as found by Weiss and Sanderson in [10]. The advantage of calculating the kinematics for the Katana robot arm using planar matrices, will permit the rotation angle ‘ $\phi$ ’ to be calculated separately, thus reducing the complexity of calculations.

Chapter 2 included descriptions of the ancillary devices used to ensure the accuracy of the manipulator in bringing the end effector to grasp the object. The first device discussed was the inclusion of force feedback mechanism within the gripper arms to ensure that the object is not only present but also does not slide through the gripper mechanism when under transportation. The position and activation of the force sensors, housed within the gripper arms, resulted in positive response by increasing the surface area of the activation plunger and thus improving the tolerance of the position of the object within the gripper mechanism allowing additional flexibility in the control of the manipulator when manoeuvring to grasp; however the effectiveness of operation is only successful with the correct design of gripper arm that was described in Chapter 3. The excel spreadsheet again is used to gain knowledge of the required force to be measured by the force sensors in order to transport the object, without damage, to its destination. All the information required by the main manipulator control is stored within the same spreadsheet providing efficient access not only to positional information but also links to the image database: the spreadsheet can also be amended and enhanced through the main program or edited by the user without specialist training. A discussion on the visual servoing mechanism ended the chapter describing how the effective operation of the mechanism related to the efficient functioning of the image processing system by ensuring the recognised object, from the previous manipulator pose, in central to the image for the next image acquisition stage: to ensure the ROI is away from the image borders. The ability to operate the visual servoing system on the manipulator ‘neck’ also provides additional feedback from the servo-motor control system, which permits ‘homing’ of the end effector to the object; it also provides additional options for control of the vision system to be used under different applications i.e. 3D imaging, object tracking. The main advantage of the servo positioning is the facility to update the coordinate positions for the end effector as the manipulator manoeuvres closer to the desired location, than using a fixed

camera external to the robots workspace as the position of the object in the acquired image and the servo positions are also used when updating the positional coordinates. The advantage of the camera constantly moving closer to the desired object is that image quality improves as the distance away reduces. This permits the use of a low quality pixel camera instead of the expense of a High Definition (HD) camera, as proven with the research project. Although the use of HD quality could prevent the issue with one of the GBOPO objects in the long distance scan being detected nowhere near its location. A failsafe design with the ancillary devices is also discussed and how the ability to disable resources when not needed improves the efficiency of operation, with an additional advantage of no permanent fixing being required within the workspace for the vision system and the mounting bracket can easily be transferred from the manipulator and placed onto another without the use of tools, which is ideal for maintenance and uptime.

Chapter 3 described the design weaknesses of the manufacturer's supplied gripper mechanism that would affect the efficient operation of the gripper; as such the design methodology of a new gripper mechanism was presented. The new gripper arms are designed to grasp differently shaped and deformed objects by permitting flexibility within the third finger to allow forming around the object; the degree of displacement however, ensures adequate applied load on the grasped object. The characteristics of the gripper mechanism is also programmed into the main control kinematics, to permit the manipulator to make a decision about the location of the object with respect to the end of the gripper arm, in addition to ensuring the gripper mechanism does not come into contact with the arm itself or the workspace. A replacement manipulator was designed and developed to permit quick and easy access and replacement of parts. The basis of the design was that access to the Katana 6M180 was difficult to accomplish and required several tools and patience to remove the end effector, however in a real world environment quick resolution of faults is required. The new designed manipulator is based on quick release methodology that provides easy access to the internal mechanics and electro-mechanical components and thus improves uptime of the attached robot arm working in an industrial environment. Within a glovebox environment, numerous dissimilar tasks are required to be undertaken: sorting of machine parts, separation of radioactive liquids or materials, are two such examples. Therefore it is imperative that a robot arm placed in this environment has the ability for a quick change of end effector or faulty

component. As such the end effector and associated workings can be removed with two screws (can be modified to release with a solenoid plunger), then a new end effector (rotary tool, suction cups etc.) can be secured to the manipulator to complete a different task, with little change over time.

Chapter 4 contains the algorithms used for the operation of the vision system. Included in this chapter is a distinctive method for calibrating the acquired image, which not only provides a reliable solution to perspective error that occurs with mounting a camera at an angle to the workspace, but also provided an effective transformation from pixels to real world coordinates all in one algorithm. The main advantage of this is that no matter where the robot arm is positioned, the real world coordinates returned by the calibration algorithm, will be identical as such the robot arm can work in a unfamiliar environment with the confidence that the workspace calibration is already accomplished. The additional image processing algorithms that were introduced in this chapter are designed for efficiency with utilising a coarse-to-fine search strategy that allows a template image to be moved around the acquired image more effectively, than moving pixel-to-pixel. The inclusion of a match score, as used by Gomez and Eggenberger in [22] enables a hill climbing algorithm to identify an accurate match coordinate around the areas in the image that produced the highest match score from the previous search strategy. The results shown in Chapter 5 prove the effectiveness of the vision system algorithms. The algorithm used for greyscale pattern matching was developed to detect an object matching a template, from the image database, even when the object has been rotated. This will enable the manipulator to receive a degree of rotation of the match and thus rotate joint 3 and joint 4 respectively (refer to Figure 7), to compensate for the displaced component. As such, when sorting through machine parts (which is a task conducted in a nuclear glovebox) the robot arm can adapt to an acquired image that shows the recognised part rotated from the template image, and take appropriate actions.

Chapter 5 contains the main results from both kinematic and image processing algorithms. The effectiveness of the additional algorithms working in conjunction with the kinematic control has shown to prevent hazardous conditions (collision), but also enables one joint angle to be controlled by the other interconnected joints if the task requires it to be so. A demonstration of how combining the three different methods of kinematics, discussed in

Chapter 2, can correct the operation of the manipulator when the initial equations become unresolved; the results shown in this research prove that full control of joint space can be accomplished. A number of image processing trials were also introduced to prove the effectiveness of object recognition and location even in poor quality, high noise images. Unlike the work conducted by Kelly in [15] and, Saxena and Driemeyer in [26], with designing the image control to permit two images to be processed within the operation: first to ensure a recognised object is present and secondly to identify the colour difference, resources are saved and the operation proved to be efficient and effective: proving the camera is not required throughout the entire operation to ensure the manipulator can decide the correct grasp position. A weakness found in the first two trials of the long distance scan: shades of grey that represents the colour sectors of the objects, proved to be an advantage in the short distance scan, which identifies the difference in the tapered sectors of each object. The implementation of the three input AND gate, to generate a Boolean expression for the coloured object, proved effective in preventing detection of an incorrectly recognised object in the poor quality image. The use of the fitness function similar to the ones used by Gomez and Eggenberger in [22] and Harri in [24], in order to determine the position of the manipulator and the colour detected was of interest. This fitness function was used within the research specifically for colour matching and calibration functions. A distinct software management scheme introduced by the work conducted by Harri in [24] that encompasses all elements of the manipulator control system, has shown to produce a fast and effective response during real-time tests. Ensuring that each sub-control systems are only engaged when required, has proven a big advantage in real-time processing in removing unwanted delay times from operation.

Principles from numerous fields have been utilised to produce a manipulator control system that is versatile and can adapt to circumstance. Multiple sensory inputs, including information from databases, are used in order to correctly determine the manipulator movements. Software management techniques similar to Harris[23] and Koshizen [43] ensure resources are used efficiently and effectively. The selection of which inputs to use is fully independent and depends on the decisions made from external influences on the control system. With built in failsafes, both in hardware and software, the manipulator can continue to function when a failure of a subsystem is reported, using its own secondary reserved

system [44] (e.g. A camera becomes faulty, the additional camera can be engaged in addition if one force sensor fails to record force change whilst the opposite arm does the control system can adapt, whilst recording an error on the Graphic User Interface (GUI). Work done prior to this thesis, on connecting the Katana 6M180 robot arm to the LabView environment can easily be integrated with the operation of the virtual robotic manipulator to provide an supervisor with real time positional information of the physical robot arm and assist in resolving any functional issues that may occur.

By combining all relevant monitoring information that a supervisor requires to ensure correct operation of the physical manipulator within its environment to appear on the Graphic User Interface (GUI) as Figure 78, any fault condition can be quickly seen and acted upon. Although substantial information is displayed, depending on user specifications all responses can be monitored in the background and only displayed when there are significant discrepancies between the virtual operation and the real world robot arm – all of which has been described in detail. Information includes:-

- Program Sequence Number – As described in Chapter 2, the operation of the virtual manipulator is placed in a sequence structure to enable efficient fault rectification. The sequence structure is designed to distinguish the operation for the different recognised objects within the workspace. Thus if the robot arm ‘pauses’ for a length of time, the supervisor can obtain instant knowledge of where, in the program sequence, the robot arm is halted and take appropriate actions to restart operation. It will also permit additional programmes to be added easily, which can be selected by the supervisor on the GUI, to adapt the functioning of the manipulator to suit different tasks.
- Iteration Count – To be used mainly in conjunction with the sequence number to visually identify that the virtual simulation is still functioning: if the iteration count ceases then the program has ‘crashed’.
- Alteration in rotation angle at the base of the arm – For the operation set out in this thesis, there is a position on the workspace that the object should ideally be located on ( $Id_{loc}$ ), if the object is found not to be at this location, the base of the robot arm

will be rotated to compensate. As such it is recorded on the GUI and can be used to inform the supervisor that positional error (if the object is conveyed into place) has occurred.

- Distance to object – This is used as an indicator that the object can be reached by the robot arm (dependent on the length of links and whether any transient movement is viable), it also indicates the position of the end effector from the object, this will show 200mm ( $\pm 2$ mm) for the short image acquisition scan position.
- Cartesian Coordinates of end effector – Used as a quick reference for the 3D position of the end effector. A negative value in the ‘y’ axis will incur an error.
- PWM waveform Generation – This will produce a waveform when the vision system is active as such will function in operation with the stereo vision system. If the generated waveform is not present on the GUI, then the servo system is non-functional and operation of the physical robot arm will require verifying.
- Encoder Feedback value – On all joints of the robot arm, attached to the motors, are encoders, which are defaulted to the values shown in Appendix C once calibration sequence has occurred. The encoder values are used to describe the operation and rotation position of each motor attached to the links of the robot arm.
- Gripper arm operation and applied force – The operation of the gripper mechanism can be seen virtually along with the applied force from the force sensors. The force feedback should register for each gripper, if only one value is variable when the gripper mechanism is operational, then a fault condition with a description is present within the error message prompts for each gripper arm. This will ensure the supervisor can quickly diagnose any issues with the gripper system.
- Stereo vision servo position – A clear indication that the camera system is operating correctly is seen. As the manipulator manoeuvres closer to the object, the stereo vision servo system should rotate inwards at a predetermined angle to provide an acquisitioned image where the object is directed towards the centre of the image.

- Image acquired from the vision system – The acquire greyscale image is illustrated on the GUI that will indicate that the object present is in the centre of the image and also provides details of the object on the workspace.
- Manipulator movements from virtual robot arm – The virtual manipulator operation is displayed within the windows which illustrates the movements of the robot arm, which can be recorded for playback in-case of any functional issues. Once a physical robot arm is attached, the virtual robot arm can be used as a slave to the physical robot arm to maintain monitoring of its operation.

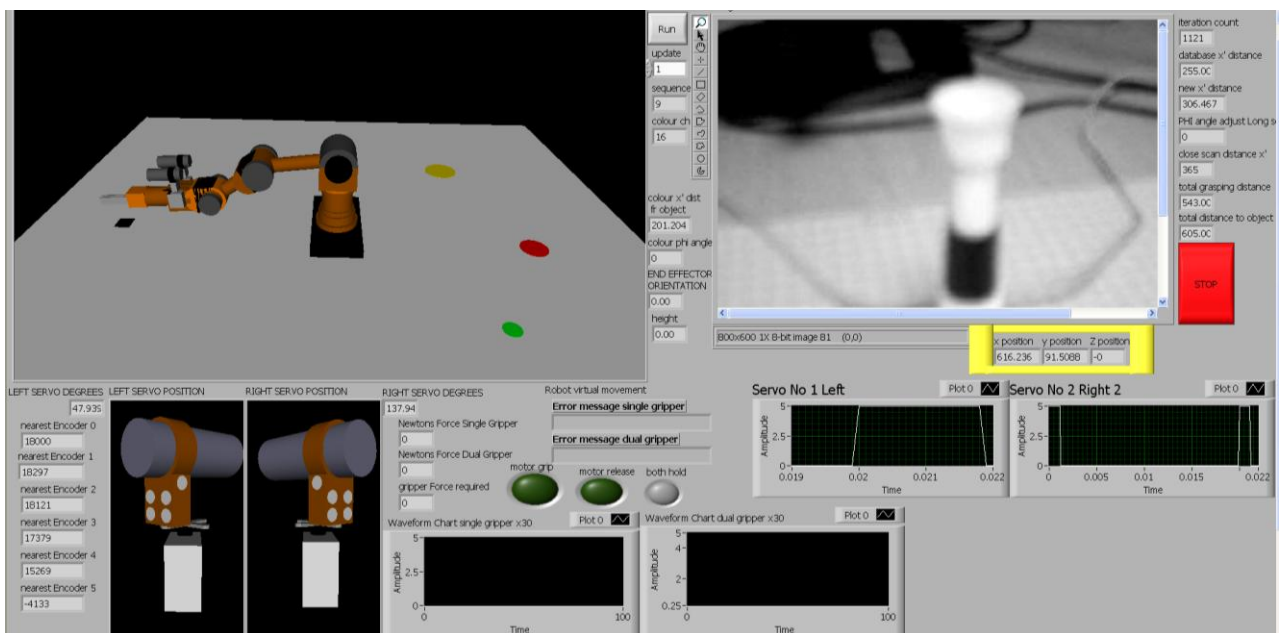


Figure 78 Opertor GUI for Manipulator Control System

## 6.1 Further Work and improvements

The obvious improvement to the research is to use high picture quality cameras, such as HD would enable the image processing algorithms to become more efficient. Without significant noise within the acquired image, positional information can be calculated with a greater degree of accuracy even at the long distance image acquisition position. When the manipulator has grasped the object the vision system can be used in combination with the force sensors to ensure no slippage occurs. The camera lens is in close proximity to the object once grasped and any slight movement can be easily recorded; a fixed camera system would

not allow for this type of control – or be as effective if used from distance. Placing an image mask over the acquisitioned image, a vertical line can be placed through the centre of the object and the best edge can be found with using edge detection. The standard edge detection techniques can be modified to produce a failsafe system working in conjunction with the force feedback system to ensure the object does not slip during transportation. Edge detection is used to detect the variations in greyscale pixel values from neighbouring pixels. A value of edge strength determines the maximum difference between the edge and the surrounding background on an image; A number of pixels can be used to identify the edges, by using a parabolic fit to the edge-detected data points, the peak value is found along with the values of one pixel either side of the peak. Using three coefficients a, b, and c, the expression  $ax^2+bx + c$  to create a parabolic interpolation, determining the coefficients is carried out as follows:

Let the three points (one peak and two neighbours) locations be represented by  $(X_0, Y_0)$ ,  $(X_1, Y_1)$ , and  $(X_2, Y_2)$ . Let  $X_0 = -1$ ,  $X_1 = 0$ , and  $X_2 = 1$ , substituting these point in the equation for the parabola to solve for a, b, and c:

$$a = \frac{Y_0 + Y_2 - 2Y_1}{2}$$

$$b = \frac{Y_2 - Y_0}{2}$$

$$c = Y_1, \text{ not needed}$$

The maximum of the function is computed by taking the first derivative of the parabolic function and setting the result equal to zero. Therefore:

$$x = -\frac{b}{2a}$$

Providing a sub-pixel offset where the estimate of the true edge location lies, thus from the parabolic fit as in Figure 79:-

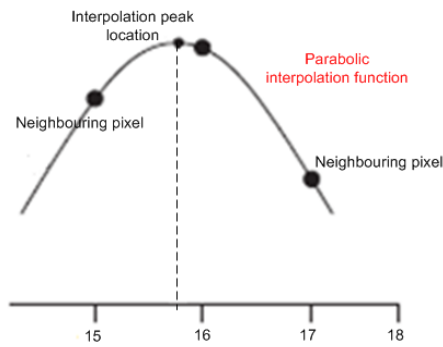


Figure 79 Parabolic Interpolation for Sub-pixel Location

This line can be used to find a best edge detection point between the different sectors of the objects once grasped [41]. The returned coordinates can be monitored throughout the movement to the ‘drop-off’ location and any change in coordinate value can constitute a slippage of the object. Used in conjunction with the force sensor feedback mechanism through an OR gate will ensure that either detection system can produce an appropriate response from the gripper mechanism, an example of the image mask can be seen below in Figure 80.

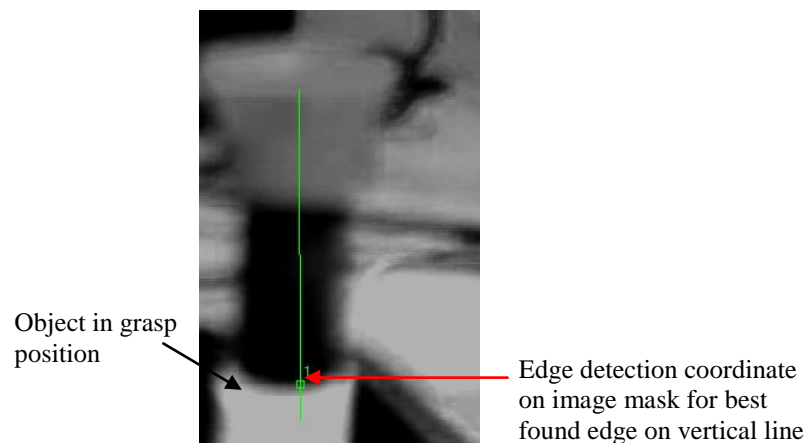


Figure 80 Edge Detection Once Object is Grasped

With engaging both cameras on the stereo vision system and comparing the difference in the acquired images, it is possible to design an algorithm based of the partially observable Markov decision processes (POMDP) to identify a few points within the image that correspond to good locations for which the attached gripper arm can grasp; especially for those objects that are not recognised/stored within the image database, similar to the work conducted by Hsiao and Perez in [45]. Measurements can be taken by the use of an edge detection algorithm and correlate this with the manipulator parameters in order to identify the

acceptable grasp locations. Operator prompts can then be used in order to add the object to the database and enter the drop-off locations, thus the Excel spreadsheet can then be updated.

Research into improving the current Kinematic operation so that the rotation of the main body can encompass the positional information directly, some attempts have already been made, but with poor speed of operation and considerable loss of control of the manipulator arm as discussed by Asfour and Azad in[46] in relation to ARMAR-III humanoid robots. Further improvements to the kinematics of the manipulator to include probabilistic algorithms; using pre- and post-positional information to allow the manipulator to make a decision on the pose of the end effector. This information can be used within a learning algorithm to predict the movement of the manipulator and therefore reduce the number of calculations. The recursive Bayesian updating algorithm below, will determine the value of  $x$  from the measurements of  $z, \dots$ ;  $z$  is commonly named as diagnostic reasoning and its value is within the range of 0 to 1: the probability that an object is there which will increase the number of times that an object is found to be there and vice-versa. Therefore the control will work on the most likely outcome from previous activities thus advance the calculations with previous knowledge of events

$$p(x : z_1, \dots, z_n) = \frac{p(z_n : x, z_1, \dots, z_{n-1})p(x : z_1, \dots, z_{n-1})}{p(z_n : x, z_1, \dots, z_{n-1})}$$

With most of the processing occurring within the PC from the virtual manipulator, the amount of control required at the manipulator is kept to a minimum. This means that numerical values and colour images are communicated between the virtual robot and the PC, therefore very low bandwidth is required for communication and thus will enable multiple manipulators to be monitored from one central supervisor station; therefore multiple GUI's can be reduced onto one display. The GUI informs the supervisor of numerous robot operations, with full view of the pose of each and of any occurring errors. These errors can be combined so as to not overcome the human supervisor with too much information, the individual error code that will be required, is to identify which robot arm has incurred the error. This will prove to be a distinct advantage when a production line has numerous different types of robot arm/mobile robot in operation.

## References

- [1] C Bauckhage, G Sayerer (2001): An integrated system for cooperative man-machine interaction; IEEE Int. Symposium in Computational Intelligence in Robotics and Automation, pp328-333, Banff, Canada.
- [2] SA Robotics (2008): remote and robotic manipulators; Hazardous and Radioactive Containment Structures and Gloveboxes;  
<http://powertechnology.com/contractors/powerplantequip/sarobotics>
- [3] Robotworx (1999): <Http://robots.com/faq.php?question=robopt+manipulator>.
- [4] E Rome, J Hertzberg (2006): Towards Affordance-based Robot Control; International Conference and Research Centre for Computer Science Seminar 06231, June 5-9, Schloss Dagstuhl, Germany.
- [5] E Acar, H Choset (2002): Sensor-based coverage of unknown environments; International Journal of Robotic Research, July 1, Vol.21 no. 4 pp. 345-366.
- [6] Y Nasai, S Morita (2003): A Constructive model for the development of joint attention; Connection Science, Vol.15, no.4 pp. 211-229.
- [7] F.A. Marian and H.T. Rowan (1987): The Cost-Benefit of Robotic Devices in Nuclear Power Plants; Public Service Electric and Gas Company.
- [8] Anonymous (1990): Robots deliver real benefits for PSE&G; Nuclear Engineering International, vol.35, No.435, pp.120-121.
- [9] RC Bollies (1975): Verification vision within a Programmable Assembly System; Proceedings of the 5<sup>th</sup> International Joint Conference on Artificial Intelligence, August 22-25, Vol.2, pp/569-575, San Francisco, California, USA.
- [10] IE Weiss, AC Sanderson (1987): Dynamic Sensor-based control of Robots with visual feedback; IEEE Journal of Robotics and Automation, Vol.3, No5, pp404-417.
- [11] D. Howe, N Popp, MR Cutkosky (1990): Grasping, Manipulation and Control with tactile sensing; IEEE International Workshop on Intelligent Motion Control, August 20-22, Istanbul, pp.1258-1264.
- [12] G.S. Bell, W.J. Wilson, and C.C.W.Hulls (1996): Relative end-effector control using cartesian position based visual servoing; IEEE Transactions on Robotics and Automation, Vol.12, No.5, pp 684-696.
- [13] D. E. Koditschek, A. A. Rizzi (1996): An active visual estimator for dexterous manipulation; IEEE Transactions on Robotics and Automation, Vol.12, No.5, pp.697-713.
- [14] C. Malcom (1996): Dynamic effects in visual closed-loop Systems; IEEE

- Transactions on Robotics and Automation, Vol.12, No.5, pp 671-683.
- [15] R. Kelly (1996): Robust asymptotically stable visual servoing of planar robots; IEEE Transactions on Robotics and Automation, Vol.12, pp.756-766.
- [16] D Cojocaru, RV Tanasie (2008): Graphic simulation for camera calibration in visual-servoing applications Robust visual servoing in 3d reaching; ISCGAV'08 Proceedings of the 8<sup>th</sup> Conference on Signal Processing, Computational Geometry and Artificial Vision, Wisconsin, USA, August 20-22.
- [17] P Eggenberger (1997): Creation of neural networks based on developmental and evolutionary principles; In Proceedings of the International Conference on Artificial Neural Networks, October 8-10, p337-342, Lausanne, Switzerland.
- [18] R Horaud and T Skordas (2001): Model-based strategy Planning for recognizing Partially Occluded Parts; Computer, Vol.5, pp.58-65.
- [19] B Agarwalla, P Hutto (2004): A Multisensor data fusion Architecture; Technical Report, Centre of Experimental Research in Computer Systems, Georgia Institute of Technology, Atlanta.
- [20] J Llinas, DL Hall (1994): A challenge for the data fusion community II - Infrastructure imperatives; Proceedings 7<sup>th</sup> National Symposium on sensor fusion, Vol.85, no.1, Albuquerque NM.
- [21] FR Bach, and M. I. Jordan (2002): Kernel independent component analysis; Journal of Machine Learning Research 3, July 3, pp 1-48.
- [22] G Gomez, P Eggenberger (2004): Investigations on robustness of an evolved learning mechanism for a robot arm; ATR International, Kyoto, Japan.
- [23] V Harri (2004): Behaviourally meaningful representations from normalisation and context-guided denoising; Artificial Intelligence Laboratory, University of Zurich.
- [24] V Harri (2009): Meaningful representations from normalisation and context-guided denoising; Artificial Intelligence Laboratory, University of Zurich.
- [25] S Ashutosh, J Driemeyer (2008): Robotic grasping objects using vision; Proceedings of International Journal of Robotic Research, Vol.27, No2. pp.157-173.
- [26] A Saxena, J Driemeyer (2009); Robotic grasping of novel objects using vision; In IEEE International Conference on Robotics and Automation, ICRA, Vol 27, Issue 2.
- [27] L Rong, A. K. C. Wong, R. V. Mayorga, and X Liang (1996): A vision based on-line motion planning of robot manipulators; In IROS 96 - Intelligent Robots and Systems, Vol.2, pp.940-948, Osaka, Japan.
- [28] J Angeles (2003): Fundamentals of Robotic Mechanical Systems: Theory, Methods, and

- Algorithms; 2<sup>nd</sup> Edition, Springer, pp.19-63, Hong Kong.
- [29] AJ Kelly (1994): Essential Kinematics for Autonomous Vehicles; Technical Report CMU-RI-TR-94-14, Robotics Institute, Carnegie Mellon University.
- [30] GR Pennock, AT Yang (1985): Application of Dual-Number matrices to the inverse kinematics problem of robot manipulators. *Journal of Mechanism Transmission and Automation Design* 107, pp.201-208.
- [31] J Duffy (1980): Analysis of mechanism and robot manipulators; John Wiley, New York, pp419.
- [32] H Cruse, M Bruwer (1990): Simple network controlling the movement of a three joint planar manipulator; *Parallel Neural Systems and Computers*, pp.409-412.
- [33] GD Hager, W-C Chang and AS Morse (1995): Robot Hand-Eye Co-ordination Based on Stereo Vision; *Machine Vision and Applications*, Vol.10, No.3, pp136-143.
- [34] Intelligent robots and computer vision XXV (2007): Algorithms, techniques and active vision; *Proceedings of the Society of Photo-optical Instrumentation Engineers (SPIE)*, Vol. 6764, pp.17640-17640.
- [35] S Hutchinson, G Hager and P Corke (1996): A tutorial on visual servo control; *IEEE Transactions on Robotics and Automation*, Vol.12, No.5, pp.651-670.
- [36] J Modersitski: Numerical methods of Image recognition; Oxford University Press, 2004
- [37] D Kragie and HL Christensen (2003): Robust Visual servoing; *International Journal of Robotics Research (IJRR)*, Vol.22, No.10, pp.923-939.
- [38] SK Pal (1992): Fuzzyness, image information and scene analysis; *An Introduction to Fuzzy Logic Applications in Intelligent Systems*, Kluwer, Boston, pp147-183.
- [39] F Chaumette and E Malis (2000): 2 1/2 D visual servoing: a possible solution to improve image-based and position-based visual servoings; In *IEEE International Conference on Robotics and Automation*, 760345, ICRA, May 3-8, Anchorage, Alaska.
- [40] J Amat, A Casal (1993): Tracking system for dynamic control of convoys; *Robotics and Autonomous systems*, Vol.11, pp.269-277, Issue3-4.
- [41] F Bergholm (1987): Edge focussing; *IEEE Transaction on Pattern Analysis and Machine Intelligence*, Vol.9, pp.726-741.
- [42] RD Howe (1994): Tactile sensing and control of robotic manipulation; *Journal of Advanced Robotics*, Vol.18, No.3, pp.245-261.
- [43] T Koshizen (2001): Improved Sensor Selection Technique by Integrating; *Journal of Intelligence and Robotic Systems*, Vol.29, No1, pp.79-92.

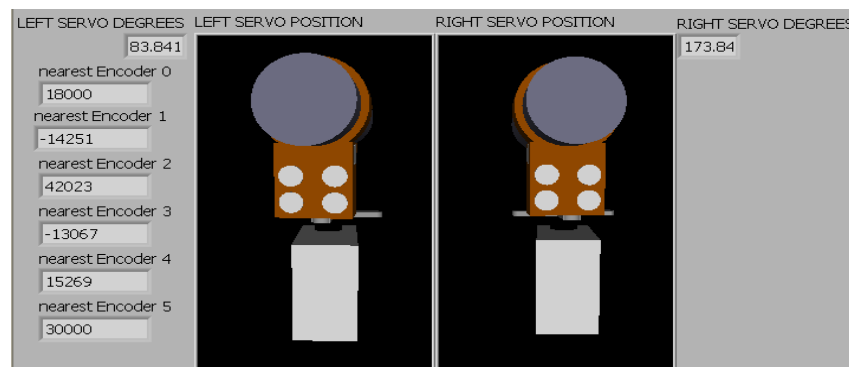
- [44] SP Brooks (1998): Markov chain Monte Carlo method and its application; Journal of the Royal Statistical Society, The Statistician, Vol.47, No.1, pp.69-100, Blackwell Publishing.
- [45] K Hsiao, T Lozano-Perez (2007): Grasping POMDPs; In International Conference on Robotics and Automation, October 17-21, pp.4485-4692, Rome, Italy.
- [46] T Asfour, K Regenstein, P Azad, J Schroder, A Bierbaum, N Vahrenkamp and R Dillmann (2006): ARMAR-III: An Integrated Humanoid Platform for Sensory-Motor Control; IEEE-RAS International Conference on Humanoid Robots, December 12-15, pp.169-175, Genova, Italy.
- [47] M. Charlwood, N Worsell (2004): A methodology for assignment of safety integrated levels (SILs) to safety-related control functions implemented by safety-related electrical, electronic and programmable electronic control systems of machines; UK Health and Safety Executive Research Report 216, Crown copyright 2004, HSE Books.



## Appendix B

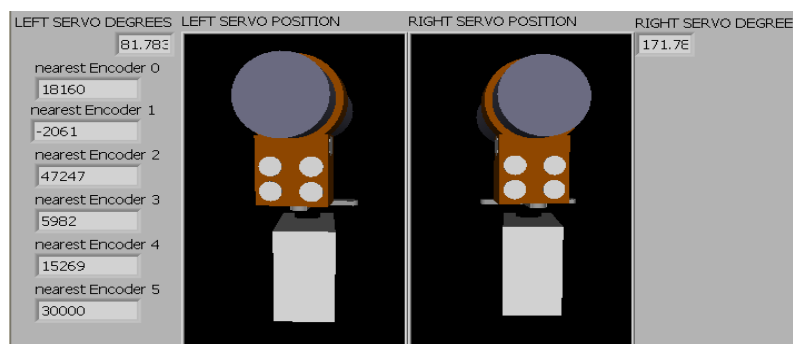
### Visual Servoing Mechanism Commissioning Information

FigureB 1 illustrates the position of the servo motors at the first image acquisition position, directed towards  $Id_{loc}$ . There is little adjustment in servo angle at the first scan coordinates from looking straight ahead, this is caused by the significant distance between the destination coordinates and current manipulator position and pose.



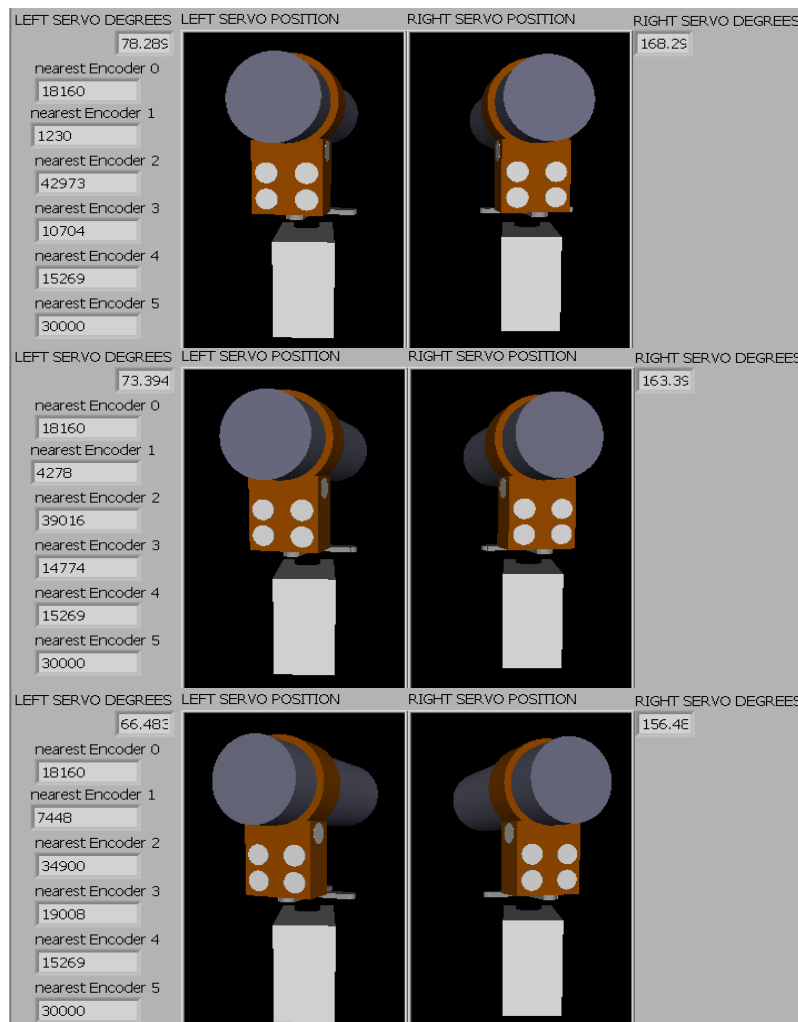
FigureB 1 Servo Adjustment From First Scan Position  
The simulated encoder values are for each joint on the robot arm.  
Information on calibration of encoder values, see Appendix C

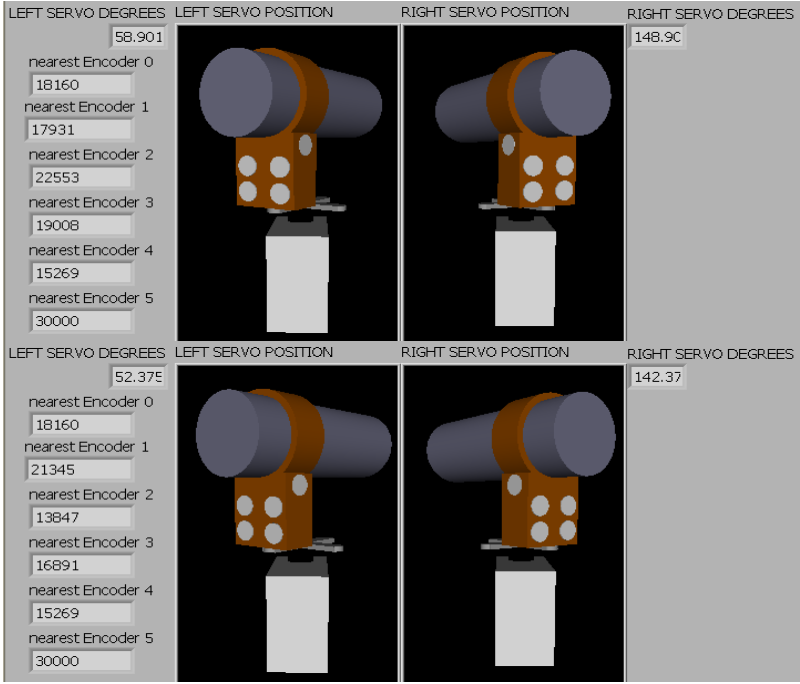
FigureB 2 depicts the adjustment in angle of the servo motors from the first scan position to the short scan position. Only  $1.714^\circ$  adjustment in servo motor angle has occurred. Thus indicating there is still considerable distance for the manipulator to move toward the detected object, hence a wide focus is still required with the manipulator pose in this position.



FigureB 2 Servo Adjustment From First Scan Coordinates to Short Scan Coordinates

As seen in FigureB 2, as the manipulator moves closer to the detected object the servo motors incur a greater variation of angular position. By checking the calculated angles shown in the LabView application to the real world manipulator, it becomes apparent that the servo motor angles does adjust the ROI towards the centre of the field of view of the cameras (as seen in Chapter 4). The LabView frame shown in the bottom of FigureB 3 illustrates the position of the servo motors when the manipulator has grasped the object. At this position the vision system if required can be used to determine any object movement, functioning in cooperation with the tactile (FS force sensor) feedback system. (Using a logical operator to compare one previously acquired image with a newly acquired one).





FigureB 3 LabView Frames Describing Servo Adjustment From Short Scan Coordinates to Grasp Position

## Appendix C

### Virtual Manipulator Commissioning Information

To simulate the real world encoder values from the katana robot in addition to the eventual connection of the virtual control to the real world robot, synchronisation between both is required. The calibration cycle allows for the sequencing and homing of the encoder feedback control. This procedure will reset the joint encoders to pre-programmed values shown in the TableC 1. With Joint 0 controlling  $\Phi$  through to Joint 5, which controls the gripper mechanism.

TableC 1 Calibration Encoder Settings

Joint No.	Motor No.	Encoder pulses / cycle	Enc. calibration value
Joint 0	Motor 5	51200	+3000 (dir positive)
Joint 1	Motor 0	51200	+3000 (dir positive)
Joint 2	Motor 1	94976	-3000 (dir negative)
Joint 3	Motor 2	81408	-3000 (dir negative)
Joint 4	Motor 3	51200	+3000 (dir positive)
Joint 5	Motor 4	51200	+3000 (dir positive)

As seen in Figure 56, the virtual robot arm will commence with all joint angles at  $0^\circ$  (default setting). The real world robot arm calibration procedure also finds the location of the mechanical constraints for each joint angle: whereas for the virtual robot these mechanical stops are programmed in as angle positional limits; which have to be used for the kinematics solution as a checksum (to ensure that the virtual robot arm cannot exceed the rotational requirement for the real world robot arm). Mechanical constraints of the real world robot are specified and angle constraints for the virtual robot, as such referring to Figure 7 a&b.

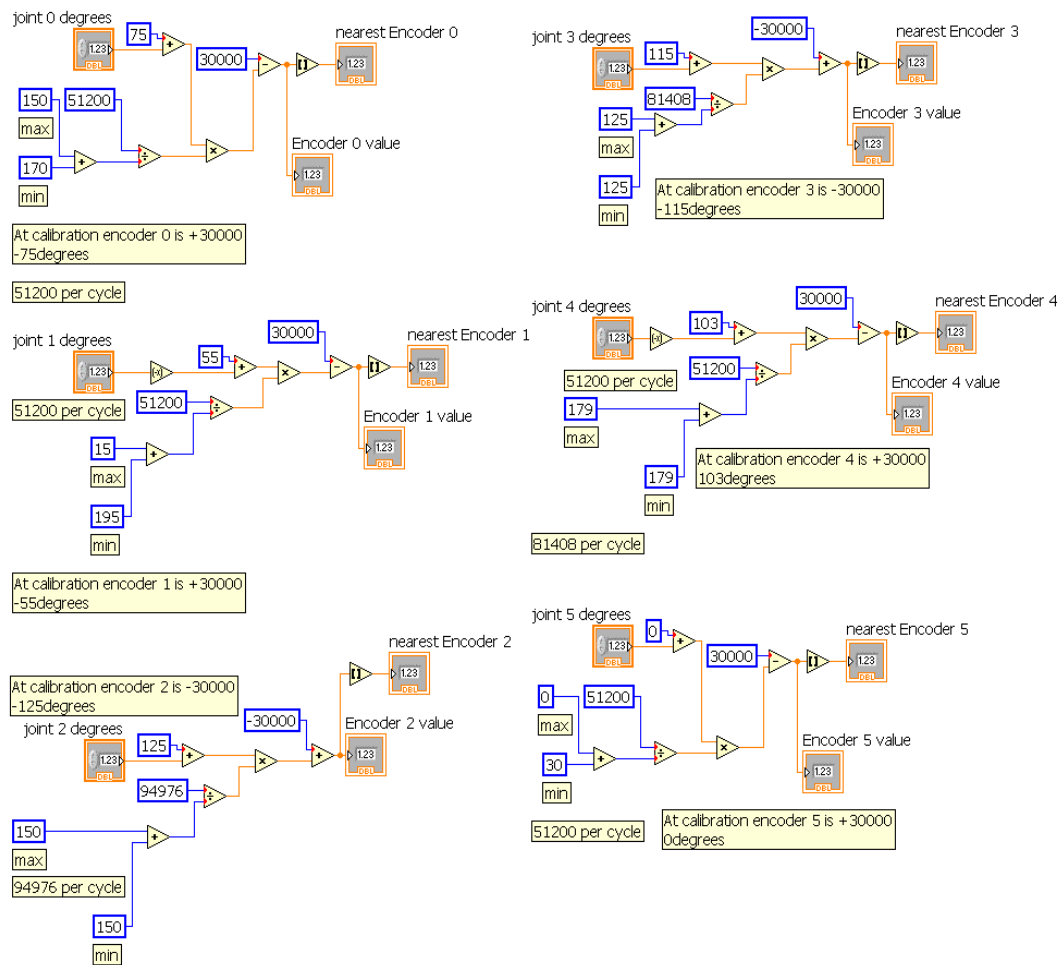
$$\Phi = -170^\circ \text{ to } 150^\circ \longrightarrow 320^\circ \text{ of movement}$$

$$\theta_1 = -195^\circ \text{ to } 15^\circ \longrightarrow 210^\circ \text{ of movement}$$

$$\theta_2 = -150^\circ \text{ to } 150^\circ \longrightarrow 300^\circ \text{ of movement}$$

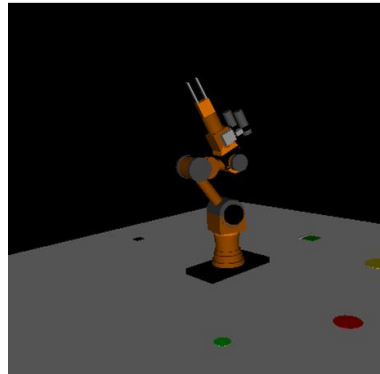
$$\theta_3 = -125^\circ \text{ to } 125^\circ \longrightarrow 250^\circ \text{ of movement}$$

$$\Phi_2 = -180^\circ \text{ to } 180^\circ \longrightarrow 360^\circ \text{ of movement}$$



FigureC 1 Calibration Encoder Settings Algorithm

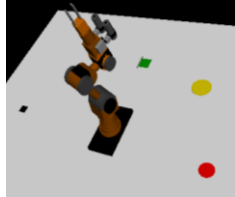
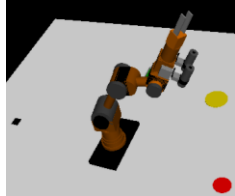
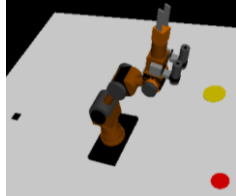
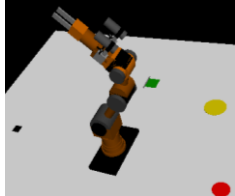
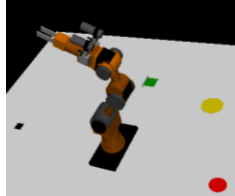
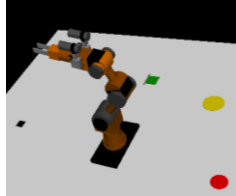
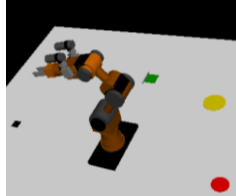
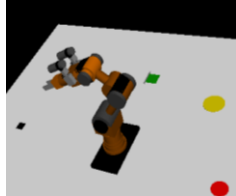
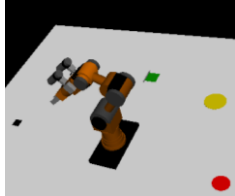
From the initial starting position (Figure 56) the virtual robot will move to the calibration coordinates; loaded from the software database. At the calibration coordinates the virtual robot will synchronise to the real world robot, as seen by the algorithm illustrated in FigureC 1, the calibration position is seen in FigureC 2.



FigureC 2 Virtual Manipulator Calibratation Position

At this position the virtual encoder coordinates illustrated in FigureC 2, would match those shown in TableC 1, when the received encoder feedback correspond to these values, the manipulator begins its operation automatically without the need for any human intervention. LabView frames shown in TableC 2 illustrates how the virtual manipulator manoeuvres from the calibration position to the first image acquisition position (long distance scan) loaded from the excel database, along with the expected encoder values from the real world robot arm.

TableC 2 Labview Frames from Calibration to First Image Scan Position

 <pre> nearest Encoder 0 28720 nearest Encoder 1 1230 nearest Encoder 2 -27467 nearest Encoder 3 -27395 nearest Encoder 4 28856 nearest Encoder 5 30000                     </pre>	 <pre> nearest Encoder 0 27600 nearest Encoder 1 -476 nearest Encoder 2 -25251 nearest Encoder 3 -25116 nearest Encoder 4 27855 nearest Encoder 5 30000                     </pre>	 <pre> nearest Encoder 0 26160 nearest Encoder 1 -2670 nearest Encoder 2 -22402 nearest Encoder 3 -22185 nearest Encoder 4 26568 nearest Encoder 5 30000                     </pre>	 <pre> nearest Encoder 0 24240 nearest Encoder 1 -5596 nearest Encoder 2 -18603 nearest Encoder 3 -18277 nearest Encoder 4 24851 nearest Encoder 5 30000                     </pre>	 <pre> nearest Encoder 0 21920 nearest Encoder 1 -9131 nearest Encoder 2 -14012 nearest Encoder 3 -13556 nearest Encoder 4 22778 nearest Encoder 5 30000                     </pre>
 <pre> nearest Encoder 0 19600 nearest Encoder 1 -12667 nearest Encoder 2 -9422 nearest Encoder 3 -13067 nearest Encoder 4 20704 nearest Encoder 5 30000                     </pre>	 <pre> nearest Encoder 0 18000 nearest Encoder 1 -14251 nearest Encoder 2 -3723 nearest Encoder 3 -13067 nearest Encoder 4 18130 nearest Encoder 5 30000                     </pre>	 <pre> nearest Encoder 0 18000 nearest Encoder 1 -14251 nearest Encoder 2 709 nearest Encoder 3 -13067 nearest Encoder 4 16127 nearest Encoder 5 30000                     </pre>	 <pre> nearest Encoder 0 18000 nearest Encoder 1 -14251 nearest Encoder 2 7041 nearest Encoder 3 -13067 nearest Encoder 4 15269 nearest Encoder 5 30000                     </pre>	 <pre> nearest Encoder 0 18000 nearest Encoder 1 -14251 nearest Encoder 2 15588 nearest Encoder 3 -13067 nearest Encoder 4 15269 nearest Encoder 5 30000                     </pre>
 <pre> nearest Encoder 0 18000 nearest Encoder 1 -14251 nearest Encoder 2 21762 nearest Encoder 3 -13067 nearest Encoder 4 15269 nearest Encoder 5 30000                     </pre>	 <pre> nearest Encoder 0 18000 nearest Encoder 1 -14251 nearest Encoder 2 26986 nearest Encoder 3 -13067 nearest Encoder 4 15269 nearest Encoder 5 30000                     </pre>	 <pre> nearest Encoder 0 18000 nearest Encoder 1 -14251 nearest Encoder 2 33951 nearest Encoder 3 -13067 nearest Encoder 4 15269 nearest Encoder 5 30000                     </pre>	 <pre> nearest Encoder 0 18000 nearest Encoder 1 -14251 nearest Encoder 2 37433 nearest Encoder 3 -13067 nearest Encoder 4 15269 nearest Encoder 5 30000                     </pre>	 <pre> nearest Encoder 0 18000 nearest Encoder 1 -14251 nearest Encoder 2 42023 nearest Encoder 3 -13067 nearest Encoder 4 15269 nearest Encoder 5 30000                     </pre>

At each point within the movement, each joint location in 3D space is calculated in order to resolve the end effector movement in the shortest time possible. The encoder values displayed are those values expected to be received from the real world robot motor encoders. Stringent control is maintained to ensure the real world manipulator corresponds to the

movement from the virtual manipulator; by comparison of feedback encoder values to the virtual encoder values.

Long scan position to short scan position

The new coordinate location for the end effector is supplied by the vision system. The pose and distance away from the object is uploaded from the database. The manipulator uses this information to position itself for a closer inspection of the detected object, as seen in TableC 3.

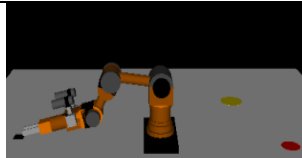
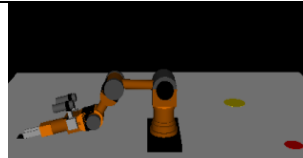
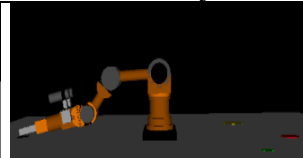
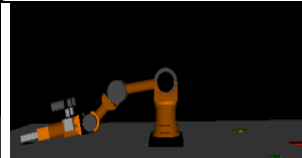
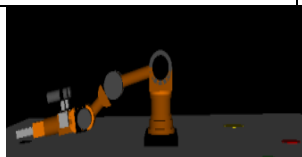
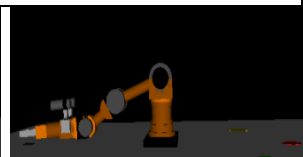
TableC 3 Labview Frames from Long Scan Position to Short Scan Coordinates

 <p>nearest Encoder 0 18160 nearest Encoder 1 -11570 nearest Encoder 2 45823 nearest Encoder 3 -9485 nearest Encoder 4 15269 nearest Encoder 5 30000</p> <p>x position y position Z position 254.12 142.17 4.4356</p>	 <p>nearest Encoder 0 18160 nearest Encoder 1 -9497 nearest Encoder 2 47247 nearest Encoder 3 -6717 nearest Encoder 4 15269 nearest Encoder 5 30000</p> <p>x position y position Z position 257.658 106.347 4.4974</p>	 <p>nearest Encoder 0 18160 nearest Encoder 1 -6571 nearest Encoder 2 47247 nearest Encoder 3 -2810 nearest Encoder 4 15269 nearest Encoder 5 30000</p> <p>x position y position Z position 287.665 86.2891 5.0212</p>
 <p>nearest Encoder 0 18160 nearest Encoder 1 -2305 nearest Encoder 2 47247 nearest Encoder 3 2889 nearest Encoder 4 15269 nearest Encoder 5 30000</p> <p>x position y position Z position 322.464 46.9406 5.6286</p>	 <p>nearest Encoder 0 18160 nearest Encoder 1 -2061 nearest Encoder 2 47247 nearest Encoder 3 5982 nearest Encoder 4 15269 nearest Encoder 5 30000</p> <p>x position y position Z position 360.247 73.4295 6.2881</p>	 <p>nearest Encoder 0 18160 nearest Encoder 1 -2061 nearest Encoder 2 47247 nearest Encoder 3 6145 nearest Encoder 4 15269 nearest Encoder 5 30000</p> <p>x position y position Z position 362.236 75.3011 6.322E</p>

Short scan position to object grasp position

The position shown bottom right in TableC 3 shown the end effector positioned 200mm away from the object. With the end effector directly behind the object the manipulator, (simulated as though the robot arm is working in a nuclear environment), will position itself horizontal to the workspace with adequate ground clearance, so as to ensure object is gripped without obstruction, shown by the LabView frames in TableC 4. Another image acquisition can be actioned to reinforce the information gathered from the short scan. More detailed measurements can be taken by the use of edge detection system.

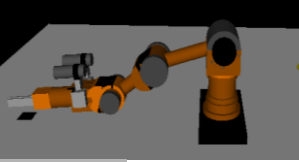
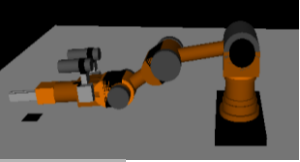
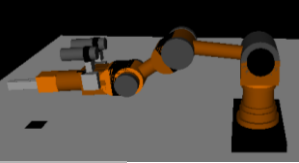
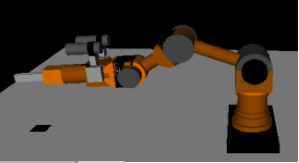
TableC 4 End Effector Position to Enable Object Grasp

 <pre> nearest Encoder 0 18160 nearest Encoder 1 14762 nearest Encoder 2 32051 nearest Encoder 3 23892 nearest Encoder 4 15269 nearest Encoder 5 30000 x position y position Z position 555.289 41.4944 9.6926                     </pre>	 <pre> nearest Encoder 0 18160 nearest Encoder 1 16103 nearest Encoder 2 28569 nearest Encoder 3 22101 nearest Encoder 4 15269 nearest Encoder 5 30000 x position y position Z position 568.434 29.8425 9.922C                     </pre>	 <pre> nearest Encoder 0 18160 nearest Encoder 1 17200 nearest Encoder 2 24769 nearest Encoder 3 20147 nearest Encoder 4 15269 nearest Encoder 5 30000 x position y position Z position 584.861 33.5543 10.20E                     </pre>	 <pre> nearest Encoder 0 18160 nearest Encoder 1 18419 nearest Encoder 2 20970 nearest Encoder 3 18194 nearest Encoder 4 15269 nearest Encoder 5 30000 x position y position Z position 596.869 33.979 10.41E                     </pre>
<b>Point A</b>			
 <pre> nearest Encoder 0 18160 nearest Encoder 1 19638 nearest Encoder 2 17488 nearest Encoder 3 16891 nearest Encoder 4 15269 nearest Encoder 5 30000 x position y position Z position 605.242 39.4943 10.564                     </pre>	 <pre> nearest Encoder 0 18160 nearest Encoder 1 20857 nearest Encoder 2 14480 nearest Encoder 3 16891 nearest Encoder 4 15269 nearest Encoder 5 30000 x position y position Z position 609.926 56.8273 10.646                     </pre>	 <pre> nearest Encoder 0 18160 nearest Encoder 1 21345 nearest Encoder 2 13847 nearest Encoder 3 16891 nearest Encoder 4 15269 nearest Encoder 5 30000 x position y position Z position 607.822 50.5381 10.605                     </pre>	
<b>Point B</b>			

The movement begins with the end effector only 26mm above the robots workspace; as a result any movement produced by the manipulator has to occur with great care and precision. The end effector position to the robot workspace is best seen during the movement at Point A to point B.

The movement from the grasp location to the clearance height is seen below in TableC 5. The manipulator remains horizontal to the workspace (to ensure if manipulating a liquid, no spillage occurs). There is no significant movement forwards (x) or sideways (z), only the height (y) is increased to clear the workspace. At this position, the manipulator will make a decision of how to achieve the finishing coordinates, with the knowledge that the manipulator has to remain horizontal to the workspace.

TableC 5 Manipulator Movement to Lift Grasped Object Clear of Workspace

 <pre> nearest Encoder 0 18160 nearest Encoder 1 20248 nearest Encoder 2 15588 nearest Encoder 3 17379 nearest Encoder 4 15269 nearest Encoder 5 -4133 x position y position Z position 611.085 65.4884 10.666                     </pre>	 <pre> nearest Encoder 0 18160 nearest Encoder 1 18907 nearest Encoder 2 17330 nearest Encoder 3 17379 nearest Encoder 4 15269 nearest Encoder 5 -4133 x position y position Z position 614.953 83.3049 10.734                     </pre>	 <pre> nearest Encoder 0 18160 nearest Encoder 1 16956 nearest Encoder 2 19862 nearest Encoder 3 17379 nearest Encoder 4 15269 nearest Encoder 5 -4133 x position y position Z position 617.493 109.69 10.77E                     </pre>
 <pre> nearest Encoder 0 18160 nearest Encoder 1 15128 nearest Encoder 2 22237 nearest Encoder 3 17379 nearest Encoder 4 15269 nearest Encoder 5 -4133 x position y position Z position 616.518 134.524 10.761                     </pre>	 <pre> nearest Encoder 0 18160 nearest Encoder 1 13543 nearest Encoder 2 24295 nearest Encoder 3 17379 nearest Encoder 4 15269 nearest Encoder 5 -4133 x position y position Z position 613.055 155.788 10.70C                     </pre>	 <pre> nearest Encoder 0 18160 nearest Encoder 1 11958 nearest Encoder 2 26352 nearest Encoder 3 17379 nearest Encoder 4 15269 nearest Encoder 5 -4133 x position y position Z position 607.208 176.522 10.59E                     </pre>

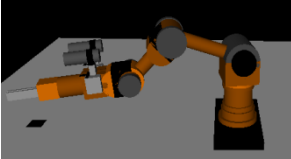
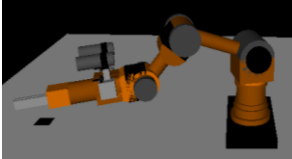
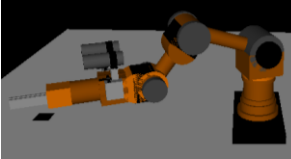
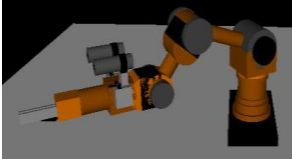
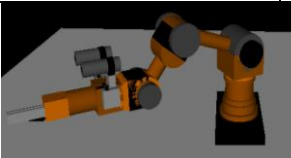
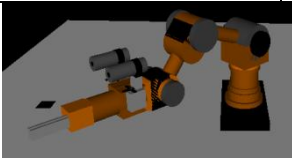
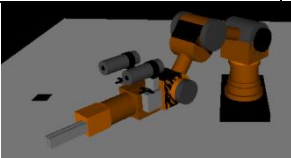
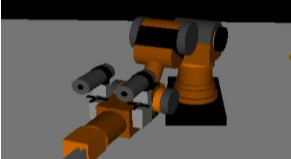
For each of the three different objects there are three different locations, shown as different coloured area on the robots workspace:

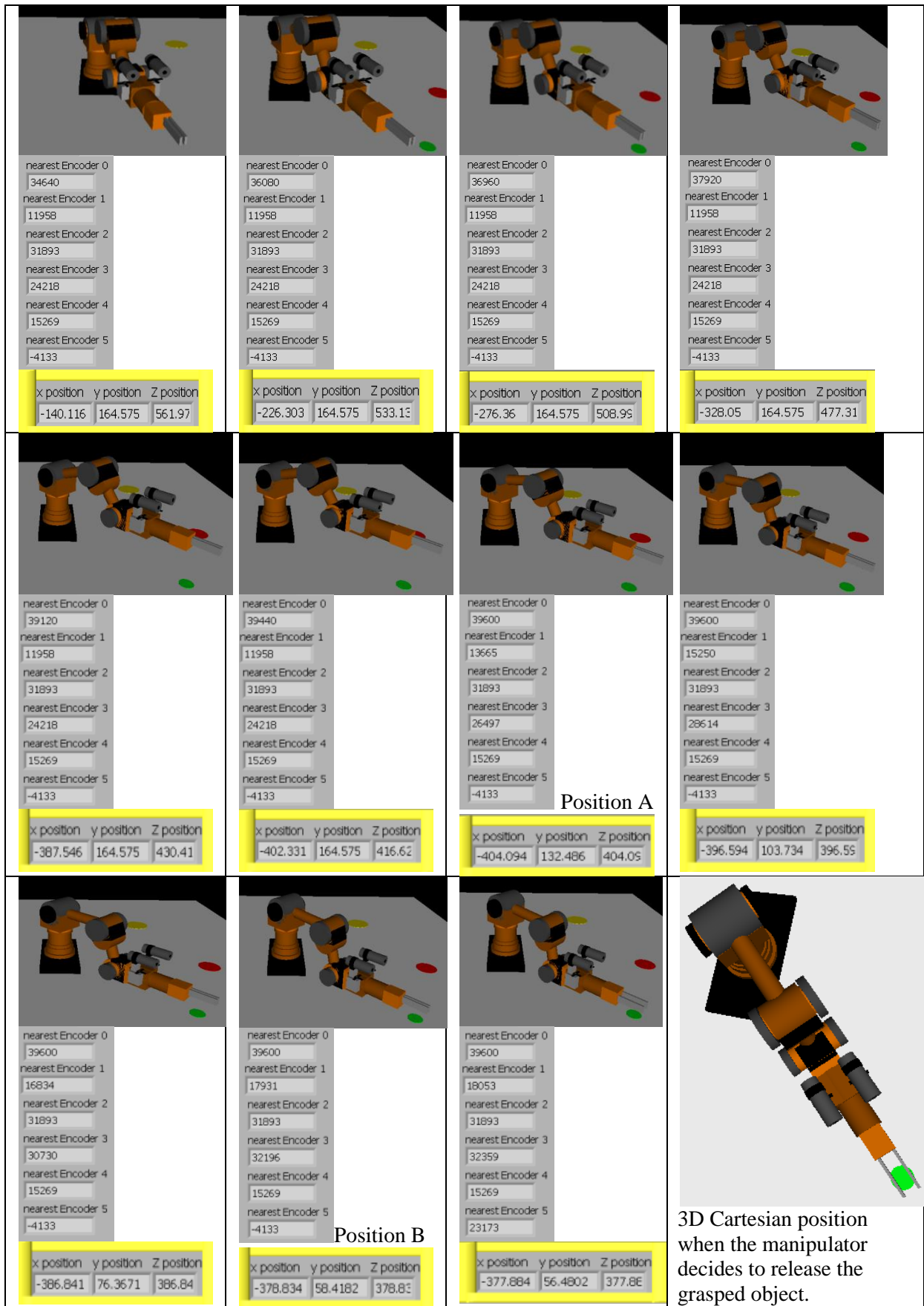
- 1) The object coloured 'Green Blue Orange Pink Orange' (GBOPO) – Green.
- 2) The object coloured 'Pink Orange Blue Green' (POBG) – Red.
- 3) The object coloured 'Pink Blue Orange green' (PBOG) – Yellow.

#### Manipulator movement to 'drop-off' the GBOPO object

The GBOPO object being detected, the manipulator is required to move to the light green spot on the virtual workspace, position itself at the same height as when the object was grasped; then release the object. The LabView frames of the movement are seen in TableC 6, illustrates how the manipulator moves from the clearance position to the 'drop-off' position. Throughout the movement, the applied force is continuously monitored for any variance, to ensure that the object does not slip or become damaged due to the applied force of the gripper mechanism. At the start of the movement the height of the manipulator drops to 143mm. At this point the kinematic equation is unresolved and as a result the manipulator, for a limited time, cannot decide on the appropriate position in joint space. However the manipulator quickly corrects this error with the additional algorithms used in conjunction with the kinematic solutions, and increases the height to 164.5mm for the majority of the movement before reducing in height near the 'drop-off' location.

Table C 6 LabView Frames Illustrating Movement to Drop GBOPO Object

 <p>nearest Encoder 0 19760 nearest Encoder 1 11958 nearest Encoder 2 29835 nearest Encoder 3 20636 nearest Encoder 4 15269 nearest Encoder 5 -4133</p> <p>x position y position Z position 579.132 150.512 112.57</p>	 <p>nearest Encoder 0 20480 nearest Encoder 1 11958 nearest Encoder 2 31260 nearest Encoder 3 22101 nearest Encoder 4 15269 nearest Encoder 5 -4133</p> <p>x position y position Z position 560.791 143.104 155.52</p>	 <p>nearest Encoder 0 21440 nearest Encoder 1 11958 nearest Encoder 2 31893 nearest Encoder 3 24055 nearest Encoder 4 15269 nearest Encoder 5 -4133</p> <p>x position y position Z position 538.866 161.844 212.26</p>	 <p>nearest Encoder 0 22640 nearest Encoder 1 11958 nearest Encoder 2 31893 nearest Encoder 3 24218 nearest Encoder 4 15269 nearest Encoder 5 -4133</p> <p>x position y position Z position 506.561 164.575 280.75</p>
 <p>nearest Encoder 0 22640 nearest Encoder 1 11958 nearest Encoder 2 31893 nearest Encoder 3 24218 nearest Encoder 4 15269 nearest Encoder 5 -4133</p> <p>x position y position Z position 506.561 164.575 280.75</p>	 <p>nearest Encoder 0 24800 nearest Encoder 1 11958 nearest Encoder 2 31893 nearest Encoder 3 24218 nearest Encoder 4 15269 nearest Encoder 5 -4133</p> <p>x position y position Z position 427.015 164.575 391.2E</p>	 <p>nearest Encoder 0 26160 nearest Encoder 1 11958 nearest Encoder 2 31893 nearest Encoder 3 24218 nearest Encoder 4 15269 nearest Encoder 5 -4133</p> <p>x position y position Z position 364.489 164.575 450.1C</p>	 <p>nearest Encoder 0 27440 nearest Encoder 1 11958 nearest Encoder 2 31893 nearest Encoder 3 24218 nearest Encoder 4 15269 nearest Encoder 5 -4133</p> <p>x position y position Z position 298.299 164.575 496.4E</p>
 <p>nearest Encoder 0 28960 nearest Encoder 1 11958 nearest Encoder 2 31893 nearest Encoder 3 24218 nearest Encoder 4 15269 nearest Encoder 5 -4133</p> <p>x position y position Z position 212.269 164.575 538.87</p>	 <p>nearest Encoder 0 30800 nearest Encoder 1 11958 nearest Encoder 2 31893 nearest Encoder 3 24218 nearest Encoder 4 15269 nearest Encoder 5 -4133</p> <p>x position y position Z position 100.573 164.575 570.37</p>	 <p>nearest Encoder 0 32080 nearest Encoder 1 11958 nearest Encoder 2 31893 nearest Encoder 3 24218 nearest Encoder 4 15269 nearest Encoder 5 -4133</p> <p>x position y position Z position 20.213 164.575 578.82</p>	 <p>nearest Encoder 0 33520 nearest Encoder 1 11958 nearest Encoder 2 31893 nearest Encoder 3 24218 nearest Encoder 4 15269 nearest Encoder 5 -4133</p> <p>x position y position Z position -70.5841 164.575 574.86</p>

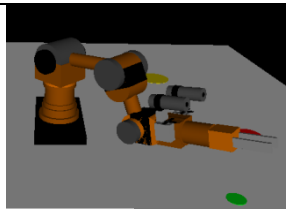
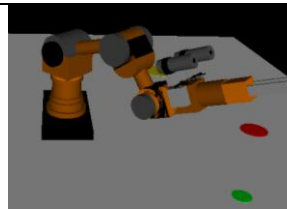
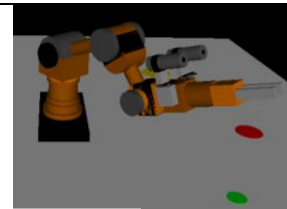
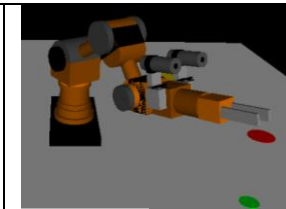
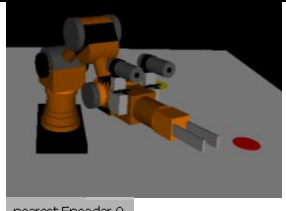
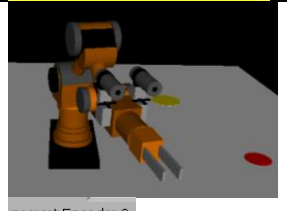


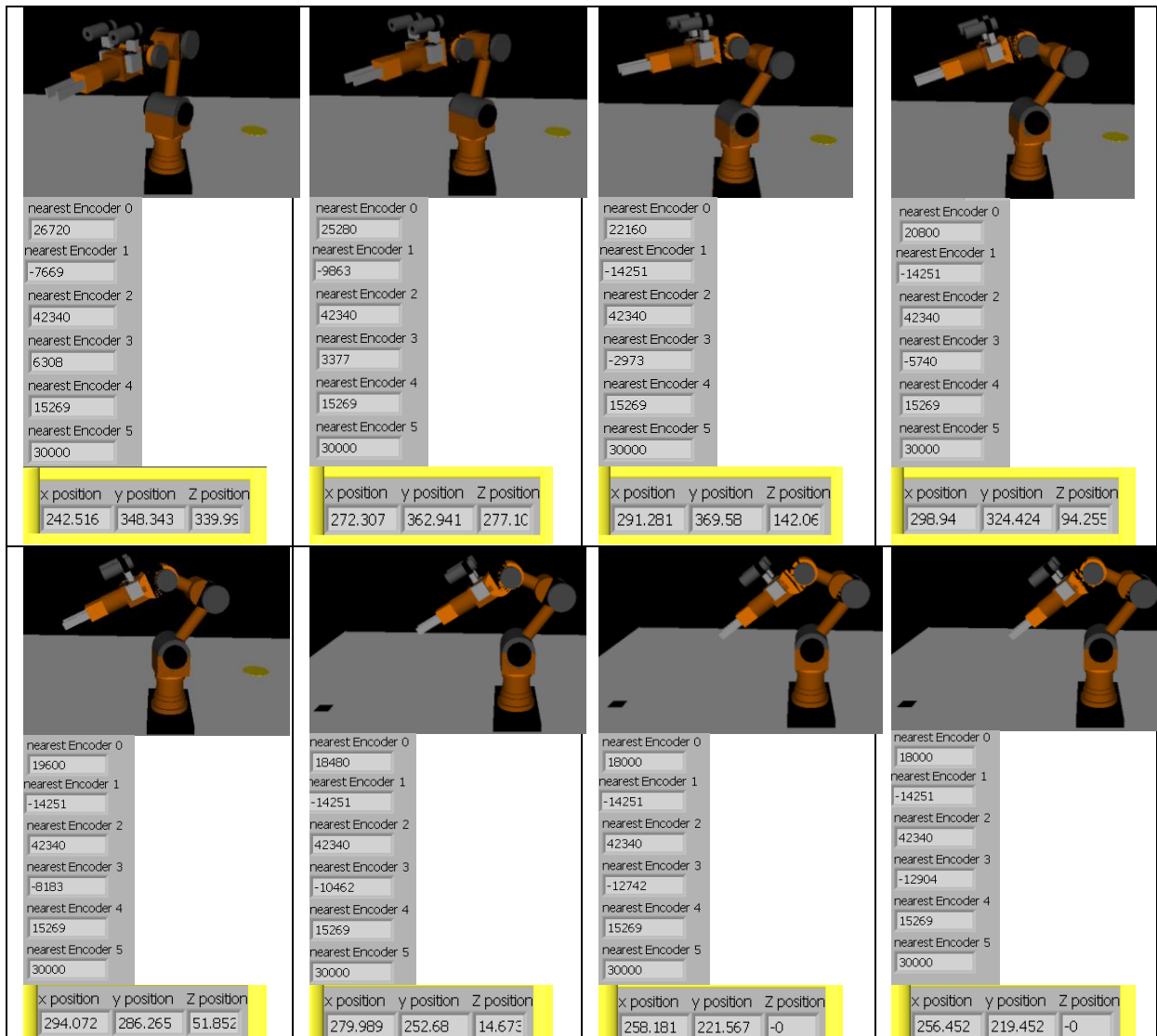
At position A (shown in TableC 6), the manipulator decides to decrease in height towards the ‘drop-off’ point; whilst ensuring the 0° orientation. At position B, the manipulator has checked the correct position and is confident to release the grasped object. The overhead view of the final position within this movement is shown bottom-right within the table.

Return to scan position from GBOPO ‘drop-off’ location

In order for the manipulator to continue to function in an efficient manner, the manipulator is required to return to the first image acquisition position. TableC 7 illustrates the LabView frames of how the kinematics resolves this movement.

TableC 7 LabView Frames Describing Movement From GBOPO 'drop-off' Position to First Scan Coordinates

 <pre> nearest Encoder 0 39600 nearest Encoder 1 15250 nearest Encoder 2 31893 nearest Encoder 3 32521 nearest Encoder 4 15269 nearest Encoder 5 30000 x position y position Z position -391.758 168.81 391.75                     </pre>	 <pre> nearest Encoder 0 39600 nearest Encoder 1 12202 nearest Encoder 2 31893 nearest Encoder 3 32521 nearest Encoder 4 15269 nearest Encoder 5 30000 x position y position Z position -389.005 289.736 389.00                     </pre>	 <pre> nearest Encoder 0 38960 nearest Encoder 1 10983 nearest Encoder 2 33159 nearest Encoder 3 31219 nearest Encoder 4 15269 nearest Encoder 5 30000 x position y position Z position -362.569 291.671 417.00                     </pre>	 <pre> nearest Encoder 0 37520 nearest Encoder 1 8789 nearest Encoder 2 36008 nearest Encoder 3 28288 nearest Encoder 4 15269 nearest Encoder 5 30000 x position y position Z position -293.172 271.148 469.17                     </pre>
 <pre> nearest Encoder 0 36240 nearest Encoder 1 6838 nearest Encoder 2 38541 nearest Encoder 3 25683 nearest Encoder 4 15269 nearest Encoder 5 30000 x position y position Z position -221.311 249.405 497.07                     </pre>	 <pre> nearest Encoder 0 34880 nearest Encoder 1 4766 nearest Encoder 2 41232 nearest Encoder 3 22915 nearest Encoder 4 15269 nearest Encoder 5 30000 x position y position Z position -140.211 223.185 505.50                     </pre>	 <pre> nearest Encoder 0 32000 nearest Encoder 1 377 nearest Encoder 2 42340 nearest Encoder 3 17054 nearest Encoder 4 15269 nearest Encoder 5 30000 x position y position Z position 21.683 261.234 496.62                     </pre>	 <pre> nearest Encoder 0 28720 nearest Encoder 1 -4621 nearest Encoder 2 42340 nearest Encoder 3 10378 nearest Encoder 4 15269 nearest Encoder 5 30000 x position y position Z position 177.213 320.907 417.40                     </pre>

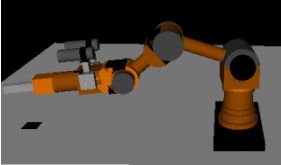
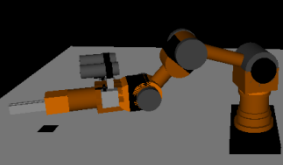
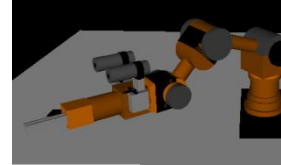
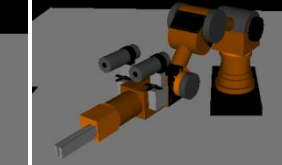
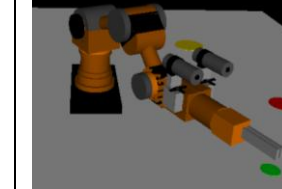
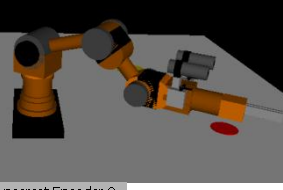
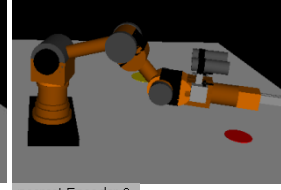
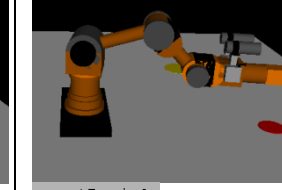


With the manipulator now returned to the first image acquisition position, the vision system is again engaged and scans the robots workspace for an object that matches the images saved within the image database.

Manipulator movement to ‘drop-off’ the POBG object

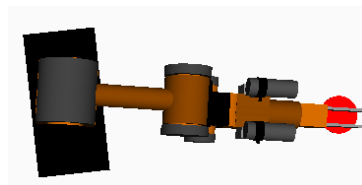
The ‘drop-off’ coordinates for the POBG object is 180° from the  $Id_{loc}$  coordinate. The movement from the clearance position and the final ‘drop-off’ position is shown by the LabView frames in TableC 8.

Table C 8 LabView Frames Illustrating Movement to Drop POBG Object

 <p>nearest Encoder 0 19040 nearest Encoder 1 11958 nearest Encoder 2 28569 nearest Encoder 3 19333 nearest Encoder 4 15269 nearest Encoder 5 -4133</p> <p>x position y position Z position 592.753 157.608 67.53E</p>	 <p>nearest Encoder 0 21200 nearest Encoder 1 11958 nearest Encoder 2 30151 nearest Encoder 3 22427 nearest Encoder 4 15269 nearest Encoder 5 -4133</p> <p>x position y position Z position 553.673 173.37 201.52</p>	 <p>nearest Encoder 0 24080 nearest Encoder 1 11958 nearest Encoder 2 30151 nearest Encoder 3 22427 nearest Encoder 4 15269 nearest Encoder 5 -4133</p> <p>x position y position Z position 464.301 173.37 362.7E</p>	 <p>nearest Encoder 0 27440 nearest Encoder 1 11958 nearest Encoder 2 30151 nearest Encoder 3 22427 nearest Encoder 4 15269 nearest Encoder 5 -4133</p> <p>x position y position Z position 303.464 173.37 505.04</p>
 <p>nearest Encoder 0 29680 nearest Encoder 1 11958 nearest Encoder 2 30151 nearest Encoder 3 22427 nearest Encoder 4 15269 nearest Encoder 5 -4133</p> <p>x position y position Z position 172.267 173.37 563.4E</p>	 <p>nearest Encoder 0 32080 nearest Encoder 1 11958 nearest Encoder 2 30151 nearest Encoder 3 22427 nearest Encoder 4 15269 nearest Encoder 5 -4133</p> <p>x position y position Z position 20.563 173.37 588.84</p>	 <p>nearest Encoder 0 34640 nearest Encoder 1 11958 nearest Encoder 2 30151 nearest Encoder 3 22427 nearest Encoder 4 15269 nearest Encoder 5 -4133</p> <p>x position y position Z position -142.542 173.37 571.7C</p>	 <p>nearest Encoder 0 36720 nearest Encoder 1 11958 nearest Encoder 2 30151 nearest Encoder 3 22427 nearest Encoder 4 15269 nearest Encoder 5 -4133</p> <p>x position y position Z position -267.494 173.37 524.9E</p>
 <p>nearest Encoder 0 39200 nearest Encoder 1 11958 nearest Encoder 2 30151 nearest Encoder 3 22427 nearest Encoder 4 15269 nearest Encoder 5 -4133</p> <p>x position y position Z position -398.062 173.37 434.4C</p>	 <p>nearest Encoder 0 41600 nearest Encoder 1 11958 nearest Encoder 2 30151 nearest Encoder 3 22427 nearest Encoder 4 15269 nearest Encoder 5 -4133</p> <p>x position y position Z position -496.931 173.37 316.5E</p>	 <p>nearest Encoder 0 43520 nearest Encoder 1 11958 nearest Encoder 2 30151 nearest Encoder 3 22427 nearest Encoder 4 15269 nearest Encoder 5 -4133</p> <p>x position y position Z position -551.893 173.37 206.34</p>	 <p>nearest Encoder 0 45200 nearest Encoder 1 11958 nearest Encoder 2 30151 nearest Encoder 3 22427 nearest Encoder 4 15269 nearest Encoder 5 -4133</p> <p>x position y position Z position -580.255 173.37 102.31</p> <p style="text-align: right;">Position A</p>



The manipulator realises that there is an angle constraint, if rotated clockwise toward the destination and therefore repeats the identical route taken for the GBOPO object. However this time with the ‘drop-off’ point being position further away from the centre of the robot arm, the kinematics has been efficiently resolved (joint space is not as close together); hence the height of the manipulator remains constant from the lift position (173mm). At position A the manipulator realises that it is close to the destination coordinates and begins the descent to the ‘drop-off’ location, as seen in FigureC 3.

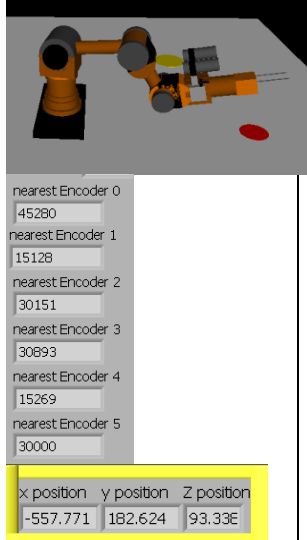
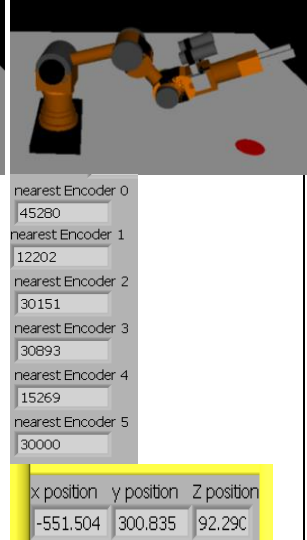
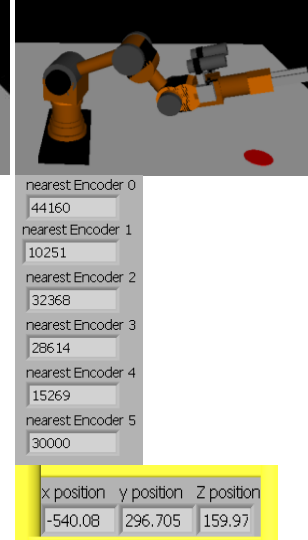
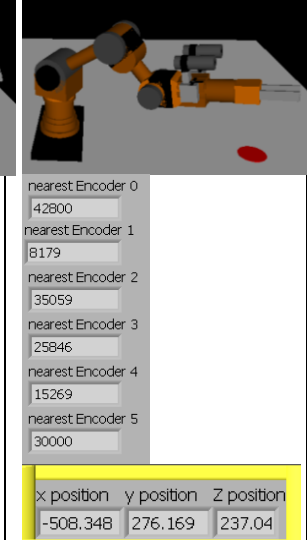
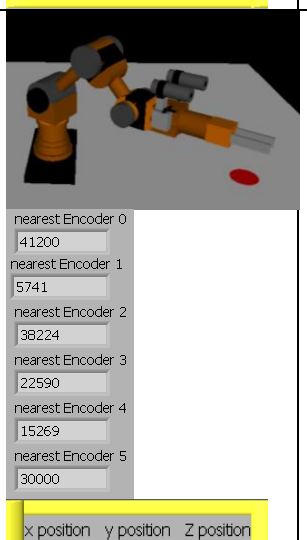
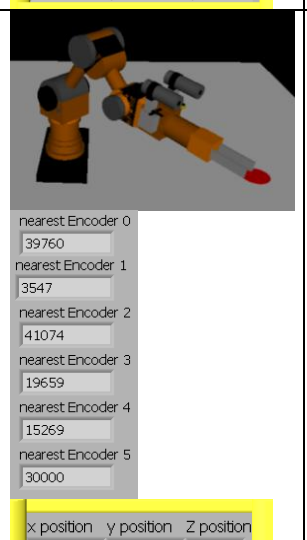
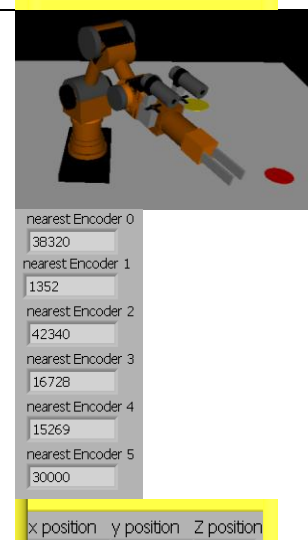
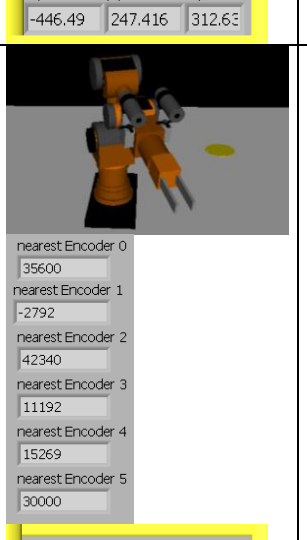
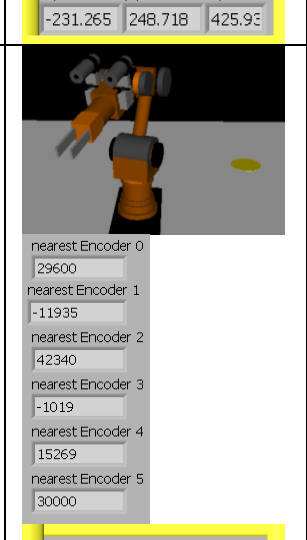


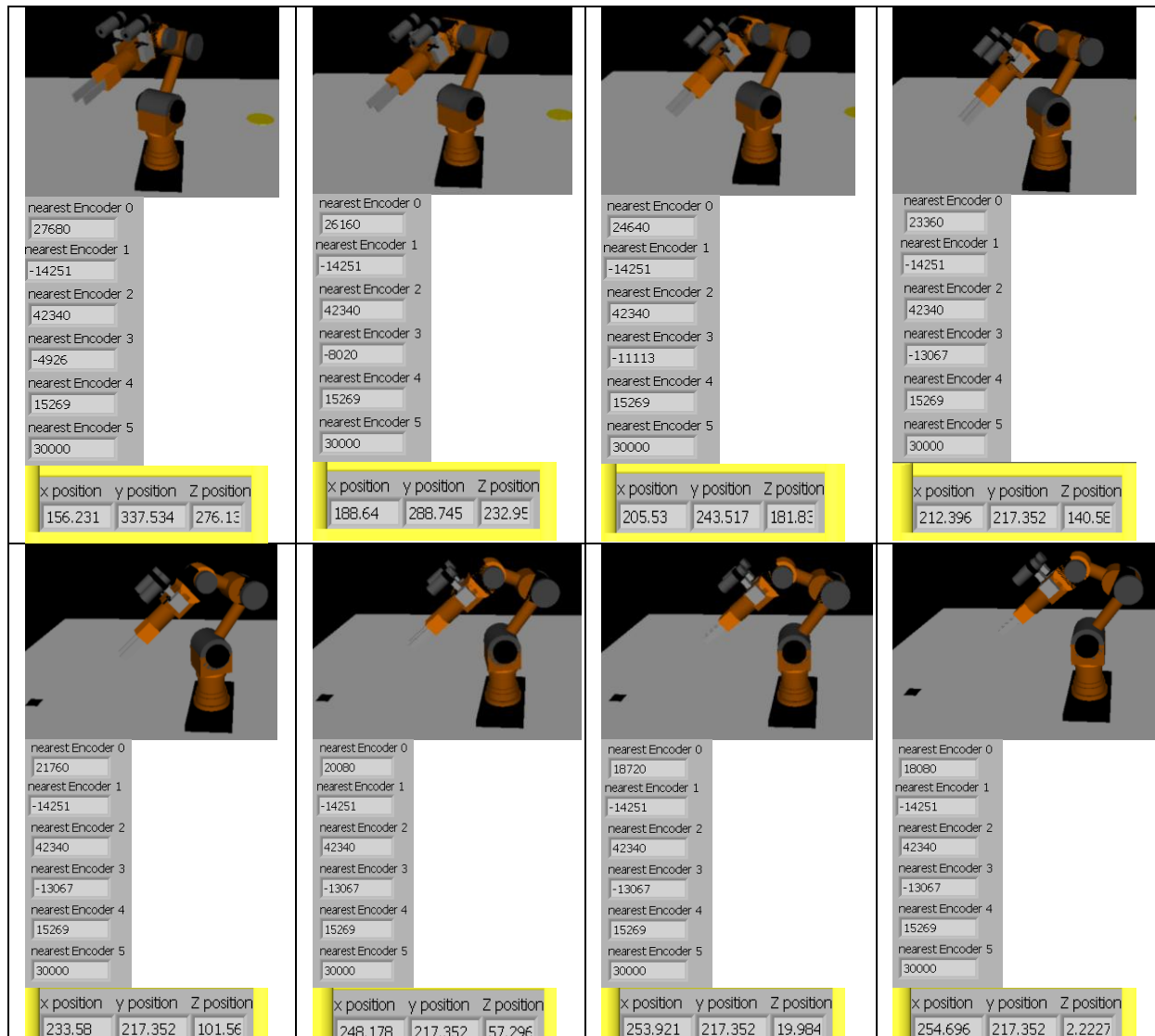
FigureC 3 POBG 'drop-off' Destination Position of Manipulator

Return to scan position from POBG ‘drop-off’ location

The manipulator is required to return to the first image acquisition position, therefore the kinematics is resolved to ensure a quick return to this position, the LabView frames for this movement is seen in TableC 9.

Table C 9 LabView Frames Depicting Movement from POBG 'drop-off' position to First Scan Position



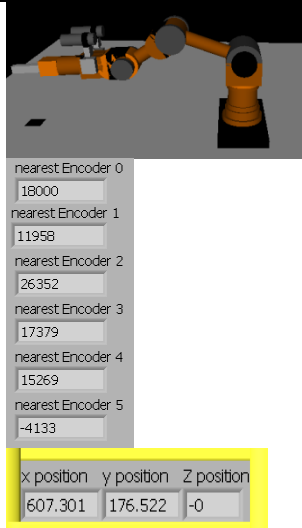
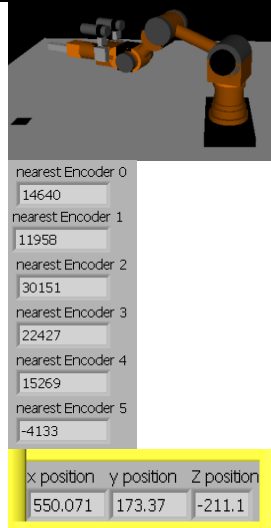
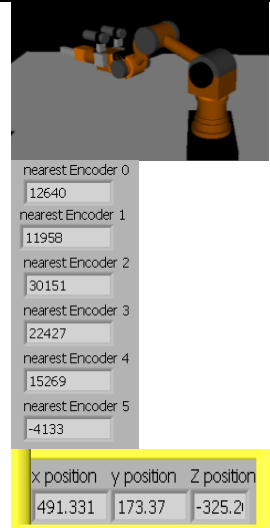
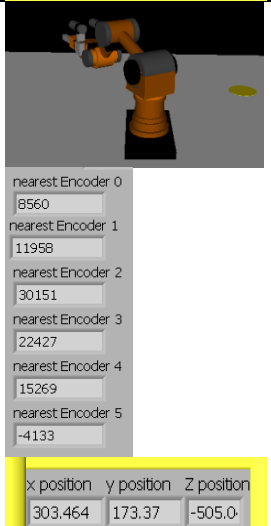
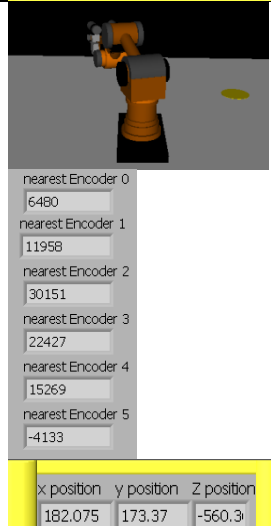
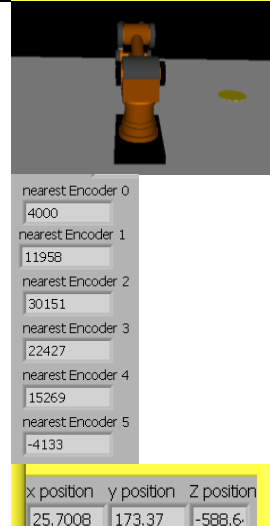
Due to the difference in joint space, the manipulator returns to the first scan position slightly different than the GBOPO ‘drop-off’ point. Although the rotation of Joint 0 is identical the manipulator orientation reaches its final position sooner, therefore the manipulator waits until the rest of the robot arm has completed the revolution to the first scan position.

Manipulator movement to ‘drop-off’ the PBOG object

The ‘drop-off’ location for the PBOG object is situated at it nearest, in the opposite direction to the other ‘drop-off’ locations and just before the location of the programmed angle limit. As seen in TableC 10, the manipulator decides that the ‘drop-off’ position for this respective object is before the programmed mechanical stop, and uses the Euler’s calculation to make the robot arm rotate clockwise towards the destination. For the manipulator to reach the destination coordinates, the joint space is as

compact as the drop-off coordinates for GBOPO object, therefore at the start of movement the kinematics are unresolved. However the calculations quickly correct themselves and return to the required height for the movement to destination. At position A the manipulator is in close proximity to the destination and begins the descent toward the target, again ensuring that the manipulator is horizontal to the workspace. When the feedback from the joint position matches the same height that the manipulator grasped the object, the gripper mechanism released the object.

TableC 10 LabView Frames Illustrating Movement to Drop PBOG Object

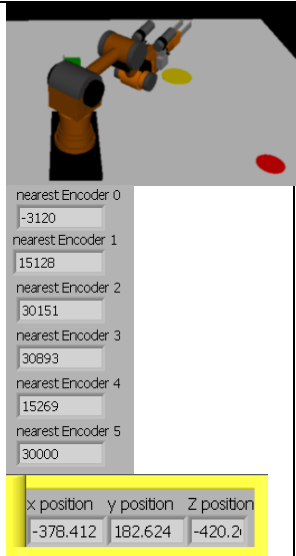
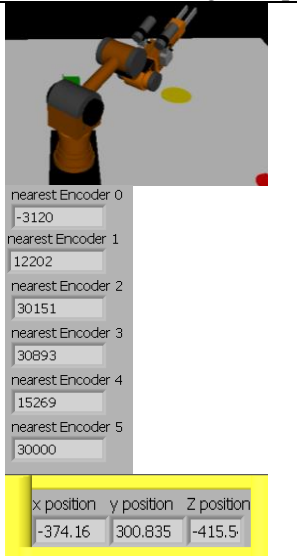
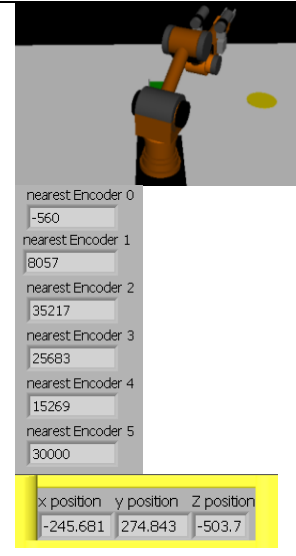
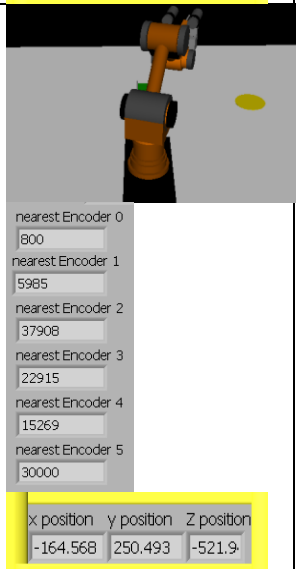
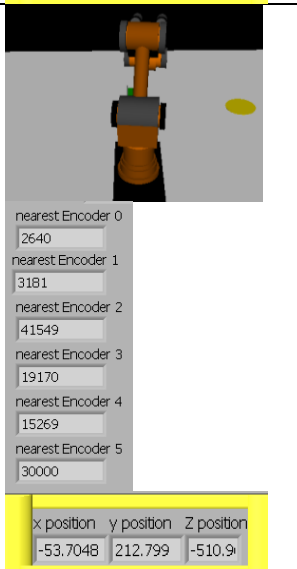
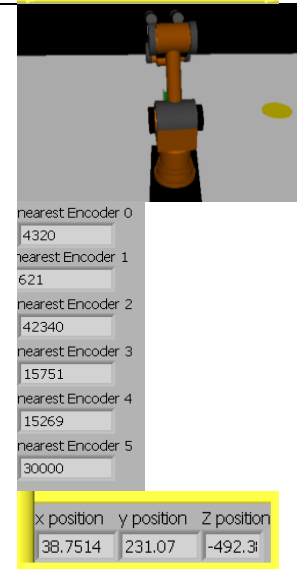
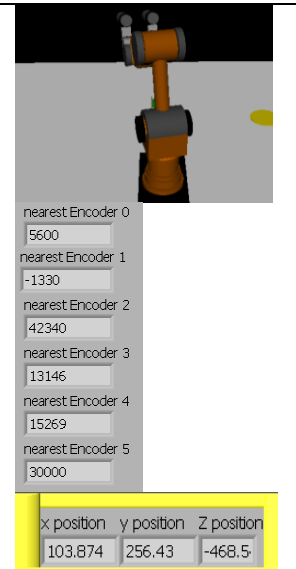
			
			

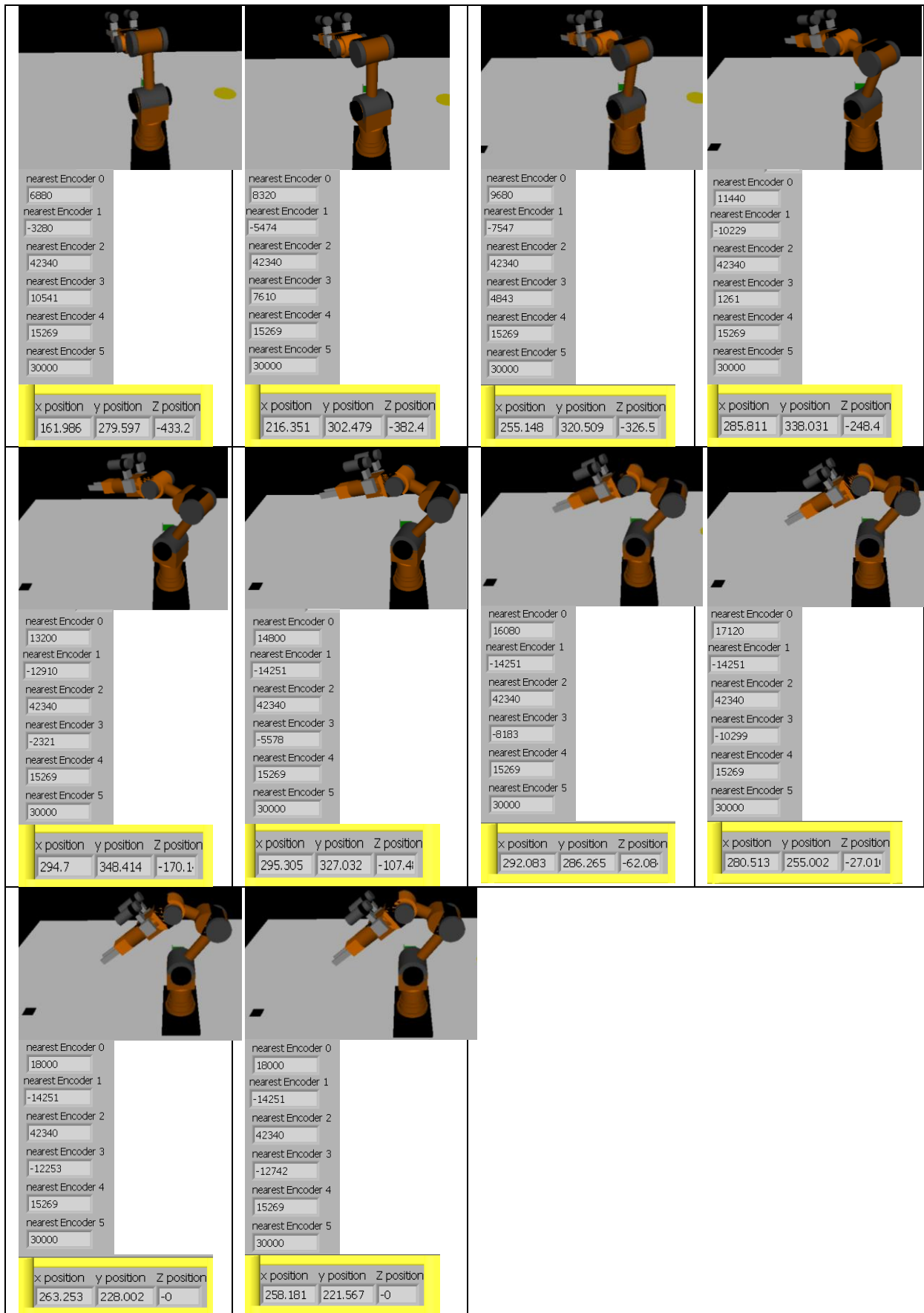


Return to scan position from PBOG ‘drop-off’ location

The manipulator is required to return to the first image acquisition position, the manipulator returns to the exact position for the long distance scan; this is seen in TableC 11. The manipulator automatically realises the shortest distance to move for all joints and ensures this movement then checks the end position. This enables for the next image acquisition to take place and continue its autonomous operation.

TableC 11 LabView Frames Illustrating Movement From PBOG 'drop-off' Location to Following Image Acquisition Scan



## Appendix D

### Annealed Stainless Steel Gripper Arms Analysis

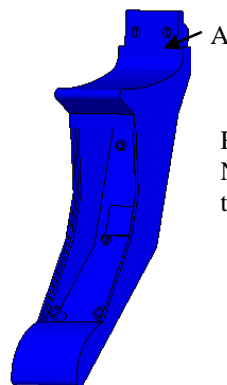
Within the research PC-10 versions of the gripper arms are used to ensure that feedback can be accomplished and sufficient grasp can be accomplished in order to transport the objects to their destination. However, for the gripper arms to be used in a real world industrial environment, SS equivalents are required to be produced; as such determination of the gripper specifications is required to be produced in order to establish limitations of use. Thus additional simulations were conducted to determine Maximum Permitted Load Before Failure (MPLBF). A comparison between the manufacturers supplied gripper arms discussed in Chapter 3 to the new developed ones is discussed. The Factor of Safety (FOS) will be utilised to determine MPLBF for both Gripper Arms.

### Simulation of prototype Stainless Steel gripper arms

As shown in TableD 1, the single gripper arm is 0.07557kg heavier than the manufacturer's supplied Gripper arm. The design for the prototype SS single gripper arm scored an FOS of 3.6519, which shows a positive improvement from the results obtained with the existing gripper; this is further clarified from the FOS simulation shown in FigureD 1.

TableD 1 Annealed SS Single Gripper Arm Properties

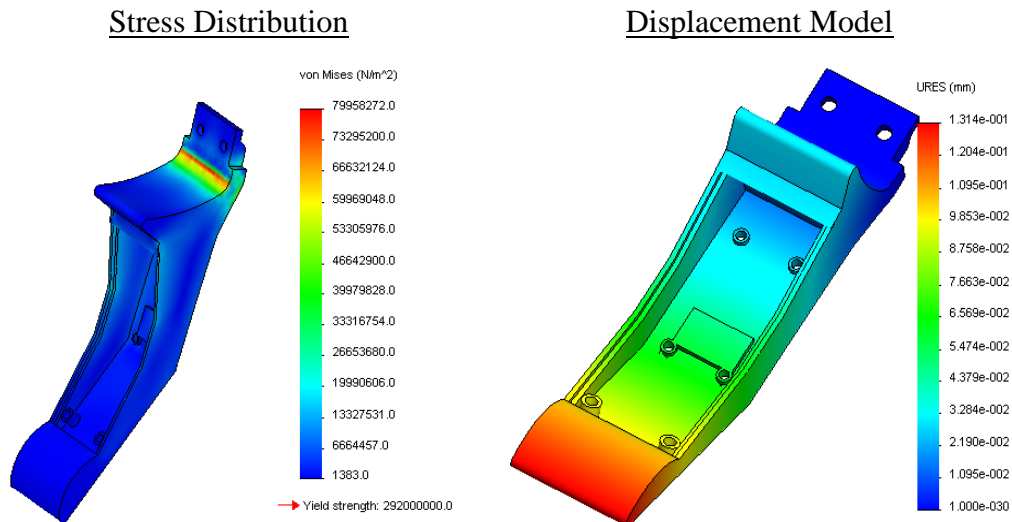
Mass properties of single gripper	
Mass	0.10549 kg
Volume	0.0000134215 $m^3$
Surface area	0.01046774 $m^2$



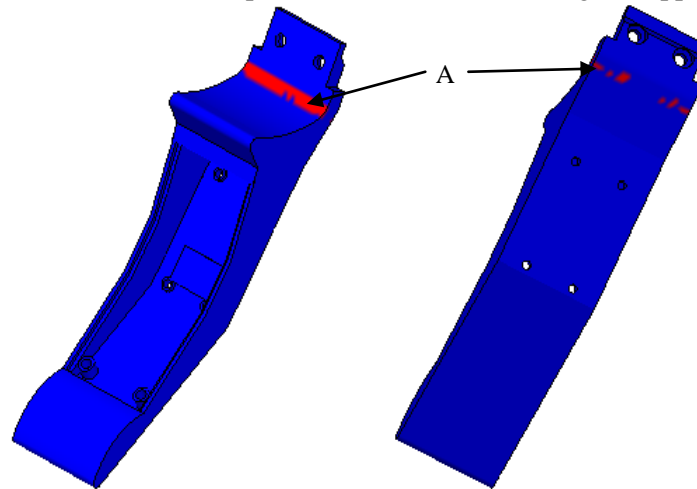
Red = Factor of safety (FOS)= 1  
Notice there is no area of the part that fails with the applied load.

FigureD 1 FOS for Prototype SS Single Gripper Design

As seen in FigureD 2, the stress distribution illustrates considerable improvement to the original, thus, causing an improvement to the grasp quality of the manipulator. By conducting simulations, the maximum permitted load before the part fails is 4.721N, as seen in FigureD 3.

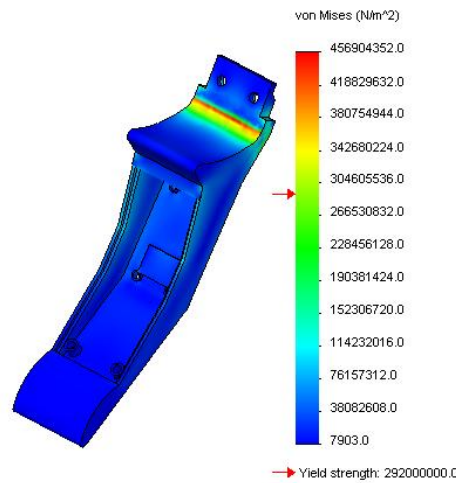


FigureD 2 Stress and Displacement Model for SS Single Gripper Arm



FigureD 3 FOS Limit for SS Single Prototype Gripper Arm Design

The maximum stress is established at the location of the red arrow on the bar chart at the right hand side of FigureD 4. Any stress on the part that exceeds this value has the potential of causing catastrophic failure. From further simulations the part will work continue to work at a load of 4.473N, as long as the applied load is only subjected to the part in a time limited method.



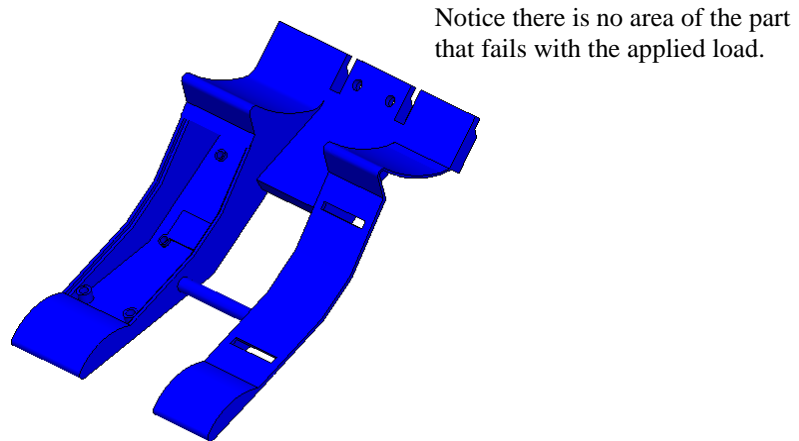
FigureD 4 Failure Analysis for SS Single Gripper Arm

TableD 2 depicts the properties of the dual gripper arm, there is a considerable difference in the mass when compared to the single gripper arm due to the addition of the support finger and the support beam/bar being attached to the main finger. The design scored an FOS of 3.58003, which is lower than the FOS for the single gripper due to the inclusion of the flexible design of the support finger that permits displacement to allow for forming around objects, and thus inherently weaker than the solid construction of the single gripper arm.

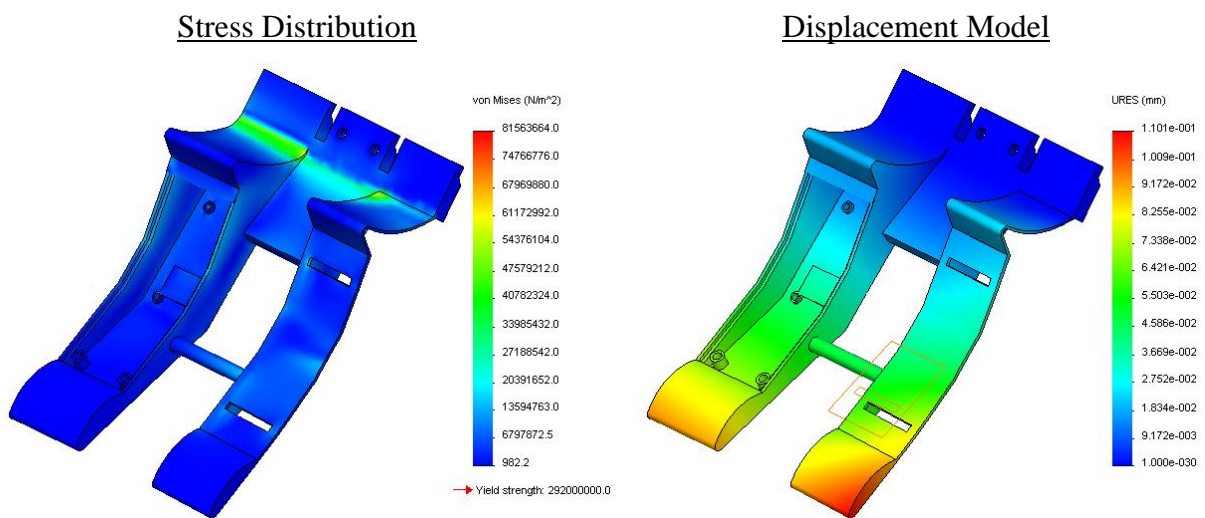
TableD 2 Annealed SS Prototype Dual Gripper Arm Properties

Mass properties of dual gripper	
Mass	0.19124 kg
Volume	0.000024331 $m^3$
Surface area	0.02059547 $m^2$

FigureD 5 illustrates the part can continue to work under the specified load without causing significant damage as there is no areas of the part shown to be under strain. The support finger is 1.5mm deep and subjected to increased displacement, as seen in FigureD 6.

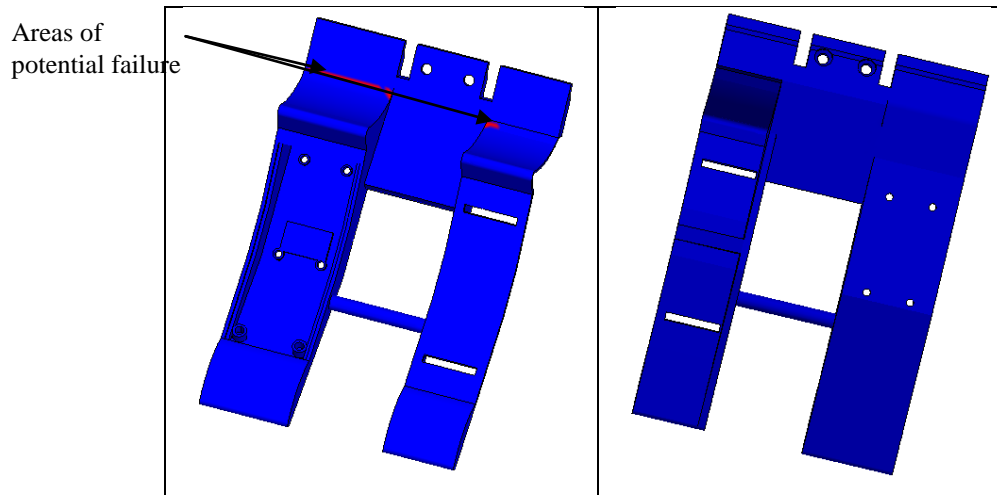


FigureD 5 FOS for Prototype Design SS Dual Gripper Arm



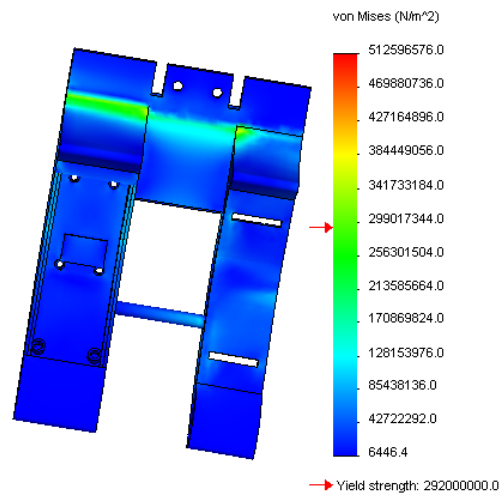
FigureD 6 Stress and Displacement Model for SS Dual Gripper Arm

With numerous simulations, the maximum load before failure is calculated as 4.946N, the FOS is calculated as 0.56949 which is less than the FOS for the single gripper but with greater applied load. Further inspection shows that the area of potential failure is directed along the identical location as with the single gripper, as seen in FigureD 7.



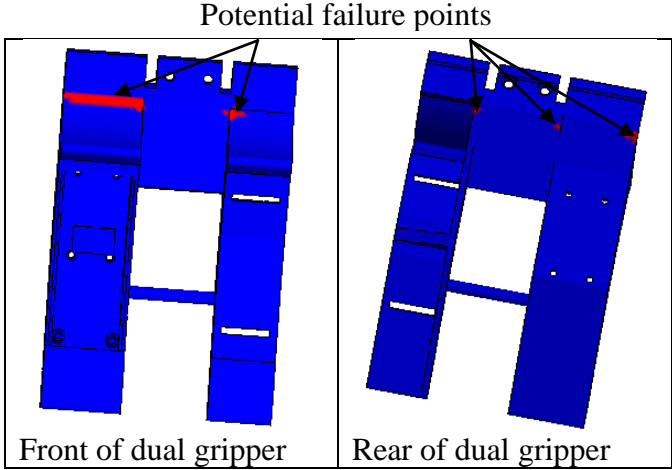
FigureD 7 FOS for Prototype Design SS Dual Gripper Arm

As seen in FigureD 8, the stress analysis for the part determines that the gripper can withstand 4.946N of applied load, with no critical strain 'red' areas illustrated within the analysis. Thus proving the dual gripper can withstand increased load when compared with the single gripper design.



FigureD 8 Failure Stress Analysis for SS Dual Gripper Arm

With increasing the maximum allowable load to determine the FOS for the part, the maximum allowable load without damage is found to be 7.42N, as illustrated in FigureD 9. The main location of stress, depicted in red, is across the main finger that houses the main electronic circuitry. Thus determining the part will operate with this applied load for a limited time before failing. If the part continues to operate under load of 7.42N, the number of potential failure points shown on the rear of the part will increase, eventually causing a failure in the main gripper finger.



FigureD 9 FOS Limit for Prototype SS Dual Gripper Arm Design

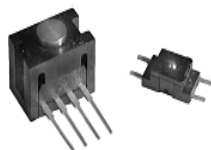
The type of sensor that can be fitted within the gripper housing can vary from optical to colour to other tactile sensors or switches. It is this reason why the maximum load for the part is required, to account for different operational needs that will suit this design of gripper mechanism.

# Appendix E

## FS-Series Force Sensor Manufacturers Datasheet

### Force Sensors FSG and FSL Series

FS Series



#### FEATURES

- Compact commercial grade package
- Robust performance characteristics
- Adaptable product design
- Precision force sensing
- Electrically ratiometric output
- Extremely low deflection (30 microns typ. @ Full Scale)
- High ESD resistance 10 KV
- Available signal conditioning
- Optional terminal configurations

The FS Series Force Sensors provide precise, reliable force sensing performance in a compact commercial grade package. The sensor features a proven sensing technology that utilizes a specialized piezoresistive micro-machined silicon sensing element. The low power, unamplified, noncompensated Wheatstone bridge circuit design provides inherently stable mV outputs over the force range.

Force sensors operate on the principle that the resistance of silicon implanted piezoresistors will increase when the resistors flex under any applied force. The sensor concentrates force from the application, through the stainless steel plunger, directly to the silicon sensing element. The amount of resistance changes in proportion to the amount of force being applied. This change in circuit resistance results in a corresponding mV output level.

The sensor package design incorporates a patented modular construction. The use of innovative elastomeric technology and engineered molded plastics results in load capacities of 4.5 Kg over-force. The stainless steel plunger provides excellent mechanical stability and is adaptable to a variety of applications. Various electrical interconnects can accept pre-wired connectors, printed circuit board mounting, and surface mounting. The unique sensor design also provides a variety of mounting options including mounting brackets, as well as application specific mounting requirements.

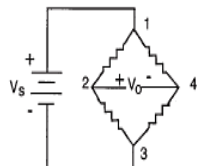
#### MOUNTING

Sensor output characteristics do not change with respect to mounting orientation. Care should be taken not to obstruct the vent hole in the bottom of the housing. Improper venting may result in unstable output.

#### APPLYING FORCE

Evaluation of the sensor is to be performed using deadweight or compliant force. Application of a rigid, immobile force will result in output drift (decrease) as elastomeric seals relax. Off-center plunger loading has minimal effect on sensor performance and maintains operation within design specifications.

#### ELECTRICAL CONNECTIONS



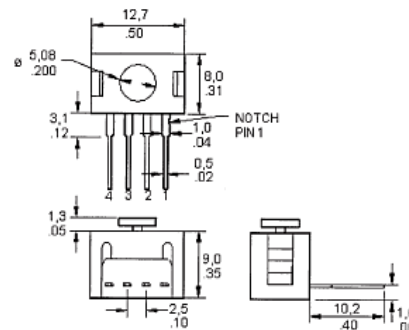
#### FS SERIES CIRCUIT NOTES

1. Circled numbers refer to Sensor Terminals (interface pins).  
Pin 1 =  $V_s$  (+)  
Pin 2 = Output, (+)  
Pin 3 = Ground, (-)  
Pin 4 = Output, (-)
2. The force sensor may be powered by voltage or current.  
Maximum supply voltage is not to exceed 12 volts.  
Maximum supply current is not to exceed 1.6 mA. Power is applied across Pin 1 and Pin 3.
3. The sensor output should be measured as a differential voltage across Pin 2 and Pin 4 ( $V_o = V_2 - V_4$ ). The output is ratiometric to the supply voltage. Shifts in supply voltage will cause shifts in output. Neither Pin 2 nor Pin 4 should be tied to ground or voltage supply.

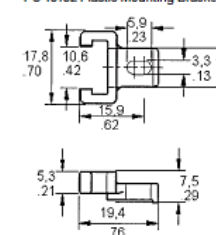
### Force Sensors FSG and FSL Series

FS Series

#### MOUNTING DIMENSIONS (for reference only) FSG15N1A



#### ACCESSORY (FSG Sensor only) PC-15132 Plastic Mounting Bracket



#### PERFORMANCE CHARACTERISTICS @ 10.0 ± 0.01 VDC, 25°C

Parameter	Min.	Typ.	Max.	Units
Excitation*	—	10.0	12.0	VDC
Null offset	-30	0	30	mV
Operating Force	0	—	1500	grams
Sensitivity	0.20	0.24	0.28	mV/gram
Linearity (B.F.S.L.)**	—	±22.5	45	grams
Null Shift	+25°C to 0°C, +25°C to +50°C	—	±1.0	mV
Sensitivity Shift	+25°C to 0°C	—	0.012	mV/gram
	+25°C to +50°C	—	-0.012	mV/gram
Hysteresis	—	45	180	grams
Repeatability (@ 1500 grams)	—	30	120	grams
Input Resistance	4.0 K	5.0 K	6.0 K	Ohms
Output Resistance	4.0 K	5.0 K	6.0 K	Ohms
Overforce	—	—	4,500	grams

#### ENVIRONMENTAL SPECIFICATIONS

Operating Temperature	-40° to 85°C (-40° to +185°F)
Storage Temperature	-55° to +105°C (-131° to +221°F)
Vibration	Qualification tested to 10 Hz to 2 kHz, 20 g sine
Shock	Qualification tested to 150 g, 6 ms, half-sine
Solderability	5 sec at 315°C per lead
Output ratiometric	Within Supply Range

\*B.F.S.L. - Best Fit Straight Line  
 Note: All force related specifications established using dead weight or compliant force.

#### FS SERIES ORDER GUIDE

Catalog Listing	Force Range (grams)	Sensitivity mV/V/gram			Span mV (at 10 VDC)	Over Force grams
		Min.	Typ.	Max.		
FSG15N1A	1,500	.02	.024	.028	360	4,500

#### Constant Current Excitation Schematic

\*Non-compensated force sensors, excited by constant current instead of voltage, exhibit temperature compensation of Span. Application Note #1 briefly discusses current excitation.

Constant current excitation has an additional benefit of temperature measurement. When driven by a constant current source, a silicon pressure sensor's terminal voltage will rise with increased temperature. The rise in voltage not only compensates the Span, but is also an indication of die temperature.

